THE
PHYSICAL REVIEW

A journal of experimental and theoretical physics established by E. L. Nichols in 1893

SECOND SERIES, VOL. 73, NO. 5 MARCH 1, 1948

Threshold for the Proton-Neutron Reaction in Copper*

W. E. SHOUPP, B. JENNINGS, AND W. JONES
Electronics and Nuclear Physics Department, Westinghouse Research Laboratories, East Pittsburgh, Pennsylvania

(Received November 14, 1947)

The direct determination of the (p, n) threshold for Cu^{65} has been found. The energy of the $Li^7(p, n)$ threshold had been previously checked against the $F(p, \gamma)$ resonances, and the value, 1.85 ± 0.01 Mev of this threshold of Li^7 was used as the voltage standard in this experiment. The value for the Cu^{65} (p, n) threshold was found to be 2.164 ± 0.01 Mev. If the mass of Cu^{65} is taken as 64.955, the mass for Zn^{65} is computed to be 64.9565 ± 0.001. If after positron emission the resultant nucleus is in the ground state, the maximum energy of the positron spectrum may be computed to be 0.355 ± 0.001.

INTRODUCTION

THE first observation of (p, n) reactions was made by Du Bridge, Barnes, and Buck[1] by measurement of the activities induced by the neutrons in silver foils. Since then the values of the proton energy threshold, for the (p, n) reactions in Li^7, Be^9, B^{11}, and C^{13} have been observed and accurately measured[2–5] yielding accurate mass data for Be^7, B^9, C^{11}, and N^{13} as well as furnishing accurate and easily reproducible voltage calibration points for the nuclear energy scale. The (p, n) threshold for Cu^{65} has now been determined using the $Li^7(p, n)$ threshold for voltage reference. This enables us to make a computation of the mass of Zn^{65}, and establishes accurately the maximum energy of the positrons emitted from Zn^{65} when it decays into Cu^{65}.

EXPERIMENT

The Westinghouse pressure electrostatic generator[6, 7] was used as a source of high energy protons. The voltage stability was approximately 0.1 percent for short times and was not controlled by automatic means. The magnetically deflected spot of mass one (H^+) was used to avoid any possible deuterium contamination. The target arrangement is shown in Fig. 1, in which the tantalum aperature of the Faraday cage was small enough to insure that all protons entering the cage would strike the target. The beam alignment was checked by means of a quartz plate which could be let down over the target. The proton beam current was integrated with a device similar to one described by B. E. Watt[8] except that a 300-v battery was installed in series with the input so as to suppress secondary electrons formed at the entrance to Faraday cage and 313C tube was used instead of the neon glow

* This work was performed under contract with the Office of Naval Research N6ori-156.

[1] L. A. Du Bridge, S. Barnes, J. H. Buck, Phys. Rev. **51**, 995 (1937).
[2] L. A. Du Bridge, S. Barnes, J. H. Buck, Phys. Rev. **53**, 447 (1938).
[3] J. E. Hill and G. E. Valley, Phys. Rev. **55**, 678A (1939).
[4] J. E. Hill, Phys. Rev. **57**, 567A (1940).
[5] R. O. Haxby, W. E. Shoupp, W. E. Stephens, W. H. Wells, Phys. Rev. **58**, 1035 (1940).
[6] R. O. Haxby, W. E. Shoupp, W. E. Stephens, W. H. Wells, Phys. Rev. **57**, 348, 567 (1940).
[7] R. O. Haxby, W. E. Shoupp, W. E. Stephens, W. H. Wells, Phys. Rev. **58**, 162 (1940).
[8] B. E. Watt, Rev. Sci. Inst. **17**, 334 (1946).

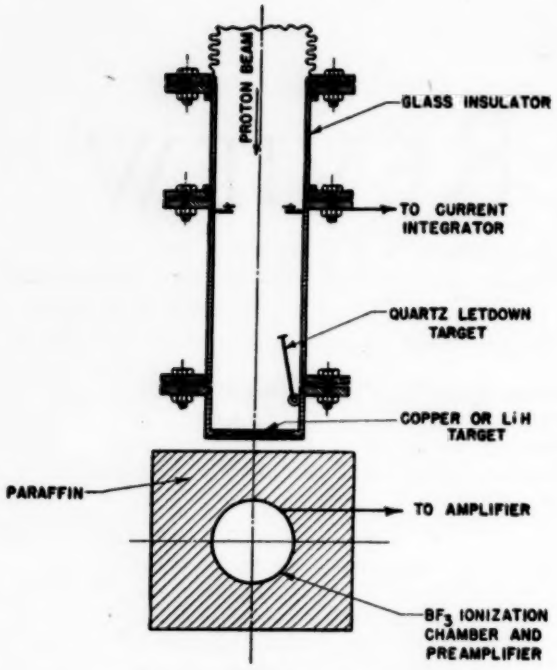

FIG. 1. Arrangement of target, paraffin, and BF_3 ionization chamber.

lamp. Neutrons emitted by the target were slowed down by paraffin, detected by means of a BF_3 chamber, a preamplifier, and a linear amplifier, and recorded through a scale of 16 and an integral recorder. The design of the BF_3 chamber was patterned after Segrè and Wiegand.[9] Commercial unenriched BF_3 was used and the ionization chamber was operated slightly above atmospheric pressure. A Geiger counter γ-ray monitor was operated simultaneously with the neutron detector. The compensating generating voltmeter used was the same as that previously employed[7] and had been checked for linearity against the 0.862-Mev fluorine gamma-ray resonance using the H^+, HH^+, and HHH^+ beams. The voltage was varied by means of a single corona point mounted on the end of a remotely controlled rod that was moved towards or away from the high voltage electrode. The energy of the $Li^7(p, n)$ threshold had been previously checked against the $F(p, \gamma)$ resonances and the value, 1.85 ± 0.01 Mev, of this (p, n) threshold of Li^7 was used as the voltage standard in these experiments. These measurements are established for the same voltage scale[7] previously used for Li^7, Be^9, B^{11}, and C^{13}. This scale may be in error in absolute value by as much as 1 or 2 percent, however, the relative scale should be accurate to about 0.1 percent.

RESULTS

The number of neutrons counted by the BF_3 ionization chamber per current integrator count is plotted as a function of proton energy, read by the generating voltmeter, to give the curves shown in Figs. 2 and 3. A thick target of lithium

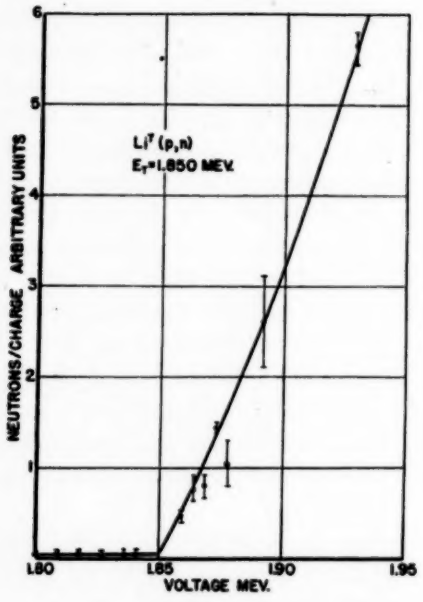

FIG. 2.

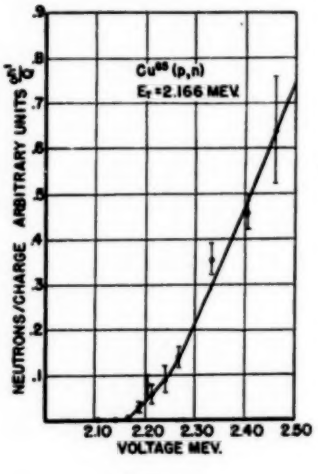

FIG. 3.

[9] E. Segrè and C. Wiegand, Rev. Sci. Inst. 18, 86 (1947).

hydride was used for the $Li^7(p, n)$ voltage calibration data and a pure metallic copper target was used for the $Cu(p, n)$ data, otherwise the detection and measuring equipment was the same for lithium hydride and for copper targets. Beam currents of about 0.1 μa of resolved protons were used. The vertical lines indicated at the experimental points on Figs. 2 and 3 represent the expected statistical fluctuations in recorded neutrons.

In general, the (p, n) reaction may be written

$$ {}_zX^A + {}_1H^1 \rightarrow {}_{z+1}Y^A + {}_0n^1 + Q_1, \quad (1) $$

where Q_1 is a negative quantity since the reaction is endoenergetic. The value of Q_1 is determined from the energy threshold (E_t) by,

$$ Q_1 = -E_t A/(A+1). \quad (2) $$

The product nucleus Y may be radioactive and return to X by positron emission

$$ {}_{z+1}Y^A \rightarrow {}_zX^A + 2M_e + \mu + E_+, \quad (3) $$

or by K-electron capture

$$ {}_{z+1}Y^A \rightarrow {}_zX^A + \mu + Q_2. \quad (4) $$

In these equations X and Y are the atomic masses involved, M_e is the electronic mass, E_+ is the maximum energy of the positron spectrum, Q_2 is the energy balance, and μ is the rest mass of the neutrino. The threshold for Cu^{63} has been previously observed[10] to occur at 4.1 ± 0.1 Mev and the maximum of the positron spectrum (half-life 38 min.) was given as 2.3 ± 0.15 Mev. These data are in good agreement with the energy relations involved (Eqs. (1), (2), (3)). A long-life activity (235 days) was also observed in the $Cu(p, n)$ reaction and was assigned to Zn^{65}. The threshold energy (E_t) for the (p, n) reaction in copper observed here occurs at $2.164 \pm .01$ Mev. This threshold energy is considerably lower than that of Cu^{63} and must then be assigned to the remaining less abundant copper isotope Cu^{65} (29.87 percent). The reaction observed in this work is then

$$ {}_{29}Cu^{65} + {}_1H^1 \rightarrow {}_{30}Zn^{65} + {}_0n^1 + Q_1. \quad (5) $$

From the threshold $E_t = 2.164 \pm .01$ Mev,

$$ Q_1 = -A/A + 1, \quad E_t = -2.131 \pm .01 \text{ Mev}. \quad (6) $$

If we use for the neutron-hydrogen mass difference $({}_0n^1 - {}_1H^1)^{11} = 0.755 \pm .016$ Mev, the $(Zn^{65} - Cu^{65})$ mass difference is,

$$ (Zn^{65} - Cu^{65}) = 2.131 - 0.755 = 1.376 \pm 0.02 \text{ Mev} = 0.00147_7 \pm 0.00003 \text{ MU}. $$

Using the mass of Cu^{65} as 64.955 MU gives the mass for Zn^{65} the value 64.9565 ± 0.001 MU. If after positron emission, the resultant nucleus is in the ground state, the maximum energy of the positron spectrum may be computed from Eq. (3) (assuming μ to be zero),

$$ E_+ = 1.376 - 1.021 = 0.355 \pm .001 \text{ Mev}. $$

This value is in agreement with, but much more accurate than, the cloud-chamber value of 0.4 Mev obtained by the Rochester[10] group.

[10] C. V. Strain, Phys. Rev. **54**, 12 (1021).

[11] W. E. Stephens, Rev. Mod. Phys. **19**, 19 (1947).

Development of the Frequency Modulated Cyclotron

J. REGINALD RICHARDSON,* BYRON T. WRIGHT,* E. J. LOFGREN,** AND BERNARD PETERS***
Radiation Laboratory, Department of Physics, University of California, Berkeley, California

(Received November 12, 1947)

The experimental development of the phase stability principle as applied to the 37-inch f-m cyclotron is discussed. The ions were required to pass through an over-all radial decrease in magnetic field of 13 percent. Some theoretical estimates of the yield *vs.* modulation frequency are given and these were found to be in satisfactory agreement with the experimental results. It is found that some of the ions emerge as late as four or five modulation cycles after their initial acceleration. Observations were made of the time of flight of the ions and evidence was found of the actual phase oscillations in the shape of the ion current patterns. The ion current received by a probe at different radii and different pressures using a pulsed source was analyzed, and indicates a considerable loss of beam at dee voltages less the 60 kev. The data confirm the variation of ion beam loss as the reciprocal of the square of the ion energy and extend the validity of this relation to 600 kev for deuterons. The variation of ion current with dee voltage is quite steep. A deflected beam amounting to 10 percent of the circulating current was obtained, taking advantage of the precessional motion of the ion orbits. Circulating ion currents of 3 μa of 7.5-Mev deuterons and 2 μa of 14.6-Mev protons were obtained.

1. INTRODUCTION

THIS is a report on the experimental development[1] of the phase stability principle[2,3] as applied to the frequency modulated cyclotron. The purpose of this development was to ascertain the chances of the successful application of the phase stability principle to the 184-inch cyclotron[4] by using the 37-inch Berkeley cyclotron as a model.

The cyclotron frequency for an ion of kinetic energy W (units Mc^2) in a magnetic field H is

$$f=f_cH/(1+W)H_c, \qquad (1)$$

where f_c is the frequency the ion would have with very low energy in the field H_c, H_c being the field at the cyclotron center. This relation exhibits the difficulty one encounters in trying to accelerate ions to high energies ($W>0.02$) in an ordinary cyclotron. In order to maintain vertical focusing of the ions it is necessary that the magnetic field fall off as the ion energy increases. The decrease in H and increase in W combine to produce a lowering of the resonant frequency f as the ion energy increases. This means that after a certain number of turns, the ions will be so far out of phase with the accelerating dee voltage that they will be decelerated and will never attain the full energy desired. In the past, the usual solution to this problem has been to increase the dee voltage until the number of ion turns was relatively small (<100). Then the ions would never get so much out of phase with the dee voltage that they would be decelerated.

For really high energies this solution requires very large dee voltages. In designing the 184-inch cyclotron for the acceleration of 100-Mev deuterons, for example, it was clear that something of the order of one million volts on the dees would be required. Although by no means insoluble, the handling of such large r-f voltages is a serious technical problem, and since the required dee voltage varies as the square of the desired energy[5] this would soon place a ceiling on the possible ion energy produced by the cyclotron.

The possibility of using the phase stability principle together with frequency modulation on the cyclotron was suggested by McMillan, but it was not clear what would be required in the way of ion injection to get them into the region of stable phase. However, one of us (JRR) was able to show by means of graphical integration that no special ion injection technique would be required and that a yield of some one to five percent (depending upon various conditions of the acceleration) of the total ion current would

* Now at the University of California, Los Angeles, California.
** Now at the University of Minnesota.
*** Now at the University of Rochester.
[1] J. R. Richardson, K. R. MacKenzie, E. J. Lofgren, and B. T. Wright, Phys. Rev. 69, 669 (1946).
[2] E. M. McMillan, Phys. Rev. 68, 143 (1945).
[3] V. Veksler, J. Phys. U.S.S.R. 9, 153 (1945).
[4] Brobeck, Lawrence, MacKenzie, McMillan, Serber, Sewell, Simpson, and Thornton, Phys. Rev. 71, 449 (1947).
[5] R. R. Wilson, J. App. Phys. 11, 781 (1940).

be picked up normally in the phase stable region. Since yields of this magnitude would certainly be adequate for most experiments at very high energies, it was decided to make experimental tests on this technique.

Looking at Eq. (1) we see that it is possible to simulate a combined frequency change caused by energy increase and magnetic field decrease by a change in magnetic field alone. The field on the 37-inch cyclotron was accordingly tailored[6] to fit an over-all frequency change of 13 percent from ion source to exit radius, and the experimental results described in this paper were obtained under these conditions.

2. EXPERIMENTAL APPARATUS

The field from the 37-inch magnet was adjusted to conform to the relation

$$H=H_c/(1+9\times10^{-4}r^2)^{\frac{1}{2}}, \qquad (2)$$

where H_c is the field at the center and r is the radius in inches. This relation was followed out to a radius of 18 inches. Equation (2) is derivable on the assumptions of a geometrical similitude of the resonant ion frequency between the 37-inch and the 184-inch, that the frequency change caused by mass change is negligible on the 37-inch, and that the frequency change on the 184-inch is entirely due to the mass change. The last assumption is true only as a first approximation. The radial variation in field was obtained by the use of shims of circular symmetry.

Figure 1 is a plan view showing the four-foot square steel vacuum tank with 41-inch pole tips $2\frac{1}{4}$ inches thick welded in the top and bottom. The atmospheric load is carried by heavy non-magnetic steel[7] corner posts welded to the $2\frac{1}{4}$-inch disks. The vertical walls of the tank are also non-magnetic (this was probably not necessary) while the top and bottom are of ordinary steel. This type of construction is very easy to build, and the welds if reasonably well done are almost certain to be vacuum tight. Magnetic shims to shape the field are screwed to the pole tip disks. The magnet gap where the shims are thickest is $5\frac{1}{2}$ inches. Two entire sides of the tank are open for ready access.

Since the dee voltage required in the f-m cyclotron is quite moderate, the primary reason for having two dees has disappeared. The plate covering the opening on the left of Fig. 1 carries a single dee on a stem passing through a zircon insulator. The dee stem is part of the half-wave line of the f-m radiofrequency system.[8] The inside dimensions of the dee are $2\frac{1}{2}$ inches in height and 19 inches in radius. The opposite face plate carries the arc source, probe, and deflector. The source consists of a d.c. heated tungsten 100-mil filament enclosed in a gas tight copper box with a graphite top. The graphite has the advantage over most metals in that it resists sputtering and it can run hot enough to dissipate its heat by radiation. The ion column emerges from the box through a 0.090-inch by 0.625-inch slot, the long dimension parallel to the dee edge.

Both the grounded and negative deflector electrodes, Fig. 1 and Fig. 2, are hinged at the entrance to the deflected ion channel and are provided with cam and flexible shaft mechanisms to permit adjustment to optimum positions from outside the tank. Internally, the entrance to the deflector channel may be set to a given distance from the geometrical center of the tank. This radius is usually $17\frac{3}{4}$ inches. The exit strip is 0.006-inch tantalum sheet. The deflector face plate also carries a probe which may be inserted

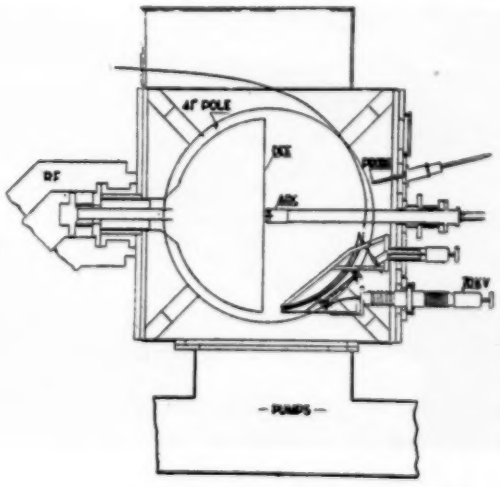

FIG. 1. A plan view of the cyclotron showing the single dee, arc source, and deflector assembly.

[6] Our thanks are due Mr. Duane Sewell for considerable assistance in this part of the work.

[7] Jessop non-magnetic steel Mn $10\frac{1}{2}$–$12\frac{1}{2}$ percent Ni 7–8 percent.

[8] K. R. MacKenzie and V. Waithman, to be published when patent release can be obtained.

along a radius to various distances from the center. A rectangular extension (top of Fig. 1) was added to the tank to give clearance to the deflected beam when it was brought outside the tank into the air.

The frequency modulation is produced by a rotating mechanical capacitor as previously described.[9] This capacitor is connected to the end of the half-wave resonant line which is opposite to that carrying the dee. The shape of the frequency time curve could be adjusted during operation by means of a moveable stator ring.

The ion source could be pulsed[10] with a condenser discharge which could be repetitiously tripped at any desired instant in the modulation cycle. The width of the pulse was variable from about three to 50 microseconds. Under steady operation, the 100-mil tungsten filaments in the ion source had an average useful life of about 60 hours. However, under pulsed operation this lifetime was increased by more than a factor ten.

A d.c. bias voltage was applied to the dee system, including the resonant line and the rotor of the capacitor. This voltage acted as a clearing field[8] to sweep out residual ionization which otherwise so loads up the oscillator that it is unable to establish a large dee voltage. For low r-f dee voltages a positive bias of 1000–2000 volts was definitely beneficial in beam output-giving a factor of ten at three kv r-f on the dee. As the dee voltage was increased the benefit was less marked and was perhaps 20 percent at 10-kv dee voltage. This effect is not completely understood.

FIG. 2. A photograph showing the deflector and arc source face plate as it is removed from the tank.

[9] F. H. Schmidt, Rev. Sci. Inst. 17, 301 (1946).

[10] We are indebted to James Vale for the design and construction of the ion pulser.

The problem of measuring the true ion beam current by means of a probe is a serious one. In addition to the usual difficulties with the rectification of r-f signals, and secondary emission, the probe currents sometimes acted similarly to those encountered in a plasma. It was usually necessary to check the probe current by putting both positive and negative voltages on the probe. These deleterious effects disappeared when the pulsed ion source was used. They could also be eliminated at the high ion energies by totally shielding the probe with aluminum foil.

Sufficient precautions were taken so that we are confident that the figures given in this paper are substantially correct for the ion beam currents.

Considerable experimenting was done with different arc source geometries, including round holes and slots of different dimensions for the arc column and graphite cones of different sizes and shapes. The one described was, however, the most successful under our particular conditions. It is possible that an arc column of larger cross section would be better if one had more r-f power available, but in our case it made the operation unstable. A dummy or vestigial dee was tried both at ground and plus and minus d.c. voltages, but it had little effect on the ion current. Some attempts were made to use small accelerating electrodes near the arc column with attractive voltages on them in order to increase the ion current, but these attempts, in general, were not successful. The principal difficulty encountered was in arranging the accelerating electrodes so that they would not be hit by the ions in subsequent revolutions.

3. THEORETICAL CONSIDERATIONS

The ions as picked up in the cyclotron from the ion source at the center are very quickly brought into phase (within ~ 0.1 radian) with the dee voltage after one or two r-f cycles.[11] This holds true independently of the actual phase angle at which they start being accelerated. Thus one can regard all the ions as being picked

[11] A. C. Helmoltz, private communication.

up with essentially zero phase. If α is the phase angle ($\alpha=0$ for maximum ion acceleration), V_D is the dee voltage, and f is the resonant frequency of the ion, then the kinetic energy gained by the ions (in electron volts) is

$$T=2\sum V_D f\cos\alpha\Delta t. \quad (3)$$

If the applied r-f frequency is f_a, we define $h=f-f_a/f_c$, where f_c is the resonant ion frequency at the center of the cyclotron. Then

$$\alpha=2\pi f_c\sum h\Delta t. \quad (4)$$

When the kinetic energy T can be considered small compared to the rest energy, W_0, we can use

$$h=(H/H_c)(T_a-T/W_0), \quad (5)$$

where H is the magnetic field at the ion path and H_c is the field at the center. T_a is the kinetic energy that an ion would have if it were exactly in resonance with the applied frequency f_a. Now we can define the phase stability factor, ρ, which is the value of $\cos\alpha$ which would be required to keep the ion of energy T_a always in step with the applied frequency f_a. If averaged over several phase oscillations, it will be true that

$$\rho=\frac{\text{average energy gain per turn}}{\text{maximum possible energy gain per turn}}. \quad (6)$$

Thus we can write

$$h=(2/W_0)(H/H_c)[\sum V_D f_a\rho\Delta t-\sum V_D f\cos\alpha\Delta t]. \quad (7)$$

If we are concerned only with the initial stages of the acceleration, we can simplify this to

$$h=(2/W_0)(H/H_c)V_D f\sum(\rho-\cos\alpha)\Delta t. \quad (8)$$

Equations (4) and (8) can be solved simultaneously by graphical integration to obtain the phase and frequency oscillations which occur in such a system, then Eq. (3) can be used to obtain the ion energy as a function of the time. The efficiency of ion pick-up, that is, the ratio of the number of ions accelerated to those available for acceleration, can be estimated from the ratio of the time during which ions are picked up to the total time of one complete modulation cycle. The area under the $h(t)$ curve is proportional to the phase angle α. Since $\Delta h/\Delta t$ is proportional to V_D, it follows that for a constant ρ the time over which ions are picked up is proportional to $1/(V_D)^{\frac{1}{2}}$. But for a constant ρ the modulation period is proportional to $1/V_D$. Therefore the efficiency of ion pick-up varies as $(V_D)^{\frac{1}{2}}$ for a constant ρ.

TABLE I. Variation of the ion pick-up efficiency with the value of the phase stability factor ρ.

ρ	1.0	0.9	0.8	0.7	0.6	0.5
ϵ (percent)	0	0.8	1.3	1.7	2.1	2.6

In general, if we neglect the change in magnetic field we will have

$$\epsilon=\text{efficiency}=\frac{(V_D W_0)^{\frac{1}{2}}}{T_f}\left(\frac{2}{\pi}\langle\cos\alpha-\rho\rangle_{Av}\cos^{-1}\rho\right)^{\frac{1}{2}}, \quad (9)$$

where T_f is the final kinetic energy of the ions and $\langle\cos\alpha-\rho\rangle_{Av}$ is an average value over the first quarter phase oscillation. For ρ between 1.0 and 0.5 the approximation

$$\langle\cos\alpha-\rho\rangle_{Av}=1-\rho-\frac{\alpha_1^2}{10},$$

where $\alpha_1=\cos^{-1}\rho$ is satisfactory. This gives

$$\epsilon=\frac{(V_D W_0)^{\frac{1}{2}}}{T_f}\left(\frac{2}{\pi}\cdot\alpha_1\cdot\left(1-\rho-\frac{\alpha_1^2}{10}\right)\right)^{\frac{1}{2}}. \quad (10)$$

In this expression for the efficiency it has been assumed that the period of acceleration occupies half of the total modulation cycle.

As an example we can consider the ion pick-up efficiency for the acceleration of deuterons to $T_f=200$ Mev with $V_D=50$ kev. The variation with different values of ρ is given in Table I.

A more elegant method of calculating these results was later introduced by McMillan and extended by Bohm and Foldy[12] to include the condition that the ions not return to the center. If the ions return to the center of the cyclotron they will be effectively lost, at least as far as that cycle is concerned. This condition applies for $\rho\leqslant 0.5$, and the results are shown in the theoretical curve of Fig. 3.

In the case of the 37-inch cyclotron we know H as a function of r and df_a/dt as a function of

[12] Bohm and Foldy, to be published.

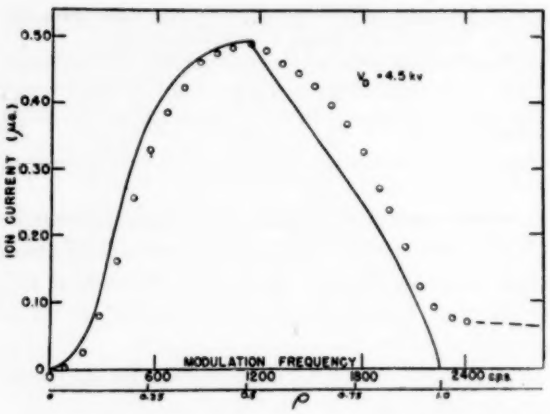

FIG. 3. The variation of ion current with modulation frequency. The solid curve is the theoretical expectation on the yield *vs.* ρ. The displacement of the experimental points from the curve is probably due to the variation of the pressure effect with ρ. See Fig. 9. The dashed line indicates the experimental trend at high modulation frequencies as indicated by the other data.

time. The latter can be evaluated at different values of r, and, then if one neglects the change in ion frequency caused by the change in mass, it is easily shown that

$$\rho=\frac{2\pi^2}{c^2}\frac{W_0}{V_D}\frac{df_a}{dt}r^2\left(1+\frac{1}{(r/H)(\partial H/\partial r)}\right), \quad (11)$$

where W_0 is here expressed in electron volts.

When the magnetic field is of the form (2) the expression

$$r^2\left(1+\frac{1}{(r/H)(\partial H/\partial r)}\right)$$

is a constant. Thus for ρ to be a constant throughout the ion motion we must have $(1/V_D)(df_a/dt)$ =constant. In our experimental arrangement only moderate efforts were made to have these relations hold so that a variation in the instantaneous value of ρ of almost 30 percent over the total ion path was sometimes encountered.

4. EXPERIMENTAL RESULTS

In Fig. 3 is shown a graph of the beam current received at a probe as a function of the angular speed of the rotating condenser. Since for a given radius and magnetic field variation the phase stability constant ρ is simply proportional to df_a/dt, this figure shows the experimental variation of the beam current with ρ. The theoretical curve is that predicted by Bohm and Foldy, and Eq. (10) for $\rho>0.5$.

Presumably the average value of ρ over the first half-cycle of phase oscillation is the important criterion in catching the ions for further acceleration. This first half-cycle of phase oscillation in our instrument corresponded to a radius up to about 6 inches. A precise determination of ρ would involve an exact knowledge of the variation of the dee voltage with the time and corresponding information concerning the radius and the quantity $(r/H)(dH/dr)$. If ρ is to be kept constant, then one has to tailor these quantities accordingly. Only moderate efforts were made to do this, since from the practical viewpoint it is quite unnecessary, and its only virtue would lie in an exact comparison with theory. As a result of these efforts, ρ was found to vary by 10 percent over the first six inches of radius. We estimate that the experimental value of ρ, which we assigned for comparison purposes, has an over-all uncertainty of about 20 percent. It is clear that in view of these facts the comparison with the theoretical curve is quite good. The conclusion is that the optimum value for the phase stability constant is near $\rho=0.5$. The absolute magnitude of the yield or efficiency is rather more uncertain. We estimate that our maximum efficiency is about one to three percent, which is in satisfactory agreement with the theoretical predictions.

Further evidence that the experimental variation in Fig. 3 is due to a change in ion pick-up efficiency is given by the following: If the ion source were to be pulsed for a duration short in comparison with the ion pick-up time involved, it would be expected that the total charge accelerated per pulse would be constant, and independent of the modulating frequency, as long as the dee voltage and other conditions were maintained the same. Therefore one would expect that under these conditions the time average accelerated current would be directly proportional to the frequency of the modulator until the limit of stability near $\rho=1$ was reached. This was confirmed experimentally to the extent that it was found that for short ion pulses the maximum ion beam current was moved toward the $\rho=1$ condition. Also for different modulating frequencies the minimum duration of arc pulse

was determined which would just give the maximum possible beam at that modulating frequency. The qualitative variation of this duration with ρ was in agreement with the expected variation of ion "pick-up" time with ρ as predicted by the theory.

An interesting feature of the curves of beam current against ρ was that the beam did not decrease to zero $\rho>1$ but actually remained at a value as much as 10 percent of the maximum even under these conditions when there was presumably no phase stability. Under the straightforward theory of the f-m cyclotron it should be impossible for ions to get out when the phase stability factor is greater than 1. However, if the ions can spend several modulating cycles in being accelerated, it might be possible for them to get out even when there is no phase stability present in the ordinary sense. With the aid of Eqs. (3), (4), and (8) we can obtain rather easily through graphical construction the kinetic energy of the ions as a function of the time for the case where $\rho>1$. Figure 4 shows this function for the three cases where the ions start early ($f_a>f_c$), on time ($f_a=f_c$), or late ($f_a<f_c$). It is seen, therefore, that in a given modulating cycle as the applied frequency gets far out of resonance with the natural frequency of the ion, a large band of ions is left circulating in the chamber from zero radius up to a maximum radius determined by those ions which start early. In particular, the maximum radius will be attained by those ions which start just early enough so that they reach a phase lag of just $\pi/2$ before starting their large gain in phase which occurs when the applied frequency rapidly drops below their natural frequency. It can be estimated from curves such as those shown in Fig. 4 that in the case of the 37-inch f-m cyclotron and a ρ of 1.4 and V_D of 6 kev these ions would get out to a radius of about 8 inches on the first modulation cycle. Then they would circulate with approximately constant energy and radius until the applied frequency again approached the new natural frequency of the ions. Then, depending upon the phase in which they found themselves, the ions would be accelerated or decelerated for the period during which the applied frequency was within one percent, say, of the natural ion frequency. This would be true even when the applied frequency passes through as it is increasing in the unused part of the modulation cycle. Every time the applied frequency passes through the region the ions are "blurred out"—some being accelerated and some decelerated. Eventually after a series of such passes, some of the ions will receive the full energy and emerge from the cyclotron. This gives a picture of the way in which ions can be accelerated by the f-m cyclotron even when there is no phase stability.

This picture was investigated experimentally by pulsing the arc source once every ten modulation cycles and using a synchroscope to look at the probe current at different radii. At a radius of 17 inches and ρ of about one, it was found that beam came out over a series of four successive modulation cycles in pulses of somewhat decreasing magnitude and at times corresponding to the periods when f_a approximated the ion frequency at that particular radius. When this occurs on the decreasing part of the frequency-time cycle, we will call it a direct pass; when it occurs on the increasing frequency part of the modulation cycle, we will call it an inverse pass. For a radius of 5 inches and below, all ions were

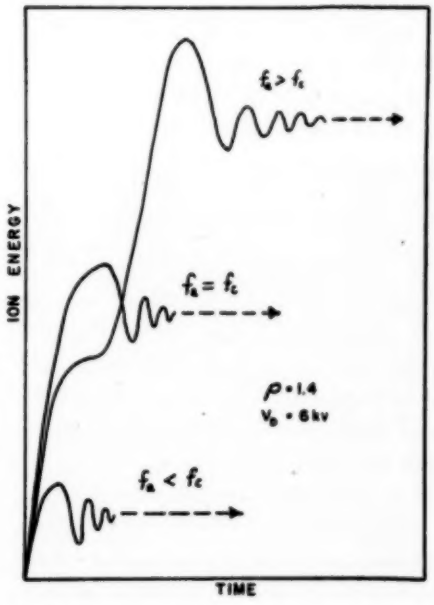

FIG. 4. This shows the kinetic energy of the ions as a function of the time for ions starting early ($f_a>f_c$), on time ($f_a=f_c$), or late ($f_a<f_c$). Particularly for the first two cases, the ions apparently remain circulating with the energy shown by the dotted arrows until the applied frequency again approaches the ion frequency, when they are either accelerated further or decelerated.

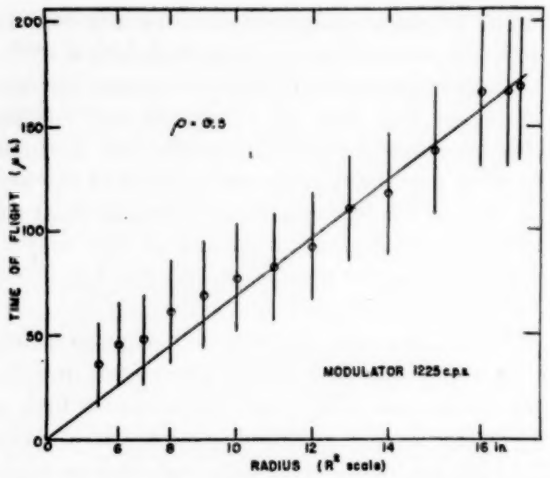

FIG. 5. The time of flight of the ions plotted against $(HR)^2$. The length of the vertical lines indicate the time over which current is received at the probe for that particular radius. The circles are just the centers of the vertical lines. The slanting line would be the expected curve if there were no phase oscillation.

brought out on the first direct pass. Ions appeared on the first inverse pass for radii between six and twelve inches. The ions from the second direct pass appeared at a radius of seven inches, and in general the evidence was in agreement with the idea that for $\rho \sim 1.2$ the ions came out to full radius in a series of four or five passes. One would expect that if this were true the order of magnitude of yield would be $1/2^4$ which is not out of line with the actual yield observed, which was 5 to 10 percent of the maximum beam.

5. TIME OF FLIGHT

Some observations were made using the synchroscope on the time of flight of the ions in normal phase stable operation. Figure 5 shows the results of a typical investigation with $\rho \sim 0.5$. It can be seen that the time over which beam is received at the probe is quite a large fraction of the time of flight of the ions.

This is probably due to the existence of the phase oscillations of the ions and their consequent oscillations about the frequency time curve. Precession of the orbits, an effect which we shall mention later, is too small by a factor of at least five to account for the breadth of the beam pulse. In the case of Fig. 5 we see that the ions must be receiving acceleration when the applied frequency is as much as 2 percent greater or smaller than the ion frequency. Since the total frequency change here is about 12 percent, this probably means that the energy oscillations have an amplitude in this case $2/12 \sim 17$ percent. At any instant, then, near the end of the acceleration period we must have a rather broad band of ions with a total energy spread of about one-third of the mean energy and in our case a total spread in radius of about 3 inches.

When the phase stability factor ρ is less than one-half, many of the ions undergo deceleration during part of their phase oscillation. It is presumed that this is the reason for the series of peaks observed in the beam pattern for low values of ρ as indicated in Fig. 6. This figure shows an oscilloscope pattern of the beam current to a probe as a function of the time. If during part of the time the ions are undergoing deceleration, this will show up as a reduction in the current reaching the probe during that period, and this should be followed by a period during which larger numbers of ions would reach the probe. A typical set of conditions for this type of observation was $\rho \sim 0.3$ and $V_D = 10$ kv. Under these circumstances one would expect the ions to undergo about 10 phase oscillations before attaining their full energy. At first sight one might expect that these oscillations would be smeared out by the time the full energy was attained, particularly since the ions which start late or early are in quite different portions of the energy oscillation. However, if one draws these oscillations out graphically one sees that there is a grouping tendency. This tendency is particularly marked for those ions which start early and on time; this persists throughout their path so that these ions are presumably the ones which produce the peaks in the beam pattern. The period of the oscillation, which is predicated by graphical integration to be 15μ sec. for these conditions, is in very good agreement with the experimentally observed value of 13μ sec. The fact that the time duration of the peaks was independent of the radius from 10 to 17 inches is in agreement with the supposition that they actually represent the oscillations in the natural frequency of the ions. The peaks then would represent successive scrapings by the probe of the ion beam as it oscillates outward. About twice as many peaks were found to be present at

a radius of 17 inches as there were at 11 inches. The amplitude of the frequency oscillation is not damped very much in the small number of oscillations used in the f-m cyclotron so that we can say that it is approximately constant and that therefore the number of peaks present is approximately inversely proportional to df_a/dt. This was found to be the case since we generally operated on the lower section of the available frequency-time curve.

6. VARIATION OF ION CURRENT WITH DEE VOLTAGE

There are many reasons why the beam current will vary as the dee voltage is changed. Among them are:

1. Change in the source current. The accelerating field which pulls the ions out of the source is principally supplied by the dee voltage. One peculiar aspect of the d.c. dee bias is that its optimum value is positive and so tends to reduce this effect.

2. At constant modulation frequency, a change in the dee voltage results in a change in the phase stability factor ρ, which in turn means a change in the ion pick-up efficiency.

3. At constant ρ a change in the dee voltage will cause a change in the ion pick-up efficiency proportional to $(V_D)^{\frac{1}{2}}$.

4. If the beam is pressure sensitive, that is, if some ions are lost because of charge exchange, etc., with gas molecules in the chamber, then since the probability of these processes is very sharply dependent on the energy of the ions, a marked variation with dee voltage might be expected (see the next section). Because of this situation it is rather difficult to get strictly reproducible results on the variation of beam current with dee voltage.

However, some measurements were made which eliminated (2) by changing the modulation frequency in proportion to the dee voltage so that ρ was kept constant. Figure 7 shows the results of a typical set of observations of the ion beam current as a function of the dee voltage with the phase stability factor ρ held constant. It is seen that the dependence on dee voltage is quite steep. However, it is still not as steep as one might expect from reasons (1), (3), and (4), which would lead to a dependence of the form:

$$I \sim V_D^2 e^{-K/V_D}.$$

The presence of the d.c. bias certainly introduces some complication here.

7. VARIATION OF ION CURRENT WITH PRESSURE

In this section we wish to discuss the effect of the general chamber pressure on the ion current.[6] The presence of a large number of gas molecules in the path of the ion beam will cause a loss in the beam because of charge exchange, electron capture, and very large angle scattering. We shall assume in this discussion that the cross section for these processes varies inversely as the square of the energy of the ions. At least we shall assume that this is true above a certain energy, E_0, which in our experiment is taken to be about 25 kev.

If the cross section at the energy E_0 is σ_0 and the corresponding ion radius is r_0, then we assume

$$\sigma(E) \simeq \frac{\sigma_0}{(E_0+E^2)} \sim \frac{\sigma_0}{(r_0+r)^4}.$$

For our purposes we can ignore the variation of E with H in comparison with the variation with r. Then if I_0 is the value of the beam current I at r_0 we can write in the usual way $(dI)/I = -\sigma N ds$, where N is the number of gas molecules per cc and ds is the element of ion path length.

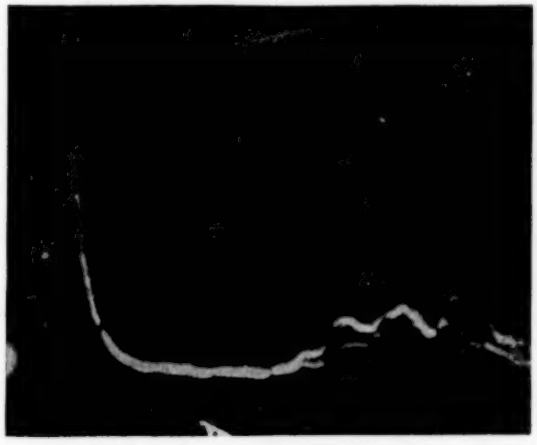

FIG. 6. This oscilloscope photograph shows the ion current to the probe as a function of the time. The markers are at 10-microsecond intervals. The peak on the left is the arc pulse, and those on the right represent the effect of the phase oscillations. There are three modulation cycles in this photograph.

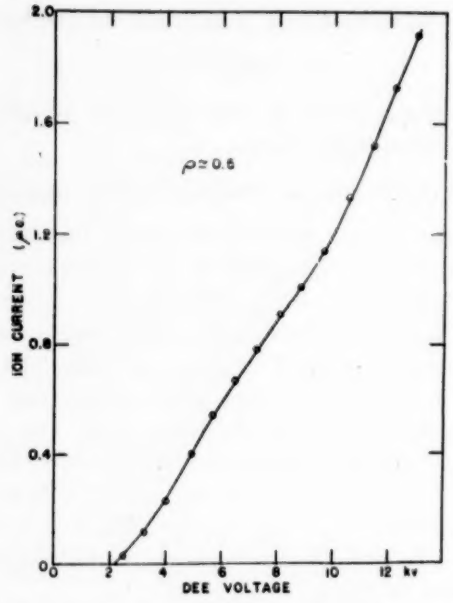

FIG. 7. The ion beam as a function of dee voltage, showing the rapid increase of current as the dee voltage is raised.

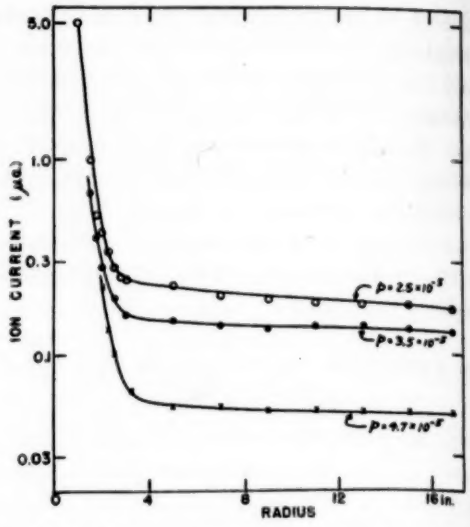

FIG. 8. The ion current to a probe as a function of the radius. The phase stable pick-up of ions does not enter here because the arc pulse was made short in comparison with the time of ion pick-up. Note that most of the losses occur at less than four inches radius.

We shall not investigate here the variation of the ion loss with the phase stability constant, ρ, but shall assume that the experiments are carried out at constant ρ. We shall also concern ourselves just with the radial variation of ion current over less than half of the first phase oscillation. Over this region we shall assume that the increase in path length per ion revolution is approximately proportional to the radius. Then in increasing the ion energy by ΔE we increase the ion path length by

$$\Delta S \sim 2\pi r \frac{\Delta E}{V_D},$$

and since

$$\frac{\Delta E}{E} = 2\frac{\Delta r}{r},$$

$$\Delta S \sim \frac{E}{V_D}\Delta r \sim \frac{(r_0+r)^2}{V_D}\Delta r.$$

If we substitute these results into the above differential equation and integrate, we obtain

$$\ln\frac{I_R}{I_0} \sim -\frac{N}{V_D}\int_0^{R-r_0}\frac{dr}{(r_0+r)^2} = \frac{KN}{V_D}\left(\frac{1}{r_0}-\frac{I}{R}\right),$$

or

$$\frac{I_R}{I_0} = \exp\left[-\frac{KN}{V_D}\left(\frac{1}{r_0}-\frac{1}{R}\right)\right],$$

where I_R is the ion current at the radius R and K is a dimensional constant.

It is interesting to note that for large radii the ion current approaches a constant value. This is, of course, a direct result of the assumption on the functional relationship between σ and E. The variation with pressure is what one would expect from this type of phenomenon. The variation of the ion current with dee voltage is of importance and expresses the fact that for low dee voltage the ions have a long path at low energies so that the ion loss is large. The effect on the ion loss of increasing the pressure in the chamber could be compensated for by increasing the dee voltage in proportion (provided that ρ is kept constant).

Figure 8 shows some experimental results on the ion beam at different radii and different pressures. These results were obtained with the arc source pulsed in a time short compared with the pick-up time for the ions into stable acceleration. Thus the radial loss of beam is presumably entirely due to the loss of charge of the ions which we have been considering. The pressures were measured by means of an ionization gauge on the pump line and therefore is only a rough approximation to the true pressures inside the chamber. The pressure was varied by letting air into the chamber.

If we plot the $\ln I_R/I_0$ *vs.* the reciprocal of the radius we should, according to the above equation, obtain a straight line if ρ, p, and V_D are held constant. Figure 9 gives such plots for these different sets of conditions. It is observed that within the expected experimental error the data are quite linear. The data are sufficiently good to be in definite disagreement with variations of the cross section σ either as the three halves or five halves power of the ion energy. This was checked by plotting $\ln I_R/I_0$ *vs.* $\ln R/r_0$ and *vs.* $1/R^2$ for the 3/2 and 5/2 assumptions, respectively. In both cases the deviation from linearity was very marked. It is important to note that even under our most favorable operating conditions ($p=2\times10^{-5}$ mm and $V_D=11$ kv) fully 90 percent of the ion beam was lost in going from a radius of $1\frac{1}{4}$ inches to a radius of 5 inches. Of course, a larger dee voltage would improve this situation considerably, so that if $V_D=40$ kv one would expect only 50 percent ion loss in this region.

It is certainly unsafe to extrapolate these relations to lower energies and radii, but it seems clear that there must be additional large ion losses in the region below $1\frac{1}{4}$ (extrapolating from the data given here one would guess at least another 80 percent loss at 11 kv or a thirty percent loss at 40 kv). These losses would be the same, naturally, for a large cyclotron as for the 37-inch at equal dee voltage.

One can think of various injection schemes for getting around these difficulties by giving the ions a high initial energy, but the most straightforward solution is to increase the dee voltage until the effect becomes negligible. At a dee voltage of 60 kv, for example, only fifty percent of the ions should be lost over-all due to this effect. The same result, of course, could be attained by improving the vacuum, but this may be difficult to do in view of the desire for heavier arcs and larger gas flows in the ion source.

8. TIME VARIATION OF FREQUENCY AND DEE VOLTAGE

From Eq. (11) under conditions (2) we have:

$$\rho V_D = \text{const.} df_a/dt$$

for the 37-inch operation. It can be shown from phase stability considerations that either an increase in ρ or a decrease in V_D during the ion acceleration will result in some loss of ions. The theoretical curve in Fig. 3 for $\rho>0.5$ is a measure of the loss of ions on increasing ρ, since the amount of damping of the phase oscillations in the case of the f-m cyclotron is rather small. (There are usually less than a dozen oscillations in the whole acceleration.)

Some qualitative tests were made on the effect of distortion of the frequency-time curve on the ion beam output. These were made by adjusting the variable stator ring of the rotating condenser (9) during operation. By this means the slope of the frequency time curve could be distorted over a range of perhaps 50 percent. The ion current was not very sensitive to this distortion, and the maximum loss in current was only 30 percent.

No systematic studies were made concerning the effect of differing V_D *vs.* time variations on the ion current. However, it was observed that the presence of sharp peaks or breaks in this function was definitely deleterious. As mentioned above, there would be some ion loss if the dee voltage were allowed to decrease during the acceleration. This loss would not be very large, and because of the great sensitivity of the ion

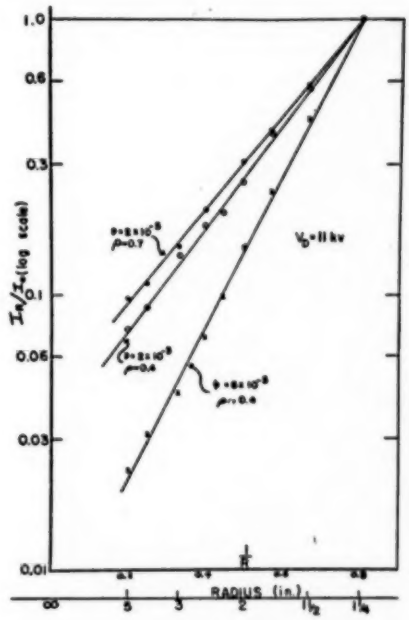

FIG. 9. This shows excellent verification of the expression developed in the paper and confirms the ion loss variation as one over the square of the energy up to deuteron energy of 600 kev. This also would indicate little ion loss from five inches radius to infinity.

current to dee voltage there might be some advantage in having the dee voltage abnormally high during the few microseconds of ion pick-up time. From the practical point of view this might be easier than holding V_D continuously at the higher value.

9. DEFLECTION OF THE BEAM

Shortly after it became clear that a substantial current of high speed ions was obtainable, a bombardment was planned for the purpose of comparing the actual energy of the beam with the expected value, as determined from the magnetic field and radius. A stack of Cu foils was placed on a probe, and the well-known 12.8-hour Cu^{64} activity was produced. The resulting excitation curve gave agreement between the actual and expected values of the beam energy to better than 5 percent, which is as good as could be expected because of the uncertain position of origin of the ions, and the uncertainties inherent in the method.

Of great interest was another result of such bombardments. Each foil was cut into several pieces so as to determine roughly the curve giving the *relative activity vs. radial distance back from the edge of the foil.* The result of one such experiment with four one-mil foils is shown in Fig. 10. Consider foil number 1. One sees that a quite appreciable amount of activity is found at distances greater than 7/64 inch from the edge of the probe.

In a cyclotron, if ΔE = maximum available energy increase per turn, at a radius R the maximum possible gain in radius per turn $=\Delta R = R\Delta E/2E$, where E is the energy of an ion at radius R. In the case of the above experiment, $R=17$ inches, $E=7$ Mev, and $\Delta E=2$ kev, so $\Delta R \cong 5$ mils.

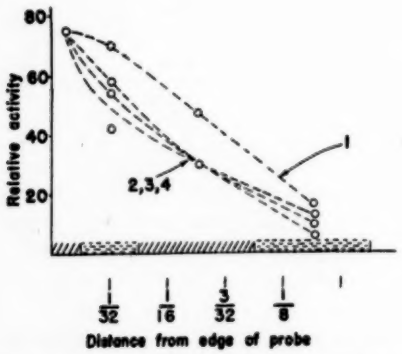

FIG. 10. Curves of *relative activity vs. radial distance from the edge of the probe* for a stack of four 0.001-inch Cu foils. The foils were sliced into the radial widths indicated.

So we have a maximum possible increase of 5 mils per revolution for the radius of an ion trajectory, but an observed increase in the *distance from the cyclotron center* of more than 100 mils in one revolution.

The observed *fact* immediately offered, at least, a possibility of using a conventional d.c. deflector to withdrawn the beam; the apparent discrepancy posed an interesting problem.

That the curves of *relative activity vs. radial distance from probe edge* for the second, third, and fourth foils (Fig. 10) in the stack have the same shape proves that the ions falling some distance from the probe edge have the full energy. The different shape of curve 1 opens the possibility that the circulating current has a considerable relatively low energy tail.

The ability of an ion to increase its distance from the cyclotron center in one revolution as much as 20 or 30 times the amount of increase of its radius of curvature is based on the *precession* of the orbits.

In Fig. 11, O represents the geometric and magnetic center of the cyclotron. As mentioned previously, the magnetic field was made to decrease radially in such a fashion as to simulate a relativistic increase in mass. We may express the field near any radius r_0 in this fashion.

$$H(r)=H(r_0)(r_0/r)^n.$$

In Fig. 11 the dotted circle represents the path of a particle which has an energy, E_0, appropriate to the radius r_0 and the field $H(r_0)$. Now consider a particle which has the same E_0, but which, for one reason or another, exists at a distance x beyond the dotted circle and with its center of curvature at A on the radius OAJ (i.e., $OA=x$). It can be shown[13] that for $x \ll r_0$, and if n is constant in the region involved, that the distance of the particle from the dotted circle will vary in a simple harmonic manner. Moreover, if we call f_x the frequency of this motion and f the radiofrequency of the dee voltage, then $f_x=f(1-n)^{\frac{1}{2}}$, and the number of r-f cycles per cycle of radial oscillation $=1/(1-n)^{\frac{1}{2}}$. Consider

[13] McMillan, Bohm, and Foldy, unpublished.

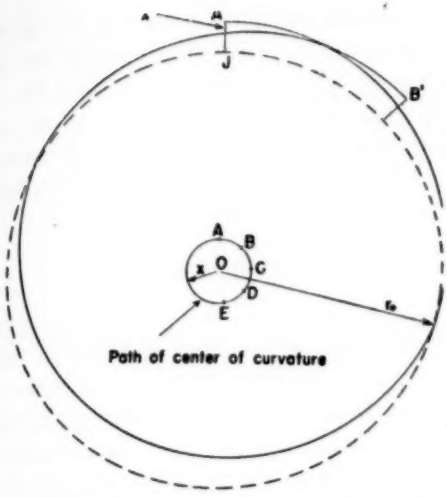

FIG. 11. The solid line represents the approximate path of an ion in a radially decreasing magnetic field during one cycle of radial oscillation.

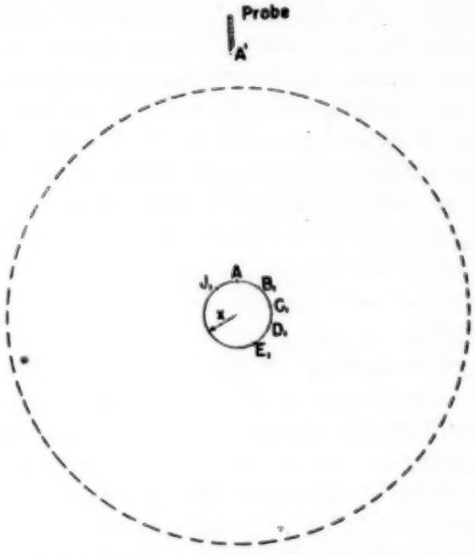

FIG. 12. The points, A, B_1, C_1, D_1, etc., represent the position of the center of curvature of an ion in a radially decreasing magnetic field after successive cycles of the radiofrequency voltage which is applied to the cyclotron dee.

a particular case in which $n=0.2$ in the region about r_0, then

$$\frac{\text{number of r-f cycles}}{\text{cycle of radial oscillation}}=1.12.$$

So after 1.12 r-f cycles, one cycle of radial oscillation would be completed. The particle follows the solid curve, Fig. 11, and in further cycles of radial oscillation the particle's path forms a rosette. The orbit is said to precess. In the above motion the center of curvature has moved from A to B. After subsequent cycles of radial oscillation the center of curvature takes the positions C, D, E, etc.

Of more interest is the position of the center of curvature after successive r-f cycles.

$$\beta=\frac{\text{number of degrees of advance of center of curvature}}{\text{r-f cycle}}=360(1-(1-n)^{\frac{1}{2}}).$$

For our example $\beta=36°$.

In Fig. 12, then, we plot the position of the center of curvature after successive r-f cycles.

Now consider the case in which a particle at A', at the beginning of motion, just misses a probe P. Because of the progression of its center of curvature, it must certainly miss the probe on the next few r-f cycles. Now, depending on the ratio of r_0 to x, and depending on the amount of increase in the radius of curvature per cycle because the particle is being accelerated, we may obtain the case in which, after several cycles, the center of curvature is at J_1, with the particle just missing the probe, i.e., now having a radius of curvature J_1A'. Then during the *next* r-f cycle the center of curvature shifts to A. The particle after this cycle will strike the probe. Because of the shift in the center of curvature from J_1 to A, the distance back from the leading edge of the probe at which the particle strikes may be much greater than that which could be due to the increase in its radius of curvature in one turn.

It is clear that when one proceeds from a discussion of a probe to that of deflector, the question as to whether or not an appreciable fraction of the ions will enter the deflector channel under conditions such that they can be successfully deflected becomes involved. In the case of the 37-inch cyclotron these points bore consideration:

1. By the very nature of process making the

deflection possible, many of the ions could be expected to have relatively large radial components of velocity upon entering the channel.

2. In the range of radii from 17 inches to 19 inches, n varies from 0.25 to 1.1. The amplitude of the radial oscillation was expected to be at least an inch. With such a large variation of n over the range of the radial oscillation, the simple picture of the means whereby these oscillations might lead to a mechanism for deflection does not hold.

It was decided, however, to determine by direct experiment whether a conventional d.c. deflector would remove any ions. Accordingly, the deflector, whose mechanical details have been described, was installed. It operated very satisfactorily. With 7.5-Mev deuterons under optimum adjustment, about 10 percent of the circulating current was extracted. In a conventional cyclotron about 25 percent of the circulating current may be deflected.

With 14.5-Mev protons, it was possible to deflect 5 percent of the circulating current.

The above deflections amounted to a 11–14 percent increase in radius through a channel whose angular length was 60°.

The center of curvature could be shifted away from the geometric and magnetic center of the cyclotron by (1) simply adjusting the position of the ion source away from the cyclotron center, or (2) by the application of the positive d.c. bias on the dee. This bias produces an asymmetric acceleration, and tends to build up a radial oscillation.

It was found that the magnitude of the deflected beam was much more sensitive to the operating value of the magnetic field than was the circulating current. The value of n at a particular radius did depend somewhat on the magnitude of H, so by adjusting H it was apparently possible to adjust the average n at radii near that of the exit strip to a more or less favorable value. Note that $n=\frac{3}{4}$, which gives $\beta=180°$, would not be expected to be favorable for deflection, for after two r-f cycles the center of curvature would shift once around its circle, allowing an insufficient number of r-f cycles during which to increase the radius of curvature. Values of n greater or less than $\frac{3}{4}$ would be expected to be more effective.

10. PERFORMANCE

A steady ion current of three microamperes of 7.3-Mev deuterons was obtained at an internal target. Approximately 10 percent of this current was brought out through the deflecting channel.

At the conclusion of these experiments and tests on the f-m cyclotron it was decided to convert the 37 inch to the acceleration of protons. The f-m technique has a considerable advantage in simplicity even in the energy range of 14.6-Mev protons which was the energy produced in this case. It would probably require a dee voltage of 150 kv to produce a satisfactory beam of this energy without frequency modulation. In our case a dee voltage of 8 kv was sufficient to produce a proton beam of two microamperes to an internal target. The deflection of the 14.6-Mev protons was considerably more difficult than that of the 7.3-Mev deuterons, and the maximum current obtained down the deflector channel was five percent of the circulating current. This beam after it had emerged from between the coil tanks had a current density of 1.4×10^{-9} amp./cm^2.

It is a pleasure to express our thanks to Professors E. M. McMillan and R. L. Thornton for many helpful suggestions and criticisms, and our gratitude to Professor Ernest O. Lawrence whose inspiration and encouragement made this development possible.

This paper is based on work performed under Contract No. W-7405-eng-48 with the United States Atomic Energy Commission, in connection with the Radiation Laboratory, University of California, Berkeley, California.

Note on the Milne Problem for a Sphere

T. H. BERLIN
Rowland Physical Laboratory, Johns Hopkins University, Baltimore, Maryland
(Received November 28, 1947)

A formal solution to the Milne problem for the sphere is presented which exhibits the shadow of the sphere and the corresponding discontinuity in the neutron distribution function. Two limiting cases leading to the Milne problem for the plane are briefly discussed.

STATEMENT OF THE PROBLEM

An infinite non-capturing medium which scatters neutrons isotropically without changing their velocity surrounds a sphere which completely absorbs all incident neutrons. A current density $1/r^2$ in the direction $-r$ is supposed to exist in the infinite medium. The problem is to determine the neutron distribution function in the medium.

The transport equation for the distribution function is:

$$\mu\frac{\partial\psi(r,\mu)}{\partial r}+\frac{(1-\mu^2)}{r}\frac{\partial\psi(r,\mu)}{\partial\mu}+\psi(r,\mu)=\tfrac{1}{2}\int_{1-}^{+1}\psi(r,\mu')d\mu'\equiv f(r). \quad (1)$$

The center of the sphere is taken as the coordinate origin and μ is the cosine of the angle between the direction of motion of the neutron and the radius vector r. $\psi(r,\mu)d\mu$ is the number of neutrons per unit volume at r with direction cosine between μ and $\mu+d\mu$. $2f(r)$ is the neutron density at r. The neutron mean free path is the unit of length.

The current density

$$j(r)=-\int_{-1}^{+1}\mu\psi(r,\mu)d\mu,$$

and on integrating Eq. (1) over μ it is seen that $4\pi r^2 j(r)$ is a constant. This constant is taken as 4π so that $j(r)=1/r^2$.

A solution of Eq. (1) is to be found such that $\psi(r,\mu)$ is finite everywhere in the medium and satisfies the boundary condition for a black sphere,

$$\psi(a,\mu)=0 \quad \text{for } 0<\mu\leqslant 1, \quad (2)$$

where a is the radius of the sphere.

The statement of the problem given here follows that of Marshak.[1] An exact solution appears to be difficult and for practical reasons approximate solutions have been obtained.[1] One would expect to see the shadow of the sphere and, as a result, a discontinuity in the neutron distribution function. The solutions previously given do not show this effect, and it is our purpose to present a formal solution which demonstrates the shadow and discontinuity.

THE FORMAL SOLUTION

Our method shall consist of the reduction of the transport Eq. (1) to a homogeneous integral equation for the neutron density. This is the usual treatment, for example, of the Milne problem for the plane.

If it is supposed that $f(r)$ is a known function, Eq. (1) is a first-order partial differential equation for ψ. A formal solution for ψ in terms of $f(r)$ can be obtained which exactly fulfills the boundary condition. This procedure demonstrates the discontinuity in ψ. Substitution of this ψ in the definition of $f(r)$ leads to a homogeneous integral equation for $f(r)$. The solution of the integral equation, normalized by the condition $j(r)=1/r^2$, yields the complete solution of the problem.

Supposing that $f(r)$ is known, we have for the subsidiary equations:

$$dr/\mu=rd\mu/(1-\mu^2)=d\psi/(-\psi+f(r)). \quad (3)$$

Integrating the relation between r and μ gives $r(1-\mu^2)^{\frac{1}{2}}=c$. The parameter c has the range $0<c<\infty$. For c fixed, we require $c\leqslant r<\infty$ in order that $|\mu|\leqslant 1$.

We also have the relation

$$d\psi/dr=-(1/\mu)\psi+(1/\mu)f(r).$$

[1] R. E. Marshak, Phys. Rev. 71, 443 (1947). References to previous work are given in this paper.

Expressing μ in terms of r and c, and holding c fixed, we find on integrating that

$$\psi(r,\mu)\exp[\pm(r^2-c^2)^{\frac{1}{2}}]\mp\int^r dyyf(y)(y^2-c^2)^{-\frac{1}{2}}\times\exp[\pm(y^2-c^2)^{\frac{1}{2}}]=h_\pm(c). \quad (4)$$

The signs $\pm$ refer to the sign of μ as we shall always take the positive square root.

The characteristics $c=$ constant are sketched in Fig. 1. We can now discuss the determination of ψ.

$$-1\leqslant\mu<0$$

In this region $\mu=-(r^2-c^2)^{\frac{1}{2}}/r$. Let us denote the distribution function in this region by $\psi^-(r,\mu)$. Then, from (4),

$$\psi^-(r,\mu)\exp[-(r^2-c^2)^{\frac{1}{2}}]+\int^r dyyf(y)(y^2-c^2)^{-\frac{1}{2}}\times\exp[-(y^2-c^2)^{\frac{1}{2}}]=h_-(c). \quad (5)$$

Let the point (r,μ) move to infinity along $c=$ constant. As $r\to\infty$, $\mu\to-1$. Since $\psi^-(\infty,-1)$ must be finite,

$$\int^\infty dyyf(y)(y^2-c^2)^{-\frac{1}{2}}\exp[-(y^2-c^2)^{\frac{1}{2}}]=h_-(c). \quad (6)$$

Consequently,

$$\psi^-(r,\mu)=\exp[+(r^2-c^2)^{\frac{1}{2}}]\int_r^\infty dyyf(y)(y^2-c^2)^{-\frac{1}{2}}\times\exp[-(y^2-c^2)^{\frac{1}{2}}]. \quad (7)$$

If we hold c fixed and let $r\to c$, then $\mu\to0^-$. Thus,

$$\psi^-(c,0^-)=\int_c^\infty dyyf(y)(y^2-c^2)^{-\frac{1}{2}}\times\exp[-(y^2-c^2)^{\frac{1}{2}}]. \quad (8)$$

$$0<\mu\leqslant+1$$

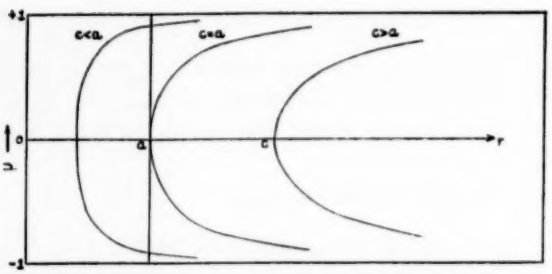

FIG. 1. The characteristics $r(1-\mu^2)^{\frac{1}{2}}=c$ for $0<c<\infty$.

In this region $\mu=+(r^2-c^2)^{\frac{1}{2}}/r$. We shall denote the distribution function in this region by $\psi^+(r,\mu)$. Then, from (4),

$$\psi^+(r,\mu)\exp[+(r^2-c^2)^{\frac{1}{2}}]-\int^r dyyf(y)(y^2-c^2)^{-\frac{1}{2}}\times\exp[+(y^2-c^2)^{\frac{1}{2}}]=h_+(c). \quad (9)$$

We see from Fig. 1 that in this region the sub-regions defined by $c\gtrless a$ must be considered separately. When $c>a$, the characteristics do not cut the line $r=a$; whereas, when $c<a$ the curves cut the line $r=a$ and, therefore, allow the introduction of the boundary condition (2).

Sub-Region $c>a$

Let us denote the distribution function in this sub-region by $\psi^+(r,\mu;>)$. The distribution function must be continuous across the line $\mu=0$ when $r>a$, i.e., $\psi^+(r,0^+;>)=\psi^-(r,0^-)$. This condition enables $\psi^+(r,\mu;>)$ to be determined.

Holding c fixed and letting $r\to c$, then $\mu\to0^+$. From (9),

$$\psi^+(c,0^+;>)-\int^c dyyf(y)(y^2-c^2)^{-\frac{1}{2}}\times\exp[+(y^2-c^2)^{\frac{1}{2}}]=h_+(c;>). \quad (10)$$

Now, using the continuity condition and (8), we have

$$\psi^+(r,\mu;>)=\exp[-(r^2-c^2)^{\frac{1}{2}}]\times\int_c^\infty dyyf(y)(y^2-c^2)^{-\frac{1}{2}}\exp[-(y^2-c^2)^{\frac{1}{2}}]+\exp[-(r^2-c^2)^{\frac{1}{2}}]\int_c^r\cdot dyyf(y)(y^2-c^2)^{-\frac{1}{2}}\times\exp[+(y^2-c^2)^{\frac{1}{2}}]. \quad (11)$$

Sub-Region $c<a$

The distribution function is denoted by $\psi^+(r,\mu;<)$. Since the curves for $c<a$ cut the line $r=a$, set $r=a$ in (9). This yields

$$\psi^+(a,\mu;<)\exp[+(a^2-c^2)^{\frac{1}{2}}]-\int^a dyyf(y)(y^2-c^2)^{-\frac{1}{2}}\exp[+(y^2-c^2)^{\frac{1}{2}}]=h_+(c;<). \quad (12)$$

μ and c are connected by

$$\mu=(a^2-c^2)^{\frac{1}{2}}/a, \quad 0<c<a. \tag{13}$$

Using the boundary condition (2), $\psi^+(a, \mu; <) =0$, we find $h_+(c; <)$ and, consequently,

$$\psi^+(r, \mu; <)=\exp[-(r^2-c^2)^{\frac{1}{2}}]$$

$$\times\int_a^r dyyf(y)(y^2-c)^{-\frac{1}{2}}\exp[+(y^2-c^2)^{\frac{1}{2}}]. \tag{14}$$

The boundary condition (2) is now exactly fulfilled and $\psi(r, \mu)$ is defined in the region $a<r<\infty$, $|\mu|\leqslant 1$ in terms of the function $f(r)$ by Eqs. (7), (11), and (14). ψ is continuous across $\mu=0$ when $r>a$. But we note that ψ is not continuous across $\mu=0$ when $0<r<a$, and $\psi^+(r, a; <)$ is negative when $r<a$. Although the region $r<a$ has no physical sense in that it is the inside of the black sphere, yet ψ is mathematically well defined in terms of $f(r)$.

We also see that the point $\mu=0$, $r=a$ $(c=a)$ is a singular point of ψ. The function ψ is essentially indeterminate at this point and this lack of determination is carried along the curve $c=a$, when $0<\mu<1$. Equations (11) and (14) immediately show that

$$\Delta\equiv\operatorname*{Lim}_{c=a}[\psi^+(r, \mu; >)-\psi^+(r, \mu; <)]$$

$$=F(a)\exp[-(r^2-a^2)^{\frac{1}{2}}], \tag{15}$$

where

$$F(a)=\int_a^\infty dyyf(y)(y^2-a^2)^{-\frac{1}{2}}\exp[-(y^2-a^2)^{\frac{1}{2}}].$$

When $c=a$, the relation between μ and r is

$$\mu\equiv\mu_r=(r^2-a^2)^{\frac{1}{2}}/r. \tag{16}$$

The geometrical significance of relation (16) is shown in Fig. 2.

From the point at a distance r from the center of the sphere, the tangent to the sphere is drawn. Then, of course, $\mu_r=\cos\theta_r=(r^2-a^2)^{\frac{1}{2}}/r$. The arrow in Fig. 2 indicates the neutron direction of motion. The critical value of θ, θ_r, defines the shadow of the sphere. The shadow at the point r is within the cone of apex angle θ_r. With respect to Fig. 1, the shadow region, for the various r, is the region covered by the curves for which $c<a$ $(0<\mu<1)$, and it is these curves which cut the line $r=a$.

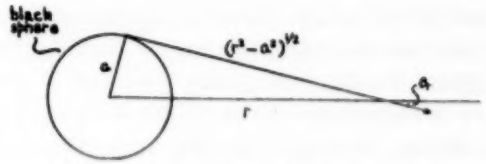

FIG. 2. The geometrical significance of $\mu_r=\cos\theta_r=(r^2-a^2)^{\frac{1}{2}}/r$.

Integral Equation for $f(r)$

The definition of $f(r)$ is given in (1). On substituting the ψ given by (7), (11), and (14) into this definition we are led, after some manipulation, to the following equation for $f(r)$ when $a<r<\infty$.

$$rf(r)=\int_a^\infty K(r, y)yf(y)dy, \tag{17}$$

where[2]

$$K(r, y)=\tfrac{1}{2}E_1(|r-y|)$$

$$-\tfrac{1}{2}E_1[(r^2-a^2)^{\frac{1}{2}}+(y^2-a^2)^{\frac{1}{2}}]. \tag{18}$$

The function $f(r)$ is normalized by the requirement that

$$-\int_{-1}^{+1}\mu\psi(r, \mu)d\mu=1/r^2.$$

This completes the formal solution of the problem for the range of the variables $a<r<\infty$, $|\mu|\leqslant 1$.

DISCUSSION

An exact solution of the integral equation (17) is difficult to obtain. There are two limiting cases of physical interest, however, which lead to the same soluble specialization of (18). In one case $r\gg a$. Then the kernel $K(r, y)$ is essentially determined by the first integral in (18) as this integral is large for $y\simeq r$ and the second integral is small for all y. In the second case $a\to\infty$ and $r\to\infty$ so that $r-a$ is finite. The kernel $K(r, y)$ is again given by the first integral in (18). This limiting kernel is found in the Milne problem for the plane, and the exact solution of the integral equation is well known.[3] The first case has been discussed by Marshak[4] and Davison.[5] The

[2] $E_1(x)=\int_1^\infty[e^{-xt}]dt/t$.

[3] G. Placzek and W. Seidel, Phys. Rev. **72**, 550 (1947). These authors have discussed the solution for the plane in a form adapted to problems in neutron diffusion.

[4] R. E. Marshak, Phys. Rev. **71**, 688 (1947).

[5] B. Davison, Phys. Rev. **71**, 694 (1947).

shadow of the sphere plays no significant role in this case as the points of interest are far from the sphere. In the second case the shadow of the sphere is important as the points of interest are close to the boundary. In the limit, the region $c>a$ for $\mu>0$ disappears. The distribution function at points near the sphere may be discussed from the point of view of this approximation.

Because of the existence of the shadow and the discontinuity in ψ, measurements of the critical angle θ_r and Δ can, in principle, determine the radius a of the sphere and the mean free path λ of the neutrons. If it is supposed that μ_r is determined at two positions along a radius so that $\delta r=r_2-r_1$ is known, then, from (16),

$$a^2=r_1^2(1-\mu_{r1}^2)=r_2^2(1-\mu_{r2}^2).$$

There are three equations for the three unknowns a, r_1, and r_2. In (15), r is expressed in terms of λ as the unit of length. We then write, from (15),

$$\ln\Delta=-(1/\lambda)r\mu_r+\ln F.$$

The slope of the line obtained from a plot of $\ln\Delta$ against $r\mu_r$ determines λ. The quantity Δ may be measured in an arbitrary unit and the quantity $r\mu_r$ is provided by the measurements of μ_r and δr.

PHYSICAL REVIEW VOLUME 73, NUMBER 5 MARCH 1, 1948

Angular Correlation of Scattered Annihilation Radiation*

HARTLAND S. SNYDER, SIMON PASTERNACK, AND J. HORNBOSTEL
Brookhaven National Laboratory, Upton, New York

(Received November 24, 1947)

If the two photons emitted in an annihilation process are scattered, their initial cross-polarization leads to an angular correlation of the scattered radiation. This correlation effect is calculated, and yields a substantial azimuthal asymmetry. It is shown that one may regard the scattering of one photon as performing a partial analysis of the polarization of the other photon.

1. INTRODUCTION

ACCORDING to pair theory[1] the dominant type of annihilation is one in which the positron-electron pair has zero relative angular momentum. Associated with this is the cross-polarization of the two quanta emitted in the annihilation process. If one photon is linearly polarized in one plane, the other photon, which goes off in the opposite direction, is linearly polarized in the perpendicular plane. A similar relation exists for any state of polarization of one photon.

Wheeler[2] has suggested an experiment to test this prediction, involving coincidence measurements of the scattering of both of the annihilation photons. The arrangement is represented schematically in Fig. 1.

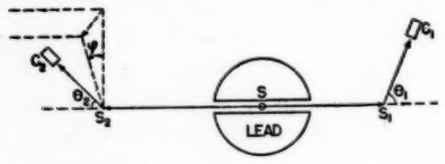

FIG. 1. Schematic diagram of experimental arrangement.

A source S of annihilation radiation (a radioactive source of slow positrons covered with a foil) is placed at the center of a lead sphere with a narrow channel drilled through it. The photons, each of energy mc^2, passing through the channel are scattered by scatterers S_1 and S_2 and recorded by gamma-ray counters C_1 and C_2. Coincidences between the two counters are recorded when the azimuths of the two counters are identical ($\varphi=0$) and when the azimuths differ by a right

* Research carried out at the Brookhaven National Laboratory under the auspices of the Atomic Energy Commission.

[1] P. A. M. Dirac, Proc. Camb. Phil. Soc. 26, 361 (1930).

[2] J. A. Wheeler, Ann. N. Y. Acad. Sci. 48, 219 (1946).

angle ($\varphi=\pi/2$), and the ratio is determined. According to Wheeler, the calculated ratio ($N_{\varphi=\pi/2}/N_{\varphi=0}$) for the case of ideal geometry is 1.080 when the scattering angles θ_1 and θ_2 are 90°; and the theoretically most favorable ratio of 1.100 is obtained when the scattering angles are reduced to 74°30′.

The theory of this proposed experiment has been re-examined, using two different approaches, and results different from those of Wheeler are obtained.[3] The following ratio is obtained for the case in which the two photons are scattered through the same angle θ:

$$\rho=\frac{N_{\varphi=\pi/2}}{N_{\varphi=0}}=1+\frac{2\sin^4\theta}{\gamma^2-2\gamma\sin^2\theta};$$
$$\gamma=2-\cos\theta+\frac{1}{2-\cos\theta}. \quad (1)$$

For scattering angles of 90° the ratio reduces to 2.60. The maximum ratio of 2.85 is obtained for scattering angles of 82°. The asymmetry ratio ρ is plotted as a function of θ in Fig. 2.

2. PARTIAL POLARIZATION ANALYSIS METHOD

One approach to the problem is to view the scattering of one photon as performing a partial analysis of the polarization of the other photon. That is, the observation of one scattered photon gives information about the initial state of polarization of the other photon.

The statement that the two light quanta are polarized at right angles to each other is readily expressed in terms of the Schroedinger wave functionals. Let $\psi(\cdots, N_{\mathbf{k}\lambda}, \cdots)$ denote the wave functional for the light quanta when there are $N_{\mathbf{k}\lambda}$ quanta, having momenta $\mathbf{k}$ and polarization indicated by the index λ. The annihilation radiation consisting of two quanta having momenta $\mathbf{k}_0$ and $-\mathbf{k}_0$ may then be described by the following wave functional

$$\frac{1}{\sqrt{2}}\{\psi(\cdots 1_{\mathbf{k}_0 1}, 0_{\mathbf{k}_0 2}, \cdots 0_{-\mathbf{k}_0 1}, 1_{-\mathbf{k}_0 2}, \cdots)$$
$$+\psi(\cdots 0_{\mathbf{k}_0 1}, 1_{\mathbf{k}_0 2}, \cdots 1_{-\mathbf{k}_0 1}, 0_{-\mathbf{k}_0 2}, \cdots)\}, \quad (2)$$

with arguments of 0 for all quanta not explicitly indicated. The polarization indices 1 and 2 for $\mathbf{k}_0$ and $-\mathbf{k}_0$ refer to the plane-polarization directions as shown in Fig. 3, in which the $\boldsymbol{\varepsilon}$'s are unit vectors.

For the above expression to represent correctly the fact that the quanta with the momenta $\mathbf{k}_0$

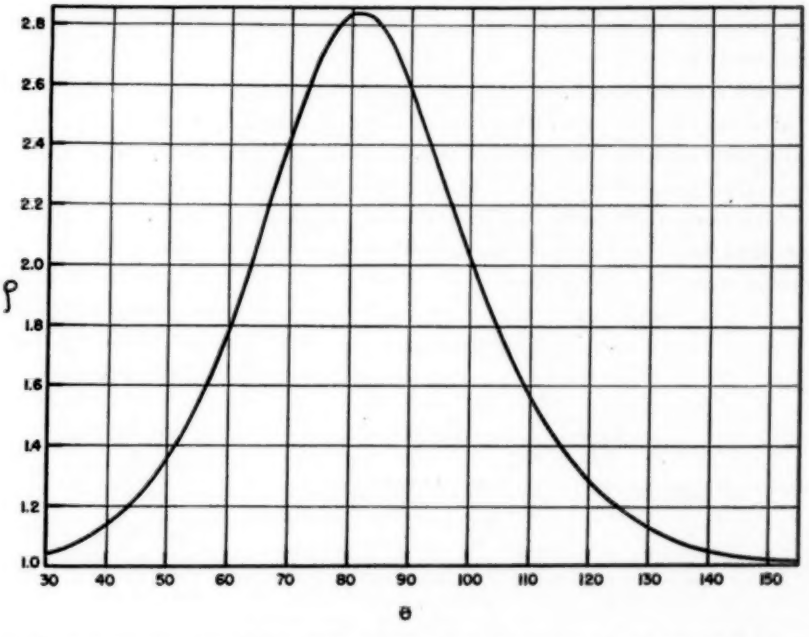

FIG. 2. Asymmetry of coincidence counting rate, ρ, for ideal geometry, as a function of the scattering angle θ.

[3] Since these results were obtained there has appeared a brief article by M. H. L. Pryce and J. C. Ward (Nature 160, 435 (Sept. 27, 1947)) in which the result of similar calculations is reported. Their formula agrees with the one obtained here (Eq. (19)).

and $-\mathbf{k}_0$ are polarized at right angles to each other, the phases of the wave functionals are chosen so that $\psi(\cdots 1_{\mathbf{k}_{01}}, 0_{\mathbf{k}_{02}}, \cdots)\cos\mu + \psi(\cdots 0_{\mathbf{k}_{01}}, 1_{\mathbf{k}_{02}}, \cdots)\sin\mu$ represents a plane-polarized quantum making an angle μ with the $\varepsilon_{\mathbf{k}_{01}}$ direction, and an angle $\pi/2-\mu$ with the $\varepsilon_{\mathbf{k}_{02}}$ direction for all momenta $\mathbf{k}_0$. It may now be easily verified for a new system of axes for the resolution of the polarization of the light quanta,

$$\varepsilon_{\mathbf{k}_{01}'} = \varepsilon_{-\mathbf{k}_{01}'} = \varepsilon_{\mathbf{k}_{01}}\cos\mu + \varepsilon_{\mathbf{k}_{02}}\sin\mu,$$
$$\varepsilon_{\mathbf{k}_{02}'} = -\varepsilon_{-\mathbf{k}_{02}'} = -\varepsilon_{\mathbf{k}_{01}}\sin\mu + \varepsilon_{\mathbf{k}_{02}}\cos\mu,$$

that the wave functional above becomes

$$\frac{1}{\sqrt{2}}\{\psi(\cdots 1_{\mathbf{k}_{01}'}, 0_{\mathbf{k}_{02}'}, \cdots 0_{-\mathbf{k}_{01}'}, 1_{-\mathbf{k}_{02}'}, \cdots) + \psi(\cdots 0_{\mathbf{k}_{01}'}, 1_{\mathbf{k}_{02}'}, \cdots 1_{-\mathbf{k}_{01}'}, 0_{-\mathbf{k}_{02}'}, \cdots)\}.$$

It is now clear on inspection that this wave functional represents two light quanta with opposite momenta; each quantum is unpolarized, but the two quanta are polarized at right angles to each other.

We now consider the manner in which the scattering of a light quantum by an electron partially analyzes the polarization of the original quantum. According to the Klein-Nishina formula[4] the polarization dependence of the differential scattering cross section for a photon of momentum $\mathbf{k}_0$ scattered into a photon of momentum $\mathbf{k}$ is given by the factor $k/k_0+k_0/k-2+4\cos^2\Theta$, in which Θ is the angle between the direction of polarization of the incident quantum and the direction of polarization of the scattered quantum. If we average this over the polarization directions of the scattered quantum we find for the polarization dependence of the initial quantum the factor

$$\frac{k}{k_0}+\frac{k_0}{k}-2\sin^2\theta\cos^2\phi, \qquad (3)$$

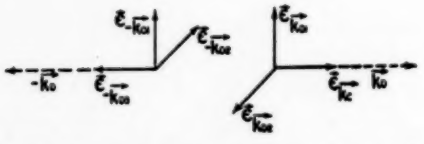

FIG. 3. Coordinate systems for representing polarization directions of the initial quanta. *Note added in proof:* $\mathbf{k}_0$, the subscript to the first unit vector from the right, should read $\mathbf{k}_{02}$.

[4] O. Klein and Y. Nishina, Zeits. f. Physik 52, 853 (1929); Y. Nishina, *ibid.* 52, 869 (1929).

in which θ is the angle of scattering and ϕ is the angle between the plane of the scattering and the direction of polarization of the incident quantum. For a quantum polarized in the plane of scattering (3) gives us the factor $k/k_0+k_0/k-2\sin^2\theta$; for a quantum polarized perpendicular to the plane of the scattering we obtain $k/k_0+k_0/k$. If the quantum is polarized making an angle ϕ with the plane of scattering, then the probability that it is polarized in the plane of the scattering is $\cos^2\phi$ and the probability that it is polarized at right angles to the plane of scattering is $\sin^2\phi$. Factor (3) may now be obtained by multiplying the probability that the light is polarized in the plane of the scattering by the factor $k/k_0+k_0/k-2\sin^2\theta$, and adding to this product the product of the probability that the light is polarized at right angles to the plane of scattering by its corresponding factor $k/k_0+k_0/k$. The fact that the relative intensity for an arbitrary angle of polarization can be computed in terms of the probability of polarization in the plane and at right angles to the plane of scattering shows that the scattering of a quantum by an electron produces a partial analysis in terms of plane-polarized light in the plane of scattering, and at right angles to this plane. This result holds if and only if the polarizations of the quanta are resolved in this particular way.

We now suppose that the quantum with momentum $\mathbf{k}_0$ is scattered through an angle θ_1 into a photon of momentum $\mathbf{k}_1$. The *a priori* probability that this light quantum had its plane of polarization in the plane of scattering is one-half, and that it had its plane of polarization at right angles to the plane of scattering is one-half. Thus, as a consequence of the scattering the *a posteriori* probability that this quantum had its plane of polarization in the plane of the scattering is

$$\left(\frac{k_1}{k_0}+\frac{k_0}{k_1}-2\sin^2\theta_1\right)\Big/2\left(\frac{k_1}{k_0}+\frac{k_0}{k_1}-\sin^2\theta_1\right),$$

and the *a posteriori* probability that its plane of polarization was perpendicular to the plane of scattering is

$$\left(\frac{k_1}{k_0}+\frac{k_0}{k_1}\right)\Big/2\left(\frac{k_1}{k_0}+\frac{k_0}{k_1}-\sin^2\theta_1\right).$$

According to the wave functional (2) this means that the probability that the second quantum, whose momentum is $-\mathbf{k}_0$, has its plane of polarization in the plane of scattering of the first light quantum is

$$\left(\frac{k_1}{k_0}+\frac{k_0}{k_1}\right)\Big/2\left(\frac{k_1}{k_0}+\frac{k_0}{k_1}-\sin^2\theta_1\right),$$

and the probability that the second light quantum's plane of polarization is perpendicular to the plane of scattering of the first light quantum is

$$\left(\frac{k_1}{k_0}+\frac{k_0}{k_1}-2\sin^2\theta_1\right)\Big/2\left(\frac{k_1}{k_0}+\frac{k_0}{k_1}-\sin^2\theta_1\right).$$

If we now apply the above probabilities to the calculation of the scattering of the second quantum by an electron we find that the normalized probability distribution, dP, for the two light quanta, assuming that both the quanta are scattered, is given by

$$dP=\frac{k_1^2k_2^2(\gamma_1\gamma_2-\gamma_1\sin^2\theta_2-\gamma_2\sin^2\theta_1+2\sin^2\theta_1\sin^2\theta_2\sin^2\phi)d\Omega_1d\Omega_2}{4\pi^2k_0^4\left(\frac{40}{9}-3\ln 3\right)^2}, \tag{4}$$

$$\gamma_1=\frac{k_1}{k_0}+\frac{k_0}{k_1},\quad \gamma_2=\frac{k_2}{k_0}+\frac{k_0}{k_2}.$$

In this equation $d\Omega_1$ and $d\Omega_2$ are differential solid angles for the scattered first and second light quanta, k_1 and k_2 are the magnitudes of their momenta, θ_1 and θ_2 are their scattering angles, and φ is the angle between the two planes of scattering. Also, for the case of practical interest, in which the kinetic energies of the positron and electron are small, the two quanta have an energy of mc^2 each and the Compton formula gives

$$k_1=\frac{k_0}{2-\cos\theta_1},\quad k_2=\frac{k_0}{2-\cos\theta_2}. \tag{5}$$

Equations (5) were used in the normalization of (4). When $\theta_1=\theta_2=\theta$, Eq. (4) leads to the ratio given in Eq. (1).

3. PERTURBATION THEORY METHOD

It is of interest to verify the above conclusion by a direct application of time-dependent perturbation theory. The process involved is a four-quanta process, corresponding to absorption and emission of quanta by the two electrons involved in the scattering. However, since the scattering processes are independent (except for the connection between polarizations of the initial quanta) the problem reduces to consideration of a pair of two-quanta processes.

In the standard time-dependent perturbation theory[5] the perturbation H' is replaced by $\lambda H'$, and the wave function ψ is expressed as a power series in λ.

$$\psi=\psi^{(0)}+\lambda\psi^{(1)}+\lambda^2\psi^{(2)}+\cdots, \tag{6}$$

where $\psi^{(0)}$ is the wave function of the unperturbed state. The $\psi^{(s)}$ are then expanded in terms of the eigenfunctions of the unperturbed time-dependent wave equation

$$\psi^{(s)}=\sum_n a_n^{(s)}u_ne^{-iE_nt/\hbar}\quad(s=0,\,1,\,2,\,\cdots).$$

Substitution into the perturbed wave equation, equating coefficients of equal powers of λ, and setting $\lambda=1$, yields the equations

$$\dot{a}_m^{(0)}=0,\quad \dot{a}_m^{(s+1)}=\frac{1}{ih}\sum_n H'_{mn}a_n^{(s)}e^{i\omega_{mn}t},$$

where

$$\omega_{mn}=(E_m-E_n)/h;\quad H'_{mn}=\int u_m^*H'u_n\,d\tau.$$

For a two-quanta process, the solution of these

[5] See, for example, W. Heitler, *The Quantum Theory of Radiation* (Oxford University Press, New York, 1944), second edition, p. 87. We shall follow essentially Heitler's notation in the remainder of this section. In particular, the wave functions of the plane waves involved in the determination of matrix elements are normalized to unit volume, and the momenta are expressed in energy units (i.e., the quantity $c\times$ momentum is called momentum).

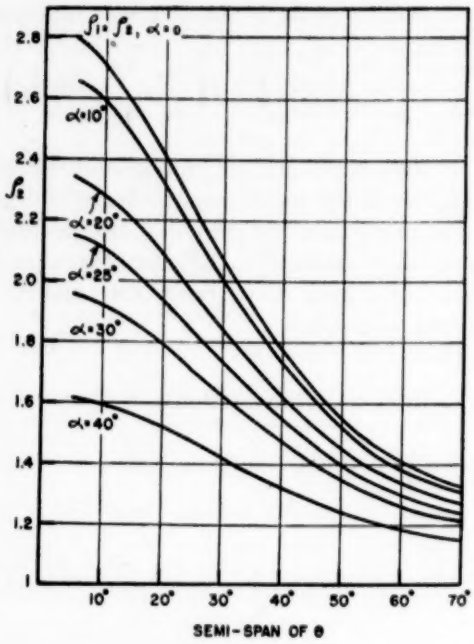

FIG. 4. Asymmetry in coincidence counting rates, $\rho_2 = P_{\text{orthogonal}}/P_{\text{coplanar}}$, for finite geometry, as function of half-span in θ for various half-spans in azimuth, α. Curve for $\alpha = 0$ also represents asymmetry ratio $\rho_1 = \Delta P_{\phi=\pi/2}/\Delta P_{\phi=0}$.

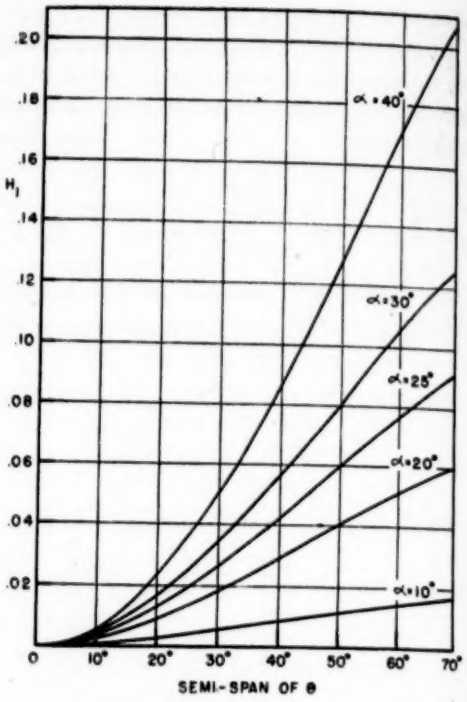

FIG. 5. Geometric efficiency, H_1, of coincidences in orthogonal position, as function of half-span in θ for various half-spans in azimuth, α.

equations subject to the initial conditions

$$a_m^{(0)} = \delta_{mP},$$

is

$$a_P^{(2)}(t, P) = \frac{1}{\hbar^2} \sum_n H'_{Fn} H'_{nP} \frac{1}{\omega_{nP}} \times \left\{ \frac{e^{i(\omega_{nP}+\omega_{Fn})t} - 1}{\omega_{nP}+\omega_{Fn}} - \frac{e^{i\omega_{Fn}t} - 1}{\omega_{Fn}} \right\}. \quad (7)$$

Here the wave functional of the unperturbed state is (deleting for convenience the functions representing the electrons)

$$\frac{1}{\sqrt{2}} \{ \psi_A(1)\psi_B(2) + \psi_C(1)\psi_D(2) \}, \quad (8)$$

where

$$\begin{aligned} \psi_A(1) &= \psi(\cdots 1_{k01}, 0_{k02}, \cdots), \\ \psi_B(2) &= \psi(\cdots 0_{-k01}, 1_{-k02}, \cdots), \\ \psi_C(1) &= \psi(\cdots 0_{k01}, 1_{k02}, \cdots), \\ \psi_D(2) &= \psi(\cdots 1_{-k01}, 0_{-k02}, \cdots). \end{aligned} \quad (9)$$

The Hamiltonian of the unperturbed system and the perturbation Hamiltonian may both be written as sums of Hamiltonians for the two subsystems. If we replace $H'(1)+H'(2)$ by $\lambda_1 H'(1) + \lambda_2 H'(2)$, the wave functional for the complete system may be written in the form

$$\psi = \frac{1}{\sqrt{2}} \{ \psi_a(1)\psi_b(2) + \psi_c(1)\psi_d(2) \}, \quad (10)$$

where $\psi_a(1)$, $\psi_c(1)$ may separately be expanded as power series in λ_1 of the form (6), and $\psi_b(2)$, $\psi_d(2)$ may be expanded as power series in λ_2; and

$$\begin{aligned} \psi_a^{(0)}(1) &= \psi_A(1), \quad \psi_b^{(0)}(2) = \psi_B(2), \\ \psi_c^{(0)}(1) &= \psi_C(1), \quad \psi_d^{(0)}(2) = \psi_D(2). \end{aligned} \quad (11)$$

The usual reduction procedure then replaces (7) by

$$a_P^{(2,2)}(t_1, t_2) = a_P^{(2)}(t_1, A) a_P^{(2)}(t_2, B) + a_P^{(2)}(t_1, C) a_P^{(2)}(t_2, D). \quad (12)$$

The transition probability for the joint scattering process (if one observes one sub-system at time t_1 and the other at time t_2) is $|a_P^{(2,2)}|^2$. It may be reduced in the usual manner, by assuming for each sub-system that in the neighborhood of the final state there are a large number of states with the same physical properties and that $\rho_E dE$ represents the number of these states with energy

between E and $E+dE$. The probability dP' of finding the system with the photons in any one of the appropriate states is

$$dP' = \int_{\Delta E_1}\int_{\Delta E_2} |a_F^{(2,2)}|^2 \rho_{E_1}(1)\rho_{E_2}(2)dE_1 dE_2$$

$$= \frac{4\pi^2 t_1 t_2}{h^2}\rho_{E_1}\rho_{E_2}\cdot\tfrac{1}{2}|R(1)S(2)+S(1)R(2)|^2$$

$$= \frac{2\pi^2 t_1 t_2}{h^2}\rho_{E_1}\rho_{E_2}\{|R(1)|^2|S(2)|^2 + |S(1)|^2|R(2)|^2 + R(1)S^*(1)R^*(2)S(2) + R^*(1)S(1)R(2)S^*(2)\}, \quad (13)$$

where

$$R=\sum_{n'}\frac{H'_{An'}H'_{n'F}}{E_0-E_{n'}}, \quad S=\sum_{n'}\frac{H'_{Cn'}H'_{n'F}}{E_0-E_{n'}},$$

$$E_0=\tfrac{1}{2}E_A=\mu+k_0, \quad E_i=\mu+k_0-k_i \ (i=1,2), \quad (14)$$

and the arguments refer to the two photons. The electronic mass μ and the momenta k_0, k_1, and k_2 are expressed in energy units in accordance with Heitler's notation.

It is of interest to note here that for small times t_1 and t_2 (but t_1 and $t_2 \gg h/E_0$) the transition probability dP' is proportional to the product $t_1 t_2$. This is to be expected, since we deal here with a joint probability of two scattering processes. It is therefore inappropriate to define a transition probability per unit time. Similarly, it is not appropriate to call $dP'/c^2 t_1 t_2$, which has the dimensions of (length),[4] a "differential cross section" for the scattering. However, the difficulty is of no consequence in the problem we are treating, since we are concerned only with the relative probability of different angular relations of the scattered photons.

A result equivalent to (12) and (13) could also be obtained by regarding the process as a four-quanta process, corresponding to absorption and emission of quanta by the two electrons involved in the scattering. For any sequence of absorptions and emissions there are five other sequences involving the same energy differences, namely those in which the same four absorption and emission processes take place in a different order, retaining, however, the order of absorption and emission of quanta by each electron. If in summing over intermediate states we sum first over such permutations, the resultant terms involving exponentials in t factor into a product of two terms of the form given in Eq. (7). The coefficient $a_F^{(4)}(t)$ is thus reduced to $a_F^{(2,2)}$ as given in Eq. (12), with $t_1=t_2=t$. The transition probability dP' is then proportional to t^2.

The matrix elements R and S may be reduced by the procedure used in treating the scattering of one photon, and yield

$$R(i)=\frac{2\pi e^2h^2c^2}{(k_0k_i)^{\frac{1}{2}}}\sum\left\{\frac{(u_0^*\alpha_{01}u')(u'^*\alpha u)}{\mu+k_0-E'} + \frac{(u_0^*\alpha u'')(u''^*\alpha_{01}u)}{\mu-k_i-E''}\right\},$$

$$S(i)=\frac{2\pi e^2h^2c^2}{(k_0k_i)^{\frac{1}{2}}}\sum\left\{\frac{(u_0^*\alpha_{02}u')(u'^*\alpha u)}{\mu+k_0-E'} + \frac{(u_0^*\alpha u'')(u''^*\alpha_{02}u)}{\mu-k_i-E''}\right\}, \quad (15)$$

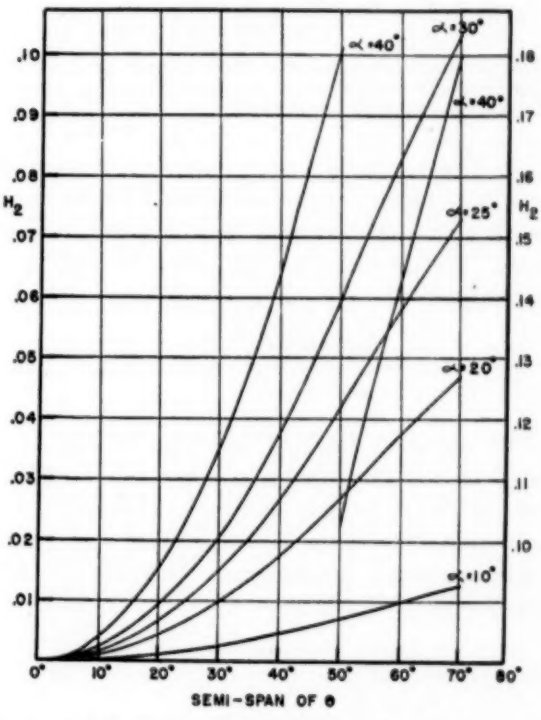

FIG. 6. Geometric efficiency, H_2, of coincidences in coplanar position, as function of half-span in θ for various half-spans in azimuth, α. Ordinate scale at right for curve $\alpha=40°$, $\theta>50°$.

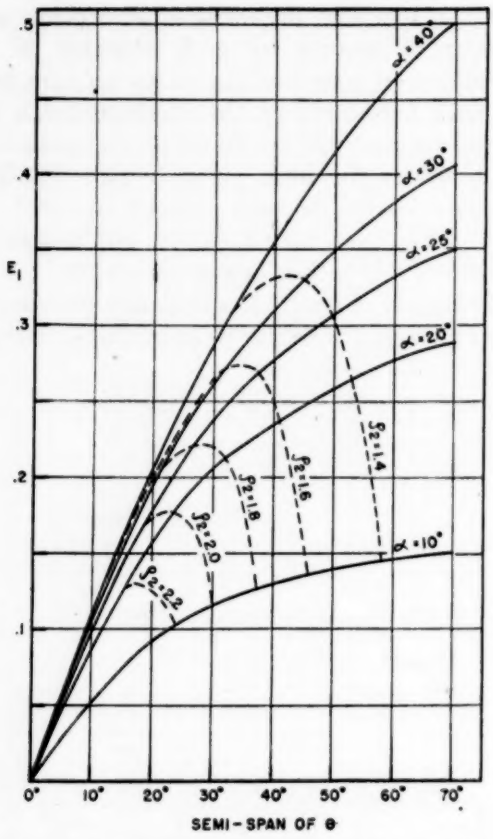

FIG. 7. Relative geometric efficiency for coincidences following single counts, E_1, in orthogonal position. Dashed curves connect points ρ_2=constant.

where i takes the values 1 and 2. The symbols α_{01} and α_{02} represent the components of the Dirac vector $\boldsymbol{\alpha}$ in the directions $\boldsymbol{\varepsilon}_{k01}$ and $\boldsymbol{\varepsilon}_{k02}$, respectively. The densities ρ_{E_i} are given by the usual expression

$$\rho_{E_i}=\frac{E_i k_i}{\mu k_0}\frac{[k_i^2 d\Omega_i}{(2\pi\hbar c)^3} \quad (i=1, 2). \tag{16}$$

The terms in Eq. (13) may be evaluated in the usual way, by summing over the spin directions of the scattering electrons, averaging over their spin directions in the initial state, and evaluating spurs. For instance, the Klein-Nishina formula derivation gives

$$|R(1)|^2=\frac{\pi e^2\hbar^2c^2}{2\mu E_0 k_0 k_1}\times\left(\frac{k_1}{k_0}+\frac{k_0}{k_1}-2+4\cos^2\Theta_{1,01}\right), \tag{17}$$

where $\Theta_{1,01}$ is the angle between the polarization direction of $\mathbf{k}_1$ and $\boldsymbol{\varepsilon}_{k01}$. Similar expressions hold for $|R(2)|^2$, $|S(1)|^2$, and $|S(2)|^2$. We must also sum over the states of polarization of the scattered quanta, since we are interested in all the photons of momenta $\mathbf{k}_1$ and $\mathbf{k}_2$.

The evaluation outlined in the preceding paragraph is simplified considerably by the proper choice of two mutually perpendicular directions for the polarization of one of the scattered photons. For instance, if the polarization directions of $\mathbf{k}_1$ are taken to be perpendicular to the scattering plane ($\boldsymbol{\varepsilon}_1=\boldsymbol{\varepsilon}_{k02}$) and in the scattering plane ($\boldsymbol{\varepsilon}_1=\boldsymbol{\varepsilon}_{k01}\cos\theta_1-\boldsymbol{\varepsilon}_{k03}\sin\theta_1$) the cross-product terms in Eq. (13) vanish. For these terms reduce in the usual way to an evaluation of spurs of which a typical example is

$$\text{spur } \alpha_{02}K'\alpha_1(E-\beta\mu-\boldsymbol{\alpha}\cdot\mathbf{p}_1)\alpha_1K'\alpha_{01}(1+\beta), \tag{18}$$

where

$$K'=\mu(1+\beta)+k_0+\boldsymbol{\alpha}\cdot\mathbf{k}_0,$$
$$\mathbf{p}_1=\mathbf{k}_1-\mathbf{k}_0.$$

The given choices of polarization directions give $\alpha_1=\alpha_{02}$, and $\alpha_1=\alpha_{01}\cos\theta_1-\alpha_{03}\sin\theta_1$, and in either case it is evident that the spur (18) contains an odd number of α_{02} terms and hence vanishes. We may now choose also any two mutually perpendicular polarization directions for the scattered quantum $\mathbf{k}_2$. A convenient pair are perpendicular to the scattering plane of $-\mathbf{k}_0$ and in its scattering plane.

Combining Eqs. (13), (16), and (17), and summing over the polarization directions of $\mathbf{k}_1$ and $\mathbf{k}_2$, we obtain

$$\frac{dP'}{c^2t_1t_2}=\frac{1}{16}r_0^4 d\Omega_1 d\Omega_2\frac{k_1^2}{k_0^2}\frac{k_2^2}{k_0^2}(\gamma_1\gamma_2-\gamma_1\sin^2\theta_2-\gamma_2\sin^2\theta_1+2\sin^2\theta_1\sin^2\theta_2\sin^2\varphi), \tag{19}$$

where

$$r_0=e^2/\mu=e^2/mc^2,$$
$$\gamma_i=(k_i/k_0)+(k_0/k_i),$$
$$k_i=k_0/(2-\cos\theta_i) \quad (i=1, 2). \tag{20}$$

Since we are interested only in the correlation of the scattering quanta when both original quanta are known to be scattered, Eq. (19) should be normalized so that the integral over all directions of scattering of both quanta gives unit probability. This yields the result given in Eq. (4).

In Eq. (13), it is evident that the sum of $|R(1)|^2$ over the polarization states of $\mathbf{k}_1$ will give the same value no matter which two perpendicular directions are chosen for $\boldsymbol{\varepsilon}_1$ (so long as they are perpendicular to $\mathbf{k}_1$, of course). Similar statements hold for $|S(1)|^2$, $|R(2)|^2$, and $|S(2)|^2$. The cross-product terms must therefore vanish when summed over the polarization states of the final quanta. (However, it is only for the choices of $\boldsymbol{\varepsilon}_1$ mentioned above that they vanish before the sum is taken.) This reduction of the expression in brackets in Eq. (13) to $\{|R(1)|^2|S(2)|^2 + |S(1)|^2|R(2)|^2\}$ is equivalent to the conclusion in Section 2 that the scattering of one quantum by an electron produces a partial analysis in terms of plane-polarized light in the plane of scattering and at right angles to this plane, and hence gives a partial analysis also of the second quantum emitted in the annihilation process.

4. FINITE GEOMETRY

If an experimental verification of the expected asymmetry in coincidence counting rates is attempted, it will be found that a close approach to ideal geometry is impractical. It is, therefore, desirable to extend the calculations to the case where the gamma-ray counters subtend finite angles.

We set $\varphi=\varphi_2-\varphi_1$, with φ_1 and φ_2 the azimuths of an element of counters 1 and 2, respectively, relative to the axis of counter 1. In integrating Eq. (4) over finite ranges in θ_1, θ_2, and φ_1, φ_2 it will be sufficient to consider the arrangement in which the two counters subtend equal angles.

First we perform the integration over θ. With $d\Omega_i=\sin\theta_i d\theta_i d\varphi_i$, $(i=1,2)$, $1/q=4\pi^2(40/9-3\ln 3)^2$, and the abbreviations $x=2-\cos\theta$, $\gamma=x+1/x$ and

$$J=\int \gamma(k/k_0)^2\sin\theta d\theta=\ln x-1/2x^2,$$
$$J'=\int (k/k_0)^2\sin^3\theta d\theta=-x+4\ln x+3/x, \tag{21}$$

we obtain from Eq. (4)

$$\Delta P=d\varphi_1 d\varphi_2\int dP d\theta_1 d\theta_2$$
$$=q(J^2-2JJ'-2J'^2\sin^2\varphi)d\varphi_1 d\varphi_2, \tag{22}$$

and for the asymmetry for finite range in θ but infinitesimal range in φ

$$\rho_1=\frac{\Delta P_{\varphi=\pi/2}}{\Delta P_{\varphi=0}}=1+\frac{1}{\frac{1}{2}(J/J')^2-(J/J')}. \tag{23}$$

The integrals J and J' were evaluated for intervals symmetrical about $\theta=82°$ which is the approximate location of the maximum of ρ (see Fig. 2). ρ_1 as a function of the half-span of such intervals is included in Fig. 4 ($\alpha=0$).

The calculations are then extended to finite ranges in φ_1 and φ_2. We obtain P_1 by integrating Eq. (22) over the intervals $-\alpha<\varphi_1<\alpha$ and $\pi/2-\alpha<\varphi_2<\pi/2+\alpha$, and P_2 for the intervals $-\alpha<\varphi_{1,2}<\alpha$. With

$$\int_{-\alpha}^{\alpha}\int_{-\alpha}^{\alpha}\sin^2(\varphi_2-\varphi_1)d\varphi_1 d\varphi_2=2\alpha^2-\tfrac{1}{2}\sin^2 2\alpha=u,$$

$$\int_{-\alpha}^{\alpha}\int_{-\alpha}^{\alpha}\cos^2(\varphi_2-\varphi_1)d\varphi_1 d\varphi_2=2\alpha^2+\tfrac{1}{2}\sin^2 2\alpha=w,$$

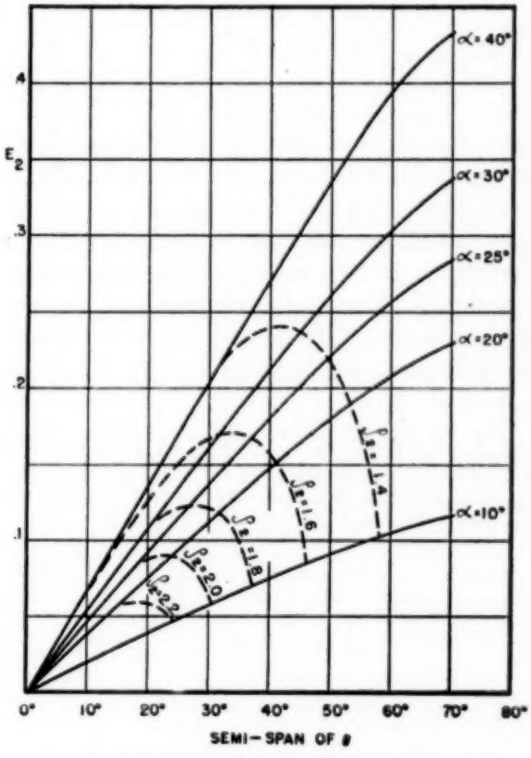

FIG. 8. Relative geometric efficiency for coincidences following single counts, E_2, in coplanar position. Dashed curves connect points ρ_2=constant.

and $z=u/w$, the asymmetry $\rho_2=P_1/P_2$ can be written as

$$\rho_2=(z+\rho_1)/(1+z\rho_1). \tag{24}$$

Curves of ρ_2 as a function of the above-mentioned half-spans in θ and for various values of α are shown in Fig. 4.

In setting up the experiment it is also required to know the efficiencies. We shall here give the geometric part of the efficiencies, which are defined as the number of pairs of scattered quanta reaching both counters divided by the number of all scattered pairs. To obtain over-all efficiencies, the geometric factors must, of course, be multiplied by the efficiencies of the counters[6] and the fractions of the incident intensities scattered by the targets.

Using, as before, subscripts 1 and 2 for the orthogonal and coplanar positions, we derive from Eq. (22) the efficiencies η_i for "semifinite" geometry

$$\eta_2=\frac{J^2-2JJ'}{J_0^2-2J_0J_0'}=\frac{J'^2}{J_0'^2}\left(\frac{\rho_{10}-1}{\rho_1-1}\right),$$
$$\eta_1=\frac{\rho_1}{\rho_{10}}\eta_2. \tag{25}$$

Here, the η's have been normalized to unity for the range $0<\theta<\pi$, i.e., $\eta_i=\Delta P_i/\Delta P_0$; the subscript 0 referring to this range.

Integration of Eq. (22) leads to the following expressions for the geometric efficiencies H_i for finite longitudinal and azimuthal apertures: (In the following equations we assume two detectors on each side, relatively displaced by 180° in azimuth and covering the same range in θ.)

$$H_2=\frac{2}{\pi^2}\left(\frac{u\eta_1}{1+1/\rho_{10}}+\frac{w\eta_2}{1+\rho_{10}}\right),$$
$$H_1=\rho_2H_2=\frac{2}{\pi^2}\left(\frac{w\eta_1}{1+1/\rho_{10}}+\frac{u\eta_2}{1+\rho_{10}}\right). \tag{26}$$

The functions H_1 and H_2 are shown, for the same intervals as before, in Figs. 5 and 6.

Also needed in designing the experiments are the relative geometric efficiencies E_i, i.e., the probabilities of registering a coincidence once a single count has been observed. These are obtained in terms of H_i and the efficiency D for single counts

$$E_1=H_1/D,$$
$$E_2=H_2/D, \tag{27}$$

with

$$D=\frac{2\alpha}{\pi}\left(\frac{J-J'}{J_0-J_0'}\right). \tag{28}$$

Equation (28) is, of course, directly obtained by integration of the Klein-Nishina formula with respect to θ (after summing over polarization directions of the incident and scattered quanta). The factor of 2 enters since there are two single scattering processes for each scattered pair.

The functions E_i are plotted in Figs. 7 and 8. The dotted curves in these plots connect the points $\rho_2=$constant. It is seen that for a given value of ρ_2 best efficiencies are obtained for approximately square apertures.

ACKNOWLEDGMENTS

We are indebted to Dr. E. O. Salant and Dr. H. Primakoff for some stimulating discussions on this problem. We also wish to express our appreciation to Miss Jean Snover who performed the numerical computations for the finite geometry case.

[6] See, for example, Bradt, Gugelot, Huber, Medicus, Preiswerk, and Scherrer, Helv. Phys. Acta. 19, 77 (1946). Note that our calculations do not take into account the energy dependence of the counter sensitivity which results in a dependence of detector sensitivity on θ.

Interaction of Cosmic-Ray Primaries with Sunlight and Starlight*

E. FEENBERG AND H. PRIMAKOFF
Washington University, St. Louis, Missouri
(Received November 20, 1947)

This paper discusses collision processes between cosmic-ray primaries (protons and electrons) and the thermal photons of sunlight and starlight. In particular, electron-positron pair production and Compton scattering in interplanetary, intragalactic, and intergalactic space are treated in detail. It is found that the number of collisions between primary particles and thermal photons in single traversals of the solar system and the local galaxy is not sufficiently large to cause either appreciable energy loss to the particles or appreciable production of secondary pairs and energetic scattered photons. The same statement holds for the primary protons even on an intergalactic scale. On the other hand, energetic primary electrons may experience a sufficient number of Compton collisions in intergalactic space (travel time of the order 2×10^9 years) to eliminate them effectively from the cosmic radiation reaching the neighborhood of the earth.

The stopping power for electrons of the observed interstellar radiofrequency spectrum is also estimated and found to be comparatively large.

1. INTRODUCTION

THE primary cosmic radiation incident on the earth's atmosphere is now thought to consist largely of protons.[1] In addition, highly energetic photons and positive and negative electrons must inevitably accompany the primary protons, if only because they are produced when the protons collide with interstellar diffuse matter and with the low energy "thermal" photons which constitute the major portion of starlight and sunlight. The present study is concerned chiefly with collisions between thermal photons and primary cosmic-ray particles taken as either protons or electrons.[2] Such collisions are found to produce, under certain conditions, large changes both in the composition and in the energy distribution of the original primary radiation. A variety of interaction processes between the primaries and the thermal photons may occur, depending on the energies and momenta of the colliding particles. Thus one may anticipate (for primary protons):

1. Electron-positron pair production (when the energy ϵ^* of the thermal photon in the rest frame of the proton exceeds $2\ mc^2$).[3]
2. Production of energetic recoil photons by Compton scattering (no restriction on ϵ^*).
3. Double Compton scattering—one photon incident, two recoiling—a bremsstrahlung process (no restriction on ϵ^*).
4. Single meson creation ($\epsilon^*>200\ mc^2$).
5. Meson pair creation ($\epsilon^*>400\ mc^2$).
6. Nucleon pair creation ($\epsilon^*>6000\ mc^2$).[4]

Each such process reduces the energy of the original primary particle and at the same time contributes a new component to and possibly removes an original component from the cosmic radiation. In the present paper the emphasis is on processes (1) and (2). We compute the energy losses from Compton scattering and electron-positron pair production, as well as the numbers of scattered photons and pairs, (i) for a particle (proton or electron) falling radially through the sun's radiation field to the earth's orbit, (ii) for a particle traversing the local galaxy, and (iii) for a particle traveling the distance 1.85×10^9 l.y. in intergalactic space (the distance parameter in the empirical red shift formula).[4a]

* The research described in this paper was supported in part by contract N60RI-117, U.S. Navy Department.

[1] T. H. Johnson, Rev. Mod. Phys. 11, 208 (1939); M. Schein, W. P. Jesse, and E. O. Wollan, Phys. Rev. 59, 615 (1941); 59, 930 (1941).

[2] Collisions between high energy photons, considered as cosmic-ray primaries, and thermal photons, with resultant electron-positron pair creation have been considered by G. Breit and J. A. Wheeler, Phys. Rev. 46, 1087 (1934); 45, 134 (A) (1934). Extensive calculations similar to the present have been carried out by J. W. Follin, Bull. Am. Phys. Soc. July 11, 1947, Abstract D5. Through the courtesy of Dr. J. R. Oppenheimer, we have seen a manuscript copy of Dr. Follin's paper.

[3] Because of the relativistic Doppler and aberration effects, a more or less isotropic distribution of low energy photons ($\epsilon\sim1$ ev) in the earth's frame of reference appears as an extremely anisotropic distribution of high energy photons ($\epsilon^*\gg1$ ev) in the rest frame of the primary. Thus from the viewpoint of an observer traveling with the primary, the electromagnetic field in interstellar and intergalactic space consists of extremely energetic photons filling a small cone of directions opposite to that in which the primary itself is moving.

[4] H. Feshbach and L. Schiff, Phys. Rev. 72, 254 (1947).

[4a] For glossary of symbols used, see end of paper.

2. THE PHOTON POPULATIONS OF INTERPLANETARY, INTERSTELLAR (INTRAGALACTIC), AND INTERGALACTIC SPACE

We require estimates of the total number and energy distribution of the thermal photons occurring in the spaces traversed by the primary particles. Considering case (i) first, it is convenient to refer to the number of solar thermal photons, $n_s(\epsilon/kT)$, per unit volume and unit energy range, at the earth's orbit.[5] Evidently n_s can be expressed in terms of the solar constant, η, and the equivalent blackbody spectral distribution function. Thus,

$$n_s(u)d\epsilon = A\frac{u^2du}{e^u-1}, \quad u\equiv\frac{\epsilon}{kT}; \quad A\equiv\frac{15}{\pi^4}\frac{\eta}{ckT}. \tag{1}$$

With $\eta=1.94$ cal./min. cm^2 [6] there are 2×10^7 photons/cm^3 of mean energy $2.7kT\cong1.35$ ev at the earth's orbit corresponding to a total radiation energy density $\cong2.7\times10^7$ ev/cm^3 $(=\eta/c)$. The total number Q_s of thermal photons in a cylinder of unit cross section extending radially from the earth's orbit (radius R_e) to infinity has the value[7]

$$Q_s=\int_0^\infty d\epsilon\int_{R_e}^\infty n_s(u)\left(\frac{R_e}{R}\right)^2dR=2.4AR_e$$
$$=3.1\times10^{20}\text{ photons/cm}^2. \tag{2}$$

Case (ii) is treated next. The galaxy is represented by a collection of N stars all of the same absolute magnitude and spectral type as the sun. To further simplify the calculation the average number of stars per unit volume, $p(x, y, z)$, is given the simple form

$$p(x,y,z)=\frac{N}{R_g^2R_g'\pi^{\frac{1}{2}}}\exp\left\{-\frac{x^2+y^2}{R_g^2}-\frac{z^2}{(R_g')^2}\right\}; \tag{3}$$
$$R_g\cong5R_g'.^8$$

If one now considers the number of photons (per unit energy range) in an infinitely long cylinder of unit cross section enclosing the x axis, one finds that the contribution $\Delta Q_g(u)$, to this number from a single star located at x, y, z is given by

$$\Delta Q_g(u)=\frac{\pi R_e^2n_s(u)}{(y^2+z^2)^{\frac{1}{2}}}. \tag{4}$$

Thus the total number of photons in the cylinder in question is

$$Q_g=\int_0^\infty d\epsilon\int\int\int\Delta Q_g(u)p(x,y,z)dxdydz$$
$$=6.1\pi^{-\frac{1}{2}}\frac{NR_e}{R_g}Q_s. \tag{5}$$

Inserting the values $N\cong8.5\times10^7$ and $R_g\cong10^4$ l.y.,[9] one obtains

$$Q_g\cong1.5Q_s=4.5\times10^{20}\text{ photons/cm}^2.$$

Again using Eq. (3), the ratio of the intragalactic and solar (at earth's orbit) total photon energy densities or number densities is

$$N\left(\frac{R_e}{R_g}\right)^2 2\ln\left(\frac{2R_g}{R_g'}\right)\cong10^{-9}.^{9a} \tag{5a}$$

The magnitudes of Q_s, Q_g and of the cross sections expected for the collision processes (1)–(6) indicate that neither the radiation of the sun nor that of the local galaxy possesses an effective stopping power for the primary particles in a single traversal.

We turn now to the photon population in intergalactic space. A simple treatment will be presented, based on general assumptions of uniformity in space and static conditions in time. The cosmic-ray primaries are pictured as traveling in a uniform, unbounded, and static universe, meeting everywhere and always the same

[5] Here ϵ is the energy of the thermal photon in the earth's frame of reference, and T is the surface (equivalent blackbody) temperature of the sun$\cong$6000° Abs.

[6] See *Smithsonian Physical Tables* (Smithsonian Institution, Washington, D. C., 1933), eighth revised edition, p. 608.

[7] The inverse square law used in the derivation of Eq. (2) holds rigorously for the photon energy current density, but not for the photon energy or number densities. However, the deviations from the inverse square law are inappreciable at distances from the center of the sun greater than two or three solar diameters.

[8] B. J. Bok and P. F. Bok, *The Milky Way* (The Blakiston Company, Philadelphia, 1941), p. 18.

[9] E. Hubble, *The Realm of the Nebulae* (Yale University Press, New Haven, Connecticut, 1936).

[9a] Equation (5a) predicts a total intragalactic energy density of $10^{-9}\times2.7\times10^7$ ev/cm^3 $=4.3\times10^{-14}$ erg/cm^3. This value seems to be some ten times smaller than the estimate given by T. Dunham, Proc. Am. Phil. Soc. 81, 277 (1939). Also the spectral distribution observed by Dunham is not exactly blackbody. Our choice for the intragalactic spectral distribution thus probably underestimates the magnitude of the effects here considered.

average density and spectral distribution of thermal photons—namely, that observed at present on the earth—and losing energy only through encounters with these photons or with diffuse matter. Such a treatment should be useful for a preliminary orientation and may be of help in formulating a more rigorous discussion within the framework of non-static cosmological models.[10] More specifically we assume:

(a) The average density $\mathfrak{N}$ of galaxies or nebulae (independent isolated stellar systems comparable to the local galaxy) is constant in Euclidean space.

(b) The individual nebulae radiate like N stars of the same spectral type and absolute magnitude as the sun.

(c) At the distance R from a particular nebula, the photon number density produced by it, in the energy range $d\epsilon$, is

$$\Delta n_n(u, R)d\epsilon = N\left(\frac{R_e}{R}\right)^2 g(R)A\frac{(u/f(R))^2 du/f(R)}{e^{u/f(R)}-1}, \quad (6)$$

so that $n_n(u)d\epsilon$, the photon number density in the energy range $d\epsilon$ due to all the nebulae, is the same at all points in space and has the value

$$n_n(u)d\epsilon = d\epsilon\int_0^\infty \Delta n_n(u, R)\mathfrak{N}4\pi R^2 dR$$

$$= 4\pi\mathfrak{N}NR_e^2 A u^2 du\int_0^\infty \frac{g(R)f(R)^{-3}dR}{e^{u/f(R)}-1}. \quad (7)$$

In Eqs. (6) and (7), the constant A and the nebular temperature T (in $u=\epsilon/kT$) are identified with the corresponding quantities in Eq. (1). The function $f(R)$ measures the red shift in the photon's energy, while $g(R)$ is an associated reduction factor in the radiation intensity and, therefore, in the photon number density at R. Thus, if the red shift is interpreted as a Doppler effect arising from nebular recession, one has $g=f\cong 1-v(R)/c$, where $v(R)$ is the radial velocity of the nebula at the distance R from the point of observation. On the other hand, the observations of Hubble[11] (out to $R\cong 2.5\times 10^8$ l.y. from the earth) show that

$$f(R)\cong 1-R/R_0; \quad R_0=1.85\times 10^9 \text{ l.y.}, \quad g(R)\cong 1.^{12} \quad (8)$$

In the present discussion the behavior of f and g out to $R\cong R_0$ is important, but cannot be determined from the observational material now available. The red shift and the (still uncertain) reduction in intensity associated with the red shift determine the linear terms in R/R_0 in the power series expansions of f and g and yield no evidence for higher order terms. It is therefore necessary, if one wishes to evaluate the photon number density, to extrapolate $f(R)$ and $g(R)$ to distances of the order of R_0. Two simple, but extreme, procedures for such an extrapolation will be discussed. In the first, the red shift is neglected except insofar as it suggests an "effective" radius, R_0, for the matter in the universe. The conditions $g=f=1$ for $R<R_0$, and $g=0$, for $R\geqq R_0$ describe a universe with no red shift and no nebulae outside of a sphere of radius R_0. In this case

$$n_n(u)d\epsilon = [4\pi\mathfrak{N}NR_e^2R_0]A\frac{u^2du}{e^u-1}. \quad (9)$$

The second procedure utilizes the relations[13]

$$g=1, \quad f=\exp(-R/R_0), \quad (10)$$

in agreement with Eq. (8) for $R\ll R_0$.

Equations (7), (10) and the change of variable $y=u\exp(R/R_0)$ now yield

$$n_n(u)d\epsilon = [4\pi\mathfrak{N}NR_e^2R_0]A\frac{du}{u}\int_u^\infty \frac{y^2dy}{e^y-1}. \quad (11)$$

The "red shifted" spectral distribution of Eq. (11) predicts a strong concentration of thermal photons at very low energies ($\epsilon\ll kT$) and thus

[10] See, for example, H. P. Robertson, Rev. Mod. Phys. 5, 62 (1933); E. Hubble and R. C. Tolman, Ap. J. 82, 302 (1935); E. A. Milne, *Relativity Gravitation and World Structure* (Oxford University Press, London, 1935).

[11] See reference (9) and also Hubble's article in *Science in Progress* (Yale University Press, New Haven, Connecticut, 1942), third series.

[12] This relation (described by Hubble as the absence of the number effect) is still in dispute. J. L. Greenstein, Ap. J. 88, 605 (1938) presents evidence for the inadequacy of both $g=f$ and $g=1$.

[13] Within the framework of a uniform static cosmological model, the exponential form for $f(R)$ can be derived from the assumption that the frequency red shift in the distance ΔR is proportional to the frequency and to ΔR. The same expression for $f(R)$ is deduced by G. J. Whitrow, Phil. Mag. 37, 469 (1946), on the basis of considerations involving kinematic relativity.

exhibits an entirely different behavior than the "no shift" blackbody distribution of Eq. (9). Other reasonable extrapolations of Hubble's f and g functions to large R result, in general, in spectral distributions intermediate between those of Eqs. (9) and (11); in what follows only the more or less extreme cases of Eqs. (9) and (11) are considered explicitly.[14]

We note that the "red shifted" and the "no shift" spectral distributions yield the same total photon energy density:

$$\int_0^\infty \epsilon n_\epsilon(u)d\epsilon=[4\pi\mathfrak{N}NR_e^2R_0]\eta/c. \quad (12)$$

With $N\cong 8.5\times10^7$, $\mathfrak{N}\cong 2\times10^{-19}$ (l.y.)$^{-3}$, and $R_0=1.85\times10^9$ l.y.[11] one has

$$[4\pi\mathfrak{N}NR_e^2R_0]\cong 10^{-10}, \quad (13)$$

so that the ratio of the radiation energy density in intergalactic space to the radiation density produced by the sun at the earth's orbit is 10^{-10}. This same number is also the ratio of the intergalactic "no shift" photon number density and the solar photon number density at the earth's orbit. For the present discussion, however, a better comparison is provided by the ratio of the radiation energy in intergalactic space in a cylinder of volume 1 cm$^2\times R_0$ to the energy of solar radiation in a cylinder of unit cross section extending radially from the earth's orbit to infinity. This ratio is

$$[4\pi\mathfrak{N}NR_eR_0^2]\cong 10^4. \quad (14)$$

Finally, in the special case of "no shift," the total number of photons in the cylinder of volume 1 cm$^2\times R_0$ has the value[15]

$$Q_n=[4\pi\mathfrak{N}NR_eR_0^2]Q_e\cong 3\times10^{24}. \quad (15)$$

The connection of Q_n with the yield from processes (1)–(6) will be treated below.

In the whole above discussion we have supposed that the photon populations in the various spaces considered are well represented (apart from red shift effects) by blackbody distributions appropriate to a temperature of some 6000° Abs. On the other hand, observation shows that a "radiofrequency tail" is present in the radiation from the local galaxy (and presumably in the radiation from intergalactic space as well) which arises from proton-electron recombination in interstellar space.[16] A discussion of the contributions to process 1–2 from the intragalactic and intergalactic "radiofrequency" photons appears in Appendix A; the possible importance of such contributions was first recognized by Follin.[2]

3. ELECTRON—POSITRON PAIR CREATION IN PROTON—PHOTON AND ELECTRON-PHOTON COLLISIONS

We shall now consider the creation of electron-positron pairs as a result of collisions between the cosmic-ray primaries (protons) and the thermal photons of starlight and sunlight. The processes involved are described in two coordinate systems: (a) in the rest frame of the proton where some of the incident photons have energies large enough to produce pairs in collisions with originally stationary particles and (b) in a frame of reference fixed in the earth where the electromagnetic field of the rapidly moving proton may be replaced by a set of virtual photons, some of which possess enough energy to create pairs by collisions with thermal photons. As might be expected, the two treatments give essentially the same results; however, it will be helpful to discuss them both, particularly since the second is especially well suited to describe any possible effect on pair creation of the anamolous magnetic moment of the proton, or, in general, of any

[14] A more general discussion can be based on the one-parameter family of functions

$$f(R)=(1+R/R_0p)^{-p};\quad p\neq0,$$

with the special restriction $f=0$, $R>-pR_0$ for $p<0$, and, either $g=1$ or $g=f$. The range $-\frac{1}{2}<p<0$ may be excluded by the observed linearity of the red shift out to the limit of observation ($R\leqq R_0/6$), while the requirement of finite energy density excludes the special cases $g=1$, $0<p\leqq1$ and $g=f$, $0<p\leqq\frac{1}{2}$. The exponential form occurs for $p=\pm\infty$. It will be observed that the paired conditions $g=1$, arbitrary p, and $g=f$, $p'=p/(p+1)$ yield identical values for n_n.

[15] Equation (15) and the relation $Q_\gamma\sim Q_e$ (Eq. (5)) show that the number of thermal "no shift" photons encountered by a primary particle in the distance R_0 in intergalactic space is of the same order as the number of photons encountered by a primary in a time 10^9 years in the local galaxy. The primary may actually spend such a time in the galaxy if it is originally produced there and if an intragalactic magnetic field of sufficient magnitude exists and prevents its escape. See H. Alfvén, Zeits. f. Physik 107, 579 (1937); L. Spitzer, Phys. Rev. 70, 777 (1946); H. Babcock, Phys. Rev. 72, 83 (1947).

[16] G. Reber, Ap. J. 91, 621 (1940); L. G. Henyey and P. C. Keenan, *ibid.*, 91, 625 (1940).

manifestation of the meson charge cloud surrounding the latter.

We begin with the treatment appropriate to the rest frame of the proton. Here a photon of energy $\epsilon^* > 2\ mc^2$ [17] incident on a fixed proton may be converted into an electron-positron pair with energies ϵ_+^* and ϵ_-^* ($\equiv \epsilon^* - \epsilon_+^*$) and directions of motion falling in the elements of solid angle $d\Omega_+^*$ and $d\Omega_-^*$. The differential cross section for this process with ϵ_+^* falling in the range $d\epsilon_+^*$ is denoted by

$$\phi^{\pm *}(\epsilon^*; \epsilon_+^*, \theta_+^*, \theta_-^*) d\epsilon_+^* d\Omega_+^* d\Omega_-^*.$$

The average rate at which pairs are produced per proton, $dN^{\pm}/dt$, as measured in the earth's reference frame, is then given directly in terms of the total cross section,

$$\phi^{\pm *}(\epsilon^*) \equiv \int_{mc^2}^{\epsilon^* - mc^2} \int\int \phi^{\pm *}(\epsilon^*; \epsilon_+^*, \theta_+^*, \theta_-^*) \times d\epsilon_+^* d\Omega_+^* d\Omega_-^* \quad (16)$$

by the relation

$$\frac{dN^{\pm}}{dt} = \gamma^{-1} \frac{dN^{\pm}}{dt^*} = c\gamma^{-1} \int_{2mc^2}^{\infty} \int n^*(\epsilon^*, \theta^*) \times \phi^{\pm *}(\epsilon^*) d\epsilon^* d\Omega^* \quad (17)$$

in which $\gamma = (1-\beta^2)^{-\frac{1}{2}} = E/Mc^2$, E and M are the total energy and rest mass, respectively, of the proton, m is the rest mass of the electron and $n^*(\epsilon^*, \theta^*) d\epsilon^* d\Omega^*$ is the number of photons per unit volume in the energy range $d\epsilon^*$ which are traveling in directions lying in the element of solid angle $d\Omega^*$. The polar axis from which θ_+^*, θ_-^*, and θ^* are measured is directed opposite to the velocity of the proton. Also, if dW^*/dt^* and dP^*/dt^* denote the average rates (in the proton's rest frame) at which energy and momentum are transferred to the pairs, then, from the transformation properties of energy and momentum and from the time dilatation, one has for $-dE^{\pm}/dt$, the average rate at which the proton loses energy because of pair creation (in the earth's coordinate system), the expression,

$$\frac{-dE^{\pm}}{dt} = \frac{dW}{dt} = \frac{dW^*}{dt^*} + c\beta \frac{dP^*}{dt^*} = c \int_{2mc^2}^{\infty} \int n^*(\epsilon^*, \theta^*) d\epsilon^* d\Omega^* \int_{mc^2}^{\epsilon^* - mc^2} \times \int\int \phi^{\pm *}(\epsilon^*; \epsilon_+^*, \theta_+^*, \theta_-^*) \times [\epsilon_+^* + \epsilon_-^* - c\beta(p_+^* \cos\theta_+^* + p_-^* \cos\theta_-^*)] d\epsilon_+^* d\Omega_+^* d\Omega_-^*. \quad (18)$$

Finally, the average energy of a pair has the value

$$\langle \epsilon_+ + \epsilon_- \rangle = -\frac{dE^{\pm}}{dt} \Big/ \frac{dN^{\pm}}{dt}. \quad (19)$$

We first evaluate the rate of pair production. With the aid of the relativistic transformation formula [18]

$$\frac{n^*(\epsilon^*, \theta^*) d\epsilon^* d\Omega^*}{n(\epsilon, \theta) d\epsilon d\Omega} = \frac{\epsilon^*}{\epsilon} = \gamma(1 + \beta \cos\theta), \quad (20)$$

the integral in Eq. (17) can be reduced to the form

$$\frac{dN^{\pm}}{dt} = c \int d\Omega \int_{\epsilon(\theta)}^{\infty} n(\epsilon, \theta)(1 + \beta \cos\theta) \times \phi^{\pm *}(\gamma[1 + \beta \cos\theta]\epsilon) d\epsilon, \quad (21)$$

where $\epsilon(\theta) = 2mc^2/\gamma(1+\beta\cos\theta)$. Thus, in the earth's coordinate system $\phi^{\pm}(E, \epsilon, \theta) = \phi^{\pm *}(\epsilon^*)$ plays the role of the total cross section for pair creation in the collision of a proton and a photon with energies E and ϵ, respectively, and angle $\pi - \theta$ between their directions of motion. The factor $c(1+\beta\cos\theta)$ multiplying $n(\epsilon, \theta)$ arises from the relative velocity of proton and photon in the earth's reference frame. The actual expression employed for $\phi^{\pm *}(\epsilon^*)$ is based on the Bethe-Heitler formulae for the differential and total

[17] In what follows, starred and unstarred symbols always refer to quantities measured in the proton's rest frame and in the earth's frame, respectively. Most of the relativistic transformation formulae used (connecting corresponding quantities in the two frames) may be found in W. Pauli, *Relativitatstheorie* (Teubner, Leipzig, 1921).

[18] Equation (20) follows from $n(\epsilon, \theta) d\epsilon d\Omega \sim A^2/\epsilon$, where A is the amplitude of the corresponding electromagnetic wave, and from $A/\epsilon = A^*/\epsilon^*$, a consequence of the transformation properties of the electric and magnetic field strengths. Alternatively, Eq. (20) can be derived from the transformation law for the time component of the null radiation energy current-density four-vector.

pair creation cross sections,[19] which treat the proton as a point electric charge, so that for the time being, any possible effect of the latter's anomalous moment (or more generally, of its enveloping meson charge cloud) is disregarded. For convenience an analytic approximation to the Bethe-Heitler $\phi_{\pm}^*(\epsilon^*)$ is used, *viz.*,

$$\phi_{\pm}^*(\epsilon^*)\cong\frac{28}{9}\left(\frac{e^2}{\hbar c}\right)\left(\frac{e^2}{mc^2}\right)^2\left[\ln\left(\frac{\epsilon^*}{6.7mc^2}\right)+\frac{1}{6}\left(\frac{\epsilon^*}{mc^2}-2\right)^3\exp\left(-0.6\frac{\epsilon^*}{mc^2}\right)\right],\quad \text{for } \epsilon^*\geqq 6.7mc^2$$
$$\cong\frac{14}{27}\left(\frac{e^2}{\hbar c}\right)\left(\frac{e^2}{mc^2}\right)^2\times\left[\left(\frac{\epsilon^*}{mc^2}-2\right)^3\exp\left(-0.6\frac{\epsilon^*}{mc^2}\right)\right]\quad \text{for } 2mc^2\leqq\epsilon^*<6.7mc^2 \tag{22}$$

where exact numerical values of $\phi_{\pm}^*$ at $\epsilon^*/mc^2=3$, 4, 5, 6, 10, 20, and 50 have been employed to fit the exponential correction term.

Consider now the case of a proton falling through the sun's radiation field. If the fall is radial, θ is effectively zero, i.e.,

$$n(\epsilon,\theta)\cong(R_\odot/R)^2 n_\odot(u)\delta(\theta)/4\pi\ ^{20}$$

so that Eq. (21) yields

$$(c\beta)^{-1}\frac{dN^{\pm}}{dt}=\frac{dN^{\pm}}{dR}\cong 2\left(\frac{R_\odot}{R}\right)^2\int_{mc^2/\gamma}^{\infty}\times n_\odot(u)\phi_{\pm}^*(2\gamma\epsilon)d\epsilon. \tag{23}$$

Equation (23) can be integrated at once to yield, $N_\odot^{\pm}$, the number of pairs produced by a proton falling radially in the sun's radiation field from infinity to the earth's orbit. With the aid of Eqs. (1) and (22), the result is,

$$N_\odot^{\pm}=2R_\odot\int_{mc^2/\gamma}^{\infty}n_\odot(u)\phi_{\pm}^*(2\gamma\epsilon)d\epsilon \tag{24}$$
$$=\frac{280}{3\pi^4}\frac{e^2}{\hbar c}\left(\frac{e^2}{mc^2}\right)^2[\Psi_{1\odot}(u_{\pm})+\Psi_{2\odot}(u_{\pm})]\left(\frac{\eta R_\odot}{kT_\odot}\right)$$
$$\cong 2.5\frac{e^2}{\hbar c}\left(\frac{e^2}{mc^2}\right)^2[\Psi_{1\odot}(u_{\pm})+\Psi_{2\odot}(u_{\pm})]Q_\odot,$$

in which

$$u_{\pm}\equiv\frac{mc^2}{kT}\frac{Mc^2}{E}$$

and

$$\Psi_{1\odot}(u_{\pm})=\sum_{p=1}^{\infty}\frac{1}{p^3}\left[(3+3.35pu_{\pm})\exp(-3.35pu_{\pm})+2\int_{3.35pu_{\pm}}^{\infty}\frac{e^{-x}}{x}dx\right], \tag{25}$$

$$\Psi_{2\odot}(u_{\pm})=8u_{\pm}^3\sum_{p=1}^{\infty}\frac{1}{(1.2+pu_{\pm})^6}[(pu_{\pm}+1.2)^2+8(pu_{\pm}+1.2)+20]\exp(-pu_{\pm}-1.2). \tag{26}$$

In the "extreme relativistic" case ($\epsilon^*\gg mc^2$, i.e., $u_{\pm}\ll 1$ or $E\gg mc^2Mc^2/kT\cong 10^6Mc^2\cong 10^{15}$ ev) the infinite sums in Eqs. (25) and (26) can be transformed into simple closed expressions (which are listed below in Table II) and one obtains from Eq. (24).

$$N_\odot^{\pm}(R_\odot)\cong 1.1\times 10^{-6}\ln\left(\frac{0.6}{u_{\pm}}\right). \tag{27}$$

According to Eq. (27), a proton with energy $E=10^8Mc^2$ produces, on the average, 5×10^{-4} electron-positron pairs in falling radially through the radiation field of the sun to the earth's orbit.[21]

[19] See, for example, W. Heitler, *The Quantum Theory of Radiation* (Oxford University Press, London, 1944), second edition, pp. 194–204. One sees from Eq. (20) that $\epsilon^*\sim(E/Mc^2)\epsilon\sim(E/Mc^2)kT$, so that, for example, energies E as high as 2×10^{18} ev (protons) or 10^{15} ev (electrons) correspond to rest frame photon energies ϵ^* of only 10^9 ev. Such photon energies lie in the range where the Bethe-Heitler pair creation cross section (and presumably also the Klein-Nishina scattering cross section) are at least in approximate agreement with observations on cascade showers.

[20] $\delta(\theta)$ is a Dirac delta-function normalized according to $\int\delta(\theta)d\Omega=4\pi$.

[21] The 5×10^{-6} pairs of Eq. (27) are created in the encounter of a proton with the 3×10^{20} photons/cm² of Eq. (2). This number of photons encountered by the proton in passing (essentially) across the solar system may be compared with the number, 10^{15}, of material particles (mostly hydrogen atoms) encountered in the same passage. The last number is calculated assuming the number density of diffuse interplanetary atoms as 1/cm³. Also, protons passing through the solar system in directions other than radial generally meet numbers of photons comparable with 3×10^{20}; an exceptional case is that of grazing passage near the sun's edge where the number of photons encountered may be greater by a factor of several hundred.

More generally, without restriction on $u_{\pm}$, Ψ_{1u}, and Ψ_{2u} can be evaluated in numerical form. The results for $N_u^{\pm}$ appear in Table I. The numbers in the last column are proportional to the number of pairs per unit energy range of the primary spectrum, the latter being assumed to follow an inverse third power law.

We now estimate the integral in Eq. (18) for the average rate of energy transfer from the protons to the pairs which it creates. The difficult angular integration over θ_+^*, θ_-^* can be reduced to a known result by using the inequality

$$\epsilon_+^*+\epsilon_-^*-\beta c(p_+^*\cos\theta_+^*+p_-^*\cos\theta_-^*) > (mc^2)^2\left[\frac{1}{\epsilon_+^*+cp_+^*}+\frac{1}{\epsilon_-^*+cp_-^*}\right], \quad (28)$$

where, near the threshold for pair production, the left- and right-hand sides of Eq. (28) are each $2\ mc^2$, while far from the threshold $\langle\cos\theta^*\rangle \cong\langle\cos\theta_+^*\rangle\cong\langle\cos\theta_-^*\rangle\cong 1^{19}$ and the left- and right-hand sides are again equal. Consequently, the left- and right-hand sides of Eq. (28) are always of comparable magnitude, differing by no more than a factor of 2 for average deviations of θ^*, θ_+^*, and θ_-^* from the polar axis. Equation (28) yields an easily evaluated lower limit to the rate of energy loss:

$$-\frac{dE}{dt}>c(mc^2)^2\int_{2mc^2}^{\infty}\int n^*(\epsilon^*,\theta^*)d\epsilon^*d\Omega^* \times\int_{mc^2}^{\epsilon^*-mc^2}\int\int\phi^*(\epsilon^*,\epsilon_+^*,\theta_+^*,\theta_-^*) \quad (29)$$

$$\times\left[\frac{1}{\epsilon_+^*+cp_+^*}+\frac{1}{\epsilon_-^*+cp_-^*}\right]d\epsilon_+^*d\Omega_+^*d\Omega_-^*.$$

At "low" proton energies ($E\ll mc^2Mc^2/kT$, say $\cong 10^5Mc^2$) only the far ultraviolet portion of the thermal photon spectrum is capable of creating pairs, and these are mostly produced near the threshold. Equations (17), (18), and (19) then show that the average energy of a pair is approximately $2\gamma\ mc^2$ or 10^{11} ev for $E=10^5$ Mc².

TABLE I. Number of pairs as a function of the primary energy.

E/Mc^2	Ψ_{1u}	Ψ_{2u}	$N_u^{\pm}\times10^6$	$(10^5Mc^2/E)^2N_u^{\pm}\times10^6$
10^5	——	0.00001	6×10^{-6}	6×10^3
$\frac{1}{2}10^6$	——	0.01	6×10^{-3}	4×10^5
$\frac{1}{2}10^6$	0.01	0.13	7×10^{-2}	5×10^5
10^6	0.24	0.34	3×10^{-1}	3×10^5
10^7	4.45	0.05	2	2×10^3
10^8	10.0	——	5	5
10^9	15.5	——	7	7×10^{-3}

In the "extreme relativistic" case ($\epsilon^*\gg mc^2$)

$$\int\int\phi^*(\epsilon^*,\epsilon_+^*,\theta_+^*,\theta_-^*)d\Omega_+^*d\Omega_-^* \cong 4\left(\frac{e^2}{\hbar c}\right)\left(\frac{e^2}{mc^2}\right)^2\frac{\epsilon_+^{*2}+\epsilon_-^{*2}+\frac{2}{3}\epsilon_+^*\epsilon_-^*}{\epsilon^{*3}} \cdot\left[\ln\frac{2\epsilon_+^*\epsilon_-^*}{\epsilon^*mc^2}-\frac{1}{2}\right], \quad (30)$$

and

$$-\frac{dE^{\pm}}{dt}>c\left(\frac{2e^2}{\hbar c}\right)\left(\frac{e^2}{mc^2}\right)^2(mc^2)^2\int d\Omega \times\int_{2\epsilon(\theta)}^{\infty}\frac{n(\epsilon,\theta)}{\epsilon}\left(\ln\frac{\gamma\epsilon(1+\beta\cos\theta)}{4mc^2}\right)^2d\epsilon, \quad (31)$$

where the approximations made in the derivation of Eq. (31) from Eqs. (29) and (30) have been such as to strengthen the inequality. In particular the lower limit of the integration with respect to ϵ does not extend down to the actual threshold. Also, in view of the fact that the approximate integrated cross section $\phi^*(\epsilon^*)$ (the logarithmic terms in Eq. (22)) computed from the right-hand member of Eq. (30) falls below the exact numerical values, particularly for small values of ϵ^*, we infer that Eq. (30) can be treated as an inequality ($\geqq$ replacing $\cong$) valid for all values of ϵ^* above the threshold for pair production. It follows then that Eq. (31) retains its validity for low values of the primary energy.

Equation (31) will now be applied to compute the average energy loss, $\Delta E_u^{\pm}$ experienced by a proton with $E\gg mc^2Mc^2/kT$ in the radial fall through the sun's radiation field to the earth's orbit. A simplification is possible just as in Eq. (22) since the angle θ is effectively zero, and one

TABLE II. Electron-positron pair production formulae.

$u_\pm$	$\Psi_{1n}+\Psi_{2n}$; Eq. (9)*	$\Psi_{1n}+\Psi_{2n}$; Eq. (11)	$\Psi_{1n}+\Psi_{2n}$; Eqs. (1) and (24)
$\ll 1$	$1.2\ln(0.4/u_\pm)$	$0.6(\ln 0.4/u_\pm)^2$	$2.4\ln(0.6/u_\pm)$
1	0.16	0.060	0.60
2	0.029	0.006	0.15
$\gg 1$	$(2.4/u_\pm^2)e^{-u_\pm}$	$(2.4/u_\pm^3)e^{-u_\pm}$	$(2.4/u_\pm)e^{-u_\pm}$

* The "no shift" blackbody directionally isotropic distribution applies in the case of a primary traversing the local galaxy. From Eq. (5) and Table II one has $N_e^* \sim N_s^*$. Hence the total pair production by a proton during a single traversal of the local galaxy is negligible.

finds

$$\Delta E_e^{\pm} = \int_{R_e}^{\infty} (c\beta)^{-1}\left(\frac{dE}{dt}\right)dR > R_e\left(\frac{2e^2}{\hbar c}\right)\left(\frac{e^2}{mc^2}\right)^2 \times (mc^2)^2 \int_{2mc^2/\gamma}^{\infty} \frac{n_e(u)}{\epsilon}\left[\ln\frac{\gamma\epsilon}{2mc^2}\right]^2 d\epsilon$$

$$\cong 0.2\ln\left(\frac{1}{u_\pm}\right)\frac{(mc^2)^2}{kT}N_e^{\pm}$$

$$\cong 10^{12} N_e^{\pm} \text{ ev at } E = 10^8 Mc^2. \quad (32)$$

Thus in the "extreme relativistic" case, the average energy of a pair varies only logarithmically with the energy of the primary particle and has a value in the neighborhood of 10^{12} ev. Recalling the result for low proton energies we conclude that the average energy with which pairs are produced remains essentially constant at 10^{12} ev in the range $E \geqq 10^8 Mc^2$.

We turn now to the problem of electron-positron pair production in intergalactic space. The quantities of interest are $N_n^{\pm}$, the average number of pairs per proton resulting from proton-photon collisions in the distance R_0, and $\Delta E_n^{\pm}$, the average energy lost by the proton in producing pairs in the same distance. Since in this case the photons are isotropically distributed over direction ($n(\epsilon, \theta) = 1/4\pi \cdot n_n(\epsilon/kT)$), Eq. (21) yields,

$$N_n^{\pm} = \frac{R_0}{4\pi}\int d\Omega \int_{\epsilon(\theta)}^{\infty} n_n(\epsilon/kT)(1+\beta\cos\theta) \times \phi_\pm^*(\gamma(1+\beta\cos\theta)\epsilon)d\epsilon$$

$$\cong 2R_0 \int_{\pm}^{\infty} du(kT)\phi_\pm^*(2\gamma kTu)u \times \int_u^{\infty} n_n(y)\frac{dy}{y^2}, \quad (33)$$

where the second integral of Eq. (33) can be derived from the first by the series of transformations: (1) change variables of integration replacing ϵ by $u = 1/2(1+\beta\cos\theta)\epsilon/kT$ and θ by $\omega = 2(1+\beta\cos\theta)^{-1}$, (2) interchange order of integration (now possible because lower limit of integration with respect to u is independent of ω), (3) replace upper and lower limits of integration with respect to ω by ∞ and 1, respectively, (4) Put $y = u\omega$. These transformations bring to light an effective "unidirectional" spectral distribution of photons,

$$[n_n(u)]_{\text{eff}} \equiv u\int_u^{\infty} n_n(y)\frac{dy}{y^2}, \quad (34)$$

for the pair-production problem in intergalactic space.

We evaluate $N_n^{\pm}$ for the "no shift" blackbody spectral distribution of Eq. (9) and the "red shifted" spectral distribution of Eq. (11). Equation (33) can be represented as a generalization of Eq. (24) in the form

$$N_n^{\pm} \cong 2.5\frac{e^2}{\hbar c}\left(\frac{e^2}{mc^2}\right)^2 [\Psi_{1n}(u_\pm)+\Psi_{2n}(u_\pm)]Q_n. \quad (35)$$

With the "no shift" distribution

$$\Psi_{1n} = \sum_{p=1}^{\infty}\frac{1}{p^3}\left[\exp(-3.35pu_\pm) + \int_{3.35pu_\pm}^{\infty}\frac{e^{-x}}{x}dx\right], \quad (36)$$

$$\Psi_{2n} = 8u_\pm^2 \sum_{p=1}^{\infty}\frac{1}{p}\left[\frac{4}{(1.2+pu_\pm)^5}+\frac{1}{(1.2+pu_\pm)^4}\right] \times \exp(-1.2-pu_\pm). \quad (37)$$

The "red shifted" distribution yields

$$\Psi_{1n} = \sum_{p=1}^{\infty}\frac{1}{p^3}\int_{3.35pu_\pm}^{\infty}\frac{1}{x}\left(1+\ln\frac{x}{3.35pu_\pm}\right)e^{-x}dx, \quad (38)$$

$$\Psi_{2n} = 8\sum_{p=1}^{\infty}\frac{1}{p^3}\left[\frac{pu_\pm}{(1.2+pu_\pm)^4}\exp(-1.2-pu_\pm) + \int_{1.2+pu_\pm}^{\infty}\frac{e^{-x}}{x}dx\right]. \quad (39)$$

TABLE III. Electron-positron pair production by proton-photon collisions in intergalactic space.

E/Mc^2	"No shift;" Eq. (9) $N_n^{\pm}$	"No shift;" Eq. (9) $(10^8Mc^2/E)^3N_n^{\pm}$	"Red shifted;" Eq. (11) $N_n^{\pm}$	"Red shifted;" Eq. (11) $(10^8Mc^2/E)^3N_n^{\pm}$
10^8	1.1×10^{-6}	4.8	1.1×10^{-7}	0.5
5×10^8	1.3×10^{-4}	1000	2.6×10^{-5}	210
10^9	7.0×10^{-4}	700	2.6×10^{-4}	260
10^7	7.3×10^{-3}	7.3	5.1×10^{-3}	5.1
10^8	2.0×10^{-2}	0.02	3.6×10^{-2}	0.04
10^9	3.2×10^{-2}	3×10^{-5}	9.6×10^{-2}	10^{-4}

These infinite sums have been evaluated for small, intermediate, and large values of $u_{\pm}$, with results which are summarized in Tables II and III.

Evidently the total number of pairs (created by all the primary particles) is not especially sensitive to the thermal photon spectral distribution. Near $E=10^8\ Mc^2$, $N_n^{\pm}$ attains the value 0.01; however, its variation with E is at best not more rapid than $\{\ln(E/Mc^2)\}^2$.

The analog of Eq. (32) in the present calculation is

$$\Delta E_n^{\pm} > R_0\left(\frac{2e^2}{\hbar c}\right)\left(\frac{e^2}{mc^2}\right)^2(mc^2)^2 \times\int_{2u_{\pm}}^{\infty}\frac{du}{u}\left[\ln\frac{u}{2u_{\pm}}\right]^2[n_n(u)]_{\text{eff}}, \quad (40)$$

derived from Eq. (31) with the help of the transformations listed in the discussion following Eq. (33). Inserting the spectral distributions of Eqs. (9) and (11) into Eq. (40), one gets

$$\Delta E_n^{\pm} > \frac{e^2}{\hbar c}\left(\frac{e^2}{mc^2}\right)^2 Q_n\frac{(mc^2)^2}{kT}\begin{cases}\displaystyle\sum_{p=1}^{\infty}\frac{1}{p}\int_{2u_{\pm}}^{\infty}\left[\ln\frac{u}{2u_{\pm}}\right]^2 e^{-pu}du & \text{(no shift)}\\ \displaystyle\sum_{p=1}^{\infty}\frac{1}{p^3}\int_{2u_{\pm}}^{\infty}\left[\ln\frac{u}{2u_{\pm}}\right]^2\left[\frac{p}{u}+\frac{1}{u^2}\right]e^{-pu}du & \text{(red shifted)}\end{cases} \quad (41)$$

which in the extreme relativistic case ($u_{\pm}\ll1$) becomes[22] (in ev units)

$$[\Delta E_n^{\pm}]^{\text{no shift}} > 5\times10^8\left[\ln\frac{2}{u_{\pm}}\right]^2 \cong 10^{11}\ln\left(\frac{2}{u_{\pm}}\right)N_n^{\pm}, \quad (42)$$

$$[\Delta E_n^{\pm}]^{\text{red shifted}} > 10^3\frac{E}{Mc^2} \cong 10^6\frac{E}{Mc^2}\left(\ln\frac{2}{u_{\pm}}\right)^{-2}N_n^{\pm}. \quad (43)$$

Both formulae agree in predicting an average energy per pair of $\sim10^{12}$ ev at $E=10^8\ Mc^2$. At higher energies, however, the "red shifted" distribution produces both an appreciably greater total energy loss and an appreciably greater average energy per pair than the "no shift" distribution.[23] For example, at $E=10^{11}\ Mc^2=10^{20}$ ev, each proton traversing a distance R_0 in the "red shifted" distribution produces, on the average, 3×10^{-1} electron-positron pairs of energy 3×10^{14} ev each.

We now discuss electron-positron pair creation in proton-photon collisions by the virtual photon method. Here one adopts the viewpoint of the earth's frame of reference and replaces the electromagnetic field of the primary proton by a set of virtual photons traveling parallel to the original direction of motion of the proton:[24] these virtual photons create pairs in collisions with thermal photons. The cross section for pair creation in the collision of a proton of energy E with a thermal photon of energy ϵ is then given by

$$\phi_{\text{pair}}(E,\epsilon,\theta)=\int_0^{\infty}d\epsilon_v Q(\epsilon_v)\sigma(\epsilon_v,\epsilon,\theta), \quad (44)$$

in which $Q(\epsilon_v)d\epsilon_v$ is the number of virtual photons with energies between ϵ_v and $\epsilon_v+d\epsilon_v$, and $\sigma(\epsilon_v,\epsilon,\theta)$ is the cross section for pair creation in the collision of two photons, with energies ϵ_v

[22] The sums in Eq. (41) approach, for $u_{\pm}\ll1$ the values $\pi/6\cdot(\ln2/u_{\pm})^2$ and $1.2/u_{\pm}$, respectively.

[23] Considering electrons in the role of cosmic-ray primaries Eq. (43) (with M replaced by m) yields $\Delta E_n^{\pm}>2\times10^{-3}E$ and an average energy loss per pair $>2E\{\ln(10^{-6}E/mc^2)\}^{-2}$. These inequalities hold in the "extreme relativistic" case ($E\gg(mc^2)^2/kT\cong5\times10^{11}$ ev). For a discussion of the applicability of the above equations to electrons, see below.

[24] The general method of virtual photons is due to C. F. Weizsacker and E. J. Williams. See, for example, reference 24, pp. 263–266.

and ϵ, and with the angle $\pi-\theta$ between their original directions of motion. The cross section $\sigma(\epsilon_\nu, \epsilon, \theta)$ determines the probability for the process inverse to the two photon annihilation so that its value can be deduced from the Dirac formula for the annihilation probability by considerations based on microscopic reversibility.

The virtual photon distribution $Q(\epsilon_\nu)$, with inclusion of the effect of the proton's anomalous magnetic moment[25] as well as of its charge, can be computed as a function of b, the minimum transverse distance at which the electromagnetic field accompanying the proton still appears equivalent to a set of independent photons. It is then known that $b\cong\hbar/mc$ yields results in agreement with the Bethe-Heitler formula for a proton originally at rest and with no anomalous magnetic moment.[26] Adopting this value for b throughout the present calculation one finds that the contribution to $Q(\epsilon_\nu)$ from the anomalous moment is smaller than that from the charge by a factor $\sim(m/M)^2$ and thus may be disregarded. An equivalent conclusion can be reached by considering the quantum perturbation theory derivation of the cross section for pair creation in a proton-photon collision, with inclusion of the effect of the anomalous moment. Here the matrix element of the interaction potential between the current density of the created electron and the anomalous moment is smaller than the matrix element of the associated electrostatic potential by a factor $\hbar/Mcb\sim m/M$, so that the anomalous moment's contribution to the cross section is again smaller than that of the charge by the factor $(m/M)^2$. In general, the proton receives, for each pair created, a transverse momentum $\sim mc$, so that most of the pairs are created at transverse distances (from the proton's path) $\sim\hbar/mc$. This distance is large compared to the presumed dimensions of the meson cloud surrounding the proton, so that the cloud can have only a small effect.[27]

We now consider briefly the possibility of primary electrons in the cosmic radiation creating electron-positron pairs by collisions with thermal photons. If the Bethe-Heitler pair-creation formula (in the electron's rest frame) can be applied to this process then all the above formulae (Eqs. 16–43) are valid with M replaced by m. Thus, for example, an electron with energy $2\times10^8\ mc^2=10^{14}$ ev will create on the average 6×10^{-6} pairs, each with average energy $\cong10^1$ ev, in a radial fall through the sun's radiation field to the orbit of the earth. However, the applicability of the Bethe-Heitler formula to the description of pair creation in electron-photon collisions is questionable because the (originally stationary) electron may acquire (in its rest frame) a large recoil energy upon impact of the photon. Consequently the interaction between the primary and the created electron will not be purely electrostatic (as is necessary for the exact validity of the Bethe-Heitler formula), but will contain magnetic and retarded contributions; in addition the equivalence of the two electrons must be considered. A complete and detailed analysis of this problem has apparently not been published,[28] but a treatment by the virtual photon method of the related process of bremsstrahlung in the collision of the two electrons indicates that the order of magnitude predicted by the Bethe-Heitler formula is correct, at least in the extreme relativistic case when the primary

---

[25] The proton's total magnetic moment is $2.79\ e\hbar/2Mc$, so that the anomalous magnetic moment is $1.79\ e\hbar/2Mc$. From the point of view of current meson theories the anomalous moment is a manifestation of the meson charge cloud surrounding the proton. Formally, the addition of a Pauli term to the Dirac equation to describe this anomalous moment makes possible a complete phenomenological description of the interaction of the proton with an electromagnetic field, without explicit reference to the meson field.

[26] E. J. Williams, Kgl. Danske Vid. Sels. Math.-Fys. Medd 13, 17 (1935).

[27] The mean transverse momentum, $p_\perp\sin(\pi-\theta_\perp)\cong\epsilon_\perp/c\cdot(\pi-\theta_\perp)$, carried off by a pair and so received by the proton can be estimated from the relation $\theta_\perp^*\sim mc^2/\epsilon^*$; $\epsilon_+ + \epsilon_-\sim(mc^2)^2/kT$ which are consequences of the Bethe-Heitler formula and of Eq. (32). From these relations and from the transformation formula, $\tan\theta_\perp=\gamma^{-1}\sin\theta_\perp^*/(\cos\theta_\perp^*-\beta)$, one immediately obtains $\pi-\theta_\perp\sim kT/mc^2\sim10^{-6}$ and $p_\perp\sin(\pi-\theta_\perp)\sim mc$. The same result follows directly from the virtual photon picture

$$(\pi-\theta_\perp\sim mc^2/(\epsilon_\nu+\epsilon)=mc^2/(\epsilon_+ + \epsilon_-)\sim kT/mc^2).$$

[28] However, see A. Borsellino, Helv. Phys. Acta 20, 136 (1947); P. Nemirovsky, J. Phys. U.S.S.R. 11, 94 (1947); J. A. Wheeler and W. Lamb, Phys. Rev. 55, 858 (1939). The Bethe-Heitler formula (for pair creation in proton-photon collisions) is, of course, not applicable to pair creation in electron-photon collisions near the threshold ($4mc^2$) of the latter process. *Note added in proof:* K. W. Watson, Phys. Rev. 72, 1060 (1947), has just given a thorough discussion of electron-positron pair creation in photon-electron collisions, and has found a cross section which, in the extreme relativistic case, is approximately double the Bethe-Heitler cross section of Eq. (22).

energy greatly exceeds the energy given the electron-positron pair.

The possibility of meson and nucleon creation in proton-photon collisions (processes 4–6) should also be mentioned. Three types of meson processes are conceivable in such collisions: (a) the transformation of a proton into a neutron and a positive meson, (b) the creation of mesons in (odd as well as even) multiples, and (c) the creation of a meson pair as a result of electromagnetic interactions alone. The cross section for (*c*) in a proton-photon collision is probably smaller than the cross section for the creation of an electron-positron pair by a factor $\sim(m/\mu)^2$ and is therefore negligible.[29] A further safeguard here (and particularly for (b)) is the high threshold energy which makes the overwhelmingly large proportion of the primary spectrum ineffective in producing meson (and, *a fortiori*, nucleon) pairs. However, in the extreme relativistic case, (a) (and/or (b)) may conceivably occur with a cross section comparable in magnitude to that for electron-positron pair creation.[30]

Finally, it may be remarked that the eventual (time dilated) radioactive decay of any neutrons and positive mesons formed in proton-photon collisions gives rise to a "delayed" electron-positron pair production.[31] Detailed investigation of such transformations must await a better understanding of the whole process of meson creation in proton-photon collisions.

4. COMPTON SCATTERING IN PROTON-PHOTON AND ELECTRON-PHOTON COLLISIONS

We shall now discuss those collisions of the primary cosmic-ray protons and electrons with thermal photons which result in Compton scattering. In the primary rest frame the photon energies ϵ^* and ϵ'^* before and after scattering, and the scattering angle χ^* are connected by the relation,[32]

$$\epsilon'^* = \frac{\epsilon^*}{1+\frac{(\epsilon^*)^2}{Mc^2}(1-\cos\chi^*)}. \tag{45}$$

Correspondingly, in the earth's frame,[33]

$$\begin{aligned}\epsilon' &= \gamma\epsilon'^*(1-\beta\cos\theta'^*)\\ &= \frac{\gamma^2\epsilon(1+\beta\cos\theta)(1-\beta\cos\theta'^*)}{1+\frac{\epsilon^*}{Mc^2}(1-\cos\chi^*)}\\ &= \epsilon\frac{1+\beta\cos\theta}{1+\beta\cos\theta'+\frac{\epsilon}{E}(1-\cos\chi)}\\ &\cong \epsilon\frac{1+\beta\cos\theta}{1+\left\{\beta-\frac{\epsilon}{E}(1+\beta\cos\theta)\right\}\cos\theta'},\end{aligned} \tag{46}$$

where Mc^2 and E are the rest energy and total energy, respectively, of the primary particle.

We require general integral expressions for the average number of scattered photons per

[29] See R. F. Christy and S. Kusaka, Phys. Rev. **59**, 405 (1941); J. R. Oppenheimer, H. Snyder, and R. Serber, *ibid.* **57**, 75 (1940); μ is the meson mass, $\sim$200 m.

[30] For example, J. Hamilton and H. W. Peng, Proc. Roy. Ir. Ac. **49A**, 197 (1944); C. Morette and H. W. Peng, Nature **160**, 60 (1947), give 5×10^{-27} cm² as the asymptotic value (for $\epsilon^*\gg\mu c^2$) of the cross section for (a), while results of the same general order of magnitude are obtained by M. Lax and H. Feshbach (private communication); this value is matched by the $\phi_+{}^*$ of Eq. (22) for $\epsilon^*\cong\mu c^2$. If, however, there is no negative meson capture by light nuclei, one must conclude that single meson creation in proton-photon collisions is an extremely rare process, at least if only one kind of meson exists and/or if nucleons have no excited "meson-pregnant" states. In this connection see, E. Fermi, E. Teller, and V. Weisskopf, Phys. Rev. **71**, 314 (1947); J. A. Wheeler, *ibid.* **71**, 320 (1947); R. E. Marshak and H. A. Bethe, *ibid.* **72**, 506 (1947); V. Weisskopf, *ibid.* **72**, 510 (1947); S. Sakata and T. Inoue, Progress of Theoretical Physics **1**, 143 (1946).

[31] "Delayed" electron-positron pairs also arise from the creation (and subsequent decay) of neutrons and mesons in collisions of primary protons with the hydrogen nuclei of interstellar diffuse matter. See Appendix C.

[32] See, for example, reference 19, pp. 146–161.

[33] The transformation properties of the photon energy-momentum four vector yields,

$$1-\cos\chi^* = [\gamma^2(1+\beta\cos\theta)(1+\beta\cos\theta')]^{-2}(1-\cos\chi)$$

with $\pi-\theta$ and $\pi-\theta'$ the angles between the original directions of motion of the primary and the directions of motion of the photon before and after the scattering. This relation and the relativistic Doppler formulae connecting ϵ'^*, ϵ', and ϵ^*, ϵ make possible the derivation of the third expression for ϵ' from the second (in Eq. (46)). This third expression can also be deduced directly by an application of the energy-momentum conservation laws in the earth's frame to the particle-photon collision. The fourth simplified, but entirely adequate form for ϵ' can be derived by considering the behavior of the denominator in the third form for small values of $\pi-\theta'$.

primary per unit time (dN^e/dt) and the average energy loss per primary per unit time ($-dE^e/dt$). A procedure analogous to that employed in the derivation of Eqs. (17), (18), and (21) yields,

$$\frac{dN^e}{dt}=c\int d\Omega\int_0^\infty n(\epsilon,\theta)(1+\beta\cos\theta)\times\phi_c^*(\epsilon^*)d\epsilon, \quad (47)$$

$$-\frac{dE^e}{dt}=c\int d\Omega\int_0^\infty n(\epsilon,\theta)(1+\beta\cos\theta)d\epsilon\times\int\phi_c^*(\epsilon^*,\chi^*)(\epsilon'-\epsilon)d\Omega^*. \quad (48)$$

Here $\phi_c^*(\epsilon^*,\chi^*)d\Omega^*$ and $\phi_c^*(\epsilon^*)$ are the differential and total cross sections for Compton scattering evaluated in the rest frame of the primary. For the time being we neglect all effects connected with the anomalous magnetic moment of the proton, or, more generally, with its surrounding meson charge cloud, and evaluate Eqs. (47) and (48) with the aid of the Klein-Nishina cross sections (presumably rigorously valid for point electric charges):[34]

$$\phi_c^*(\epsilon^*,\chi^*)\begin{cases}\nearrow \frac{1}{2}\left(\frac{e^2}{Mc^2}\right)^2(1+\cos^2\chi^*), & \epsilon^*\ll Mc^2\\ \searrow \frac{1}{2}\left(\frac{e^2}{Mc^2}\right)\frac{\epsilon'^*}{\epsilon^*}, & \epsilon^*\chi^{*2}\gg Mc^2,\end{cases} \quad (49)$$

$$\phi_c^*(\epsilon^*)\begin{cases}\nearrow \frac{8\pi}{3}\left(\frac{e^2}{Mc^2}\right)^2, & \epsilon^*\ll Mc^2\\ \searrow 2\pi\left(\frac{e^2}{Mc^2}\right)^2\frac{Mc^2}{2\epsilon^*}\ln\frac{2\epsilon^*}{Mc^2}, & \epsilon^*\gg Mc^2.\end{cases} \quad (50)$$

Employing Eqs. (47) and (50) we obtain

$$\frac{dN^e}{dR}\cong\int d\Omega\int_0^{\epsilon(\theta)}n(\epsilon,\theta)(1+\beta\cos\theta)\times\left[\frac{8\pi}{3}\left(\frac{e^2}{Mc^2}\right)^2\right]d\epsilon+\int d\Omega\int_{\epsilon(\theta)}^\infty n(\epsilon,\theta)(1+\beta\cos\theta)\times\left[2\pi\left(\frac{e^2}{Mc^2}\right)^2\frac{Mc^2}{2\epsilon^*}\ln\frac{2\epsilon^*}{Mc^2}\right]d\epsilon \quad (51)$$

in which $\epsilon(\theta)\equiv Mc^2/2\gamma(1+\beta\cos\theta)$. A similar procedure applied to Eq. (48) with explicit utilization of Eqs. (46) and (49) yields

$$-\frac{dE^e}{dR}\cong\int d\Omega\int_0^{\epsilon(\theta)}n(\epsilon,\theta)(1+\beta\cos\theta)\left[\frac{8\pi}{3}\left(\frac{e^2}{Mc^2}\right)^2\right]\Delta E^{(1)}d\epsilon+\int d\Omega\int_{\epsilon(\theta)}^\infty n(\epsilon,\theta)(1+\beta\cos\theta)\left[2\pi\left(\frac{e^2}{Mc^2}\right)^2\frac{Mc^2}{2\epsilon^*}\ln\left[1+\frac{2\epsilon^*}{Mc^2}\right]\right]\Delta E^{(2)}d\epsilon, \quad (52)$$

where the quantities

$$\Delta E^{(1)}=\frac{\gamma\epsilon^*}{1+\epsilon^*/Mc^2},$$
$$\Delta E^{(2)}=E\left[1-\frac{2\epsilon^*/Mc^2}{(1+2\epsilon^*/Mc^2)\ln(1+2\epsilon^*/Mc^2)}\right] \quad (53)$$

are approximately the average energy losses of the primary in a single Compton collision for $2\epsilon^*<Mc^2$ and $2\epsilon^*>Mc^2$, respectively.

Equations (51)–(53) and Eqs. (1) and (2) are now used to compute the average number of collisions, N_s^e, and the average energy loss, ΔE_s^e, experienced by a primary falling radially from infinity through the sun's radiation field to the orbit of the earth ($\theta\cong 0$). It is convenient to distinguish two extreme cases: "rest-frame non-relativistic" and "rest-frame extreme relativistic," depending on whether $\epsilon^*=\gamma\epsilon(1+\beta\cos\theta)$ is $\ll Mc^2$ or $\gg Mc^2$ for $\epsilon\cong 2.7\ kT$. An equivalent statement is

$$u_c=\frac{(Mc^2)^2}{EkT}\begin{cases}\gg 1 & \text{("rest-frame non-relativistic" } E\ll 2\times10^{18}\text{ ev-protons; } E\ll 5\times10^{11}\text{ ev-electrons)}\\ \ll 1 & \text{("rest-frame extreme relativistic").}\end{cases} \quad (54)$$

In the "rest-frame non-relativistic" case one

[34] See reference 19, pp. 146–160.

obtains

$$N_s^c \cong 2R_e\left[\frac{8\pi}{3}\left(\frac{e^2}{Mc^2}\right)^2\right]\int_0^\infty n_s(u)d\epsilon = 2\left[\frac{8\pi}{3}\left(\frac{e^2}{Mc^2}\right)^2\right]Q_s$$
$$\cong 1.2\times10^{-10}\text{(protons)}$$
$$\cong 4.0\times10^{-4}\text{(electrons)}, \quad (55)$$

$$\Delta E_s^c \cong 2R_e\left[\frac{8\pi}{3}\left(\frac{e^2}{Mc^2}\right)^2\right]\int_0^\infty n_s(u)2\gamma^2\epsilon d\epsilon = 2\left[\frac{8\pi}{3}\left(\frac{e^2}{Mc^2}\right)^2\right]5.4kT\gamma^2Q_s \cong \frac{10^9}{{u_c}^2}\text{ ev}. \quad (56)$$

The average energy of the scattered photons, $5.4kT\gamma^2 = 5.4E/u_c$, is comparatively large, but the total energy loss is scarcely sufficient to produce an observable intensity of scattered radiation. Recalling Eq. (5), it is clear that the same conclusion holds for a single traversal of the local galaxy.

In the "rest-frame extreme relativistic" case, Eqs. (1), (2), and (51)–(53) give

$$N_s^e \cong 2R_e\int_{u_c/4}^\infty\left[2\pi\left(\frac{e^2}{Mc^2}\right)^2\frac{u_c}{4u}\ln\frac{4u}{u_c}\right]n_s(u)kTdu \cong \frac{16\pi}{3}\left(\frac{e^2}{Mc^2}\right)^2Q_s\left[\frac{u_c}{8}\ln\frac{2}{u_c}\right] \cong 5\times10^7\frac{kT}{E}\ln\frac{2}{u_c}. \quad (57)$$

$$\Delta E_s^e \cong E\left(1-1/\ln\frac{4}{u_c}\right)N_s^e \cong 2.5\times10^7\ln\frac{0.7}{u_c}\text{ ev}. \quad (58)$$

On the average, a single Compton collision reduces the energy of the primary particle from $E(\gg(Mc^2)^2/kT)$ to $E/\ln(4/u_c)$; thus, for example, an eighty-five percent loss in a single collision requires $u_c \cong 10^{-2}$ or $E \cong 2\times10^{20}$ ev (protons), $E \cong 5\times10^{13}$ ev (electrons). It is clear that a considerable number of collisions are required to degrade a particle from "rest-frame extreme relativistic" to "rest-frame non-relativistic;" also the small value of N_s^e, even for electrons, and its decrease with E, shows that the occurence of many such collisions is extremely rare in a single traversal of the solar system or the local galaxy.

We now consider Compton collisions in intergalactic space. Here the distribution in direction of photons is isotropic $(n(\epsilon,\theta) = (1/4\pi)n_n(u))$, so that the transformations described after Eq. (34) are applicable and reduce Eqs. (51) and (52) to

$$R_0\frac{dN^e}{dR} \cong \left[\frac{16\pi}{3}\left(\frac{e^2}{Mc^2}\right)^2\right]\left[\int_0^{u_c/4}[n_n(u)]_{eff}(kTdu) + \frac{3}{4}\int_{u_c/4}^\infty\frac{u_c}{4u}\ln\frac{4u}{u_c}[n_n(u)]_{eff}(kTdu)\right], \quad (59)$$

$$-R_0\frac{dE^e}{dR} \cong \left[\frac{16\pi}{3}\left(\frac{e^2}{Mc^2}\right)^2\right]\left[\frac{1}{2}E\int_0^{u_c/4}\frac{4u/u_c}{1+2u/u_c}[n_n(u)]_{eff}(kTdu) + \frac{3}{4}E\int_{u_c/4}^\infty\frac{u_c}{4u}\ln\left(1+\frac{4u}{u_c}\right)\left\{1-\frac{4u/u_c}{(1+4u/u_c)\ln(1+4u/u_c)}\right\}[n_n(u)]_{eff}(kTdu)\right]. \quad (60)$$

The function $[n_n(u)]_{eff}$ is defined by Eq. (34); performing the integration there indicated we obtain the explicit formulae

$$[n_n(u)]_{eff}^{\text{no shift}} = \frac{Q_n}{2.4kTR_0}u\ln(1-e^{-u})^{-1}, \quad (61)$$

$$[n_n(u)]_{eff}^{\text{red shifted}} = \frac{Q_n}{2.4kTR_0}\frac{1}{u}\int_u^\infty y\ln(1-e^{-y})^{-1}dy. \quad (62)$$

Under the "rest-frame non-relativistic" condition the limit of integration $u_c/4$ in Eqs. (59) and (60) may be replaced by infinity, thus eliminating the second of the two integrals appearing in each equation. Equations (59)–(62) then give

$$R_0\frac{dN^e}{dR} \begin{cases} \cong\left[\frac{8\pi}{3}\left(\frac{e^2}{Mc^2}\right)^2Q_n\right] & \text{(no shift)} \\ \text{logarithmic infinity} & \text{(red shifted)}, \end{cases} \quad (63)$$

and

$$-R_0\frac{dE^c}{dR}\cong\left[\frac{8\pi}{3}\left(\frac{e^2}{Mc^2}\right)^2 Q_n\right]3.6kT\gamma^2$$
$$\cong\frac{3.5\times10^{12}}{u_c^2}\text{ ev}. \tag{64}$$

It is interesting that the average space rate of energy loss has the same value for both "no shift" and "red shifted" distributions since this average rate depends only on the total photon energy density—see Eqs. (60)–(62), and (12). On the other hand, Eq. (63) shows that the average space rate at which collisions occur is critically dependent on the choice of spectral distribution. In the "no shift" case, the average number of collisions per primary in the distance R_0 is

$$N_n^c\cong\frac{8\pi}{3}\left(\frac{e^2}{Mc^2}\right)^2 Q_n\begin{cases}\nearrow\cong5\times10^{-7}\text{ (protons)}\\ \searrow\cong2\text{ (electrons)}.\end{cases} \tag{65}$$

According to Eq. (65), the probability that an electron with $u_c\gg1$ suffers a collision in traveling the distance R_0 through the "no shift" distribution is $1-e^{-2}=0.85$. The corresponding average energy of the scattered photons is $3.6kT\gamma^2=3.6E/u_c$ or two-thirds the value computed earlier for unidirectional radiation moving directly towards the primary particle.

Regarding numerical values of the primary's energy loss ΔE_n^c, Eq. (64) yields $-R_0dE/dR\cong3.5\times10^{10}$ ev at $u_c=10(E\cong2\times10^{17}$ ev (protons), $E\cong5\times10^{10}$ ev (electrons)). Thus, in the distance R_0, the total energy loss of a proton is negligible; on the other hand, an electron loses a good fraction of its original energy. For an accurate evaluation of the energy loss of an electron we integrate Eq. (64), obtaining

$$\frac{mc^2}{E-\Delta E_n^c}-\frac{mc^2}{E}\cong\left[\frac{8\pi}{3}\left(\frac{e^2}{mc^2}\right)^2 Q_n\right]3.6kT/mc^2$$
$$\cong7\times10^{-6}. \tag{66}$$

At $E=5\times10^{10}$ ev, this loss amounts to 40 percent. It is clear that the energy loss experienced by such electrons as a result of their interaction with starlight (i.e., thermal photons in intergalactic space) over long periods of time ($\cong1.85\times10^9$ years) must be considered in interpreting the energy spectrum exhibited by these particles in the neighborhood of the earth (if they are indeed found to occur in the primary cosmic radiation).

We turn now to the "rest-frame extreme relativistic" case: $u_c\ll1$. It will be helpful to discuss the results for the "no-shift" and "red shifted" distributions separately beginning with the former. Introducing Eq. (61) into Eqs. (59) and (60) the first integrals in each equation may be omitted and the second readily evaluated with the results

$$R_0\frac{dN^c}{dR}\cong\frac{Q_n}{Q_s}N_s^c\cong10^4N_s^c,$$
$$-R_0\frac{dE^c}{dR}\cong E(1-1/\ln4/u_c)N_n^c. \tag{67}$$

The average number of collisions, N_n^c, and the average energy loss, ΔE_n^c, per primary in the distance R_0, predicted by Eq. (67), are quite negligible for protons ($E\gg2\times10^{18}$ ev); for electrons $N_n^c\cong0.4$ at $E=10^{12}$ ev, but decreases rapidly as E increases (compare Eq. 57). Results from Eqs. (64)–(67) may be summarized by the statement that electrons in the energy range 10^{10} to 10^{12} ev traveling a distance R_0 in intergalactic space (or a distance $\sim10^8$ l.y. in the galaxy—see reference 15a) experience a substantial fractional energy loss if the space is filled with the "no shift" photon distribution; however, if the initial energy falls outside the above-mentioned range the fractional loss of energy is relatively small.

Results of an entirely different character follow from the "red shifted" thermal photon distribution of Eqs. (11) and (62). Here $n_n(u)$ and $[n_n(u)]_{\text{eff}}$ vary inversely as u for small u so that the first integral in Eq. (59) is again infinite (as in Eq. (63)), signifying that an infinite number of "small energy transfer" collisions ($\Delta E^{(1)}$ of Eq. (53) $\ll E$) occur. The corresponding average number of "large energy transfer" collisions ($\Delta E^{(2)}$ of Eq. (53) $\sim E$) is given by the second integral in Eq. (59) with the approximate value

$$R_0\left[\frac{dN^c}{dR}\right]^{\text{red shifted}}_{\text{large energy transfer}}$$
$$\cong2\pi\left(\frac{e^2}{Mc^2}\right)^2 Q_n\begin{cases}\nearrow\cong4\times10^{-7}\text{ (protons)}\\ \searrow\cong1.6\text{ (electrons)}.\end{cases} \tag{68}$$

It is particularly interesting that Eq. (68) predicts an average number of "large energy transfer" collisions per primary independent of the primary's energy (compare with the inverse dependence on E in the "no shift" case (Eq. (67)) and in the solar problem (Eq. (57)). This behavior is a consequence of the fact that the falling off of the Klein-Nishina cross section with increasing E (Eq. (50)) is compensated for by the associated increase in the number of photons capable of producing large energy transfers

$$\left([n_n(u_c)]_{\text{eff}}^{\text{red shift}} \sim \frac{1}{u_c} \sim E\right).$$

Both integrals in Eq. (60) make finite contributions to the average energy loss $\Delta E_n{}^c$ in the distance R_0. The primary particle loses energy partly in an infinite number of small dribbles (first integral in Eqs. (52) and (60)) and partly in an occasional catastrophic collision (second integral in Eqs. (52) and (60)). Evaluating the integrals we get

$$-R_0\left[\frac{dE^c}{dR}\right]_{\substack{\text{small energy}\\ \text{transfer}}}^{\text{red shifted}} \cong \pi\left(\frac{e^2}{Mc^2}\right)^2 Q_n E \begin{cases} \cong 2\times 10^{-7}E \text{ (protons)} \\ \cong 0.8E \text{ (electrons)}, \end{cases} \tag{69}$$

$$-R_0\left[\frac{dE^c}{dR}\right]_{\substack{\text{large energy}\\ \text{transfer}}}^{\text{red shifted}} \cong 2\pi\left(\frac{e^2}{Mc^2}\right)^2 Q_n(E\ln 2) \begin{cases} \cong 3\times 10^{-7}E \text{ (protons)} \\ \cong 1.1E \text{ (electrons)}, \end{cases} \tag{70}$$

$$\begin{aligned}[\Delta E_n{}^c]^{\text{red shifted}} &\cong E\left[1-\exp\left(-2.4\pi\left(\frac{e^2}{Mc^2}\right)^2 Q_n\right)\right] \\ &\cong 5\times 10^{-7}E \text{ (protons)} \\ &\cong 0.85E \text{ (electrons)}. \end{aligned} \tag{71}$$

Equations (68)–(71) show that the distance R_0 in an intergalactic space filled with "red shifted" photons is almost perfectly transparent to protons, but is beginning to exhibit appreciable stopping power for electrons. As computed, the stopping power is not quite large enough to cut off completely a possible primary electron (or positron) spectrum above 10^{12} ev. However, the assumption that the particles reaching the earth have traveled a distance of just R_0 (in intergalactic space) is, of course, only an order of magnitude estimate. Possibly, also, the assumption of uniform conditions in space and time is seriously at fault. Thus for example, if all uncertainties in the evaluation of the energy loss are equivalent to replacing the distance traveled by $3.5R_0$, primary electrons would lose 99.9 percent of their initial energy before reaching the earth rather than 85 percent as given by Eq. (71). Thus the significant fact about the numerical coefficient for electrons in Eq. (71) is that it does not differ by an order of magnitude from the least value required to eliminate effectively the electron spectrum above 10^{12} ev.

In the light of the above remarks one sees a possible explanation for the apparent small number of high energy electrons ($E>10^{12}$ ev) among the particles striking the earth's atmosphere.[35] Even on the natural supposition that energetic protons and electrons were originally produced in comparable numbers, the attenuation due to Compton scattering, of the latter component in a travel time $\cong 1.85\times 10^9$ years (i.e., travel distance $\cong R_0$) may be sufficient to account for the observed preponderance of protons.[1]

The scattered photons produced in "large energy transfer" collisions give rise to an intergalactic cascade process. Such photons have energies of the order $0.7E$ and are therefore capable of producing electron-positron pairs by collision with the thermal photons. The cross section for this process, $\phi_{p-p}{}^{\pm}$,[2] may be ap-

[35] I. Pomeranchuk, J. Phys. U.S.S.R. 2, 65 (1940) shows that electrons with original energy $\gg 10^{17}$ ev will be degraded to $\cong 10^{17}$ ev by radiation losses in the earth's magnetic field, while the radiation losses for electrons of initial energy below 10^{17} ev are relatively insignificant.

proximated by

$$\phi_{p-p}{}^{\pm}(\epsilon_{sc},\ \epsilon,\ \theta)\begin{cases} 2\pi\left(\dfrac{e^2}{mc^2}\right)^2\dfrac{\ln 2x}{2x}, & \text{if } 2x>1 \\ 0, \text{ if } 2x<1, \end{cases} \tag{72}$$

in which $x=\epsilon_{sc}\epsilon(1+\cos\theta)/(mc^2)^2$, ϵ_{sc} and ϵ are the energies of the scattered photon and of the thermal photon, respectively, and $\pi-\theta$ is the angle between their directions of motion. Applying once more the methods used in deriving Eqs. (47), (51), and (59), we obtain

$$R_0\frac{dN^{\pm,\,p-p}}{dR}=R_0\int d\Omega\int_{\epsilon(\theta)}^{\infty} n(\epsilon,\theta)\times(1+\beta\cos\theta)\phi_{p-p}{}^{\pm}d\epsilon \cong 2\pi\left(\frac{e^2}{mc^2}\right)^2 Q_n\cong 1.6, \tag{73}$$

where $\epsilon(\theta)\equiv(mc^2)^2/2\epsilon_{sc}(1+\cos\theta)$, and the second line holds only for the "red shifted" distribution of thermal photons (compare with Eq. (68)). Thus the probability of pair creation by the high energy photon-thermal photon process is the same (about 0.8 in the distance R_0) as the probability of the "large energy transfer" collision between the original electron and the thermal photons. One can now visualize the formation of a cascade of electrons, positrons, and photons in intergalactic space with R_0 playing the role of the characteristic radiation length; the degradation of the energy of the original primary electron occurs in this cascade *via* the process of "large energy transfer" to scattered photons,[36] the subsequent and equally probable process of pair creation by these energetic photons in collisions with thermal photons[37] and the simultaneous and slightly less probable process (compare Eqs. (69) and (70)) of "small energy transfer" in electron-thermal photon collisions.[38]

The double Compton scattering (bremsstrahlung) process listed in the introduction (process 3) requires a brief discussion. In this case, there is initially a primary particle and a thermal photon; after the collision there are two energetic photons and a particle with reduced energy. The cross section for this process has been estimated by Heitler and Nordheim,[39] who find that it is smaller than the Klein-Nishina cross section by factors $e^2/\hbar c(\epsilon^*/Mc^2)^2$ and $e^2/\hbar c$, according to whether $\epsilon^*/Mc^2\ll$ or $\gg 1$. This estimate involves the restriction that both scattered photons have comparable energies, and in the case $\epsilon^*/Mc^2\gg 1$, the additional restriction that the two angles of scattering (in the rest frame) are not too small; in general these restrictions are satisfied if an appreciable energy transfer occurs. We may thus conclude that energy losses by the bremsstrahlung process are less probable than by Compton scattering in a ratio which does not exceed 1/137, so that the bremsstrahlung process is unimportant.

Much of the work reported in this paper was done during the summer of 1947 at the Brookhaven National Laboratory, Upton, New York. We wish to acknowledge many helpful discussions with members of the Brookhaven staff, in particular Dr. H. S. Snyder. We have also received a helpful communication from Dr. L. Spitzer, Jr.

APPENDIX A. THE "RADIOFREQUENCY" SPECTRUM

We have so far considered only the radiation originating from the individual stars under the simplifying assumption that the corresponding frequency distribution conforms closely to that of blackbody radiation at 6000°K. Actual measurements of extra-terrestrial radiofrequency noise, however, reveal an intensity with a pronounced maximum in the direction of the galactic center and greatly in excess of that computed from our assumption of dilute blackbody radiation.[16] The following mechanism has been proposed to account for this observation:[16] hydrogen atoms in interstellar space are ionized by stellar radiation. The resulting electron gas possesses a mean kinetic energy corresponding to a temperature $\cong$10,000° Abs. Inelastic collisions between the free electrons and protons and

[36] Analogous to photon creation by the bremsstrahlung process in an ordinary cascade.
[37] Analogous to pair creation by photons colliding with nuclei and electrons in an ordinary cascade.
[38] Analogous to the energy loss by ionization in an ordinary cascade.

[39] Reference 19, p. 178; W. Heitler and L. Nordheim, Physica **1059** (1934). See also O. Halpern and N. Kroll, Phys. Rev. **72**, 82 (1947); C. J. Eliezer, Proc. Roy. Soc. **A187**, 210 (1946); **191**, 133 (1947); R. Jost, Phys. Rev. **72**, 815 (1947).

recombination produce a radiation spectrum extending from the near infra-red down to 3×10^7 cycles/sec. with essentially constant intensity. Below 3×10^7 cycles/sec. the spectrum coincides with that of blackbody radiation at 10,000°K. With reasonable values for the electron-proton density, the computed intensity at 5 meters, for example, is then found to agree with the observations.

Guided by the plot of the theoretical spectrum we represent the intragalactic radiofrequency photon density by the simple distribution

$$n_g'(u)d\epsilon = B\frac{du}{u}e^{-\alpha u},$$

$$u \geqq 10^{-7}\ \text{ev}/kT = 2\times10^{-7} \equiv u_m$$

$$= B\frac{udu}{u_m^2}, \quad u < u_m, \quad \text{(A1)}$$

in which $B\sim 2\Omega/(10^3)^2\cdot 1$ ev$/hc\sim(\Omega/60)$ cm^{-3}. Here Ω is the effective solid angle subtended by the radiation incident on the earth. It is clear from the directional characteristics of the observed intensity that Ω is a small fraction of 4π. The value $\Omega\sim1$ steradians appears reasonable and certainly not in error by an order of magnitude. With $\Omega\sim1$ the total radiofrequency energy density has the value

$$U_g' = \int_0^\infty \epsilon n_g'(u)d\epsilon = \frac{BkT}{\alpha} \sim \frac{1}{120\alpha}\ \text{ev/cm}^3. \quad \text{(A2)}$$

We have estimated the total energy density U_g of intragalactic starlight at the solar system as 3×10^{-2} ev/cm^3 (see reference 9a). Since the energy source producing the free electron gas is stellar radiation it appears necessary to require $U_g'\ll U_g$. Consequently $\alpha\gg1$. The calculations presented below are based on the choice $\alpha=10$, which effectively cuts off the spectrum at $10u\sim1$ or $\epsilon\sim5\times10^{-2}$ ev. Fortunately, in the application to the cosmic-ray problem, the results do not depend in a critical manner on the choice of α.

The interaction of cosmic-ray primaries with the intragalactic "radiofrequency" spectrum is particularly interesting in conjunction with the hypothesis that the primaries are produced within the galaxy and prevented from escaping by an intragalactic magnetic field.[15] Adopting this hypothesis for the moment consider first the "rest-frame extreme relativistic" Compton scattering by an electron constrained to spiral indefinitely within the galaxy. Equations (60) and (34) can be adapted to the present problem by the substitution $n_g'(u)$ for $n_n(u)^{\text{no shift}}$; in this way one gets

$$[n_g'(u)]_{\text{eff}} = \frac{B}{kT}u\int_u^\infty \frac{e^{-\alpha v}}{y^3}dy, \quad u > u_m$$

$$\cong \frac{B}{kT}\frac{u}{u_m^2}\ln\frac{1.7u_m}{u}, \quad u < u_m, \quad \text{(A3)}$$

and

$$-R_0\frac{dE^e}{dR} \sim 2.5\pi\left(\frac{e^2}{Mc^2}\right)^2 R_0BE \sim 17E \quad \text{(A4)}$$

in the range $u_m\ll u_c/4\ll\alpha^{-1}\sim0.1$. For $u_c/4\ll u_m$, the second line of Eq. (A3) implies

$$-R_0\frac{dE}{dR} \sim 4\pi\left(\frac{e^2}{mc^2}\right)^2 R_0BE(u_c/4u_m)$$

$$\times\ln(1+4u_m/u_c)\ln(7u_m/u_c)$$

$$\sim 2\times10^{19}\ln(1+4u_m/u_c)\ln(7u_m/u_c)\ \text{ev}. \quad \text{(A5)}$$

From these relations it is apparent that the intensity of an electron component in the energy range 10^{12} ev$\ll E\ll5\times10^{17}$ ev is reduced by an extremely large factor in a time $\cong1.85\times10^9$ years. It will also be noted that α appears only in the determination of the upper limit on u_c. Thus, if α has been underestimated by a factor of 10, the lower limit on the energy range, 10^{12} ev, should be replaced by 10^{13} ev.

At the present stage of observational and theoretical study of the intragalactic "radiofrequency" noise and of a possible intragalactic magnetic field one may properly hesitate to draw far reaching conclusions from these numerical results. But granting the various assumptions one can understand why the cosmic radiation incident on the earth's atmosphere should contain few electrons (and positrons) in the energy range 10^{12} ev $\ll E\ll5\times10^{17}$ ev. On the other hand, this theory does not provide a mechanism for the elimination of electrons with energies $\gg5\times10^{17}$ ev.[35] Electrons of such high energy, however, must, in any event, be considered sepa-

rately since the galactic magnetic field which has been proposed[15] is not strong enough to constrain within the galaxy particles with energies in excess of 10^{16} ev.[40]

We now apply a principle of uniformity and postulate the existence of the "radiofrequency" spectrum as a feature common to all or nearly all galaxies. There must then exist an intergalactic photon number density $n_n'(u)d\epsilon$ related to the intragalactic "radiofrequency" photons in the same way that $n_n(u)d\epsilon$ is related to the intragalactic thermal photons. These considerations suggest the relations (in the range $u>u_m$),

$$n_n'(u)d\epsilon \sim \frac{1}{10}B\frac{du}{u}e^{-\alpha u} \text{ (no shift)} \quad \text{(A6)}$$

$$\sim \frac{1}{10}B\frac{du}{u}\int_u^\infty \frac{e^{-\alpha y}}{y}dy \text{ (red shifted)}, \quad \text{(A7)}$$

and, using Eqs. (A6), (A7), and (34),

$$[n_n'(u)]_{\text{eff}}^{\text{no shift}} \sim \frac{B}{20kT}\frac{1}{u}, \quad u_m \ll u \ll \alpha^{-1}, \quad \text{(A8)}$$

$$[n_n'(u)]_{\text{eff}}^{\text{red shifted}} \sim \frac{B}{20kT}\frac{1}{u}\ln\left(\frac{1}{3\alpha u}\right), \quad u_m \ll u \ll \alpha^{-1}. \quad \text{(A9)}$$

The factor 1/10 has been taken from the estimated ratio of the thermal photon energy densities in intragalactic and intergalactic space (Eqs. (5a) and (13)); the same factor is assumed to give the ratio of the corresponding radiofrequency energy densities. We substitute $[n_n'(u)]_{\text{eff}}$ for $[n_n(u)]_{\text{eff}}$ in Eq. (60) and compute the following results for electrons:

$$-R_0\frac{dE^e}{dR} \cong 1.7E \text{ (no shift)} \quad \text{(A10)}$$

$$\cong 1.7E\ln\left(\frac{1}{3\alpha u_c}\right) \text{ (red shifted)} \quad \text{(A11)}$$

in the range $u_m \ll u_c/4 \ll \alpha^{-1}$.

Because of the accidental numerical coincidence ($1.9E$ from Eqs. (69) and (70) and $1.7E$ in Eq. (A10)) the discussion of the stopping power of the "red shifted" thermal photon distribution following Eq. (71) can be immediately applied to the "no shift radiofrequency" distribution with the added restriction $E<5\times10^{17}$ ev in the latter case. Further, the presence of a "red shifted radiofrequency" spectrum renders distances R_0 in intergalactic space practically impenetrable to electrons with energies between 10^{12} and 5×10^{17} ev. For example, Eq. (A11) shows that

$$[\Delta E_n{}^e]_{\text{radiofreq.}}^{\text{red shifted}} = E\left[1-\left(\frac{3\alpha(mc^2)^2}{kTE}\right)^{0.82}\right]$$

so that at $E=10^{17}$ ev the electron loses 99.99 percent of its original energy in the distance R_0.

At still higher energies, however, the rate of energy loss becomes approximately proportional to the logarithm of the energy squared (as in Eq. (A5)), so that above $E=10^{20}$ ev, the energy loss in the distance R_0 is relatively small.

APPENDIX B. ANOMALOUS COMPTON SCATTERING BY THE MESON CHARGE CLOUD SURROUNDING THE PHOTON

We attempt in this appendix to estimate the effect of the meson cloud surrounding the proton on the scattering of photons. At small photon energies ($\epsilon^* \ll \mu c^2 \ll Mc^2$; $\mu \cong \frac{1}{10}M$) the effect of the meson cloud can presumably be expressed as an interaction between the anomalous magnetic moment of the proton and the electromagnetic field of the photons. This interaction can be described phenomenologically by a Pauli term in the Dirac equation of the proton, *viz.*:

$$-el[\beta\sigma\cdot\mathbf{H}-i\beta\alpha\cdot\mathbf{E}],^{41} \quad \text{(B1)}$$

and the resulting additional scattering estimated by a calculation similar to the Casimir (spur summation) derivation of the Klein-Nishina formula.[19] In this way, one obtains the Compton (anomalous) magnetic moment (cmm) cross

[40] The cascade formation discussed earlier is not an immediate complicating factor in the preceding discussion, since the cosmic "radiation length" is much greater than the galactic dimensions. However, the energetic photons produced within the galaxy collide with thermal photons in intergalactic space and in turn produce energetic electron-positron pairs. These pairs then constitute a particle component in intergalactic space having energies smaller than, but still comparable with, those of the primary galactic electrons.

[41] Here, $el=1.79e\hbar/2Mc$ is the anomalous magnetic moment of the proton; β, α, σ are Dirac matrices; $\mathbf{E}$, $\mathbf{H}$ are the external electric and magnetic fields.

section,[42]

$$\phi_{\text{emm}}{}^*(\epsilon^*)\sim\begin{cases}\pi\left(\frac{e^2}{Mc^2}\right)^2\left(\frac{\epsilon^*}{Mc^2}\right)^2, & \text{if } \frac{\epsilon^*}{Mc^2}\ll 1\\ \pi\left(\frac{e^2}{Mc^2}\right)^2\left(\frac{\epsilon^*}{Mc^2}\right), & \text{if } \frac{\epsilon^*}{Mc^2}\gg 1\end{cases}\tag{B2}$$

The continued linear increase of $\phi_{\text{emm}}{}^*(\epsilon^*)$ with ϵ^* in the extreme relativistic region is usually considered physically unreasonable. Certainly the interaction between the meson cloud and an external electromagnetic field cannot be represented adequately at all frequencies by the phenomenological device of a Pauli term with a constant l. In reality the effective value of the anomalous magnetic moment may well decrease with increasing frequency (for $\epsilon^* > \mu c^2$ or perhaps Mc^2) giving a scattering cross section which decreases (or remains constant) with increasing photon energy. Qualitatively such a behavior is indeed obtained in a classical non-relativistic theory if electromagnetic radiation damping is included in the calculation of the cross section. Thus, consider a point magnetic dipole with magnetic moment $e\mathbf{l}$ and spin angular momentum $\mathbf{s}$ (both of constant magnitude), the dipole being subjected to a driving torque $e\mathbf{l}\times\mathbf{H}$ (arising from an external electromagnetic field of angular frequency ω^*) and a damping torque

$$-\frac{2}{3c^3}\left(\frac{e|\mathbf{l}|}{|\mathbf{s}|}\right)\frac{d^3}{dt^3}(e\mathbf{l})$$

(arising from radiation resistance); the resulting cross section is then,[43]

$$\phi_{\text{emm}}{}^*(\omega^*)]=4\pi\left(\frac{c}{\omega^*}\right)^2\frac{\frac{4}{9}\frac{(el)^4}{(\mathbf{s})^2}\frac{(\omega^*)^4}{c^6}}{1+\frac{4}{9}\frac{(el)^4}{(\mathbf{s})^2}\frac{(\omega^*)^4}{c^6}}\tag{B3}$$

which, with the replacements $\epsilon^*=\hbar\omega^*$, $(\mathbf{s})^2=\frac{3}{4}$, $el\cong 0.9e\hbar/Mc$, becomes

$$\phi_{\text{emm}}{}^*(\epsilon^*)]_{\text{class}}\cong\begin{cases}1.6\pi\left(\frac{e^2}{Mc^2}\right)^2\left(\frac{\epsilon^*}{Mc^2}\right)^2, & \text{if } \epsilon^*\ll\left(\frac{hc}{e^2}\right)^{\frac{1}{4}}Mc^2\\ 4\pi\left(\frac{hc}{e^2}\right)^2\left(\frac{e^2}{Mc^2}\right)^2\left(\frac{Mc^2}{\epsilon^*}\right)^2, & \text{if } \epsilon^*\gg\left(\frac{hc}{e^2}\right)^{\frac{1}{4}}Mc^2.\end{cases}\tag{B4}$$

If one now supposes that essentially the same damping denominator occurs in the quantum relativistic as in the classical non-relativistic case[44] one sees from Eq. (B2) that the maximum value of $\phi_{\text{emm}}{}^*(\epsilon^*)$ is

$$\phi_{\text{emm}}{}^*(\epsilon^*)\sim\pi\left(\frac{e^2}{Mc^2}\right)^2\left(\frac{hc}{e^2}\right)^{\frac{1}{2}}$$

$$\text{at } \epsilon^*\sim\left(\frac{hc}{e^2}\right)^{\frac{1}{4}}Mc^2\tag{B5}$$

and is thus larger than the Klein-Nishina cross section (at the same energy) by a factor $\sim\hbar c/e^2=137$. Since Compton scattering effects for protons, calculated from the Klein-Nishina formula (Eq. (50)) are quite negligible, even on an intergalactic scale (see Eqs. (65)–(71)), it is clear that the above factor of 137 can hardly alter the situation.

However, in addition to the effects just estimated, there is probably present at high photon energies ($\epsilon^*\gg\mu c^2$) a manifestation of the meson charge cloud which cannot be reduced to an

[42] H. C. Corben, quoted in W. Pauli, Rev. Mod. Phys. 13, 203 (1941), Tables III and IIIa, has given exact formulae for the Compton scattering cross sections of particles of spin ½ and arbitrary magnetic moment which check the estimates in Eq. (B2) to within numerical factors of the order one. See also S. B. Batdorf and R. Thomas, Phys. Rev. 59, 621 (1941).

[43] See, for example, H. J. Bhabha and H. C. Corben, Proc. Roy. Soc. A178, 273 (1941).

[44] The argument of Heitler (see reference 20, p. 250), anent the negligible influence of the radiation resistance damping on the various cross sections in quantum electrodynamics, is applicable only to processes involving the interaction of the electric charge with the electromagnetic field, in which case the interaction energy matrix elements are proportional to $(\epsilon^*)^{-\frac{1}{2}}$. On the other hand, a (magnetic) dipole interacting with the field possesses interaction energy matrix elements proportional to $(\epsilon^*)^{\frac{1}{2}}$. This last fact vitiates the use of the perturbation theory in the derivation of Eq. (B2) for $\epsilon^* > (\hbar c/e^2)Mc^2$ (see J. R. Oppenheimer, quoted in Pauli, reference 50a) which however is greater than the ϵ^* at which damping first becomes important in Eqs. (B3) and (B4).

effective frequency dependent anomalous magnetic moment. This manifestation involves an additional photon scattering arising from the virtual creation and destruction of mesons by the photons ("virtual meson scattering" (vms) processes); thus the original photon may be absorbed by the proton with the emission of a virtual meson—the latter is then reabsorbed by the resulting neutron with emission of a photon different in general from the original one. The corresponding cross section, $\phi_{vms}{}^*(\epsilon^*)$, has been estimated by means of Heitler's quantum theory of damping,[45] and found to have the value,

$$\phi_{vms}{}^*(\epsilon^*)\cong\frac{\pi^2}{2^4}\left(\frac{eg}{\hbar c}\right)\left(\frac{\hbar}{\mu c}\right)^2\cong 5\times 10^{-27}\ \text{cm}^2. \quad \text{(B6)}$$

for $\epsilon^*\gg\mu c^2$; other estimates of the same cross section (e.g., in a weak coupling meson theory) involve other more or less arbitrary cut-off procedures, and seem to yield smaller results.

In the absence of more certain information we shall use the $\phi_{vms}{}^*(\epsilon^*)$ of Eq. (B6) to estimate the number of scattered photons per primary $N_s{}^{vms}$ and the corresponding energy loss $\Delta E_s{}^{vms}$ in the radial fall through the sun's radiation field. Equations (47) and (B6) yield, for $\epsilon^*\gg\mu c^2$

$$\left(\text{i.e., } E\gg\frac{Mc^2\mu c^2}{kT}\cong 2\times 10^{17}\ \text{ev}\right), \quad \text{(B7)}$$

$$N_s{}^{vms}\cong 2\left[\frac{\pi^2}{2^4}\left(\frac{eg}{\hbar c}\right)\left(\frac{\hbar}{\mu c}\right)^2\right]Q_s\cong 3\times 10^{-6}.$$

On the other hand, the calculation of $\Delta E_s{}^{vms}$ from Eq. (48) requires knowledge of the angular dependence of the "virtual meson scattering" which has not yet been computed. We observe that an angular dependence more pronounced than that of the Klein-Nishina cross section is unlikely since the matrix elements for the virtual emission and absorption of the mesons have a moderate, e.g., cosine, dependence on the angle between the directions of motion of the incident and scattered photons. It is thus probable that the scattered photon carries away a substantial fraction of the proton's energy (in the earth's frame) over the entire range of validity of Eq. (B7). Moreover the "substantial fraction" may well increase to over 80–90 percent in the range $E\gg(Mc^2)^2/kT=2\times 10^{18}$ ev.

It is clear that the above number of collisions per primary and the associated energy loss may well be important on an intergalactic scale (replacement of Q_s in Eq. (B7) by $Q_n\cong 10^4 Q_s$). There is thus need for an adequate theory of the differential and total scattering cross sections in proton-photon collisions at high energies.

We conclude this appendix by raising the question of the effect of the meson cloud on the double Compton scattering (bremsstrahlung in proton-photon collisions—process 3 of introduction). No calculation of this effect exists, but it seems possible that for $\epsilon^*\gg\mu c^2$ (or Mc^2?) the ratio of the double and single Compton scattering cross sections exceeds 1/137, the value which is appropriate to lower energies.

APPENDIX C. COLLISIONS OF ENERGETIC PROTONS, ELECTRONS, AND PHOTONS WITH INTERSTELLAR AND INTERGALACTIC DIFFUSE MATTER

The amount and chemical composition of diffuse matter in space is not readily accessible to measurement; nevertheless rough estimates have been obtained from the interpretation of astronomical observations. For the sake of definiteness in the statement of our results we adopt the values:

$$\begin{aligned}&\text{Interstellar(Intragalactic)}\sim 1\ \text{H atom/cm}^3.\\ &\text{Intergalactic}\ \sim 10^{-5}\ \text{H atom/cm}^3.\end{aligned} \quad \text{(C1)}$$

These estimates at least do not contradict any of the available astrophysical evidence.[46]

We also need the following cross sections:

Meson creation in primary proton—H atom collisions

$$\phi_m(E)\cong 10(\hbar/\mu c)^2\cong 4\times 10^{-25}\ \text{cm}^2.[47] \quad \text{(C2)}$$

Photon creation (bremsstrahlung) in primary electron—H atom collisions—

[45] See Hamilton and Peng, reference 30. The theory which gives this comparatively large value for $\phi_{vms}{}^*$ also predicts an equally large cross section for the creation of single mesons in photon-proton collisions—see, however, reference 34.

[46] L. Spitzer, Ap. J. 93, 369 (1941), and private communication.

[47] See W. Heitler and P. Walsh, Rev. Mod. Phys. 17, 252 (1945). Other estimates of $\phi_m(E)$ give results of more or less the same order of magnitude, essentially the cross-sectional dimensions of the meson charge cloud surrounding the proton. The observed distance traveled by primary protons in the atmosphere before absorption caused by meson creation is of the order of 100 g/cm², in agreement with Eq. (C2).

$$\phi_p(E)\cong 20\frac{e^2}{\hbar c}\left(\frac{e^2}{mc^2}\right)^2\cong 1.2\times 10^{-26}\ \text{cm}^2.^{48} \quad \text{(C2')}$$

These cross sections are considerably larger than those for any of the other processes which may occur in the collisions under consideration, e.g., electron-positron pair creation in primary proton —H atom collisions.

We can now estimate the average number of mesons N_g^m and N_n^m created in the passage of a primary proton, across the distance $R_g(\cong 10^4$ l.y.) in the local galaxy, and across the distance $R_0(\cong 1.85\times 10^9$ l.y.) in intergalactic space. One has from Eqs. (C1), (C2),

$$N_g^m\sim 4\times 10^{-3},\quad N_n^m\sim 10^{-2}. \quad \text{(C3)}$$

The neutrons and mesons produced in such collisions eventually decay, leaving as final products protons and electron-positron pairs. Also, the number of bremsstrahlung photons produced in primary electron—H atom collisions is smaller than the corresponding number of mesons by a factor $\cong 35$ (cf. Eq. (C2)). Thus it seems that the intragalactic and intergalactic matter does not constitute a serious obstacle to the cosmic-ray primaries,[49] subject, of course, to the order of magnitude validity of the matter densities and cross sections listed in Eqs. (C1) and (C2); conversely, any definite information about the nature and energy distribution of the primary particles may be employed to set limits on the cross sections and on the amount of intragalactic and, particularly, intergalactic matter.

For completeness we estimate the frequency of the various possible secondary processes. First of all, the preceding results for primary electrons can be applied immediately to secondary electron-positron pairs produced, for example, in primary proton-thermal photon collisions. Equations (C2), (C1) then show that photon creation by these electrons and positrons in collisions with diffuse matter is unimportant. Finally the very energetic Compton scattered photons (arising from primary particle—thermal photon collisions) may create electron-positron pairs in collisions with the diffuse matter; however, the pair creation cross section is of the same order as that from bremsstrahlung so that the number of such pairs, even on an intergalactic scale, is small.

[48] See reference 19, pp. 161–177.

[49] From Eq. (C3) it appears that protons and electrons constrained to move within the local galaxy by intragalactic magnetic fields (see reference 15a) would experience many meson producing and photon producing collisions in a period $\cong 1.85\times 10^9$ years. One thus finds another mechanism to eliminate the primary electron component. (The meson producing collisions of the protons ultimately only degrade the energy of the latter.) The high energy bremsstrahlung photons would, on this picture, escape from the galaxy and in turn produce energetic electron-positron pairs by collisions with thermal photons in intergalactic space (see reference 48b).

GLOSSARY OF FREQUENTLY USED SYMBOLS

η—solar constant

R_e—radius of the earth's orbit

R_g—linear dimension of a galaxy ($\sim 10^4$ light years (l.y.))

R_0—1.85×10^9 l.y. (red shift parameter)

N—effective number of stars in a galaxy

$\mathfrak{N}$—average number of nebulae per unit volume

T—effective temperature of the sun's surface

ϵ—energy of a thermal photon in the earth reference frame; also $u\equiv\epsilon/kT$

$n_{s,g,n}(u)d\epsilon$—number of thermal photons per unit volume in the energy range $d\epsilon$ from solar radiation at the earth's orbit (s), starlight averaged over the galaxy (g), and nebular radiation in intergalactic space (n). The spaces s, g, and n are defined precisely in the text.

$N^{\pm}_{g,s,n}$—number of collisions between a primary particle and thermal photons resulting in electron-positron pair production in the spaces s, g, and n.

$N^c_{s,g,n}$—number of Compton collisions between a primary particle and thermal photons in the spaces s, g, and n.

$Q_{s,g,n}$—number of photons in cylinder of unit cross section in the spaces s, g, and n

M—rest mass of the cosmic-ray primary (electron or proton)

m—electron rest mass

E—energy of the cosmic-ray primary

$\gamma\equiv(1-\beta^2)^{-\frac{1}{2}}\equiv E/Mc^2$

$u_\pm\equiv mc^2Mc^2/EkT\cong 5\times 10^5/\gamma$

$u_c\equiv(Mc^2)^2/EkT\cong 10^9/\gamma$ (protons) or $\cong 5\times 10^5/\gamma$ (electrons)

PHYSICAL REVIEW VOLUME 73, NUMBER 5 MARCH 1, 1948

The Microwave Spectroscopy of Paramagnetic Salts; the Spectrum of Chromic Alum

P. R. Weiss
Physics Department, Rutgers University, New Brunswick, New Jersey
(Received November 3, 1947)

Some measurements on the resonance absorption of chrome alum are analyzed for the purpose of obtaining a quantitative estimate of the splitting of the lowest state of the chromic ion by the electric field in the crystal. It is found that a small cylindrical field in addition to the large cubic field present is sufficient to account for the structure of the absorption curves and that the magnitude of the splitting is $0.15 \pm .01$ cm^{-1}. It is pointed out that the methods used in the case of chrome alum can be applied to other similar salts such as iron alum and the hydrated gadolinium salts.

I. INTRODUCTION

A COMMON property of the salts used in the process of adiabatic demagnetization, namely, hydrated salts of the iron group and chemically dilute gadolinum salts, is that the spin of the paramagnetic ion is free to orient itself at low temperatures in a magnetic field. This permits the entropy of the salt to be decreased by the application of a magnetic field and the subsequent decrease in temperature when the field is removed adiabatically. The mechanism by which the orbital angular momentum is quenched and the spin left free is generally accepted to be the Stark splitting of the orbital states of the ions by the electric field of the surrounding water molecules. It is clear, however, that the spins cannot be completely free for then, overlooking the question of the relaxation time, the specific heat (in the absence of a magnetic field) would be zero and absolute zero would be attained on conclusion of the process. This hindering of the orientation of the spin, and the corresponding specific heat, arise from two sources which reveal themselves in somewhat different temperature regions, both lower than 0.1 degree abs. These are a fine splitting of the lowest energy state of the paramagnetic ion by non-cubic electric fields of the surrounding ions and a finer splitting because of the magnetic interaction of the spins. The nature of the latter is well known and, although its mathematical treatment is complex, it involves no unknown parameters. The fine splitting due to the electric fields, however, does involve unknown parameters, namely, the symmetry of the field and the magnitude of the splitting.

The lack of freedom of the spin in orienting itself also has the consequence that the Curie temperature computed from the susceptibility of the salt on the supposition that the spin is perfectly free is not the true temperature. Any theoretical procedure which attempts to determine the thermodynamic from the Curie temperature must necessarily involve the parameters of the electric field. Some estimates of these have been computed by Van Vleck[1] on the basis of assumed distributions of charges in the neighborhood of the paramagnetic ion but these at best are meant to obtain an order of magnitude. A different procedure is to deduce the magnitude of the splitting from measurements of specific heat made at very low temperatures. The results of these computations[2] which must of course separate the two contributions to the specific heat show the splitting by the electric field to be of the order of several tenths of a wave number. For example, the splitting in potassium chrome alum is taken to be due to a cylindrically symmetric electric field and found to be 0.12 cm^{-1}.

In the present paper we present some computations to evaluate this splitting in the case of ammonium chrome alum from measurements[3] made (at room temperatures) on the resonance absorption at 3.20 cm. These measurements have been made on both single crystals and powder and the results can be explained by a splitting

[1] J. H. Van Vleck, J. Chem. Phys. **7**, 61 and 72 (1939).
[2] M. H. Hebb and E. M. Purcell, J. Chem. Phys. **5**, 338 (1937).
[3] P. R. Weiss, C. A. Whitmer, H. C. Torrey, and Jen-Sen Hsiang, Phys. Rev. **72**, 975 (1947).

of 0.15 cm^{-1} induced by a cylindrically symmetric field.

The experimental method and the analysis of the measurements as presented here are applicable to other salts such as the other alums of the iron group, the hydrated gadolinium salts, and some of the Tutton salts. An important one of these is ferric alum. Preliminary measurements on *diluted* ferric ammonium alum indicate the splitting to be a great deal less than has been generally accepted. A detailed discussion of this salt in which the mechanism of the fine splitting is not so clear as in the case of chrome alum is being delayed until more complete experimental data have been obtained.

In the experimental arrangement[3] the absorption is measured as a function of the magnitude of a magnetic field applied perpendicular to the r-f magnetic field. The latter had a constant frequency of 9375 mc/sec. Two different orientations of single crystals relative to the d.c. field were used: (I) the field perpendicular to a (100) plane and (II) the field perpendicular to a (111) plane. In the second case, and also when the powder was used, several absorption maxima were observed which arise as follows: Because of the splitting the energy levels of the spin ($S=\frac{3}{2}$) in the d.c. field are displaced from those of a perfectly free spin. Consequently, different pairs of levels are brought into the resonance separation by different values of the applied field. When this occurs and the corresponding transition is allowed a maximum in the absorption is measured. The spin-spin interaction serves to broaden the absorption peaks. The positions of the peaks lead to a value of 1.97 for the effective g-value and 0.15 cm^{-1} for the splitting.

II. THE CRYSTALLINE STARK SPLITTING

The spin energy levels of chrome alum in a magnetic field have already been stated by Broer[4] in connection with a different problem. In view of the high precision possible in the measurements of absorption it is worth computing the effective g-value of the spins and the magnitude of the terms quadratic in the applied field H. The x-ray analysis[5] shows that each chrome ion (Cr^{+++}) is surrounded by an octahedron of water molecules. These produce a large cubic electric field which quenches the orbital angular momentum of the normal $4F$ state of the chromic ion. However the analysis shows the symmetry about the ion is actually trigonal rather than cubic with the axis of the trigonal field along a body diagonal of the unit cube. There are four such ions per unit cell, the trigonal axes of the different ions being along the different body diagonals of the unit cell. The trigonal field about a single ion is taken to be[6]

$$Q\{(10)^{\frac{1}{2}}(Y_4^{+3}-Y_4^{-3})-(7)^{\frac{1}{2}}Y_4^0\}+aY_2^0, \quad (1)$$

where the Y's are the surface harmonics whose axes are taken along the trigonal axis of symmetry. The terms in Q represent the cubic field, that in a a field of cylindrical symmetry. In addition to this potential there are to be considered the spin orbit coupling $\lambda(L\cdot S)$ and the magnetic energy $\beta(L_z+2S_z)H_z$ (β is the Bohr magneton, the z axis is along the magnetic field which is parallel to the trigonal axis of symmetry). The cubic representation of wave functions which diagonalizes the terms in Q can be obtained in a straightforward fashion. The terms in a, the spin-orbit coupling, and the magnetic energy are then treated as perturbations. A second order perturbation computation yields the following results: (I) the separation between the levels is

$$\delta=60\bar{a}\lambda^2/(15\bar{Q})^2, \quad (2)$$

where $\bar{a}$ and $\bar{Q}$ are certain averages of a and Q over radial parts of the wave functions; (II) the effective g-value is

$$g=2\{1-4\lambda/(15\bar{Q}+5\bar{a})\}; \quad (3)$$

(III) the terms quadratic in H_z are

$$-4\beta^2H_z^2/15\bar{Q}\{1-O(5\lambda/15\bar{Q})\}, \quad (4)$$

where O indicates "of the order of." $15\bar{Q}$ is the splitting in the orbital state, between the lowest and next highest state, induced by the cubic field alone. The spin-orbit coupling parameter λ is known from spectroscopic data to be 87 cm^{-1}. Consequently, measurements of δ and g determine, though with little precision, $\bar{a}$ and $\bar{Q}$.

[4] L. J. F. Broer, Physica 9, 547 (1942).
[5] H. Lipson and C. A. Beevers, Proc. Roy. Soc. 148A, 664 (1935).
[6] J. Becquerel and W. Opechowski, Physica 6, 1039 (1939).

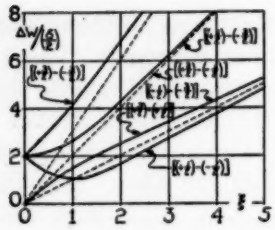

FIG. 1. Level separations (in units of $\delta/2$) as function of $\xi=2g\beta H/\delta$ in orientation I in which H is perpendicular to a (100) plane. The labeling is appropriate to very high field values.

Using $\delta=0.15$ cm^{-1} and $g=1.97$, the values are $\bar{a}=180$ cm^{-1} and $15\bar{Q}=23{,}000$ cm^{-1}. Finally, the terms quadratic in H_z are small and such terms in $1/\bar{Q}$ cancel in the separation between neighboring levels. To a high degree of precision the quadratic terms can be neglected. In view of this, the lowest state, a spin quadruplet, can be treated separately, the g-value being determined by (3). The Hamiltonian of this state can readily be shown to be[7]

$$\begin{array}{cccc} A_1 & B & C & O \\ B^* & A_2 & O & C \\ C^* & O & A_3 & -B \\ O & C^* & -B^* & A_4, \end{array} \qquad (5)$$

with

$$A_{1\atop 4}=\pm\frac{3}{2}g\beta H+\frac{\delta}{4}(1-3\cos^2\theta),$$

$$A_{2\atop 3}=\pm\frac{1}{2}g\beta H-\frac{\delta}{4}(1-3\cos^2\theta),$$

$$B=-\frac{\delta}{2}\sqrt{3}\sin\theta\cos\theta\exp-i\varphi,$$

$$C=-\frac{\delta}{4}\sqrt{3}\sin^2\theta\exp-2i\varphi,$$

θ and φ are the polar and azimuthal angles made by H with respect to the trigonal axis of symmetry.

III. SINGLE CRYSTALS

In orientation I of the single crystal, the magnetic field is perpendicular to a (100) plane, along one of the crystalline axes. In this orientation all four ions of the unit cell are equivalent in that the trigonal axes of symmetry all make the same polar angle ($\theta=\cos^{-1}1/\sqrt{3}=54°43'$) with the magnetic field. This is one of the three values of θ for which the secular equation of the Hamiltonian (5) can be solved exactly. The energy levels are,[4] in units of $(\delta/2)$,

$$W=\pm\{(\tfrac{5}{4}\xi^2+1)\pm(\xi^4+3\xi^2)^{\frac{1}{2}}\}^{\frac{1}{2}}. \qquad (6)$$

Here ξ is the magnetic energy in units of $\delta/2$, $\xi=2g\beta H/\delta$. The level separations are plotted in Fig. 1 as a function of ξ, the labeling of the curves being taken according to the nature of the spin levels at high values of the magnetic field, namely where the Paschen-Back effect is complete. Not all the transitions shown are allowed, however, over the complete range of ξ. The strengths of the different transitions are proportional to the absolute value square of the corresponding matrix elements of the perpendicular (to H) component of the spin. These have been obtained by a numerical computation at several values of ξ of the transformation matrix which diagonalizes the Hamiltonian and then applying this matrix to obtain the appropriate spin matrix. These strengths are shown in Fig. 2. For values of $\xi=2$ and greater the allowed transitions and their strengths are essentially the same as for a perfectly free spin. An additional fact to be pointed out is that because of the symmetry of the arrangement of the four axes of symmetry, no changes occur on rotating the crystal about the field direction.

On using the value $\delta=0.15$ cm^{-1} for the separation and an r-f frequency of 9375 mc/sec., the

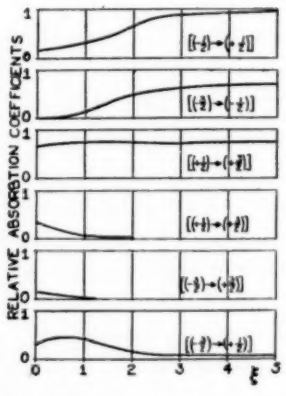

FIG. 2. Quantities proportional to strengths of absorptions as functions of ξ in orientation I. The labeling is appropriate to very high field values.

[7] H. A. Kramers, Proc. Acad. Sci. Amsterdam **33**, 953 (1930); **34**, 965, (1931).

resonance separation is found to be $\Delta W=4.17$. According to Figs. 1 and 2 the only strong transitions allowed are the $(-\frac{1}{2})\rightarrow(+\frac{1}{2})$ transitions at $\xi=4.37$ and the $(-\frac{3}{2})\rightarrow(-\frac{1}{2})$ and $(+\frac{1}{2})\rightarrow(+\frac{3}{2})$ transitions at $\xi=3.85$. Taking into account the fact that there are two coincident transitions at $\xi=3.85$, the ratio of the strength at $\xi=3.85$ to that at 4.37 is 5/3. The separation between the two is 420 gauss. The width of a single line is due practically entirely to spin-spin interaction and has a half-width at half maximum of[8]

$$\Delta H=N(2.40)^{\frac{1}{2}}g\beta S(S+1),\quad =230 \text{ gauss}. \tag{7}$$

Here N is the number of ions per cc and S is the spin per ion ($S=\frac{3}{2}$). The separation is sufficiently large compared to the widths of the lines to make the two absorption lines apparent. Actually an interference* in the absorption of the two lines is possible in the experimental arrangement used. When this is taken into account the absorption curve should have the appearance shown in Fig. 3. The interference effects emphasize the separation of the two lines. The results of measurements in this orientation are shown in Fig. 4, where only one peak is apparent. The reason for this is that insufficient care was taken in aligning the crystal in this orientation. When $\theta=\cos^{-1}1/\sqrt{3}$ the diagonal elements of the Hamiltonian are those of a perfectly free spin. Consequently the distortion of the energy levels which give rise to the separate lines arises entirely from the off-diagonal elements. A misalignment of the crystal introduces diagonal elements causing three absorption peaks for each ion. Since the misalignment could easily be different for all four ions per unit cell, there could be twelve absorption peaks all close together. The net result in such an event would be a single peak, as shown in Fig. 4, rather than two separate lines.

In orientation II the magnetic field is along one of the body diagonals of the unit cube. There are then two different types of atoms: one for which $\theta=0°$ and three for which $\theta=70°33'$.

[8] J. H. Van Vleck, J. Chem. Phys. **5**, 320 (1937).

* I am indebted to Dr. H. C. Torrey for pointing out to me this possibility. It will be considered in detail in a forthcoming paper from this laboratory concerned with the experimental method.

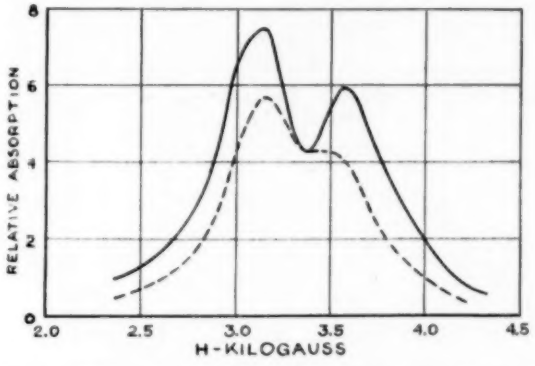

FIG. 3. Theoretical appearance of two absorption peaks when incident frequency is 9375 mc/sec. and orientation is I. The full-line curve includes the interference effects, the dashed curve does not take these into account.

The energy levels for the atom for which $\theta=0$ are

$$\pm\tfrac{3}{2}\xi-1,\quad \pm\tfrac{1}{2}\xi+1. \tag{8}$$

The separations are shown in Fig. 5 by the curves labeled I. The energy values for the case $\theta=70°33'$ cannot be obtained exactly; for $\xi\geq 2$ they were obtained by a second-order perturbation procedure while the values for $\xi<2$ were obtained from the secular equation by numerical computation. The corresponding separations are shown in Fig. 5 by the curves labelled II. The only transitions allowed in the case $\theta=0$ are those involving neighboring levels and the strengths of these are proportional to

$$[+\tfrac{1}{2}\rightarrow+\tfrac{3}{2}]:3,\quad [-\tfrac{1}{2}\rightarrow+\tfrac{1}{2}]:4,\quad [-\tfrac{3}{2}\rightarrow-\tfrac{1}{2}]:3. \tag{9}$$

In the case $\theta=70°33'$ at high fields only these transitions are allowed and their strengths are the same. At lower fields, the strengths of these

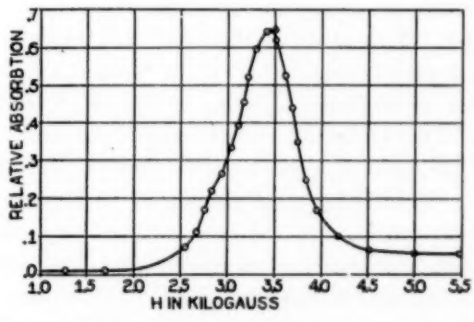

FIG. 4. Measured relative absorption as function of H in orientation I.

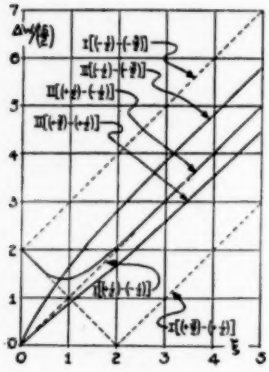

FIG. 5. Level separations (in units of $\delta/2$) as function of ξ in orientation II in which field is perpendicular to a (111) plane. The curves labeled I belong to atoms the axes of whose cylindrical electric fields make a polar angle $\theta=0$ with the magnetic field; the curves labeled II belong to atoms for which $\theta=70°33'$.

decrease and those of transitions between other than neighboring levels increases. As in the orientation (I) however, these changes are small until the field is decreased to the region $\xi=3$. A second-order perturbation theory in $1/\xi$ gives the results shown in Table I for the variation of the strengths in high fields.

The transitions allowed when δ is taken as 0.15 cm^{-1} and the r-f frequency is 9375 mc/sec. are shown in Table II. Columns 1 and 2 give the nature of the transition along with the appropriate value of θ; column 3, the value of ξ, column 4, the value of H at which the absorption peak occurs; column 5 gives the relative strength of the peak and takes into account the 3 to 1 weighting that must be assigned to the two different types of atoms.

For both values of θ the separation $(-\frac{1}{2})\rightarrow(+\frac{1}{2})$ is at these field strengths unaffected by the cylindrical field and in view of the fact that the corresponding absorption peak occurs at $H=3400$, we conclude that the effective g-value is 1.97. The values of the field strengths in column 4 were computed with this value of g. These values are shown in Fig. 6 by short vertical lines. The value of $\delta=0.15$ cm^{-1} was found by trial to give the best fit to the experimental curve. This is by trial estimated to be accurate to 0.01 cm^{-1}. The relative intensities listed in column 5 do not correspond to the strengths of the corresponding absorption peaks shown in Fig. 6. Because of the instability of the oscillator the magnitudes of peaks as measured are not reliable and this type of comparison must await the results of improved measurements. It should be noted that slight misalignments in this orientation do not smear out the absorption peaks as was the case in orientation I. In addition, this orientation is preferable because the natural growth of the crystals is along (111) planes and makes an accurate alignment of the magnetic field perpendicular to this plane extremely easy to perform.

IV. POWDER

The powder pattern obtained experimentally, Fig. 7, is notable[9] for having two small peaks in addition to the large central peak. A fair representation of these facts can be had by taking into consideration only the first-order effects, namely, only the diagonal elements of the Hamiltonian. Here it is necessary to include the interference effects. It can be shown that in the method used, the crystal current is proportional to the absolute value squared of the reflection coefficient. This in turn is proportional to the complex susceptibility which, on assuming the simple resonance formula to be valid, is proportional to

$$\gamma \propto \frac{1}{(\nu-\nu_0)-i(\Delta\nu/2)}. \tag{10}$$

Here γ is the reflection coefficient, ν the (fixed)

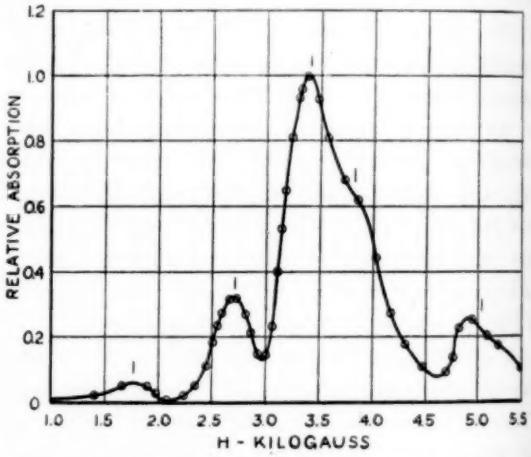

FIG. 6. Measured relative absorption as function of H in orientation II. The short vertical lines give the computed positions of the absorption peaks.

[9] See for example, E. Zavoisky, J. Phys. U.S.S.R. 10, 170 and 197 (1946).

incident r-f frequency, ν_0 the resonant frequency, and $(\Delta\nu/2)$ the half-width at half-power. Each ν_0 is a function of angle and field. It is necessary now to add (preserving phase) the contributions of the three groups of resonances: the low field one for which

$$\nu-\nu_{0-1}=3\cos^2\theta-(\xi+1-\nu), \tag{11}$$

the principle absorption

$$\nu-\nu_{00}=\nu-\xi, \tag{12}$$

and the high field one for which

$$\nu-\nu_{0+1}=(\nu-\xi+1)-3\cos^2\theta. \tag{13}$$

In 11, 12, and 13, and in what follows ν and $\Delta\nu/2$ are expressed in units of $(\delta/2)$. Thus:

$$\gamma\propto\int_0^{\pi}\sin\theta d\theta\sum_{k=-1}^{+1}\frac{g_k}{(\nu-\nu_{0k})-i(\Delta\nu/2)}. \tag{14}$$

The g_k are the weights to be assigned to the groups $\sqrt{3}$, $\sqrt{2}$, $\sqrt{3}$, in the order mentioned. The integration removes the angular dependence leaving γ a function of H and of ν. The reflected power is then proportional to $|\gamma|^2$. The integrations can be performed in the complex plane for $\xi+1-\nu$ and $\xi-\nu+1$, both near zero where the resulting expressions have maximum values. In taking the absolute value square cross product terms arise between the main maximum and the other two, which in the vicinity of $\xi=\nu-1$ and $\xi=\nu+1$ are rather large. The dependence of $|\gamma|^2$ on H is shown in Fig. 8 where one can see

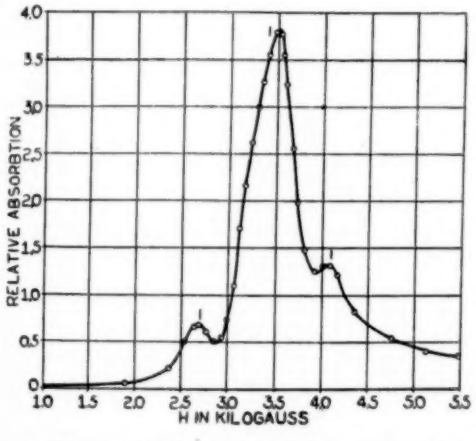

FIG. 7. Measured relative absorption as function of H in powder. The vertical lines show the computed positions of the absorption peaks as explained in the text.

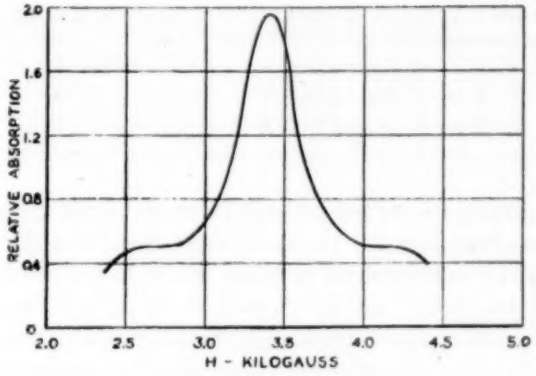

FIG. 8. Computed relative absorption of powder as function of H taking interference into account.

the principal maximum but only two flat regions rather than two subsidiary peaks. To obtain Fig. 8, $(\Delta\nu/2)$ was taken to be the equivalent of 230 gauss and ν to correspond to 9375 mc/sec. The reason why the secondary peak portions are small arises essentially from the fact that these transitions are spread by the angular dependence of the level separation over a large range of field strengths (rather than over the range $(\Delta\nu/2)$). It is likely that, on taking into account higher order terms in the level separation or by adjusting $(\Delta\nu/2)$, one could make the theoretical results show the slight secondary peaks that the measurements reveal. This is hardly worth while, however, since it is difficult, by this method, to obtain as accurate an estimate of δ as from the patterns obtained from single crystals. An arbitrary criterion used in drawing the vertical lines in Fig. 7 asserts the peaks occur at

$$\xi=\nu-1+\frac{1}{\sqrt{3}}(\Delta\nu/2)$$

and

$$\xi=\nu+1-\frac{1}{\sqrt{3}}(\Delta\nu/2). \tag{15}$$

It should be pointed out that the separation of the secondary peaks is $2-(2/\sqrt{3})(\Delta\nu/2)$, and this is roughly independent of the r-f frequency.

V. CONCLUSIONS

The analysis carried out here shows that the measurement of resonance absorption in hydrated salts like chrome alum forms a direct and very convenient method of measuring the fine

TABLE I. Variation of strengths of transitions in high fields.

$[+\frac{1}{2}\rightarrow+\frac{3}{2}]:3(1-0.592\xi^{-2})$	$[-\frac{1}{2}\rightarrow+\frac{3}{2}]:1.18\xi^{-2}$
$[-\frac{1}{2}\rightarrow+\frac{1}{2}]:4(1-0.888\xi^{-2})$	$[-\frac{3}{2}\rightarrow+\frac{1}{2}]:1.18\xi^{-2}$
$[-\frac{3}{2}\rightarrow-\frac{1}{2}]:3(1-0.592\xi^{-2})$	$[-\frac{3}{2}\rightarrow+\frac{3}{2}]:.198\xi^{-4}$

splitting of the lowest energy levels of the paramagnetic ions by the crystalline field. The difficulties encountered because of the large widths of the lines can be overcome by using single crystals properly oriented in the magnetic field and also by dilution with similar non-paramagnetic salts such as aluminum ammonium sulfate. In particular, the analysis shows the g-value of chromic ammonium sulfate to be 1.97 and that the splitting can be explained by a cylindrical electrical field, the magnitude of the splitting being $\delta=0.15\pm.01$ cm^{-1}. The constants of the electric fields are found to be $\bar{Q}=1500$ cm^{-1} and $\bar{a}=180$ cm^{-1}. The corresponding quantities computed by Van Vleck are 1000 cm^{-1} and 60 cm^{-1}, respectively. However, the accuracy with which these are determined experimentally is very small and it is questionable that there is any disagreement in these results.

TABLE II. Positions and relative intensities of absorption lines in orientation II.

$[+\frac{1}{2}\rightarrow+\frac{3}{2}]$,	$\theta=70°33'$	$\xi=3.35$	$H=2730$ gauss	9
$[-\frac{1}{2}\rightarrow+\frac{1}{2}]$,	70°33′	4.17	3400	12
$[-\frac{3}{2}\rightarrow-\frac{1}{2}]$,	70°33′	4.70	3830	9
$[-\frac{3}{2}\rightarrow-\frac{1}{2}]$,	0	2.18	1780	3
$[-\frac{1}{2}\rightarrow+\frac{1}{2}]$,	0	4.17	3400	4
$[+\frac{1}{2}\rightarrow+\frac{3}{2}]$,	0	6.17	5030	3

VI. ACKNOWLEDGMENTS

This work was supported by the Rutgers University Research Fund, the Research Corporation, and the U. S. Navy under Contract N6ori-203. I am indebted to Drs. H. C. Torrey and C. A. Whitmer and to Mr. Jen-Sen Hsiang for many valuable discussions. The experimental data referred to in reference 3 and in the text of this paper were obtained by Dr. C. A. Whitmer and Mr. Jen-Sen Hsiang.

PHYSICAL REVIEW VOLUME 73, NUMBER 5 MARCH 1, 1948

The Ionization Loss of Energy of Fast Charged Particles in Gases and Condensed Bodies

OTTO HALPERN
University of Southern California, Los Angeles, California

AND

HARVEY HALL
Bureau of Aeronautics, Navy Department, Washington, D. C.

(Received November 12, 1947)

The ionization loss of particles is treated, taking into account the polarization properties of the medium traversed. The medium is characterized by a general expression for a complex dielectric constant containing n different types of dispersion electrons, and one type of conduction electrons. Damping effects are not neglected but turn out to be significant for conduction electrons only. Formulae for the reduction in loss compared with the Bethe-Bloch expression for independent atoms, are derived and quantitatively discussed for the cases of physical interest. It is shown why qualitative and large quantitative differences occur in the results of the present multi-frequency theory compared with earlier work in which only a single dispersion frequency was assumed. Curves are given for a number of substances to show the reduction in energy loss for a wide range of momenta of the incident particles, the theory applying to all types of particles in the proper velocity range. A quantitative discussion is given which shows good agreement of the multifrequency theory with those experiments which at present allow quantitative evaluation.

I. INTRODUCTION

THE problem of energy loss of fast moving, electrically charged particles in condensed media has found a quantitative treatment in two notes published by Fermi in 1939 and 1940.[1] Fermi characterized the medium traversed by a dielectric constant produced by electrons bound with a single frequency and damped in their motion. He obtained the important result that in a condensed medium the loss depends not only on the physical parameters which enter into the Bethe-Bloch formula but also on the dielectric properties of the medium. The effects become most important if the velocity of the particle exceeds the value c/n wherein n stands for the square root of the static dielectric constant. In this case, the well-known logarithmic increase given by the classical Bohr formula disappears and the loss assumes a limiting value which is essentially independent of the particle energy.

The limiting results, although derived under the assumption of a finite damping of the electronic oscillations, turn out to be more or less independent of the damping constant and are essentially determined by the frequency and density of the oscillators in the dielectric.

Shortly after the publication of Fermi's first note and after attending a lecture given by Fermi on this theory, the present authors undertook a re-examination of the fundamental assumptions underlying Fermi's quantitative estimates. The point of special interest seemed to lie in the assumed dependence of the dielectric constant on frequency. Fermi[1] originally considered his result to be independent of the special assumption made concerning the frequency dependence of the dielectric constant of the medium. We reported[2] that the reduction in loss caused by the dielectric properties of the condensed materials depended in a very critical way on the form of the dielectric constant as a function of frequency. While Fermi's limiting law remained correct for $v \rightarrow c$, it seemed hardly possible to find any case in nature in which it applies for mesotrons and only very few in which it can be made to apply for electrons. It was found that the reduction in loss does not even follow, qualitatively, the theoretical prediction that it should increase with electronic density; for most cases the effect is, for

[1] Enrico Fermi, Phys. Rev. **56**, 1242 (1939); **57**, 485 (1940).

[2] Otto Halpern and Harvey Hall, Phys. Rev. **57**, 459 (1940).

example, larger in water than in lead, in contrast to the results for the one-electron theory presented in reference 1, Fig. 2. It also could be stated quite generally that for most cases of practical interest our results lead to a considerably smaller reduction than Fermi's.

We compared our calculations with a few existing experimental data and found very good agreement. In one of the cases,[3] it turned out that the damping of the conduction electrons, which had to be assumed in the evaluation of the experiment, played a significant role for the purpose of obtaining quantitative agreement between theory and experiment.

The present paper contains a full report of our investigation, which has been unduly delayed for reasons beyond our control. Section II contains the evaluation of the formula for the collision loss in a polarizable medium, calculated under the assumption of a most general model for the dielectric constant, including conduction electrons. In Section III, our general solution is specialized for a number of practically important cases which allow explicit evaluation. In Section IV, we discuss the physical reasons which lead to the strong modification of our result, as compared with that of Fermi. Section V contains a set of curves for various substances and velocity ranges as well as a discussion of special observations, on the basis of the theory presented here.

II. THE FORMULA FOR LOSS BY IONIZATION

The literature describing previous discussions and calculations of the ionization loss in condensed media is quoted by Fermi.[1] We follow the customary calculations up to the point where the energy loss per unit of length is given by an integral over the frequencies of the field created by the moving particle:

$$-\frac{dW}{dz}=\frac{i\rho_0}{\pi v^3}\int_0^\infty \frac{\omega^2}{\epsilon\gamma^2\gamma^*}K_0\left(\frac{\omega\rho_0}{\gamma v}\right)K_0'\left(\frac{\omega\rho_0}{\gamma^* v}\right)d\omega + \text{complex conjugate.} \quad (1)$$

In (1) ρ_0 denotes the radius of the cylinder drawn around the path of the particle and

$$\beta=v/c, \quad 1/\gamma^2=1-\beta^2\epsilon, \quad \omega=2\pi\nu.$$

Here ϵ stands for the square of the complex index of refraction and is defined in (3) below.

The cylinder functions appearing in (1) take on a very simple form for small argument:

$$K_0(x)\cong\log 2/a_0x, \quad a_0=1.78\cdots;$$
$$K_0'(x)\cong -1/x \quad \text{for} \quad |x|\ll 1.$$

Therefore, we can rewrite (1) in the form

$$-\frac{dW}{dz}=\frac{2\pi e^2}{v^2}\int_0^\infty -i\nu\left(\frac{1}{\epsilon}-\beta^2\right) \times\log\frac{A}{\nu^2(1-\beta^2\epsilon)}d\nu+\text{complex conjugate,} \quad (2)$$

with the abbreviation,

$$A=(v/\pi a_0\rho_0)^2.$$

Appendix 1 justifies in more detail the replacement of the cylinder functions by the simple expressions used in the transition from (1) to (2).

We now introduce explicitly the most general expression for the dielectric constant of a medium which contains dispersion frequencies as well as conduction electrons.

$$\epsilon=1+\left(\sum_{j=1}^{n}\frac{f_j}{\nu_j^2-\nu^2+ig_j\nu}\Big/1-\tfrac{1}{3}\sum_{j=1}^{n}\frac{f_j}{\nu_j^2-\nu^2+ig_j\nu}\right) +\frac{f_0}{-\nu^2+ig_0\nu}. \quad (3)$$

In this expression all frequencies, and g_j's are measured in units of α, which is defined by the relation

$$\alpha^2=ne^2/\pi m.$$

Here n denotes the number of electrons per unit volume. In the absence of conduction electrons we can define the static dielectric constant by putting ν equal to zero in (3).

$$\epsilon_0=1+\left(\sum_{1}^{n}\frac{f_j}{\nu_j^2}\Big/1-\tfrac{1}{3}\sum_{1}^{n}\frac{f_j}{\nu_j^2}\right). \quad (4)$$

Lorentz's correction is represented by the denominator in (3) and will be discussed later on. The quantities f_j give the fraction of electrons associated with the various dispersion frequencies, while the quantities g_j take account of the damping. g_j for the dispersion electrons will turn out to be of no practical importance; g_0 on the

[3] For example, in the application of reference 2 to the evaluation of the experiment of Rossi, Hilberry, and Hoag as reported in Phys. Rev. 56, 837 (1939). This case will be re-examined below.

other hand, which is related to the conductivity σ of the medium by

$$g_0 = n_e e^2/m\sigma,$$

will turn out to be of quantitative importance.

In connection with the Lorentz correction in Eq. (3) there exists a natural limit on the sum

$$\sum_1^n \frac{f_j}{\nu_j^2},$$

to the effect that

$$1-\tfrac{1}{3}\sum_1^n \frac{f_j}{\nu_j^2}>0.$$

This interpretation is required because otherwise the dielectric constant would become negative for small frequencies. This condition would be equivalent to the existence of conduction electrons, which are treated separately in another term.

For the purpose of evaluating the integral (2), we observe that the integrand has only one singularity in the lower half of the complex ν plane, namely, where $1-\beta^2\epsilon$ changes sign. This singularity occurs on the imaginary axis at the point, say, $\nu=-ia$. The location of the singularity as well as its value will be more thoroughly discussed later on.

We now transform the path of integration as follows: Instead of going from zero to infinity along the real axis, we move first along the imaginary axis from zero to $-ia$; then from $-ia$ to $-ir$ wherein r is a large positive quantity which later on becomes infinite; and then from $-ir$ on the arc of a circle up to the positive real axis. Denoting these three integrals by I, II, and III, respectively, we now can write (2) in the following form:

$$-\frac{dW}{dz}=\frac{2ne^4}{mv^2}\left[I+\lim_{r\to\infty}(II+III)\right]+\text{c.c.}$$

We now find successively $I+I^*=0$, since $\nu^2(1-\beta^2\epsilon)$ is real and positive on the imaginary axis as long as $|\nu|<a$;

$$II=-2\int_a^r \pi y dy\left(\frac{1}{\epsilon}-\beta^2\right),$$

$$III=\pi\left[\log\frac{A}{r^2(1-\beta^2)}-\beta^2+r^2(1-\beta^2)\right].$$

By simple algebra we can then obtain

$$II+III=\pi\left[\log\frac{A}{1-\beta^2}-\beta^2+a^2(1-\beta^2)+2J\right], \quad (5)$$

with the abbreviation

$$J=\int_a^r ydy\left(1-\frac{1}{\epsilon}\right)-\log r. \quad (6)$$

We now observe that for large values of the momentum of the incident particle expressed in units of Mc (i.e., for $p\gg1$, where $p=\beta/(1-\beta^2)^{\frac{1}{2}}$), the root a will, in general, be large. Therefore, the denominators in the defining equation for the dielectric constant (3) will be large, and we may consequently write the following relation, for the purpose of evaluation of Eq. (6):

$$1-\frac{1}{\epsilon}\cong\sum_1^n \frac{f_j}{\nu_j^2+y^2+g_j y}+\frac{f_0}{y^2+g_0 y}. \quad (7)$$

This approximation is equivalent to neglecting in the loss reduction, Eq. (17) below an additional term which is not larger than $1/4a^2$ and is negligible for all cases discussed in this paper.

We now have to evaluate an integral

$$\int_a^r \frac{ydy}{\nu_j^2+y^2+g_j y}=\log r-\tfrac{1}{2}\log(\nu_j^2+a^2+g_j a)$$
$$-\frac{g_j}{(4\nu_j^2-g_j^2)^{\frac{1}{2}}}\tan^{-1}\frac{(4\nu_j^2-g_j^2)^{\frac{1}{2}}}{2a+g_j}, \quad (8)$$

when

$$4\nu_j^2>g_j^2.$$

$$=\log r-\tfrac{1}{2}\log(\nu_j^2+a^2+g_j a)$$
$$-\frac{g_j}{2(g_j^2-4\nu_j^2)^{\frac{1}{2}}}\log\frac{2a+g_j+(g_j^2-4\nu_j^2)^{\frac{1}{2}}}{2a+g_j-(g_j^2-4\nu_j^2)^{\frac{1}{2}}}, \quad (9)$$

when

$$4\nu_j^2<g_j^2.$$

Thus, neglecting damping for all electrons except the conduction electrons, we find always, assuming $a\gg g_j$, $j\geq1$, from (5), (7), and (9),

$$J=-\log\{(\nu_1^2+a^2)^{f_1/2}\cdots(\nu_n^2+a^2)^{f_n/2}\}$$
$$-\log(a+g_0)^{f_0}. \quad (10)$$

We now introduce the following notations:

$$\nu_j^*=(\nu_j^2+a^2)^{\frac{1}{2}}, \quad j=1, 2\cdots n$$

and

$$\nu_1^{*f_1}\nu_2^{*f_2}\cdots\nu_n^{*f_n}=\nu_m^{1-f_0}. \tag{11}$$

Then (10) takes on the form

$$J=-\log\nu_m^{1-f_0}(a+g_0)^{f_0}, \tag{12}$$

and we finally obtain (from combining (2), (6), and (12)) the expression,

$$-\frac{dW}{dz}=\frac{2\pi ne^4}{mv^2}\left\{\log\frac{A}{(1-\beta^2)\nu_m^{2(1-f_0)}(a+g_0)^{2f_0}}-\beta^2+a^2(1-\beta^2)\right\}. \tag{13}$$

The complete classical expression for the loss by collision in the condensed medium is contained in (13). To obtain the reduction in loss as compared with the Bethe-Bloch formula, which is caused by polarization and conduction effects, we have to specialize for the case of very low densities of the same material. Now, for small n (3) takes on the form

$$\epsilon=1+\sum_0^n\frac{f_j}{\nu_j^2-\nu^2}. \tag{14}$$

In (14) the conduction electrons are now replaced by weakly bound dispersion electrons of frequency ν_0, and damping is everywhere neglected. We thus obtain, under the conditions of validity of the Bethe-Bloch formula, the expression

$$\left(-\frac{dW}{dz}\right)_0=\frac{2\pi ne^4}{mv^2}\left\{\log\frac{A}{(1-\beta^2)\nu_{m_0}^2}-\beta^2\right\}\cdots, \tag{15}$$

wherein the abbreviation,

$$\nu_{m_0}=\nu_0^{f_0}\nu_1^{f_1}\cdots\nu_n^{f_n} \tag{16}$$

has been used. In (16) the frequencies ν_0, ν_1, etc. are the dispersion frequencies of the compound in question when in the vapor state, rather than in the solid or liquid form, whereas in (11) the ν_j's refer to the condensed form. Finally therefore, by comparing (13) and (15) we obtain for the reduction in loss resulting from polarization and conduction effects the expression,

$$\Delta=\left(-\frac{dW}{dz}\right)_0-\left(-\frac{dW}{dz}\right)=\frac{2\pi ne^4}{mv^2}\left\{\log\frac{\nu_m^{2(1-f_0)}(a+g_0)^{2f_0}}{\nu_{m_0}^2}-a^2(1-\beta^2)\right\}. \tag{17}$$

The quantities ν_m and ν_{m_0} are defined by (11) and (16), and a is the single positive root of the following equation for y obtained from (3) for the condition $1-\beta^2\epsilon=0$.

$$\frac{1}{\beta^2}=1+\left(\sum_1^n\frac{f_j}{\nu_j^2+y^2}\Big/1-\tfrac{1}{3}\sum_1^n\frac{f_j}{\nu_j^2+y^2}\right)+\frac{f_0}{y^2+g_0y}. \tag{18}$$

While the essentially classical result, Eq. (15), cannot be expected to hold for close collisions involving a large exchange of energy, it is reasonable to suppose that Eq. (17) for the reduction in loss is valid for such collisions, since it is independent of the impact distance, or, what is the same thing, of the magnitude of energy transferred. Equation (17) will therefore be assumed to represent correctly the correction arising from dispersion and conduction effects which is to be applied to the Bethe-Bloch quantum mechanical loss formula for single atoms, Eq. (29).

Before concluding this section we have to justify the assumptions made about the singularity of the integrand in the lower half of the complex plane. This can best be done by pointing out that singularities of the integrand of (2) can only occur for real values of ϵ. These special values are:

$$\epsilon=1/\beta^2,\quad \epsilon=0,\quad \epsilon=\infty.$$

To study the behavior of ϵ as a function of ν, it is convenient to rewrite (3) by straightforward algebraic transformation as follows:

$$\sum_1^n\frac{f_j}{\nu_j^2-\nu^2+ig_j\nu}+\frac{f_0/(\epsilon+2/3)^2}{-f_0/(\epsilon-2)-\nu^2+ig_0\nu}=\frac{3(\epsilon-1)}{\epsilon+2}. \tag{19}$$

We note that (19) has the same general form that the dispersion formula would assume in the case of $\epsilon-1\ll1$ where the Lorentz correction becomes insignificant. We only have to assign to the conduction electrons a fictitious frequency

$$\nu_0'^2=-f_0/(\epsilon+2),$$

replace $\epsilon-1$ by

$$3(\epsilon-1)/(\epsilon+2),$$

and, similarly, f_0 by

$$f_0' = f_0 \Big/ \left(\frac{\epsilon+2}{3}\right)^2.$$

The condition for a singularity now takes on, by the aid of (19), the form

$$\sum_1^n \frac{f_j}{\nu_j^2-\nu^2+ig_j\nu} + \frac{f_0'}{\nu_0'^2-\nu^2+ig_0\nu} = \text{Real.} \quad (20)$$

We now put

$$\nu = x - iy, \quad x, y > 0.$$

Then the left side of (20) will take on the form

$$\sum_0^n f_j \frac{A_j - ix(2y+g_j)}{A_j^2+x^2(2y+g_j)^2} = \text{Real.} \quad (21)$$

In (21) A_j is a *real* quantity, the exact value of which is unimportant for our proof. (21) cannot hold true for a set of positive values of x, y. From this it follows that there are no singularities in the lower half of the ν plane, except possibly on the negative imaginary axis. The investigation of the case $x=0$ can then be carried out separately; for this purpose, reference should be made to (3) or to (19) in which we put

$$\nu = -iy.$$

Let us now establish that there is only one physically significant root, which corresponds to $\epsilon = 1/\beta^2$. It may be seen by inspection of Eq. (3) that there is no root at all for $\epsilon = 0$, and the root at $\nu = 0$, leading to $\epsilon \to \infty$, and caused by the presence of conduction electrons, is of no consequence because the integrand vanishes at this point.

Thus, any significant root corresponds to $\epsilon = 1/\beta^2$. That there is only one such root may be proved by inspection of Eq. (3) wherein ϵ is a monotonic function of y, for $y > 0$.

III. DISCUSSION OF SPECIAL CASES

The determination of the reduction in collision loss is, according to (17) immediately effected if we know ν_m and a. The various dispersion frequencies have, of course, to be obtained from x-ray and spectroscopic data; the only mathematical difficulty in discussing (17) lies in the determination of a, which cannot be given in explicit form but must be determined for the various cases of physical interest with the aid of (18). Although complete graphical results for certain compounds will be presented in Figs. 1, 2, and 3 below, a few special cases in which analytical results can be derived will now be discussed.

Case 1.—$p \gg \nu_n, g_0$. Here ν_n denotes the largest dispersion frequency, and g_0 is the damping constant of the conduction electrons. Under these conditions (18) gives $a \cong p$, and we obtain, inserting into (17),

$$\Delta \cong \frac{2\pi ne^4}{mc^2}\left\{\log \frac{1}{\nu_{m0}^2(1-\beta^2)} - 1\right\}. \quad (22)$$

This general result for very large p, agrees with Eq. (1) of reference 2, and with Fermi's result for $v \to c$.

Case 2.—We assume the absence of conduction electrons and also the relation $1/\beta^2 > \epsilon_0 =$ dielectric constant. In this case, which applies to the stopping of heavy particles which do not necessarily have relativistic velocities, $a = 0$. (17) does not always reduce to zero, however, in view of the fact that the more loosely bound electrons may have different frequencies in the vapor and solid states. Such an effect will be of importance only for elements of small atomic number. In this case, however, the Lorentz term may be of significance, and (7) and, consequently, (17) will then have to be corrected accordingly. This case will not be discussed further in the present paper.

Case 3.—

$$\nu_k^2 \ll p^2 \sum_0^k f_j \ll \nu_{k+1}^2,$$

$$g_0 < p\left(\sum_0^k f_j\right)^{\frac{1}{2}}.$$

Under these assumptions, (18) reduces approximately to

$$1/p^2 \cong \frac{f_0}{y^2+g_0y} + \frac{\sum_1^k f_j}{y^2}, \quad (23)$$

which can also be written in the form

$$y^2 \cong p^2\left(\sum_0^k f_j - \frac{f_0g_0}{y+g_0}\right). \quad (24)$$

(24) can now be treated by successive approxi-

mation. Using the notation,

$$F_k=\sum_0^k f_j \qquad k\leq n,$$

we find that, approximately,

$$a^2=y^2\cong p^2\left(F_k-\frac{f_0 g_0}{pF_k{}^{\frac{1}{2}}+g_0}\right). \tag{25}$$

(25) leads now to two different sub-cases:

A. When $g_0<pF_k{}^{\frac{1}{2}}$, the second term of (25) can be neglected. This case is treated below in (26).

B. When $g_0>pF_k{}^{\frac{1}{2}}$, then the second term of (25) is approximately f_0. This case is treated in more detail as case 4 (Eq. (27)).

In sub-case A, we assume

$$a\cong pF_k{}^{\frac{1}{2}}>g_0.$$

Then we obtain from (11)

$$\nu_m{}^{1-f_0}\cong a^{F_k-f_0}\nu_{k+1}{}^{f_{k+1}}\cdots\nu_n{}^{f_n},$$

and finally, as expression for the reduction in loss,

$$\Delta\cong\frac{2\pi ne^4}{mv^2}\left\{\log\frac{(F_k p^2)^{F_k}}{\nu_p{}^{2F_k}}-\beta^2F_k\right\}. \tag{26}$$

In (26) the quantity ν_p is defined by

$$\nu_p{}^{F_k}=\prod_0^k \nu_j{}^{f_j}.$$

In this special case the conduction electrons behave like bound electrons; their damping is of no significance and their only effect consists in changing the value of ν_p. In evaluating ν_p for use in (26), the frequencies for the compound in the vapor form must be used. (26) reduces to the earlier case (22) when $k=n$. In this case,

$$F_k=1$$

and

$$\nu_p=\nu_{m_0}, \quad \beta^2\sim 1.$$

(26) also agrees with the result Eq. (2) of reference (2) for the special case of two dispersion electrons.

Case 4.—

$$\nu_k{}^2\ll p^2\sum_1^k f_j\ll\nu_{k+1}{}^2$$

$$g_0>p(\sum_0^k f_j)^{\frac{1}{2}}.$$

Defining now

$$F_k'=\sum_1^k f_j,$$

we then obtain from (24) the value of $a\cong pF_k{}'{}^{\frac{1}{2}}$. Furthermore, we have from (11) the expression

$$\nu_{m_0}{}^{1-f_0}\cong a^{F_k'}\nu_{k+1}{}^{f_{k+1}}\cdots\nu_n{}^{f_n}.$$

Using these expressions in (17), we obtain for the reduction in loss,

$$\Delta\cong\frac{2\pi ne^4}{mv^2}\left\{\log\left(\frac{p^2F_k'}{\nu_p{}^2}\right)^{F_k}\times\left[\frac{(g_0+a)^2}{p^2F_k'}\right]^{f_0}-\beta^2F_k'\right\}. \tag{27}$$

The effect of the damping of the conduction electrons may thus be appreciable for light elements and will be more closely discussed in Section V.

Other cases.—Since most cases of interest in the field of high energies are covered in principle by the discussion already given in this paragraph, we shall refrain here from a detailed discussion of additional possibilities which, in every case, can be carried through without undue labor on the basis of the formulae already presented.

IV. COMPARISON BETWEEN THE ONE-FREQUENCY AND THE MANY-FREQUENCY THEORY

The discussion of the various cases in the preceding paragraph has made it abundantly clear that the results for the reduction in loss depend in a critical way on the dispersion properties of the medium traversed. The curves and numerical data given in the following paragraph will show quantitatively how much the two types of theories differ in most cases of practical interest.

Without going into any numerical discussion, we here desire to point out the physical reason which led us to expect that the frequency dependence of the dielectric constant should play so important a part in these calculations. For this purpose it is perhaps best to refer to Eq. (22) of Fermi's second paper, in which the quantities corresponding to our ϵ and $1-\beta^2\epsilon$ are defined for a single dispersion electron only.

Now, in comparing the integration of Fermi's Eq. (22) with our Eq. (1) for the case of small

damping which will suffice for the present discussion, the zeroes of the quantity $1-\beta^2\epsilon$, together with the location of the resonance points $1/\epsilon\rightarrow\infty$, for $0\leq\nu\leq\infty$, determine the regions where the integrand is important. This may be seen from the following form of our Eq. (2):

$$-\frac{dW}{dz}=\frac{2\pi e^2}{v^2}\int_0^\infty\left\{i\nu\left(\frac{1}{\epsilon^*}-\frac{1}{\epsilon}\right)\log\frac{A}{\nu^2|1-\beta^2\epsilon|}-\theta\nu\left(\frac{1}{\epsilon^*}+\frac{1}{\epsilon}-2\beta^2\right)\right\}d\nu, \quad (28)$$

where $\theta=$ampl. $(1-\beta^2\epsilon)$.

While it is true that the term in the result arising from $i(1/\epsilon^*-1/\epsilon)$ may be written in terms of a single frequency resembling our ν_{m_0} of Eq. (16), the contribution from the second term involving $\theta=$ampl. $(1-\beta^2\epsilon)$ will be determined by the magnitudes of the fractions f_j, and also ν_j and β, since $1-\beta^2\epsilon$ changes sign in the neighborhood of every absorption line. Thus, while θ is always either zero or π, the contribution from the factor

$$\nu\left(\frac{1}{\epsilon^*}+\frac{1}{\epsilon}-2\beta^2\right)$$

is characterized by the detailed dispersion properties of the material, which lead to partial cancellation in this term. These effects are illustrated especially well in the intermediate case 3, Eq. (26), where it is quite apparent that the detailed dispersion properties are important. It is only in the two limiting cases of $p\gg\nu_n$ and $p\ll\nu_1$ that a single electron theory will suffice, and even then the characteristics of this electron can be obtained from experiment only, while a theoretical expression can only be derived on the basis of the multi-frequency theory.

V. SUMMARY OF RESULTS AND COMPARISON WITH EXPERIMENT

For general purposes of comparing the results of Eq. (17) with experiment the theoretical curves of Figs. 1, 2, and 3 are provided. These curves, which cover a wide energy range, and various materials, represent the reduction in loss which must be subtracted from the Bethe-Bloch

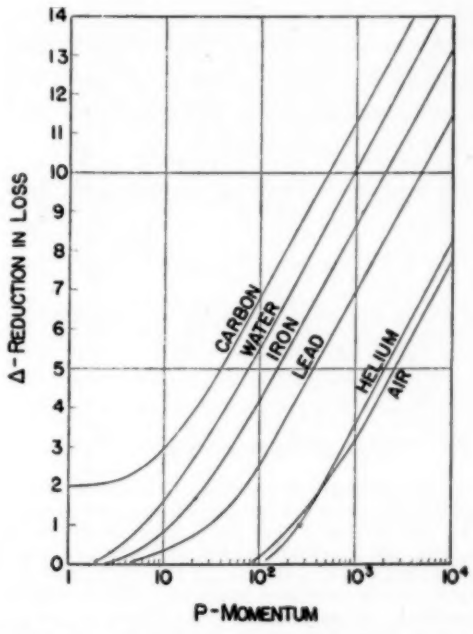

FIG. 1. The reduction in loss Δ for several materials, computed from Eq. (17). Δ is expressed here, in units of $2\pi ne^4/mv^2$, as a function of momentum of the incident particle in units of Mc. These curves are based on the data in Table I.

formula,[4] which may be written as follows for the energy range of interest here:

$$-\frac{dW}{dz}=\frac{2\pi ne^4}{mv^2}\left\{\log\frac{mv^2T}{I^2Z^2(1-\beta^2)}+1-\beta^2\right\}. \quad (29)$$

Here T is the maximum energy which can be transferred to an electron in a collision, and IZ is an average ionization energy. The quantity T according to Bhabha,[5] is given by the equation

$$T=\frac{E^2-M^2c^4}{Mc^2\left(\frac{m}{2M}+\frac{M}{2m}+\frac{E}{Mc^2}\right)}. \quad (30)$$

[4] See, e.g., W. Heitler, *The Quantum Theory of Radiation* (Oxford University Press, 1936), p. 218, Eq. (1). There are certain discrepancies in the literature between the various expressions given for the formula for collision loss. The formula of Bloch quoted by Heitler, and employed here as Eq. (29), for example, differs from the formula given by Bethe, [*Hd der Physik*, Vol. 24/1, 2nd edition, p. 523, Eq. (56.16)], for heavy particles with relativistic velocities. No attempt is made here to resolve these discrepancies which may amount to as much as several percent, since the essential points of the present paper are independent of these differences and a complete discussion of the collision loss question is beyond the scope of the present considerations.

[5] H. J. Bhabha, Proc. Roy. Soc. **164**, 257 (1937). See also reference 10.

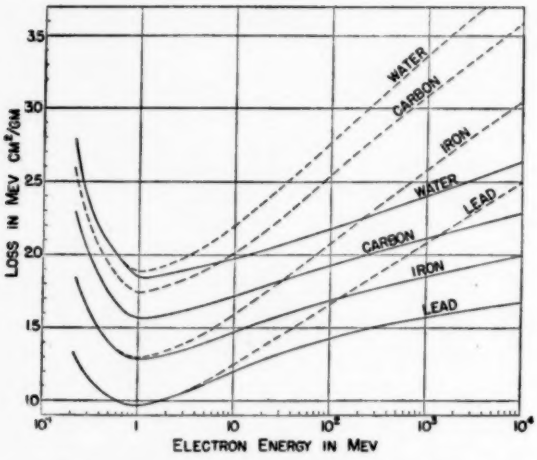

FIG. 2. The theoretical ionization loss for mesotrons in condensed materials (solid curves). These curves were obtained by subtracting Δ, Eq. (17), from the Bethe-Bloch formula, Eq. (29), for single atoms. Calculations from Eq. (29) were based on the substitution $IZ=h\nu_{m_0}$, as explained in the text. The Bethe-Bloch loss is also plotted separately (dotted curves) for purposes of comparison. In computing these curves, T was taken from Eq. (30).

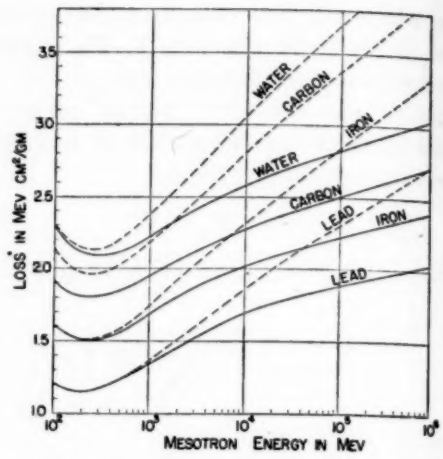

FIG. 3. The theoretical ionization loss for electrons in condensed materials (solid curves), corresponding to Fig. 2 for mesotrons. In these curves, as in Fig. 2, all calculations from Eq. (29) were based on the value $IZ=h\nu_{m_0}$. In computing these curves the maximum energy transferred in Eq. (29) was assumed to be one half the kinetic energy of the incident electron.

Here E and M refer to the energy and mass, respectively, of the moving particle.

In past applications of Eq. (29) the value of I has been assumed from experiments on gold to be 13.5 volts.[4] The present theory, however, establishes a theoretical expression for IZ, namely, the generalized geometric mean of the atomic frequencies, ν_{m_0} from Eq. (16). Actually, ν_{m_0} and $13.5Z$ may differ by perhaps 50 percent, on the basis of the dispersion models illustrated in Table I. While these dispersion models are admittedly approximate, ν_{m_0} as given in principle by Eq. (16) should be used, instead of $13.5Z$, in Eq. (29), and this change will consequently be assumed henceforth in this paper.[6]

In constructing Fig. 1 numerical values for the quantities f_j, ν_j, g_0, etc. of Eq. (3) were taken from empirical data. In assigning the f_j's, the electrons in each atomic shell (K, L, M, etc.) were generally grouped together, and an average frequency ν_j was assigned on the basis of x-ray ionization data. Table I contains the data actually employed. Here all frequencies and g_0 are expressed in units of α.

In reference 2 the authors compared the results of a two-electron dispersion model with Fermi's results (see reference 1) for a one-electron model, and with certain experiments.[7–9] While good agreement was found between reference 2 and experiment, a more detailed examination of the data in references 7–9 will now be made, in terms of our general dispersion conduction result (17), and Figs. 1, 2, and 3.

In the experiment of Rossi, Hilberry, and Hoag,[7] and similar experiments conducted subsequently,[10] a figure for the meson lifetime was obtained by comparing the ionization at two different altitudes, after compensating for the absorption over the longer path by means of a suitable amount of carbon, or other material, at the higher altitude. Since the polarization effects of Eq. (17) were neglected in reference 7, their value for the lifetime must be increased. The ratio of corrected to uncorrected lifetime for this case may be shown to be

$$\frac{\tau}{\tau_0}\cong\frac{\log N_A/N_B}{\log N_A/N_B-1.5\Delta\cdot T/\bar{E}}. \tag{31}$$

Here N_A/N_B is the ratio of observed counts at the upper and lower altitude, Δ is given by Eq.

[6] For purposes of comparison the values of $13.5Z$ and ν_{m_0} are tabulated in the same units in Table I.

[7] Rossi, Hilberry, and Hoag, Phys. Rev. **56**, 837 (1939).
[8] M. A. Pomerantz and T. H. Johnson, Bull. Am. Phys. Soc. New York Meeting February, 1940, No. 4.
[9] Crane, Oleson, and Chao, Bull. Am. Phys. Soc. New York Meeting Feb., 1940, No. 3.
[10] See, e.g., references given by W. Heisenberg, *Cosmic Radiation* (Dover Publications, New York, 1946), Sec. 8.

(17), T is the thickness of carbon, and $\bar{E}$ is of the order of the average meson energy. This result, Eq. (31), may be derived qualitatively as follows. The number of counts at the higher altitude, A, caused by mesons in the energy range dE, will be given by[10]

$$N_A \sim 1/[E+(\Delta E)_1+(\Delta E)_A]^\gamma, \qquad (32)$$

where $(\Delta E)_1$ represents the energy loss in the atmosphere above the point A, and $(\Delta E)_A$ represents the energy loss in the absorbing material placed above the counters at A. The exponent γ has a value of about 3. Similarly, at the lower altitude B,

$$N_B \sim \frac{e^{-h/c\tau_E}}{[E+(\Delta E)_1+(\Delta E)_{12}]^\gamma}, \qquad (33)$$

where h is the difference in altitude between A and B, τ_E is the meson lifetime corresponding to the energy E, and $(\Delta E)_{12}$ is the energy loss in the atmosphere between the points A and B.

In reference 7 an attempt was made to satisfy the relation

$$(\Delta E)_A \simeq (\Delta E)_{12},$$

but since our correction (17) was omitted, we must write

$$(\Delta E)_A = (\Delta E)_{12} - T\cdot\Delta. \qquad (34)$$

Equation (31) now follows by combining (32), (33), and (34), since the average meson energy is given approximately by the relation

$$\bar{E} \leqq (\Delta E)_1 + (\Delta E)_{12}$$

and

$$\log\frac{2\bar{E}+T\cdot\Delta}{2\bar{E}} \simeq \frac{T\cdot\Delta}{2\bar{E}}.$$

Thus, for the following data,

$$N_A/N_B \leqq 1.13$$
$$\bar{E} \leqq 1.4\times 10^9 \text{ ev}$$
$$T \leqq 84 \text{ g/cm}^2 \text{ (graphite)}$$
$$\text{Meson mass} = 200 \text{ electron masses}$$

and, using the value $\Delta \leqq 0.25$ Mev/g/cm² from Fig. 1, it follows that

$$\tau/\tau_0 \leqq 1.2.$$

Thus, while the influence of polarization effects can increase the lifetime, as determined by this experimental technique, by the order 20 percent, there is no possibility of explaining away the radioactivity by this means.

In the experiment of Pomerantz and Johnson[8] it was found that 890 g/cm² of water has the same effect in absorbing mesons with energies of about 10^9 ev as 1547 g/cm² of lead, or that

$$S_{H_2O}/S_{Pb} = 1.72 \pm .22. \qquad (35)$$

This result was compared in reference 8 with the value computed from the Bethe-Bloch formula

$$S_{H_2O}/S_{Pb} = 1.82. \qquad (36)$$

From Fig. 1 it is seen that Δ is negligible for lead for 10^9 ev ($p \leqq 10$), while for water $\Delta \leqq 1.6$, which represents about 6 percent in Eq. (36). Thus (36) should be reduced by 6 percent, which gives, for the theoretical ratio when polarization is included, the value

$$S_{H_2O}/S_{Pb} \leqq 1.71, \qquad (37)$$

which compares very well with Eq. (35).

For evaluating the experiment of Crane, Oleson, and Chao, on the stopping of 10 Mev electrons by carbon, we find the following data from (17), (29) and reference 9:

Observed loss	1.86
[11]Correction for radiative loss	.13
Net collision loss	1.73
[12]Theoretical Bethe-Bloch	2.02
Reduction in loss Δ from Fig. 1	.30
Theoretical loss	1.72

TABLE I. Data employed in constructing Fig. 1.

	Lead	Iron	Water	Carbon	Air (Sea level)	Helium
Z	82	26	10	6	7	2
$2\pi ne^4/mc^2$ (Mev cm²/gm)	0.0606	0.0710	0.0850	0.0765	0.0765	0.0765
α (volts)	60	53	21	28	0.74	0.40
f_0	0	0	0	1/3	0	0
f_1	22/82	2/26	2/10	1/6	3/7	1
f_2	32/82	14/26	4/10	1/6	2/7	0
f_3	18/82	8/26	2/10	1/3	2/7	0
f_4	8/82	2/26	2/10	0	0	0
f_5	2/82	0	0	0	0	0
g_0	0	0	0	7*	0	0
ν_0 (vapor)	—	—	—	0.33	—	—
ν_1 (vapor)	—	—	0.62	—	—	—
ν_1	2.0	0.25	0.27	1.7	40	100
ν_2	20	4.0	2.2	2.3	115	—
ν_3	100	32	6	15	800	—
ν_4	360	170	40	—	—	—
ν_5	500	—	—	—	—	—
$13.5Z$ (volts)	1100	350	135	81	95	27
ν_{m_0} (volts)	1200	430	80	60	96	40

* This value of g_0 (in units of α) for carbon corresponds to a specific resistance of 5000×10^{-6} ohm cm.

[11] As calculated from Heitler, p. 173.

[12] We find from Fig. 3 that the theoretical Bethe-Bloch loss for this energy is 2.02 Mev cm²/g instead of 1.93 as quoted in reference 9.

The close agreement between the present theory and experiment in these examples may perhaps be considered as somewhat fortuitous, in view of the approximate dispersion-conduction models employed for computing the reduction in loss. (See Table I.) Certain data in Table I, for example, might reasonably be changed by as much as 50 percent, and thus, for precise calculation a more detailed dispersion model which is not subject to such freedom of choice, would be required. It is unlikely, however, that such refinements will affect Fig. 1 by more than about 10 percent, or Figs. 2 and 3 by more than one or two percent, and such changes could hardly alter the excellent agreement between this theory and experiment.

It thus seems to be established that the quantitative interpretation of the experiments requires the consistent use of the multi-frequency theory.

APPENDIX

On The Expansions Used for the Cylinder Functions Appearing in Eq. (1)

We intend to justify the use of the simple expressions which allow us to pass from (1) to (2). For this purpose we rewrite (1) as follows:

$$-\frac{dW}{dz}=\frac{e^2}{\pi v^2}\int_0^\infty i\omega\left(\frac{1}{\epsilon}-\beta^2\right)x^*K_0(x)K_0'(x^*)d\omega+\text{c.c.},$$

with abbreviation

$$x=\omega\rho_0/v\gamma.$$

We then make use of the following identical transformation,

$$x^*K_0(x)K_0'(x^*)=\frac{x^*K_0(x)K_0'(x^*)+xK_0(x^*)K_0'(x)}{2}+\frac{x^*K_0(x)K_0'(x^*)-xK_0(x^*)K_0'(x)}{2}$$
$$=A+iB, \text{ where } A \text{ and } B \text{ are real.}$$

The integrand may then be written in the form

$$i\omega\left(\frac{1}{\epsilon}-\beta^2\right)(A+iB)+\text{c.c.}$$

or,

$$i\omega A\left(\frac{1}{\epsilon}-\frac{1}{\epsilon^*}\right)-\omega B\left(\frac{1}{\epsilon}+\frac{1}{\epsilon^*}-2\beta^2\right).$$

In the first term of the last expression, which gives significant contributions near the resonance points at which the real part of ϵ vanishes, we can now put $\epsilon=0$ in the factor A if damping is neglected for the dispersion electrons. Since the argument x takes on the form

$$x\cong\omega_j'\rho_0/v$$

for vanishingly small values of ϵ, the expansion is justified provided only that

$$\omega_j'\rho_0/v\ll 1,$$

or

$$\nu_j'\ll v/2\pi\rho_0$$

for the largest dispersion frequency in the atom. Now since

$$v/2\pi\rho_0 \text{ is } \tfrac{1}{3}\times 10^{18} \text{ sec}^{-1}\cong 2000 \text{ ev}$$

for $v\sim c$ and $\rho_0\sim 10^{-8}$ cm, the condition is satisfied except for very heavy elements; even in the case of lead it holds approximately true for all except the innermost electrons.

The second term containing the factor B gives its main contribution for a set of frequency ranges in which the real part of $1-\beta^2\epsilon$ is smaller than zero Throughout some of this range the argument x is small, but there is a portion of the range of integration in which x assumes sizeable values. Even there no large error arises from using the expansions of $K_0(x)$, $K_0'(x)$ for small argument, since the asymptotic expansions for large argument leads to the same result for the term in question.

This can be seen by comparing the values of

$$2iB=x^*K_0(x)K_0'(x^*)-xK_0(x^*)K_0'(x)$$

for small and large values of $|x|$ respectively.

For small $|x|$ we find

$$2iB\cong-\log\frac{2}{a_0x}+\log\frac{2}{a_0x^*}=\log\frac{x}{x^*}$$
$$=2 \text{ ampl. } x=\text{ampl. } (1-\beta^2\epsilon)$$
$$=\pi i.$$

For large $|x|$, on the other hand, we have

$$K_\nu(x)\cong(\pi/2x)^{\frac{1}{2}}e^{-x},\quad K_0'(x)=-K_1(x).$$

Therefore,

$$2iB\cong\frac{\pi}{2}[(x/x^*)^{\frac{1}{2}}-(x^*/x)^{\frac{1}{2}}]e^{-(x+x^*)}$$

or, since $x+x^*\sim 0$, when $1-\beta^2\epsilon<0$, it follows that

$$2iB\cong\frac{\pi}{2}[\exp(\text{ampl. } x)-\exp(\text{ampl. } x^*)]$$
$$=\frac{\pi}{2}(e^{(\pi i/2)}-e^{-(\pi i/2)})\cong\pi i.$$

When $1-\beta^2\epsilon>0$, ampl. $(1-\beta^2\epsilon)\sim 0$, and similarly $(x/x^*)^{\frac{1}{2}}-(x^*/x)^{\frac{1}{2}}\sim 0$, which completes the argument justifying the use of Eq. (2).

Natural Radioactivity of Rhenium

S. N. NALDRETT* AND W. F. LIBBY
Institute for Nuclear Studies, University of Chicago, Chicago, Illinois
(Received November 14, 1947)

An attempt to confirm the reported K capture activity of Os^{187}, using OsO_4 mixed with argon as the counter gas, failed to reveal any activity corresponding to a half-life of less than 5×10^{11} years. This method assumed that any K capture in Os would be followed by the emission of Auger electrons which would be recorded. The sensitivity of the system to soft Auger electrons was demonstrated by using 34.0-day A^{37} which decays by K capture. Rhenium then was examined for beta-activity, Re^{187} being isobaric with Os^{187}. An activity was found in two samples of different origin which resisted chemical purifications, including distillation of the perrhenic acid from concentrated sulfuric acid solution. The half-life appears to be $4\pm1\times10^{13}$ years calculated for Re^{187} isotope, and the range is 3.5 mg of Al/cm² corresponding to an upper energy limit of about 43 kev.

INTRODUCTION

ACCORDING to the rules of nuclear stability, it is not expected that two neighboring elements will have stable isotopes of the same nominal mass. In the cases of $_{18}A^{40}{}_{19}K^{40}{}_{20}Ca^{40}$, $_{37}Rb^{87}{}_{38}Sr^{87}$, and $_{70}Yb^{176}{}_{71}Lu^{176}{}_{72}Hf^{176}$ it has been shown that radioactive transformations occur. In three of the four other cases where neighboring isobars have been found to exist, there has not yet been any report of instability of either member of the pairs. These four pairs and their natural isotopic abundances[1,2] are as follows:

$_{48}Cd^{113}$ (12.3 percent)	$_{49}In^{113}$ (4.5 percent)
$_{49}In^{115}$ (95.5 percent)	$_{50}Sn^{115}$ (0.4 percent)
$_{51}Sb^{123}$ (44 percent)	$_{52}Te^{123}$ (0.85 percent)
$_{75}Re^{187}$ (61.8 percent)	$_{76}Os^{187}$ (1.64 percent)

A series of experiments was carried out by Zingg[3] in which particular attention was given to the detection and identification of the characteristic x-radiation of Cd, In, Sb, or Re, respectively, which would be expected to follow the capture of an orbital electron by In, Sn, Te, or Os, respectively. The observations were made by placing the subject element or one of its compounds around the outside of a cylindrical Geiger-Müller tube of 0.05-mm copper containing 10 cm Hg pressure of dry air. Copper was chosen to give the highest yield of photoelectrons from the x-rays which were sought. Within the error of his measurements Zingg found no activity in In or Te. With three samples of Sn a slight activity was found (corresponding to a half-life greater than 0.9×10^{12} years) and, moreover, absorption measurements with Cu foils gave data which fit fairly well the absorption of the In K line in Cu. However, a fourth sample of Sn gave no activity even when used as the actual counter wall, and Zingg concluded that the activity could not positively be ascribed to Sn. With Os an activity of about $\frac{1}{3}$ that found with the Sn samples was observed, but the absorption characteristics were not as predicted.

An attempt to detect the x-ray emission attending K capture was made also by Rusinov and Igelnitsky.[4] These authors used an aluminum G-M counter which was filled with 95 percent krypton and 5 percent xenon at a pressure of two atmospheres to give a high counting efficiency for soft gamma-rays. The subject material was placed around the outside of the counter. A counting yield of 100 percent is claimed for 20 kv photons (0.6A), dropping to 12 percent for 50 kv (0.24A). The K radiation of Cd, In, and Sb is 0.4 to 0.5A, within the region of high counting efficiency, but for Re, for which the K radiation is 0.2A, the efficiency would be poor. The background count was reduced over 10 times to about 9 counts per minute by shielding plus anticoincidence circuit methods. The Os-Re pair

* On leave from the National Research Council, Ottawa, Canada.
[1] K. T. Bainbridge and E. B. Jordan, Phys. Rev. **50**, 282 (1936).
[2] A. O. Nier, Phys. Rev. **52**, 885 (1937).
[3] E. Zingg, Helv. Phys. Acta **13**, 219 (1940).
[4] L. I. Rusinov and J. M. Igelnitsky, Comptes Rendus U.R.S.S. (Akademia Nauk C.R.) **47**, 333 (1945) and **49**, 343 (1945).

was not examined by these authors, but for the other three pairs, the x-rays sought were not observed, and they estimate that the half-lives must at least be greater than as follows: for In^{113}, 1×10^{14} years; for Sn^{115}, 1×10^{13} years, and for Te^{123}, 2×10^{14} years.

Neither of these investigations would have succeeded in detecting low energy beta-particles nor Auger electrons since these would have been stopped by the wall of the counter (except in Zingg's experiment in which he used Sn as the counter wall). Lougher and Rowlands[5] placed Os directly inside a cloud chamber and observed a group of electrons with a range in air of 5.0 ± 0.5 cm and with an energy of 61 ± 6 kv, both in excellent agreement with values for Re K x-radiation. They concluded Os^{187} was radioactive by K capture, and estimated the half-life as 3×10^{8} years.

The present investigation was undertaken to establish the existence of natural K capture more conclusively by placing the element inside the counter volume as a gaseous compound so that the Auger electrons emitted after the nuclear transformation might trip the counter with an efficiency high for the nuclear events. From known data it seems extremely likely that in an element such as osmium nearly every instance of K capture would be followed by the emission of at least one Auger electron, the thought being that even if the K vacancy should happen to fill by x-ray emission, the L vacancy so produced would have an even better chance of filling by the Auger process and that if even the L shell filled by x-ray emission, the M shell would not be as likely to, etc. Therefore, if the x-ray probabilities ("fluorescence yields") are W_K, W_L, etc., the chance of obtaining at least one Auger electron per nuclear event would be $(1-W_KW_LW_M\cdots)$ which from known data approaches unity for Os and most elements. This point is discussed more quantitatively later. The present report deals with an investigation of the Os-Re isobaric pair.

I. EXAMINATION OF OSMIUM

Description of Apparatus

Geiger-Müller gas counters of conventional type were used. Preliminary observations were made in a counter about 14 cm long and 2 cm in diameter; a larger counter about 30 cm long and 5 cm in diameter was then made to obtain greater sensitivity. In both cases the center wire was 0.010-in. tungsten wires, the cathode was silver, chemically deposited on the inside wall of the tube over an area which gave an effective counting volume for the small counter 70 mm long and 18 mm diameter and for the large counter 150 mm long and 50 mm in diameter. The Pyrex wall of the counter tube was pulled out in a flame to a thickness of about 30 mg/cm² for the small counter, and of 100 mg/cm² for the large counter, in order to permit the passage of some of the beta-particles from a uranium sample which could be mounted on the outside of the tube as a standard. Osmium tetroxide, purified by successive sublimations, was evaporated into the counter volume to a pressure of about 3 cm; argon was then added to bring the total pressure to 10 to 15 cm. The counter tube was kept in an oven at 60°C to prevent condensation of the osmium tetroxide. It was not found practicable to use any further shielding.

The counting equipment consisted of a scale of 64 with a stabilized high voltage supply of 2500 volts which it was necessary to supplement with a 600 volt supply from a series pack of "B" batteries, in order to provide the operating voltage required of about 3000 volts. An electronic quenching device of the Neher-Harper type was used, and an oscilloscope was connected to the center wire of the counter so that the pulses could be observed, and correct operating conditions maintained.

Procedure and Results

Observations were made with the same counter tube filled alternately with the OsO_4-argon gas mixture and with a conventional counting gas mixture of 10 mm of ethanol and 90 mm of argon. In order to check the counting efficiency of the OsO_4-argon mixture, a standard sample of uranium could be affixed to the outside of the counter tube in a reproducible manner. However, it was considered possible that the OsO_4-argon counting gas might have a sufficiently different absorption coefficient for uranium gamma-radiation so that a uranium standard would give a different count rate than with

[5] E. T. Lougher and S. Rowlands, Nature **153**, 374 (1944).

TABLE I. Comparison of count rate observed with EtOH-A and with OsO_4-A.

(1)	Alcohol-Argon (2)	(3)	(4)	OsO_4-Argon (5)	(6)	(7)	(8)
Date of observation	Count with *U* standard	Background	Date of observation	Count with *U* standard	Background	Normalized background	Apparent increment, counts/min. due to OsO_4 (7)–(3)
Small counter tube							
10 Jan. 47	663.5±1.7	49.2±0.4	8 Jan. 47	533.0±1.5	41.6±0.4	51.6±0.5	2.4±0.6
20 Jan. 47	670.8±1.3	59.0±0.3	24 Jan. 47	647.1±2.0	55.0±0.3	57.0±0.3	− 2.0±0.4
Large counter tube							
			19 Mar. 47	1931.3±6	295.6±2		
			22 Mar. 47	1934.9±7	299.6±2		
			23 Mar. 47	1899.4±5	301.1±3		
20 Mar. 47	1699.7±7	279.3±1.3	24 Mar. 47	1921.4±3.3	298.6±1.1		
21 Mar. 47	1692.3±4	271.4±1.4					
Average of above	1696.4±3.5	274.9±1.0	*Average of above*	1926.0±2.4	297.6±0.9	262.1±0.9	−12.8±1.4
15 Mar. 47	1653.2±5	260.6±2	14 Mar. 47	1672.1±1.9	257.3±0.5	254.4±0.5	− 6.2±2.1

alcohol-argon counting gas. Therefore, only the uranium beta-radiation was used for standardization. Absorption experiments showed that not over ten percent of the effect attributable to the uranium standard was due to gamma-radiation with either gas, and for this small percentage it was shown that the efficiences were similar.

Even with the use of an electronic quenching device the counting characteristics of the OsO_4-argon mixture are very sensitive to the voltage applied, or, in other words, the "plateau" of the Geiger-Müller counting region is very steep, and the count rate obtained with the uranium standard varied considerably depending upon the part of the plateau at which the counting was done. Table I shows the counting results obtained with both the small counter tube and a large one, and for each case two sets of figures are presented. The first set of results was obtained by setting the operating voltage at what appeared to be the middle of the Geiger-Müller plateau, at which voltage a higher counting rate was obtained for both the standard uranium sample and the background than with the alcohol-argon counting gas mixture. The second set of observations was made with the voltage set at the lower part of the G-M plateau, at a voltage which gave as nearly as possible the same counting rate for the uranium standard as was obtained with the alcohol-argon counting gas. In order to compare the background count obtained with OsO_4-argon and with the alcohol-argon, the count with OsO_4-argon (column 6) was multiplied by the ratio of the standard count with alcohol-argon (column 2) to the standard count with OsO_4-argon (column 5), giving the normalized OsO_4-argon background (column 7). Any activity caused by Os should be manifested in an increase of this quantity over the background with alcohol-argon (column 3).

Actually, as shown in column 8 of Table I, no increase in the counting rate was observed with OsO_4-argon as compared with that observed with alcohol-argon, which can only be interpreted as indicating that Os is not radioactive by either orbital capture or particle emission processes within the limits of error of the observations. Because of the high reactivity of OsO_4 with organic matter, it was necessary to pump out the counter tube for a long interval when fillings were changed, and, therefore, the observations with OsO_4-argon and alcohol-argon were made on different days as shown in Table I. Some fluctuation in the background counting rate of an unshielded counter under these conditions is unavoidable, and the apparent deficit in counting rate with OsO_4-argon is probably a result of such fluctuations. Better shielding of the counter, and averaging a protracted series of observations would permit the elimination of this uncertainty. However, a half-life of Os^{187} of 3×10^8 years as previously estimated (5) would have resulted in an extra activity in the large counter described above of 8,000 counts per minute. The data here presented would indicate

TABLE II. Relative response of argon-alcohol and argon-OsO_4 counting mixtures to radioactive argon.

Counter filling	Pressure of active argon mixture	Count rate	Count due A^{37}	Count per mm Hg pressure of A^{37} mixture
Argon-alcohol	none	275.0±1.7		
	115.1 mm	2782.5±4.3	2507.5	21.79
Argon-OsO_4	none	238.8±1.7		
	115.0 mm	2786.6	2547.8	22.15

a half-life about 1000 times as long. Moreover, in the second part of this report it is shown that Re, the other member of this isobaric pair, is active by beta-particle emission, and that actually the Os is therefore stable. Further evidence that the Os is inactive is presented in the following section. Refinements of technique therefore did not seem warranted.

Proof That Auger Electrons are Counted in an OsO_4-Argon Filled Geiger Counter

In order to establish that the OsO_4-argon counting mixture would respond to soft Auger electrons, some observations were made using an argon isotope, A^{37}, which was found to be radioactive by K electron capture by Weimer, Kurbatov, and Pool.[6] These authors consider that K electron capture accounts for over 99.9 percent of the total number of disintegrations; the probability of Auger emission is said to be 0.96±0.3. The sample of A^{37} for our observations was prepared by bombarding potassium chloride with deuterons in the University of Chicago 37-inch cyclotron, causing the reactions $_{19}K^{39}(d,\alpha)_{18}A^{37}$ and $_{17}Cl^{37}(d,2n)_{18}A^{37}$. The irradiated potassium chloride was placed in a tube with ice at liquid nitrogen temperature. After air had been removed from the system the ice was allowed to melt and the potassium chloride dissolved to free the A^{37} trapped in the crystals. Some inert argon was added and the gas was transferred by a Toepler pump, through a trap at −78°C to remove moisture, to a storage volume. The decay rate of a sample of the gas was followed for a period of three months and gave a half life of 34.0 days in good agreement with the value of 34.1 days reported originally.[6]

The counting rates found when similar amounts of this radioactive gas mixture were used in a standard alcohol-argon counting mixture, and in OsO_4-argon mixture are presented in Table II. The count rate obtained from the K capture process in A^{37} is the same with both counting gas mixtures.

It is, therefore, quite certain that Auger electrons from orbital capture in Os would also have been detected if they had occurred. No counting increment due to Os was observed, however. Therefore, it can be said either that no K capture process occurs in Os, or that if K capture occurs, the refilling of the orbital vacancy results only in the emission of x-rays, and never of Auger electrons, a very unlikely situation. Of course the absorption in the OsO_4-argon gas mixture of the K x-rays of Re would be slight. From observations reported for other elements it would appear that the probability of at least one Auger electron being emitted is high, although the fluorescence yields for rhenium have not been reported. For transitions to the K orbit no elements of atomic number close to rhenium have been reported, but for those examined no fluorescence yield close to unity has been reported. For example for $_{27}Co$, $_{42}Mo$, and $_{52}Te$, it is 0.29, 0.65, and 0.56, respectively, for transitions to the K orbit.[7] Moreover, for transitions to the L level, which will inevitably follow the L to K transitions, fluorescence yields are lower and have been reported to be 0.298 and 0.348 for $_{74}W$ and $_{76}Os$, respectively.[8] For succeeding orbits the fluorescence yield is still lower, being only 0.06 for the M orbit in $_{92}U$.[8] Therefore, we can say that for $_{75}Re$ at least two thirds and more likely more than 90 percent of the K capture will result in the emission of Auger electrons.

Conclusion

Assuming the limit of detectability in the above experiments to be ±10 counts per minute, a conservative limit, we are led to a lower estimate for the half-life of Os^{187} for orbital capture or positron emission of 5×10^{11} years The observations reported in the following section, however, indicate that Os^{187} is completely stable.

[6] P. K. Weimer, J. D. Kurbatov, and M. L. Pool, Phys. Rev. **60**, 209 (1944).

[7] R. J. Stephenson, Phys. Rev. **46**, 73 (1934).

[8] H. Lay, Zeits. f. Physik **91**, 533 (1934).

II. EXAMINATION OF RHENIUM

Description of Apparatus

The rhenium counts were made using solid compounds of rhenium, either metallic rhenium or rhenium heptasulfide in a "screen-wall counter," a device which has been fully described elsewhere.[9,10] In effect this type of counter avoids the loss of particles by absorption in the counter wall, since only a wire screen is interposed between the sample and the active counting volume. The sample cylinder is twice the length of the wire screen cathode and slides concentrically within the confining tube and over the wire screen, so that in one position of the sliding cylinder, the sample, which is fastened to the inside wall of the cylinder over one-half of its length, is in counting position, whereas by sliding the cylinder the sample is moved out of the counting region and the background count is obtained. The counter was operated with the sample cylinder at about 50 volts negative potential with respect to the screen, so that the sample cylinder itself became the counter wall and the geometrical efficiency was increased to nearly 50 percent.

Observations were made on rhenium received from the University of Tennessee in the form of potassium perrhenate and sintered rhenium metal. These samples were purified as described below. A sample of rhenium metal of European origin received from Johnson-Matthey Company, London, England, was also examined. The absorption characteristics of the activity found were determined by placing aluminum foils inside the slide cylinder covering both the sample and the background areas.

Method of Chemical Purification

Rhenium heptasulfide was precipitated by passing hydrogen sulfide gas into a solution of the rhenium compound which had been made $4N$ in hydrochloric acid. The rhenium heptasulfide precipitate after thorough washing was dissolved in sodium hydroxide plus hydrogen peroxide and the solution filtered to separate sulfides not soluble in this mixture. Concentrated sulfuric acid was added to the solution and perrhenic acid distilled off in a stream of carbon dioxide and steam.[11] Two such cycles resulted in a product which appeared to have no radioactivity resulting from potassium as judged by the absorption characteristics of the activity found, for certainty four such cycles were completed on the American sample of potassium perrhenate.

This purification scheme is believed to be adequate for the removal of all other elements with the possible exception of element 43, which can be expected to follow rhenium at least in part in the above separations. However, it appears doubtful in any case that this element exists in nature since the isotopes of atomic weights 97, 99, and 101, which are those most likely to be stable, have been shown to be radioactive with half-lives of 93 days,[12] 4×10^6 years and 14.0 minutes,[13] respectively. The sample was mounted simply by painting a slurry of rhenium heptasulfide in alcohol on the slide cylinder.

The sample of European rhenium was not further purified. According to a spectrographic examination of the sample made by the Johnson-Matthey Company the sample is exceedingly

TABLE III. Absorption in aluminum of activity of American and European rhenium samples.

Area of sample and thickness (1) Counts per minute (2) Percentage of original count rate	American rhenium 300 cm², 2.5 mg/cm² of Re_2S_7 (1)	 (2)	European rhenium 180 cm²; 5.6 mg/cm² of Re (1)	 (2)
Through 0 mg/cm² aluminum	31.5±1.2	100 ±3.8%	38.5±2.6	100 ±6.7%
0.8 mg/cm² aluminum	9.7±1.6	30.8±5.0%		
1.5 mg/cm² aluminum	5.6±1.4	17.8±4.3%	8.2±1.7	21.3±4.4%
2.4 mg/cm² aluminum	3.2±1.1	10.3±3.5%	4.3±1.4	11.1±3.7%
3.4 mg/cm² aluminum	0.0±0.7	0 ±2.3%	0.76±1.3	2.0±3.4%

[9] W. F. Libby, Phys. Rev. **46**, 496 (1934).
[10] D. D. Lee and W. F. Libby, *ibid.*, **55**, 245 (1939).
[11] L. C. Hurd and C. F. Hiskey, Ind. Eng. Chem. Anal. Ed. **10**, 623 (1938).
[12] E. E. Motta, G. E. Boyd, and A. R. Brosi, Phys. Rev. **71**, 210 (1947).
[13] J. M. Siegel, J. Am. Chem. Soc. **68**, 2411 (1946).

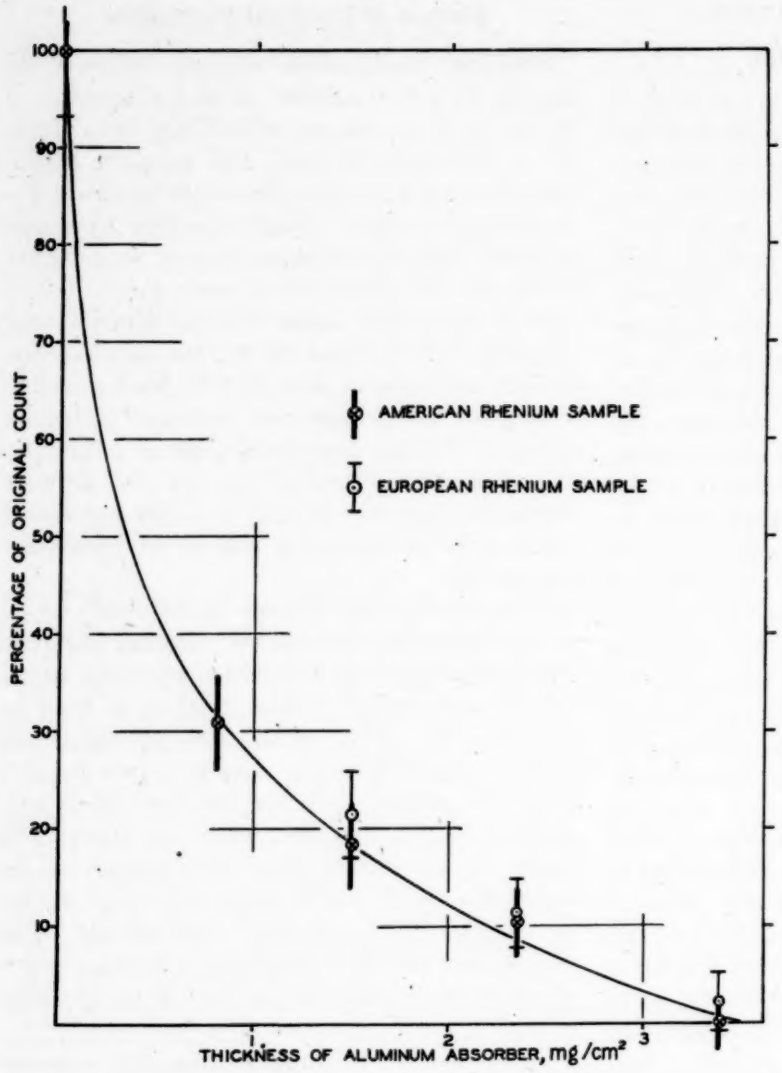

FIG. 1. Absorption in aluminum of rhenium activity.

pure, the only lines being attributed to traces of the elements calcium, silicon, magnesium, copper, and iron.

RESULTS

Table III presents the activity found in the two samples of diverse origin, *viz.*, American rhenium heptasulfide and European rhenium metal as described above. The effect of the same aluminum absorbers on the counting rates of each of these samples is also presented. The data from both samples are plotted together in Fig. 1. From this figure it can be seen that the same activity is possessed by the two widely different samples of rhenium. From these data the range of the beta-particles is estimated to be 3.5 ± 0.5 mg/cm² of aluminum. From an empirical range-energy relation,

$$\text{Range (mg/cm}^2) = \frac{[E(KV)]^{5/3}}{150},$$

which is known to hold for some other low energy beta-particle emitters,[14] the energy of the rhenium beta-particle is estimated to be 43 ± 6 kev.

Possibility That Acticity Is Caused by Emission of Alpha-Particles

The low range of these particles invited the suspicion that the activity might be alpha-particles. For this reason an attempt was made

[14] W. F. Libby, Ind. Eng. Chem. Anal. Ed. 19, 2 (1947).

to determine whether alpha-particles were involved, by determining whether the intensity of ionization produced by the particles emitted was sufficient to be observed in a counter operating in the proportional region.

The screen wall counter was used for these observations. In order to provide some known alpha-particles for comparison, a sample of samarium nitrate was mounted on the end of the sample cylinder opposite to the rhenium, in the normal background position. Under conditions which gave very well defined pulses on the oscilloscope screen when the Sm was in position, no pulses were observed when the counter was tipped to slide the Re into position, and it was concluded that the activity of Re is not emission of alpha-particles. The possibility that the activity might be due to positron emission or K capture must be eliminated, since $_{74}W^{185}$ and $_{74}W^{187}$ are both known to be radioactive by beta-emission. This leaves only the possibility of emission of beta-particles from either $_{75}Re^{185}$ or $_{75}Re^{187}$. The former process would lead to $_{76}Os^{185}$, which is known to be radioactive (I.T. 99 days; 30 hours). Since this activity is not observed, we conclude that the activity of natural rhenium is due to beta-emission from $_{75}Re^{187}$.

Half-Life of Rhenium^{187}

Estimated from European Rhenium Metal Sample

A count rate of 38.5 ± 2.6 counts per minute was given by a sample 180 cm^2 in area and 5.6 mg/cm^2 thick (Table III), of which only a layer of thickness equivalent to the range, 3.5 ± 0.5 mg/cm^2 will have contributed to the counting rate. Because of absorption and geometry factor the count observed is about 10 percent of the total disintegrations from a layer of a depth equal to the range.[84] We therefore have an indicated disintegration rate of 385 ± 26 per minute from 630 mg of rhenium of which 61.8 percent is the isotope Re^{187}. The half-life calculated from these data is 4.3×10^{12} years.

Estimated from American Rhenium Heptasulfide

A count rate of 31.5 ± 1.2 counts per minute was given by a sample 300 cm^2 in area and 2.5 mg/cm^2 thick (Table III). The total disintegration rate indicated[14] is then 320 ± 12 per minute from a calculated 1050 mg of rhenium heptasulfide, of which $373/598\times61.8/100$ is the weight of the isotope Re^{187}. The half-life calculated from these data is 2.6×10^{12} years.

This sample of rhenium sulfide covered a greater area than the sample of rhenium metal, and the counting efficiency was somewhat less because of greater end effect. A second observation was therefore made, using an infinitely thick layer of rhenium sulfide covering the same area as the rhenium metal sample. A count rate of 3.1 ± 1.4 counts per minute was observed, which gives a value for the half-life of Re^{187} of 3.3×10^{12} years.

In view of the different origins and chemical natures of the samples, the estimates of the half-life are in good agreement. Part of the discrepancy which appears is probably due to the difficulty of applying the sample in a completely uniform layer and without additives to assist adhesion. This was more difficult with the rhenium metal, which was a hard, sintered material, and the lumpiness of the sample layer probably contributed to the lower apparent activity and higher apparent half-life in this case. The average value for the half-life of Re^{187} indicated by the three observations is $3\pm1\times10^{12}$ years.

Active Nitrogen

JOSEPH KAPLAN
Institute of Geophysics, University of California, Los Angeles, California
(Received September 15, 1947)

It is shown that Mitra's hypothesis which attributes the Lewis-Rayleigh afterglow of nitrogen to the excitation of the molecules by a three-body collision,

$$N_2^+(X')+e+N_2=N_2(B\text{-state})+N_2(A\text{-state}),$$

cannot account for the spectrum of the auroral afterglow in which there is incontrovertible evidence that ions in the $N_2^+(X')$ state are present. It is proposed that the most important reactions occurring in nitrogen afterglows and probably in polar auroras are the dissociative recombination,

$$N_2^+ + e = N' + N'' \text{ (nitrogen atoms in metastable states)},$$

and collisions of the second kind involving very slow electrons and metastable atoms.

IN a series of publications which began with two notes in Science and Culture,[1] S. K. Mitra has proposed explanations of the nature of active nitrogen and the mode of excitation of the light of the night sky. These explanations depend on the presence in the active nitrogen or in the upper atmosphere of the positive ions of the nitrogen molecule in the so-called $N_2^+(X')$ state. During the past fifteen years I have studied a variety of afterglows in nitrogen and in mixtures of nitrogen and oxygen, and among these is the auroral afterglow whose existence also depends on the presence in the discharge of the first-negative bands of nitrogen. These bands persist after the discharge is cut off, and this persistence depends on the pressure and tube diameter. Recent studies indicate that the ions in the X' state last for the entire duration of the afterglow. This is illustrated in Fig. 1 in which the spectra of an auroral afterglow taken early only and very late only are shown. It is to be noted that the first-negative bands are present in each case.

It is important to note that the auroral afterglow and the afterglow of active nitrogen are not the same phenomena since they are produced differently and possess different spectra. It should also be pointed out that Mitra's hypothesis regarding the afterglow of active nitrogen is intended by him to apply to the afterglow of a condensed or electrodeless discharge in nitrogen to which I have given the name "Lewis-Rayleigh," and whose spectrum consists *only* of a few members of the first-positive system of neutral molecular nitrogen. The auroral afterglow, on the other hand, radiates the first-negative bands of ionized molecular nitrogen, the second-positive bands, the first-positive bands, the Vegard-Kaplan and the Goldstein-Kaplan bands of neutral molecular nitrogen, and the two forbidden lines of atomic nitrogen $^4S \leftarrow {}^2P$ and $^2D \leftarrow {}^2P$. The former line was observed by me many years ago, and the latter has been photographed during the past year on Eastman IZ infra-red sensitive plates. Another important difference between the Lewis-Rayleigh and auroral afterglows is that the spectrum of the former appears to be independent of the time of observation, whereas the spectrum of the auroral afterglow changes as the afterglow decays. Details and interpretations of many recent studies of this time variation will be presented soon, but this time variation is strikingly shown when one compares the spectra of Fig. 1.

It is the purpose of this note to point out that Mitra's interesting and important contributions will play a part in the explanation of the mode of excitation of auroral afterglows, but that the principal reactions which occur are not those proposed by him. Mitra's hypothesis is that in a three-body collision involving a molecular nitrogen ion in the X' state, an electron and an unexcited nitrogen molecule will yield two excited nitrogen molecules, one in the vibrational level $v=0$ of the A states (6.14 volts) and the other

[1] S. K. Mitra, Science and Culture (Calcutta) 9, 46, 49 (1943).

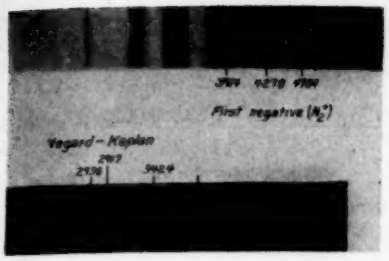

FIG. 1. (a) Auroral afterglow in pure N_2 early only. Eastman IO plate. (b) Auroral afterglow in pure N_2 late only. Eastman IO plate.

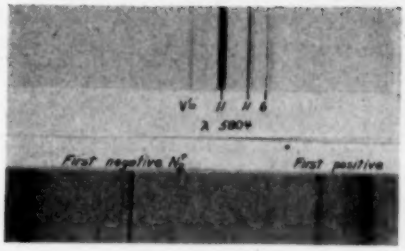

FIG. 2. (a) Auroral afterglow in N_2 (trace O_2) late. Eastman IF. (b) Auroral afterglow in pure N_2 early. Eastman IF plate.

in the level $v=11$ of the B state (9.43 volts). Since the ionization potential of nitrogen is 15.58 volts, it is clear that enough energy is available to account for these excitations. Now one of the most interesting results of the studies of the time variation of the auroral after glow spectrum has been the behavior of the first-positive and Vegard-Kaplan systems. As one photographs increasingly later portions of the auroral afterglows, there is noted a remarkable and apparently steady increase of the relative intensity of the Vegard-Kaplan bands. At the same time there is an increase in relative intensity of the first-positive bands which originate on $v=11$. It is also easy to see that the relative intensities of the first-positive bands which originate on $v=10$, 11, and 12 differ from the intensities observed in the Lewis-Rayleigh glow. These effects are illustrated in Figs. 1 and 2. In the auroral afterglow the bands which originate on $v=11$ are more intense relative to those which originate on $v=10$ and 12, than they are in the Lewis-Rayleigh glow. Furthermore, the Vegard-Kaplan bands are present when the first-positive bands from $v=11$ are enhanced. It should be stressed that the Vegard-Kaplan bands are not observed in the Lewis-Rayleigh afterglow spectrum, but also that one would not expect them since the transition probability from $A\rightarrow X$ is much smaller than from $B\rightarrow A$. The former, it is recalled, leads to the emission of the Vegard-Kaplan bands.

Now the simultaneous enhancement in the relative intensities of the Vegard-Kaplan bands and the first-positive band which originates on $v'=11$ would tempt one to ascribe this excitation to Mitra's reaction. However, if this reaction is to be the principal source of nitrogen molecules in the $A^3\Sigma$ level on which the Vegard-Kaplan bands originate, then it is difficult to explain the large intensity of these bands since they originate on a metastable state while the first-positive bands occur in an allowed transition. The failure to observe the $A\rightarrow X$ transition in the Lewis-Rayleigh glow therefore is not surprising and does not contradict Mitra's hypothesis, but their high intensity in the later stages of the auroral afterglow does.

One can also readily see on examining Fig. 2 that the first-positive band intensity distribution obtained when there is incontrovertible evidence as to the presence of nitrogen molecular ions is different from that observed in the Lewis-Rayleigh afterglow. Mitra's hypothesis alone cannot explain this, or the fact that the forbidden atomic and molecular radiations of nitrogen increase in both absolute and relative intensities with time after the interruption of the exciting discharge. Some other more probable mechanism must be used in order to explain these observations. It is therefore proposed that the two most important reactions occurring in the auroral afterglow and perhaps in the Lewis-Rayleigh glow are:

$$N_2^+ + e \rightarrow N' + N'', \quad (1)$$

and

$$N' + e \rightarrow N + e'. \quad (2)$$

Reaction (1) is a dissociative reaction[2] in which an electron recombines with a positive ion in the $N_2^+(X')$ level, producing two nitrogen atoms in the metastable ^2P state. Assuming a heat of dissociation for the neutral nitrogen molecule of 7.38 volts, the energy required for the production of two metastable nitrogen atoms in the ^2P level

[2] D. R. Bates and H. S. W. Massey, Proc. Roy. Soc. A187, 261 (1946).

would be 14.5 volts, since the energy of the ^2P state is 3.56 volts. It is therefore clear that the reaction (1) is energetically possible.

Reaction (2) is an electron-atom collision in which a metastable atom collides with a low velocity electron and gives up its potential energy to the electron in a collision of the second kind. This is the reverse of a collision of the first kind, one in which the kinetic energy of the electron is transferred to potential energy of the atom. Available evidence[3] indicates that the collisional cross section is very large for collisions of the first kind when the kinetic energy of the electron is only slightly above that necessary to raise the atom to an excited state, and the electron is therefore able to give up practically all of its kinetic energy. For electron energies higher than this the collisional cross section falls off rapidly. By the principle of microscopic reversibility a large collisional cross section should be expected for the reverse process, and here also the collisional cross section should fall off rapidly as the velocity of the impinging electron increases.

[3] I. S. Bowen, Rev. Mod. Phys. 8, 55 (1936).

If it is assumed that these are the two principal reactions which occur in *all* afterglows, it is possible for the present, to account (at least qualitatively) for the principal features of the afterglow spectra. Collisions of the second kind postulated in reaction (2) will account for the delayed maximum in the intensity of forbidden radiations. They will also provide slow electrons which can excite the first-positive bands of nitrogen by collisions with metastable molecules ($A^3\Sigma$) and highly vibrating molecules in the $X'\Sigma$ state. The latter may be produced by three body collisions in which two normal nitrogen atoms are involved. On this hypothesis one would expect a modified discharge-like spectrum in the early part of the afterglow, and this is effectively what one observes in the auroral afterglow and, incidentally, also in the spectra of polar auroras. Superposed on this may be contributions from such reactions as those of Mitra, but these do not play the principal roles. I plan, in designing future experiments and also in applying the results of laboratory studies to the physics of the upper atmosphere, to test these hypotheses as carefully as possible.

PHYSICAL REVIEW VOLUME 73, NUMBER 5 MARCH 1, 1948

The Microwave Spark[1]

D. Q. Posin*
Radiation Laboratory, Massachusetts Institute of Technology, Cambridge, Massachusetts
(Received August 6, 1947)

Electrical breakdown of air was studied at 3 microwave frequencies: wave-lengths of 1.25 cm, 3 cm, and 10 cm. Breakdown field strength was determined as a function of pressure, gap height, intensity of initial ionization, width of a single microwave pulse which sufficed for breakdown, and the pulse repetition frequency.

It is found that the field strength for breakdown is strongly dependent upon the width of the microwave pulse, the intensity of initial ionization, and, of course, upon gap height and pressure of enclosed gas. A lesser dependence is found on the repetition rate of the pulses. The validity of Paschen's law at these high frequencies is investigated, and a semitheoretical formulation of breakdown is obtained based on electron ionization competing with the process of electron attachment to neutral molecules (relatively immobile in the gas). Prediction is made from this theory as to certain expected results. For experimental conditions these were not realizable at the time the experiments were performed but they may now be realized in certain laboratories.

1. INTRODUCTION

DURING the course of the radar work at the Radiation Laboratory, M.I.T., serious problems were posed by undesired sparking of radiofrequency components when high power emanated from magnetrons. Accordingly, investigations were started to study the nature of microwave sparking.[2]

[1] This article is based on work done for the Office of Scientific Research and Development under Contract OEMsr-262 with the Massachusetts Institute of Technology.
* Now at the Department of Physics, North Dakota State College, Fargo, North Dakota.

[2] A part of the experimental material discussed in the present article appears in Radiation Laboratory Report 731, D. Q. Posin, Ina Mansur, H. Clarke, November 1, 1945.

After the completion of the spark breakdown experiments, a mathematical attempt was made to establish a sparking criterion utilizing as basic assumptions ionization by electrons which are activated by the microwave field, and disappearance of electrons by attachment to neutral molecules. For this purpose use was made of an equation giving the electron ionization as a function of pressure and ratio of field strength to pressure, similar to the functions well known in d.c.[3]

Other theories of microwave breakdown, though usually applicable only to the low pressure phenomena and for continuous waves (not pulsed microsecond bursts), have been recently developed by a number of writers[4–6] and it is hoped that more theoretical work will soon be forthcoming on electrical breakdown phenomena of centimeter waves.[7]

2. GENERAL REMARKS

To obtain reliable and repeatable breakdown data in the experiments discussed in this paper it was found necessary to provide sufficient initial ionization in the gap where breakdown was to take place. The initial ionization was supplied by placing a capsule of radioactive cobalt (of 3.2-millicurie intensity) on the outside of the wave guide above the breakdown gap. Otherwise, if the initial ionization is sporadic, like the normal ionization from cosmic rays, one might, in raising the field strength, pass the true breakdown value if no strategically placed electrons are available at the critical moment; later, electrons might appear appropriately in the gap and the spark may soon pass, but at too high a field.

It was found at microwave frequencies that with artificially provided initial ionization the breakdown field may be considerably lower than the field with only the normal natural ionization. In d.c. one does not expect the initial ionization to change the breakdown field unless the initial ionization is sufficient to cause space charge distortion[8] of the applied field. In pulsed microwave breakdown even a moderate amount of externally supplied initial ionization may change the breakdown field significantly; possibly this occurs for the following reason: If extra electrons are available when the pulse begins, then the pulse may be tall enough and wide enough to generate a sparking quantity of ions. That is, the field may be sufficiently intense and may be operative long enough to cause accumulation of electrons leading to a spark. If the initial ionization is low, the pulse may have to be made taller in order to generate the same sparking number of ions by the time the pulse has come to the end of its width. Hence, we should be guilty of overvolting.[9]

After the completion of the straightforward planned investigations, the writer observed an effect which appears to be of some interest: the lowering of the electrical breakdown field strength in certain cases for the 3-cm waves, caused by an externally applied magnetic field.[10]

Another point of interest found during the experiments is the following: when a spark or glow occurs within the narrowed wave-guide section constituting the gap, an increase in the magnitude of the standing wave occurs in the region between the discharge and the power source, and this change detected by a pick-up probe in a slotted section, may be used to advantage as an indication that breakdown is occurring, for the case of the low pressure, soft, inaudible glow discharge; or for any other, if desired. This is obviously one of the many

[3] The mathematical approach here indicated was first made by the writer in Radiation Laboratory Report 53.1, November 29, 1945, and dealt with both pulsed voltage applications and continuous wave applications.

[4] T. Holstein, Phys. Rev. 69, 50A (1946).

[5] Ernest Mayer, Phys. Rev. 69, 51A (1946).

[6] H. Margenau, Radiation Laboratory Report 967, January 10, 1946.

[7] See also T. Holstein, Phys. Rev. 70, 367 (1946), and Margenau, McMillan, Dearnley, Pearsall, and Montgomery, Phys. Rev. 70, 349 (1946).

[8] Varney, White, Loeb, Posin, Phys. Rev. 48, 818 (1935).

[9] The fact that an external supply of electrons, due ultimately to the radioactive capsule, lowers the apparent breakdown field may be used to locate weak spots in a large r-f component assembly, such as wave guides, chokes, and flanges, stub supports, rotary joints, etc., as follows: Without using the radioactive cobalt the assembly is connected on the high power bench and the power is raised until something sparks; the field strength is then lowered just out of reach of breakdown and the radioactive capsule is then passed (by a pair of long safety tweezers) on the outside along the entire assembly from end to end. The weak spot or spots will now crack electrically. This technique frequently fails to work in cases where the gap volume is very small, apparently because the gamma-rays or their ionizing secondaries miss the tiny volume. However, the method has been found well worth trying and often obviates the primitive necessity of drilling holes or putting in windows to *see* where the spark is passing.

[10] D. Q. Posin, Phys. Rev. 69, 541 (1946).

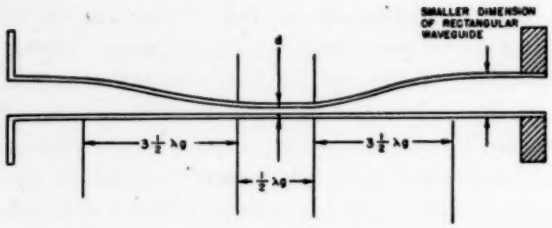

FIG. 1. Generalized drawing of "swayback" section. The breakdown gap is at *d*.

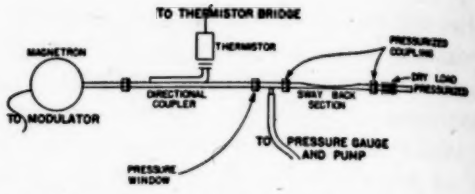

FIG. 1A. Assembly for breakdown at increased pressure. (For reduced pressure, pressure pump and pressure gauge are replaced by vacuum pump and vacuum gauge. For atmospheric pressure, pressurized windows and couplings are not used. For calibration of thermistor, dry load is replaced by water load.)

aspects of reflection of microwaves by strongly ionized layers.[11] In general, it is felt that the use of centimeter waves and the impending production of high intensity millimeter waves opens the field of gas discharge phenomena anew in the same refreshing way that the classical work of Thomson, Crookes, and Townsend did, when their efforts welcomed a host of other pioneers to investigations in the d.c. and low frequency domain.

3. APPARATUS AND EXPERIMENTAL PROCEDURE

To obtain a controlled measurable field at microwave frequencies one must either measure the field directly or use some method from which the field may be computed. In the experiments reported in this paper the second of these procedures was followed. Since it was desired that the microwave breakdown take place across a definite gap of known height, the gap within a section of wave guide had to be narrower than the rest of the wave guide. To accomplish this the wave guide was gradually narrowed in its shorter dimension, extended for a short distance with this minimum dimension, and then it was caused to taper back to normal size gradually. A typical "swayback" of the kind used is shown in Fig. 1. It is obvious that the gradual taper minimizes reflections, and since the same Poynting power now passes through a smaller guide, the field is increased in proportion to the square root of the factor by which the guide is decreased.[12] A measured amount of power was fed into the section and thus it became possible to compute the field at any power level. The procedure during the experiments was thus to increase the power from the magnetron until a spark passed in the swayback; observation of the power level at that critical point then permitted the calculation of the field corresponding to dielectric rupture.

A number of magnetrons, each of appropriate fixed frequency were utilized in turn, driven either by a hard tube or hydrogen-thyratron modulator.

4. METHODS OF MEASURING THE POWER FOR CALCULATION OF FIELD STRENGTH

A water load was used as the standard of power measurement. This type of load consists of a glass tube inserted in a wave guide; the tube is given some form of taper in order to minimize reflections, and water is circulated through the tube at an accurately known rate of flow,[13] the difference between the input and output temperatures being indicated by thermocouples. Errors due to radiation and conduction are reduced by making the temperature of the input water as close as possible to the room temperature; for this reason high flow rates, resulting in small temperature differences, are used.

A sensitive Rubicon galvanometer (0.5-microampere full-scale deflection) was used to measure the small thermocouple voltages. The voltage sensitivity of this galvanometer was varied by

[11] A somewhat related problem, treated theoretically, is that on conduction and dispersion of ionized gasses at high frequencies, by H. Margenau, Phys. Rev. 69, 508 (1946).

[12] It may be readily shown from an integration of Poynting vector over area in wave guide that the peak power, P_m, and peak field strength, E_m, are related as follows:

$$P_m = KE_m^2(\lambda_0/\lambda_g)ab,$$

where K is a constant, λ_0 is the wave-length of the waves in free space, λ_g is their length in the wave guide, and ab is the cross-sectional area of the wave guide at the particular plane where one is contemplating E_m.

[13] For a description of an accurate pump designed in the later stages of the work by H. F. Clarke, see his Radiation Laboratory Report 53.1, November 7, 1945. This also contains details relevant to measurements in microwave breakdown work.

means of a series resistance (G.R. decade, 0–1000 ohms). In order to calibrate the thermocouples and the galvanometer, it was necessary to substitute a tube containing a coiled heating element for the glass tube in water load. The coil was then connected to the 60-cycle line, and the power recorded by a wattmeter.

Although the water load is a highly desirable power measuring device, being an absolute method and giving reasonable accuracy, it nevertheless suffers from the following defects: It has to be used to terminate the line after the energy has passed through the device being studied, and this is often inconvenient. It is rather slow in its response, perhaps taking half a minute to record the reading on the lagging galvanometer. In view of the fact that discharge phenomena are practically instantaneous in their development, it is desirable that the power measuring device (ultimately field strength) be as fast as possible, especially in order to follow any fluctuations in the magnetron output. For this reason, it was found desirable to make use of a thermistor—essentially a resistance wire enclosed in a glass bead, forming one arm of a type of Wheatstone bridge. The thermistor was coupled to the main wave-guide line by means of a shunt—directional coupler—which coupled a known fraction of the r-f energy out of the line and allowed it to impinge upon the thermistor. The thermistor bridge was known at Radiation Laboratory as a "W" bridge, type TBN 3EV, and could be individually calibrated by the application of a d.c. voltage to the thermistor wire itself. Although the termistor power monitor may be used in an absolute manner, by measuring the coupling of the directional coupler, and calibrating the bridge for a known sensitivity at the thermistor, Mr. H. F. Clarke found discrepancies when using this system with the water load, especially for 1-cm waves. Accordingly, it was decided to calibrate all directional-coupler monitors against water loads. Arrangement for achieving this calibration, as well as other typical arrangements used in the study here reported, are indicated in Fig. 1A and its explanatory caption.

Inasmuch as all methods of power measurement using thermal devices measure average power, it becomes necessary to calculate the peak power from a knowledge of the repetition rate of the pulsed signals and the width of the particular pulse being generated. The determination of the repetition rate is achieved by using an oscilloscope, placing the modulator trigger voltage pulse on the vertical plates, and a sine wave from a calibrated audio oscillator on the horizontal plates. The frequency of the sine wave is then varied until one observes on the scope that one trigger occurs each cycle.

The pulse width, for purposes of power measurement,[14] is taken as the time from the center of the rise of the current pulse to the center of the fall of the pulse, as in standard procedure for pulse width measurements. The measurements were made on synchroscopes calibrated with the standard range calibrators of the Indicator Group at Radiation Laboratory.

In those experiments in which a single pulse was sent down the wave guide by pressing a button, thermal methods of power measurement could not be used, and it sufficed merely to view the height of the current pulse from the magnetron on the oscilloscope, and compare it to the heights of the pulses when repetition rate performance was employed (and power was measured by the thermistor). The reason why it suffices to study the size of the current pulse in the calculation of power is the following: the power output of a magnetron operating at a given magnetic field is found to be approximately proportional to the magnitude of the current pulse. Furthermore, it seems reasonable to assume that current pulses of the same magnitude correspond to the same power, whether single, or at some repetition rate. Therefore, one can, by using a water load with a steady string of pulses, calibrate the height of the current pulse against the power output as measured by the water load. As a matter of fact, in those portions of the present experiments where single pulse breakdown was compared to repetition rate

[14] It was clear to the writer that, insofar as ionization effects and breakdown are concerned, the width of the pulse could not be considered as the value indicated above. The problem essentially was to calculate the effective equivalent *ionization* width of the r-f voltage pulse, when the latter was shaped as a trapezoid. The ionization width of the rectangular equivalent pulse of the same amplitude as the maximum of the trapezoid was found by the writer by utilizing the ionization equation developed in the present paper. The calculation of this effective width may be obtained from the writer upon request.

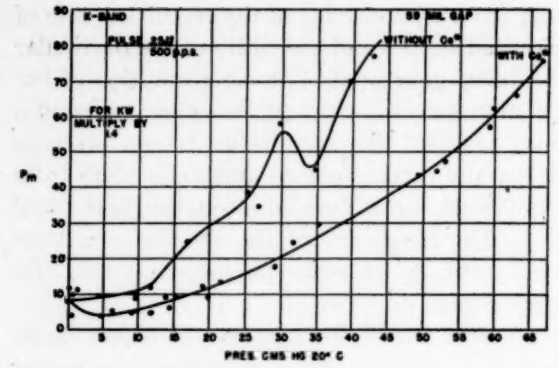

FIG. 2. One run with Co* compared to one run without Co*.

breakdown, and also in other single pulse experiments, only relative powers were of interest, and therefore it sufficed to make comparisons merely of the heights of the magnetron current pulses.

5. THE DETECTION OF THE SPARK

Ordinarily, the occurrence of the spark was evident by its sound; occasionally, when the section which terminated the wave-guide line after the swayback was an open horn, the spark could be detected also by viewing the emitted light. In other cases, especially at low pressure when the sound was extremely faint and when it was impossible to gaze down the horn because much of the assembly was under an evacuating bell-jar, the breakdown was detected by other methods. A stethoscope or a contact microphone was attached to the swayback section immediately over the enclosed gap and the sound could be detected in that way, or else a directional coupler with a power detecting device was used to pick up the sudden increased reflections due to the spark acting as an abrupt termination. This latter technique promises to develop into a form from which one might establish by quantitative definition the fact that a spark has occurred, for the amount of reflection from a cumulatively ionized gas is a function of the intensity of the ionization. In utilizing the reflection method for spark detection it is desirable that a contrivance be used which will indicate the instantaneous energy reflected, inasmuch as the sporadic reflections from an occasionally sparking gap would not register on an average power indicator, such as a resistance wire. For this reason, in these reflection method cases use was made of the set of apparatus comprising a crystal, amplifier, and synchroscope, with inverted directional-coupler pick-up inserted between the prepared sparking gap and the magnetron in position to pick up reflections from the gap should it begin to spark. The spark would thus be detected by the sudden increase in height of the pulse appearing on scope. (Even though the directional coupler in inverted position should theoretically pick up only energy reflected from the termination end of the line, in practice one always has some direct pick-up from the Poynting energy pouring outward from the source. But this may be small and rather steady until it is suddenly augmented by the reflection energy from an occurring spark.) As has been mentioned, the passage of a spark could also be detected by observing the increase in the standing-wave ratio in a slotted section located between the magnetron and the spark.

6. RESULTS

Typical experimental results are shown in Figs. 2 to 11. These graphs reveal the effects of the following parameters (after repeatability in procuring data is achieved through the use of the radioactive capsule): 1. Intensity of initial ionization. 2. Gas pressure. 3. Height of breakdown gap. 4. Repetition rate of pulses. 5. Pulse width.

In addition to presenting the typical graphs, it is felt worth while to present also an empirical summary of a portion of the results.

Figure 2 shows that, ordinarily sparking data at microwave frequencies tend to be unreliable until extra initial ionization is provided; that is in addition to the natural erratic ionization due to such sources as cosmic rays.

The use of a strong radioactive source, such as 3.2 millicuries of Co*, to provide extra ionization, brings with it also the following changes: (a) the breakdown field strength is always lower than when the radioactive source is not used; (b) the "law" of breakdown is changed from approximately straight line[15] when breakdown power ($P_m \sim E_m^2$) is plotted against pressure, to parabolic, when the Co* is used. (This effect becomes evident in the equations given in this paper.)

[15] When many non-Co* curves are averaged.

Figure 3 indicates to what extent it becomes easier to produce a microwave spark when the number of high frequency pulses running through the gap per second increases fourfold. The following is a possible interpretation of such a "repetition rate effect": If the spark does not occur on the first pulse, then some of the electrons created during the first pulse may still be roaming freely in the gas by the time that the second pulse starts (although perhaps most of the electrons have been lost through attachment, recombination, and diffusion during the rest period between two pulses). The second pulse then has an advantage, and builds on top of its inheritance; the third pulse works on a still bigger initial supply, etc., until at some pulse down the line a spark passes.

It was found that, for a given field strength, a spark that just manages to occur when the repetition rate is R_1 does not occur when the repetition rate is $R_2 < R_1$ even if we wait for it indefinitely. Certain experiments especially designed to test this matter were performed as follows: for 1.25-cm waves a certain gap broke down at 14 units of average power when the repetition rate was 1000 pulses per sec., the field was then lowered and the repetition rate set at 500 p.p.s., then the field was raised until the average power read 14/2 or 7 units; this made the two peak field strengths equal but no spark passed now even after a wait of three minutes. When the field was raised a certain amount, the spark came. From these and a number of other experiments a fairly safe conclusion is this: a fourfold increase in repetition rate (500–2000 p.p.s.) lowers the peak breakdown field strength by about 15 percent.

Figure 4 shows how the breakdown field strength for 1.25-cm waves varies with gap width at a given pulse width and repetition rate over a large range of pressures. The fact that a stronger field is necessary to crack a narrower gap might be explainable as follows: the removal of electrons by the alternating instantaneous anodes robs the gap of part of its electron density, and is more serious on a percentage basis for narrow gaps than for the wider ones, thus necessitating a higher ionizing field to make up the loss for the narrow gaps. It is worth recalling that even at d.c. the field varies with gap width especially in the lower pressure regions. That is Paschen's law is not a straight line at the lower pressures, but merely states that breakdown voltage is a function of mass between the electrodes.

Figure 4A is a plot of Paschen curves using a number of gap widths over a fairly extended pressure range. These curves are derived from those of Fig. 4 and show that the Paschen law may be considered as being approximately valid at microwave frequencies, at least for the higher products of *pxd*, that is, for the grosser air masses. (One recalls that in Paschen's law the temperature is assumed constant; otherwise a correction must be made of the pressure value.) The only unique Paschen curve at microwave frequencies may be considered to be that for a very wide gap and long pulse, or for a pulse of infinite width—that is, continuous wave. As a practical matter, at atmospheric pressure, for a gap somewhat larger than 60 mils, and for any repetition rate, a pulse greater than about 6 microseconds yields values of breakdown field substantially equal to those for a continuous wave. (This may be inferred from the rapid flattening seen in the curves of the breakdown field strength *versus* pulse width; the flattening takes place after about 6 μsec., see Fig. 8.)

Figure 5 gives a curve of breakdown power *versus* pressure up to two atmospheres, for two different repetition rates at 1 μsec. These curves were obtained with Co* in use, and again reveal the non-linear (on the average nearly parabolic) rise of peak tolerable power with pressure.

Figure 6 shows the variation of breakdown field strength with pulse width at a given repetition rate, from 1 cm to 76 cm Hg in pressure.

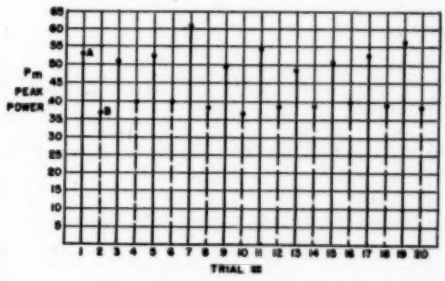

FIG. 3. Repetition rate effect on peak breakdown power at atmospheric pressure. Upper dots are for a repetition rate 500 p.p.s. Lower dots are for 1960 p.p.s. Average P_m, 30 percent.

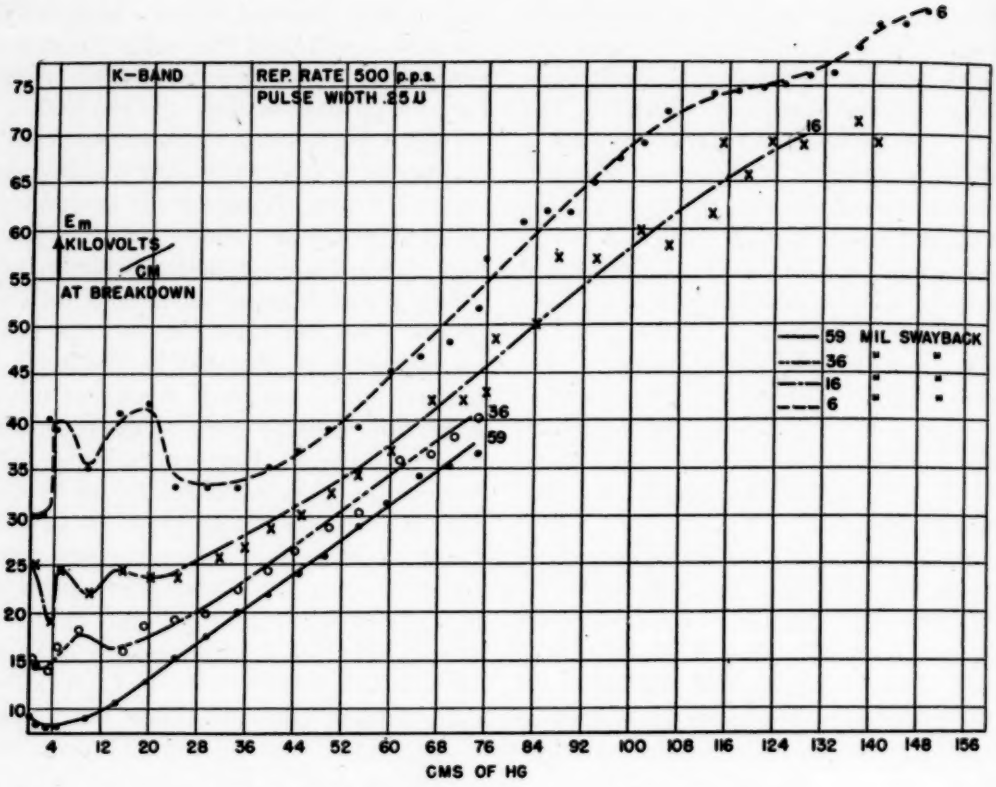

FIG. 4. Peak field strength *vs.* pressure for various swaybacks.

In Figure 7 is presented a breakdown "spectrum," showing the variation of peak power at breakdown *versus* pressure for a number of pulse widths and repetition rates. Also shown is one non-Co* curve contrasting with a Co* curve (those at 1 μsec.). The Co* curves are all parabolic and the non-Co* is practically linear.

Figure 8 reveals the dependence of breakdown power on pulse width and indicates that at atmospheric pressure, after about 4 or 5 μsec., the breakdown power is substantially independent of pulse width. That is, the "minimum formative field"** at atmospheric pressure is attained with a pulse width of about 5 μsec. (It is later shown mathematically that at lower pressures the minimum formative field becomes greater; in fact, in inverse ratio.)

It is seen from the graph that for pulses of less than about 0.3 μsec. the breakdown field becomes relatively very great.

It is perhaps possible to regard the pulse width effect in the following manner: for a narrow pulse the available and accumulating electrons may not have sufficient time to generate a sparking density of ions; hence it would be

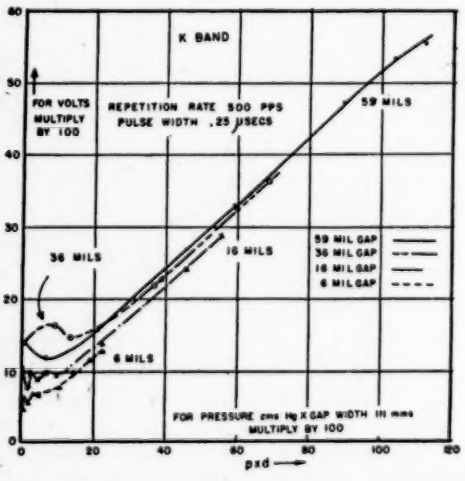

FIG. 4A. Paschen curves for various swaybacks (gap widths).

** Here arbitrarily defined as the field which is 103 percent of its minimum cw value at a given pressure.

necessary to raise the field which brings about high electron ionization by collision. In the limit, as the narrowness of the pulse approaches zero, the height of the breakdown field approaches infinity. At the other extreme, as the pulse is made broader and broader, the field necessary for breakdown becomes smaller and smaller in amplitude, the interpretation conceivably being this: although the electrons are oscillating and ionizing less vigorously, they still can generate a sparking quantity of ions if given enough time, that is, enough pulse width. There exists a limit, however, to how low the field may be (even though the width may be extraordinarily great), and this limit depends on the rate of electron production compared to the rate of electron loss by recombination, attachment, diffusion, and removal at the instantaneous anode. At atmospheric pressure the lowest breakdown field was very nearly obtained with the relatively small width of about 4 μsec. After this value of pulse width little lowering of breakdown field was discernible, and pulses greater than 4 μsec. were essentially wasting their time, literally, after 4 μsec. In principle, the lowering of field continues to a definite non-zero value asymptotically as we approach infinite pulse width or continuous wave. However, this asymptotic tapering goes on at a sub-microscopic rate, and the value of breakdown field at CW is substantially the same as that at about 5 or 6 μsec.

At lower gas densities the maximum width of the pulse after which no lowering of breakdown field is grossly discernible may be expected to be greater than the value at atmospheric pressure inasmuch as the electronic ionizing rate[16] decreases at the low pressures.

Figure 8A gives further studies of the effect of pulse width on breakdown power (or field strength) at atmospheric pressure, especially revealing the approximate minimum formative fields through the use of single pulse breakdown experiments.

Figure 9 gives a 10-cm power-pressure curve (with Co*), for the range of 1 to 1.52 atmospheres. In Fig. 10, the effect of repetition rate on breakdown is seen for the case of the 10-cm waves, the range in repetition rate being 200 to 2000 pulses per sec. The data were taken at a pulse of 0.76 μsec., at atmospheric pressure, for two different gap widths, with Co* as well as without it. One might expect the curve to flatten out at repetition rates somewhat higher than 2000, whereupon the gap would perform as though CW were being applied, or as though a pulse of 6 μsec. were active with any repetition rate whatever. For, as was indicated previously,

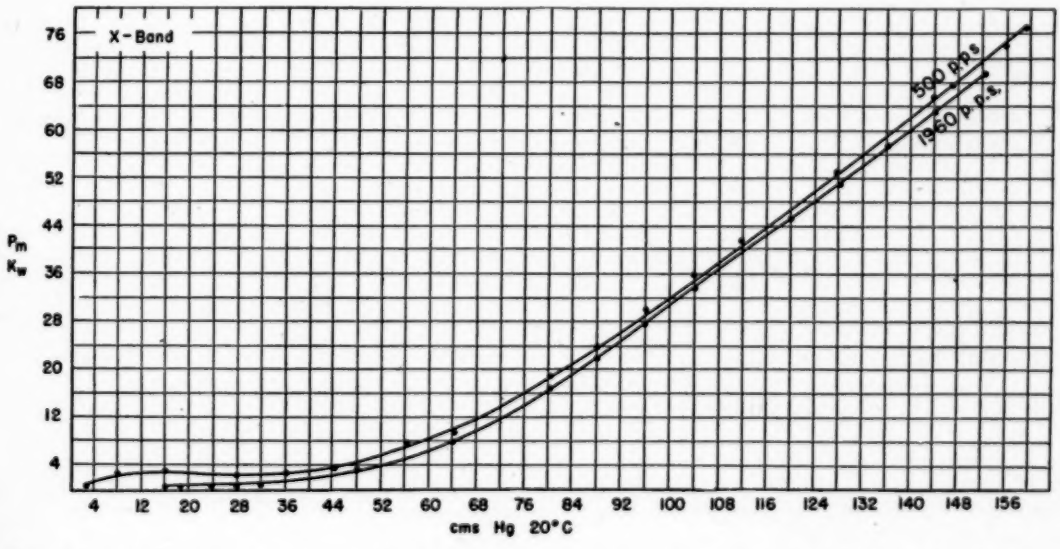

FIG. 5. Breakdown power *vs.* pressure up to two atmospheres for two different repetition rates at a pulse of 1 μsec.

[16] D. Q. Posin, Phys. Rev. 50, 650 (1936).

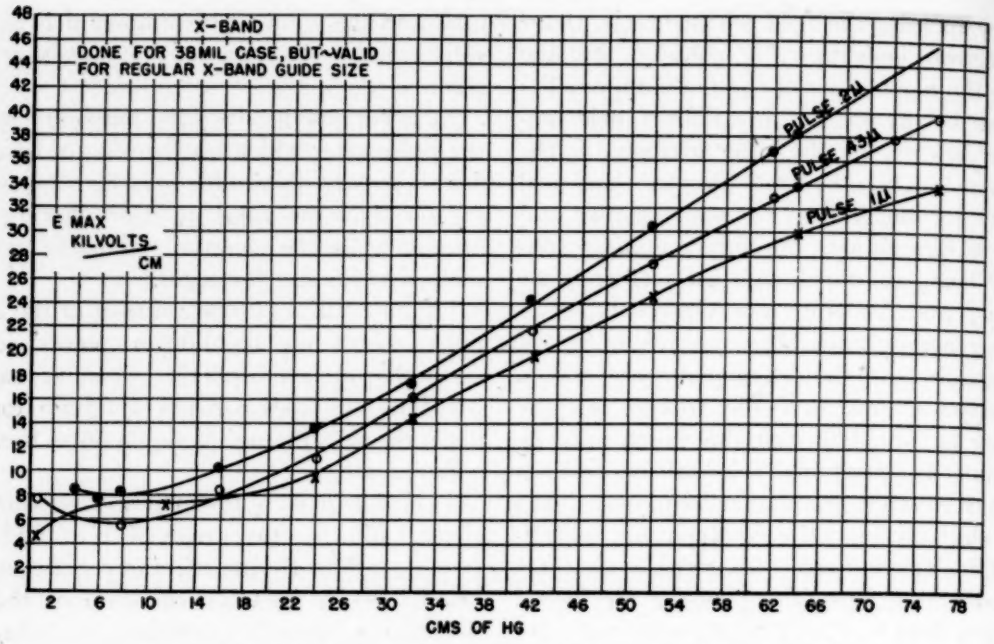

FIG. 6. Peak field strength at breakdown, and pressure, and pulse width.

CW very likely brings with it practically the same minimum breakdown field that a 6 μsec. pulse does (at atmospheric pressure).

Figure 11 shows a curve derived mathematically and predicts the manner in which the practical minimum formative field varies with pressure. Thus far, only one experimental point exists to be matched to this curve. Reference to this curve is made again in the section on mathematical formulation.

7. EMPIRICAL SUMMARY

(Peak breakdown field, E_m, in wave guide is related to peak breakdown power, P_m, by the formula

$$P_m = 6.63\times10^{-4}E_m^2\cdot\frac{\lambda_0}{\lambda_g}ab,$$

P_m in watts, E_m in volts/cm, a and b dimensions of rectangular wave guide in cm.)

1. *For 1.25-cm Waves*

$$P_m = \frac{3.74}{(\mu)^{\frac{1}{2}}}\times10^{-3}(5500-R)p^n\frac{W}{170}$$

μ is the pulse width in microseconds;
p is the pressure in atmospheres;
P_m is the peak power in kilowatts;
W is the height of the gap in mils.

Limits of verified validity: μ, 0 to 2 μsec.; for $\mu>2$, consult pulse width curves. R, 500 to 2000 pulses per sec.;

p, 5/76 to 2 atmospheres.

The exponent n is about 1 for pressures above about half an atmosphere. For the range 5-cm Hg to ½-atmosphere, $n\simeq2$.

For atmospheric pressure, 500 p.p.s. and 1-μsec. pulse,

$E_{max}\simeq27$ kv/cm,
$P_{max}\simeq187$ kw
(full-size guide, 170×420 mils, inner).

2. *For 3-cm Waves*

$$P_m = \frac{4W}{(\mu)^{\frac{1}{2}}}p^n(8000-R)\times10^{-4}\quad\text{(kw)}.$$

Limits of verified validity, including values of n: same as for the 1.25-cm waves.

$$E_m = \frac{0.38(p^n)^{\frac{1}{2}}(8000-R)^{\frac{1}{2}}}{(\mu)^{\frac{1}{2}}}\text{ kv/cm}.$$

At atmospheric pressure, 1-μsec. pulse, and 500 p.p.s.,

$E_{max}\simeq34$ kv/cm,
$P_{max}\simeq1.2$ megawatts
(full-size guide, 400×900 mils, inner).

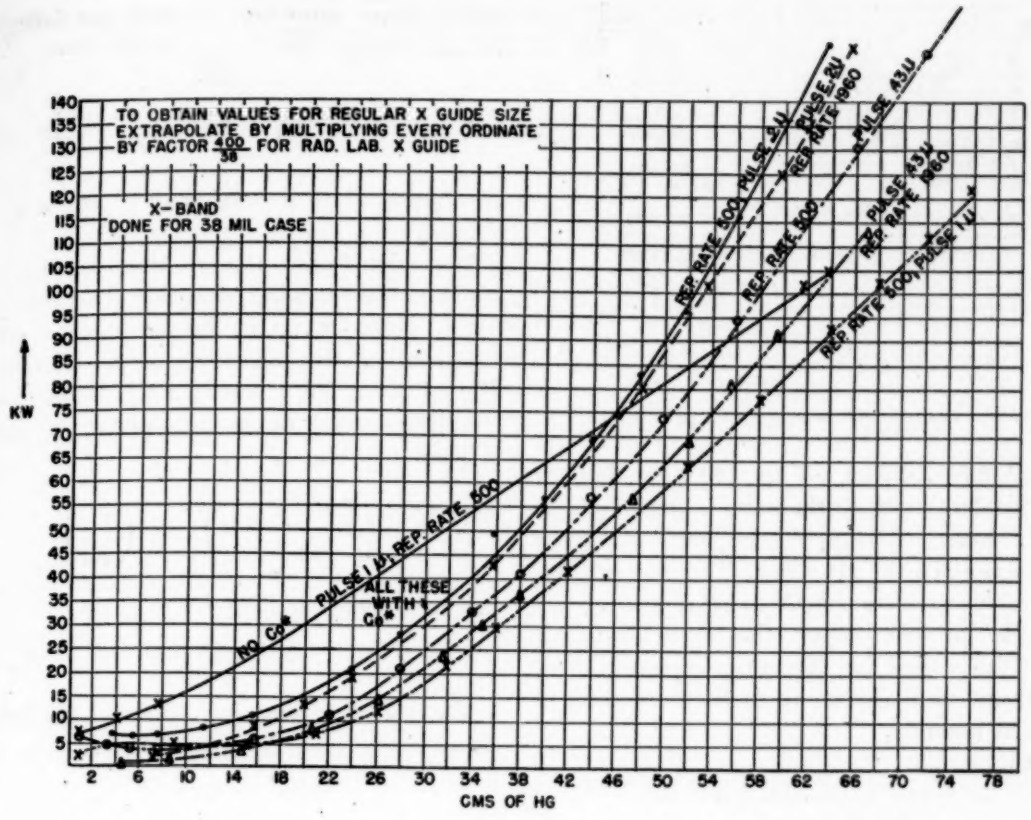
TO OBTAIN VALUES FOR REGULAR X GUIDE SIZE EXTRAPOLATE BY MULTIPLYING EVERY ORDINATE BY FACTOR 400/38 FOR RAD. LAB. X GUIDE
X-BAND DONE FOR 38 MIL CASE
KW
CMS OF HG
NO Cs*
PULSE 1 μ, REP. RATE 500
ALL THESE WITH Cs*
REP. RATE 500 PULSE 2 μ
REP. RATE 1960
PULSE 3 μ
REP. RATE 500
REP. RATE 1960
PULSE 4 μ
REP. RATE 500, PULSE 1 μ

FIG. 7. Peak power at breakdown, and pressure, repetition rate, and pulse width.

3. *For 10-cm Waves*

Limits of verified validity:
μ, 0.76 to 1.86 μsec.;
p, 1 to 1.52 atmos.;
R, 500 to 2000 p.p.s.;
$P_m = 3.45\times10^{-4}p^2(6300-R)\cdot(6.4-\mu)$;
P_m in megawatts;
p in atmospheres;
μ in microseconds.

At atmospheric pressure, 500 p.p.s., 1 μsec.; and for full-size wave guide (1.34 in.$\times$2.84 in., inner), $P_m = 10.8$ megawatts, $E_m = 30$ kv/cm.

8. MATHEMATICAL CONSIDERATIONS

Using the Townsend coefficient of ionization α as the electron generating mechanism and an electron attachment coefficient B as a loss mechanism, we may write for the net gain of electrons in a time dt

$$dn = \alpha n v dt - B n dt,$$

v being the electronic velocity.

One may now use to advantage $K_e = c/p$, where K_e is the electron mobility, and $|v| = K_e|E|$, or $v = K_e E_0 \cdot |\sin\omega t|$, together with α as a function of p and E/p. From experiment, in the region $E/p = 0$ to $E/p = 20$ (E in volts/cm, p in mm of Hg) no data are available in air; from 20 to 38 Sanders'[17] data were fitted by him, to α/p

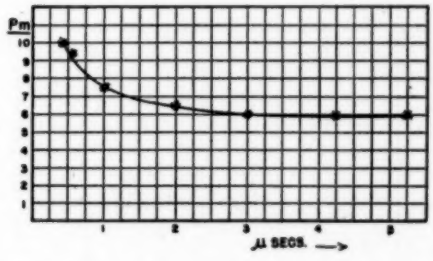

FIG. 8. Peak power as a function of pulse width (atmos. pres., rep. rate 100 p.p.s.; 17-mil gap; 3-cm waves).

[17] F. H. Sanders, Phys. Rev. **41**, 667 (1932); **44**, 1020 (1933); see also Loeb, *Fundamental Processes of Electrical Discharge in Gases* (John Wiley and Sons, Inc., New York, 1939).

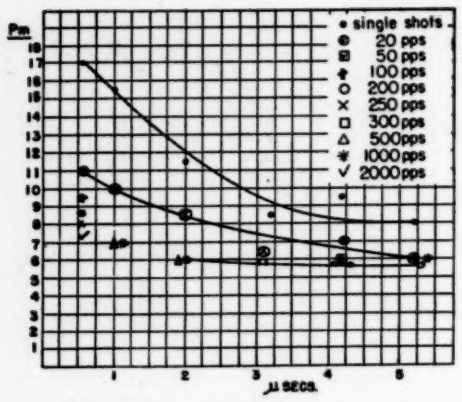

FIG. 8A. Peak breakdown power *vs.* pulse width.

$=a\exp b(E/p)$. From 38 to 140, Jodelbauer[18] fitted Sanders' data to the form $\alpha/p=[A_1(E/p)-B_1]^2$. Near atmospheric pressure Paavola[19] found $\alpha/p=A_2[(E/p)^2-B_2]^2$. The writer[20] has found similar relations in N_2, in d.c. work.

In the present paper the expression $\alpha/p=A(E/p)^2$ is used for the entire region $E/p=0$ to 140, and A is chosen to fit Sanders' data as closely as possible.

Thus,

$$dn/n=(\alpha/p)cE_0|\sin\omega t|\,dt-Bdt,$$

which gives, after substitution and integration in half-cycles,

$$n=n_0\exp\left(4/3AE_0{}^3\cdot\frac{c}{\pi p^2}-B\right)\mu$$

(the pulse width μ consists of $N=(\mu/\pi/\omega)$ half-cycles).

We might now assume that for any pulse width μ, the sparking condition is attained when for a given n_0, n/n_0 becomes large enough. Frequently, the sparking n/n_0 is equal to $K^*p/K_0p=K^*/K_0$, where K^* is defined as the sparking number of electrons per cc per mm Hg.

Then,

$$\left(\frac{4ACE_0{}^3}{3\pi p^2}-B\right)\mu=\ln\left(\frac{K^*}{K_0}\right),$$

$$\therefore\quad E_0=(3\pi/4AC)^{\frac{1}{2}}p^{\frac{1}{2}}\times[(1/\mu)\ln(K^*/K_0)+B]^{\frac{1}{2}}. \quad (1)$$

This sparking equation reduces to the following expression for a CW pulse, $\mu=\infty$:

$$E_0=(3\pi/4AC)^{\frac{1}{2}}B_0{}^{\frac{1}{2}}p,$$

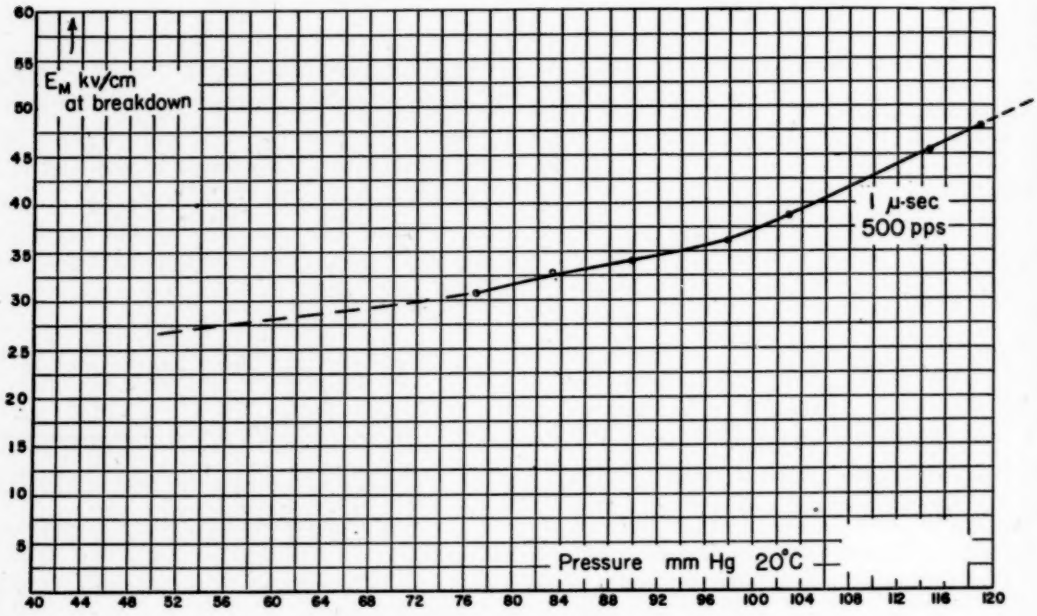

FIG. 9. Peak field *vs.* pressure (10-cm waves).

[18] Jodelbauer, Zeit. f. Physik **92**, 116 (1934); or Loeb, reference 17, p. 360.
[19] M. Paavola, Archiv. f. Elektrotechnik **22**, 443 (1922).
[20] D. Q. Posin, Phys. Rev. **50**, 650 (1936); values and formulation of α/p *vs.* E/p in N_2, from E/p 20 to 1000; or see Loeb, reference 17.

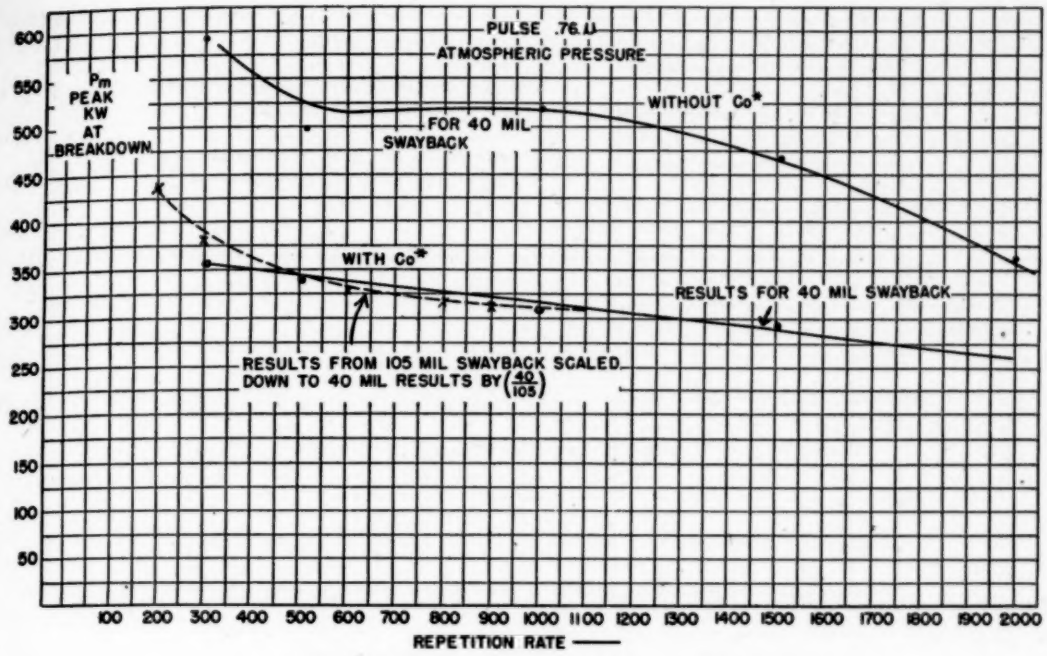

FIG. 10. Peak breakdown power *vs.* repetition rate (10-cm waves).

showing that breakdown field strength at high pressure and for long pulses is proportional directly to the pressure.

The voltage V_s across the gap is $E_0 \times d$,

$$V_s = (3\pi/4AC)^{\frac{1}{2}} B_0^{\frac{1}{2}} \cdot pd,$$

or, a Paschen law of type

$$V_s = K(pd).$$

We now see that the Paschen law may be expected to be valid at alternating frequency for continuous wave and at high gas pressure.

At lower pressures the electronic velocity is in general not in phase with the field. The equation of motion of the electron may be written as follows:

$$m\ddot{x} + f\dot{x} = E_0 e \sin\omega t,$$

where f is the friction factor and will be taken here in its average value independent of the field strength.

Then,

$$\dot{x} = \frac{efE_0 \sin\omega t}{m^2\omega^2 + f^2} - \frac{meE_0\omega \cos\omega t}{m^2\omega^2 + f^2},$$

provided that we choose the following initial condition: at $t=0$, $\dot{x} = (-E_0 e/m\omega)$. We have chosen here only electrons which have a special velocity when the field is zero. These electrons will oscillate in the gap, whereas all others will travel to an instantaneous anode and will be removed. When the oscillating electrons create new electrons by collision, again only those which have an appropriate initial velocity will oscillate in the gap. Eventually we may build up a sparking quantity of oscillating electrons. To continue analytically,

$$dx = |v|\,dt = |\dot{x}|\,dt,$$

where again we are only interested in the absolute value of the velocity, inasmuch as the new electrons formed add up whether the ionization occurs going up or down.

Integrating in half-cycles as before, we obtain for the breakdown field

$$E_0 = \left[\frac{3\pi(m^2\omega^2 + f^2)}{2Ae(m\omega - 2f)}\right]^{\frac{1}{2}} p^{\frac{1}{2}} \left[\frac{1}{\mu} \ln\left(\frac{K^*}{K_0}\right) + B_0 p\right]^{\frac{1}{2}},$$

For f, the friction term, $\to 0$,

$$E_0 = \left(\frac{3\pi m\omega}{2Ae}\right)^{\frac{1}{2}} p^{\frac{1}{2}} \left[\frac{1}{\mu} \ln\left(\frac{K^*}{K_0}\right) + B_0 p\right]^{\frac{1}{2}}. \quad (2)$$

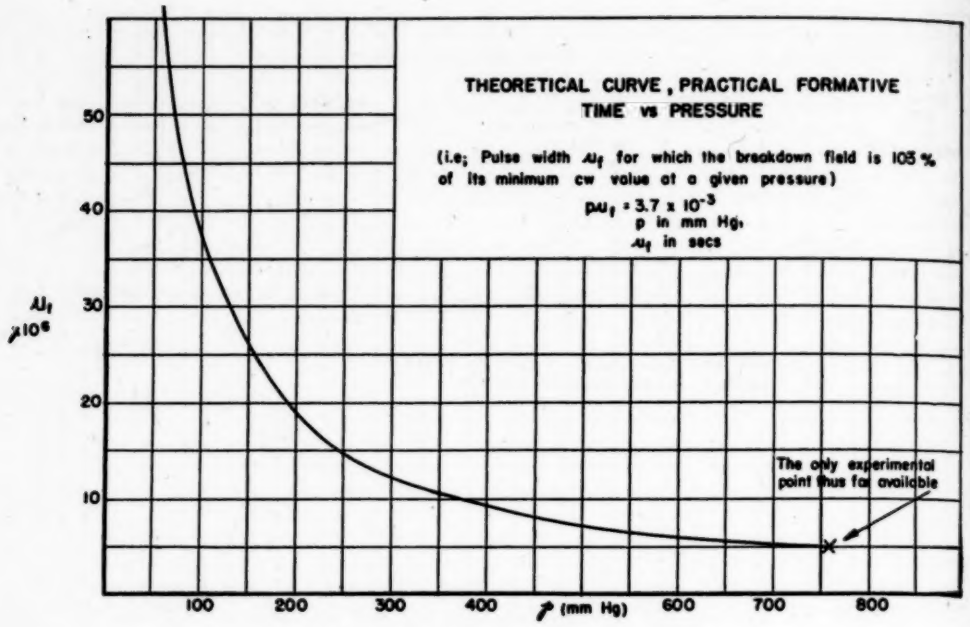

FIG. 11. Curve of "practical formative time."

For infinite pulse, or CW, this gives

$$E_0=\left(\frac{3\pi m\omega}{2Ae}\right)^{\frac{1}{2}}B_0^{\frac{1}{2}}p^{\frac{1}{2}}.$$

The sparking voltage in this case would be

$$V_s=\left(\frac{3\pi m\omega}{2Ae}\right)^{\frac{1}{2}}B_0^{\frac{1}{2}}p^{\frac{1}{2}}d,$$

and thus we note a deviation from the Paschen law at the lower pressures, inasmuch as $V_s \neq F(pd)$.

For still lower pressures we no longer use $\alpha/p=A(E/p)^2$ (with $E=E_0\sin\omega t$), but rather $(\alpha/p)^2=b^2(E/p)$ (with $E=E_0\sin\omega t$).

This general type of relation (but without the sinusoidal E) is known[21] from d.c. work, valid for $E/p=200$ to $E/p>1000$ (E in volts/cm, p in mm of Hg). Since this range is so great we will use the above α/p relationship in spite of the fact that E/p runs through zero values as the $\sin\omega t$ fluctuates; i.e., in spite of the fact that for relatively small stretches of E/p the other α/p relation is indicated.

After substitution, integration in half-cycles of $dn=\alpha n dx-Bndt$, gives

$$E_0=\left(\frac{m}{eb(0.4)^{\frac{1}{2}}}\right)^{\frac{1}{2}}\frac{\omega^{\frac{1}{2}}}{p^{\frac{1}{2}}}\left[\frac{1}{\mu}\ln\left(\frac{K^*}{K_0}\right)+B_0p\right]^{\frac{1}{2}}. \quad (3)$$

For infinite pulse width, or CW,

$$E_0=\left(\frac{m}{eb(0.4)^{\frac{1}{2}}}\right)^{\frac{1}{2}}\omega^{\frac{1}{2}}B_0^{\frac{1}{2}}p^{\frac{1}{2}}.$$

The sparking voltage becomes

$$V_s=\left(\frac{m}{eb(0.4)^{\frac{1}{2}}}\right)^{\frac{1}{2}}\omega^{\frac{1}{2}}B_0^{\frac{1}{2}}p^{\frac{1}{2}}d,$$

and this is a still greater deviation from Paschen's law, and $V_s \neq f(pd)$.

For a given gap width, we have now the following sparking voltage relations insofar as pressure is concerned:

$V_s \sim p$, at high pressure (and here alone, $V_s = f(pd)$,
$V_s \sim p^{\frac{1}{2}}$, at lower pressure,
$V_s \sim p^{\frac{1}{2}}$, at the lowest pressures.

In the formulas (1), (2), and (3), using certain convenient values of the constants, we determine

[21] D. Q. Posin, Phys. Rev. **50**, 650 (1936); for N_2.

the value of K^*/K_0 from the relation

$$36\times10^3=\left(\frac{3\pi}{4\times4\times10^{-6}\times10^3\times760}\right)^{\frac{1}{2}}760^{\frac{1}{2}}\times\left[\frac{1}{10^{-6}}\ln\left(\frac{K^*}{K_0}\right)+10^5\times760\right]^{\frac{1}{2}}.$$

(36 kv/cm is a conservative value for breakdown field strength at 1 μsec. for single pulse performance.)

We then have

$$\ln(K^*/K_0)=33;\quad (K^*/K_0)=e^{33}\text{ or }10^{14.2},$$

which is to be taken for all conditions so long as K_0 is constant.

Equations (1), (2), and (3), now become:

$$E_0=0.92p^{\frac{1}{2}}[(33/\mu)+10^5p]^{\frac{1}{2}},\qquad (1^1)$$

E_0 in volts/cm, p in mm of Hg, μ in seconds. This is for the high pressure region. For the middle pressure region,

$$E_0=4.2p^{\frac{1}{2}}[(33/\mu)+10^5p]^{\frac{1}{2}},\qquad (2^1)$$

for 1.25-cm waves. For 3-cm waves in this middle pressure region one obtains

$$E_0=4.2\left(\frac{10^{10}}{2.4\times10^{10}}\right)^{\frac{1}{2}}p^{\frac{1}{2}}\left(\frac{33}{\mu}+10^5p\right)^{\frac{1}{2}}$$

or

$$E_0=3.14p^{\frac{1}{2}}\left(\frac{33}{\mu}+10^5p\right)^{\frac{1}{2}}.$$

For 10-cm waves in this pressure range

$$E_0=4.2\left(\frac{3\times10^9}{2.4\times10^{10}}\right)^{\frac{1}{2}}p^{\frac{1}{2}}\left(\frac{33}{\mu}+10^5p\right)^{\frac{1}{2}}$$

or

$$E_0=2.1p^{\frac{1}{2}}\left(\frac{33}{\mu}+10^5p\right)^{\frac{1}{2}}.$$

For the lowest pressure range, for 1.25 cm waves one may use the value 0.2 for b, and thus readily determine E_0 in terms of known constants and the parameters of formula (3).

Calculations made with various of the formulas given above are generally in fair agreement with experimental values. Similar formulas involving the parameter R, repetition rate of pulses, may be submitted on another occasion. For the present we may conclude by making predictions as to the magnitude of the "practical formative time of the spark." By this term, as previously suggested, we mean the length of a single microwave pulse in seconds for which the breakdown field strength is about 103 percent of the minimum possible at the given pressure and initial ionization. Obviously the actual minimum field strength occurs for an infinitely wide pulse.

We form the ratio

$$\left[\frac{(33/\mu_f)+10^5p}{10^5p}\right]^{\frac{1}{2}}=1.03,$$

μ_f being the practical formative time of the spark. The formula gives

$$p\mu_f=3.7\times10^{-3},$$

and this is presented graphically in Fig. 11. For atmospheric pressure, p, of 760 mm Hg we obtain $\mu_f=4.9\times10^{-6}$ sec., which is about the value we have been obtaining experimentally. At a lower pressure, for example 20 cm of Hg, we get $\mu_f=(3.7\times10^{-3}/200)=1.9\times10^{-5}$ sec., or 19 μsec. Perhaps the means are at hand for some laboratory to test this inference; that is, the curve of Fig. 11 giving the indicated quantitative increase in the practical formative time of the spark at lower pressures.

In conclusion we would like to state that most of the apparatus for the experiments described was assembled and placed into expert order by Mr. H. F. Clarke and Mrs. Ina Mansur, who frequently assisted with the measurements. Also assisting was Miss Alice Reynolds. We appreciate the interest displayed in this work by Mr. George Yevick, Dr. George Ragan, and Professor A. G. Hill. However, any inadequacy in experiment or theory is the responsibility of the writer alone.

On the Total Vorticity of Motion of a Continuous Medium

C. TRUESDELL
*Naval Ordnance Laboratory, Washington, D. C.**

(Received October 27, 1947)

A general kinematic formula for the rate of change of the total vorticity of a finite volume of a continuous medium is deduced. Two kinematic theorems follow: (1) In a motion filling all space the total vorticity is constant in time, provided that the motion vanishes at infinity to a sufficiently high order; (2) The rate of change of total vorticity within an arbitrary volume is independent of the state of motion at all interior points of the volume. The mechanism of diffusion of total vorticity is then discussed in detail for the case of a viscous, compressible fluid.

LET $\mathbf{v}$ be a given velocity field and $\mathbf{w}$ its vorticity. The *total vorticity* $\mathbf{W}$ within a volume $\mathfrak{V}$,

$$\mathbf{W} \equiv \int_{\mathfrak{V}} \mathbf{w} d\tau, \tag{1}$$

was introduced by Poincaré.[1] He proved that *in a plane motion of an incompressible viscous fluid filling all space the total vorticity of the entire flow is constant in time*, provided that $\mathbf{v}$, $\mathbf{w}$, and **grad** $\mathbf{w}$ vanish to a sufficiently high order at ∞. His theorem was extended to general motions of an incompressible viscous fluid by Jaffé,[2] who proved that *the rate of change of the total vorticity of any fixed finite volume $\mathfrak{V}$ equals the flux* $\mathbf{vw}-\mathbf{wv}+\nu\,\mathbf{grad}\,\mathbf{w}$ through the boundary $\mathfrak{S}$, where ν is the kinematic viscosity. The method of proof employed by both Poincaré and Jaffé was integration of the Navier-Stokes equations.

We shall show that the fundamental theorem of rate of change of total vorticity is purely kinematic, and thus valid for the motion of any continuous medium. Of all the quantities connected with vorticity, the total vorticity, being in fact an average, is the least dependent upon the particular nature of the substance in which it occurs. Thus, while several properties of the vorticity of incompressible viscous fluids cease to hold for compressible fluids, the corresponding properties of the total vorticity are valid for arbitrary continuous media.

Since

$$\mathbf{a} = \frac{\partial \mathbf{v}}{\partial t} + \mathbf{w}\times\mathbf{v} + \tfrac{1}{2}\,\mathbf{grad}\,v^2, \tag{2}$$

where a is the acceleration, it follows that

$$\mathbf{curl}\,\mathbf{a} = \frac{\partial \mathbf{w}}{\partial t} + \mathbf{curl}\,(\mathbf{w}\times\mathbf{v}). \tag{3}$$

By integrating this identity over a fixed volume $\mathfrak{V}$ and then employing the Gauss-Green theorem we find that

$$\frac{\partial \mathbf{W}}{\partial t} = \oint_{\mathfrak{S}} (\mathbf{vw}-\mathbf{wv})\cdot d\mathbf{S} - \oint_{\mathfrak{S}} \mathbf{a}\times d\mathbf{S}. \tag{4}$$

This is the fundamental theorem of rate of change of total vorticity. Its validity rests upon the assumption, which we shall tacitly employ henceforth, that $\mathbf{v}$, $\mathbf{w}$, $\mathbf{a}$, and $\partial\mathbf{w}/\partial t$ are single-valued, continuously differentiable functions of position throughout $\mathfrak{V}$ and that $\mathbf{v}$, $\mathbf{w}$, and $\mathbf{a}$ are single-valued and integrable upon $\mathfrak{S}$. If $\mathfrak{V}$ is multiply connected, S must be the complete boundary, the vector element of surface $d\mathbf{S}$ being given a proper sense upon each portion. From the fundamental theorem we may draw two conclusions:

First, let the motion extend through all space. *If upon a sphere of radius r the normal component of* $\mathbf{vw}-\mathbf{wv}$ *and the tangential component of* $\mathbf{a}$ *vanish more rapidly than r^{-2} as $r\to\infty$, then the total vorticity of the motion is constant in time.* Thus Poincaré's theorem, if properly stated, is valid in the motion of any continuous medium.

Dr. Max M. Munk has pointed out to me that the total vorticity of a motion confined within

* This investigation was carried out under Contract No. 53-47 *Mechanics of Continuous Media* from the Office of Naval Research to the Naval Ordnance Laboratory.

[1] H. Poincaré, *Théorie des Tourbillons* (Paris, 1893), p. 196.

[2] G. Jaffé, "Über den Transport von Vektorgrössen mit Anwendung auf Wirbelbewegung in reibenden Flüssigkeiten," Physik. Zeits. 22, 180–183 (1921).

fixed finite walls, to which the material adheres without slipping, is always zero. Combining this result with the preceding, we may conclude that the total vorticity of a motion partly bounded by such walls and partly extending to infinity, where it vanishes as stated above, is constant in time.

Second, we recall the familiar statement that "vortex motion cannot originate in the interior of a viscous liquid, but must be diffused inward from the boundary."[3] While this theorem no longer holds for the motions of an arbitrary continuous medium, we may conclude from the fundamental identity (4) a similar but somewhat less specific statement: *The rate of change of total vorticity within an arbitrary volume is independent of the state of motion at all interior points of the volume.*

Thus far we have confined our attention to a volume fixed in space, but our general theorem may easily be modified so as to apply to a material volume. To this end we shall employ the kinematic transport theorem:

$$(D/Dt)\int_{\mathfrak{V}} \beta d\tau = (\partial/\partial t)\int_{\mathfrak{V}} \beta d\tau + \oint_{\mathfrak{S}} \beta \mathbf{v}\cdot d\mathbf{S}, \quad (5)$$

where β is any function of space and time. In words: the rate of change of the integral of β over a material volume $\mathfrak{V}$ equals the rate of change of the integral of β over a fixed volume $\mathfrak{V}$ with which the moving volume instantaneously coincides, plus the flux of $\beta\mathbf{v}$ through the boundary surface $\mathfrak{S}$. If we replace β by $\mathbf{w}$ in (5) we find that

$$D\mathbf{W}/Dt = (\partial\mathbf{W}/\partial t) + \oint_{\mathfrak{S}} \mathbf{w}\mathbf{v}\cdot d\mathbf{S}. \quad (6)$$

Hence by (4),

$$D\mathbf{W}/Dt = \oint_{\mathfrak{S}} \mathbf{v}\mathbf{w}\cdot d\mathbf{S} - \oint_{\mathfrak{S}} \mathbf{a}\times d\mathbf{S}. \quad (7)$$

Thus the second theorem stated above is equally valid for fixed and for material volumes.

[3] H. Lamb, *Hydrodynamics* (Cambridge University Press, Teddington, England, 1932), 6th edition, p. 578.

Let us now consider the very special case of barotropic motion of an inviscid fluid subject only to conservative forces; then it follows from the Euler equation of motion that $\mathbf{a}$ is a gradient, and hence the second surface integrals in both the general formulas (4) and (7) vanish:

$$\partial\mathbf{W}/\partial t = \oint_{\mathfrak{S}} (\mathbf{v}\mathbf{w} - \mathbf{w}\mathbf{v})\cdot d\mathbf{S}. \quad (8)$$

$$D\mathbf{W}/Dt = \oint_{\mathfrak{S}} \mathbf{v}\mathbf{w}\cdot d\mathbf{S}. \quad (9)$$

In describing the above class of motions we customarily state that vorticity is transported by convection only. Accordingly we shall say that the integrals

$$\oint_{\mathfrak{S}} (\mathbf{v}\mathbf{w} - \mathbf{w}\mathbf{v})\cdot d\mathbf{S}$$

and

$$\oint_{\mathfrak{S}} \mathbf{v}\mathbf{w}\cdot d\mathbf{S}$$

represent the rate of *convection* of vorticity through a fixed or a material surface $\mathfrak{S}$ respectively, and that the integral

$$-\oint_{\mathfrak{S}} \mathbf{a}\times d\mathbf{S}$$

represents that rate of *diffusion* of vorticity through $\mathfrak{S}$. In plane or axially symmetric motion the rate of convection of vorticity through a material curve is zero; in such motions the total vorticity within a material curve is changed through the effect of diffusion alone.

We may now state a third kinematic theorem: *Through a material surface accelerating only normal to itself, or through a fixed surface in crossing which the particles suffer no tangential acceleration, vorticity is transported by convection only.*

Let us now apply the fundamental theorems to the motion of a viscous compressible fluid. From the Navier-Stokes-Duhem equations[4] and the

[4] P. Duhem, "Recherches sur l'hydrodynamique", Annales de la faculté des sciences de l'université de Toulouse, 3 (2nd series), 315–431 (1901). H. Jeffreys, "The equations of viscous motion and the circulation theorem," Proc. Camb. Phil. Soc. 24, 477–479 (1928).

equation of continuity it follows easily that

$$\mathbf{a}=\mathbf{f}-\mathbf{grad}\left(\frac{p}{\rho}\right)-\mathbf{grad}\left(\frac{\lambda+2\mu}{\rho}\frac{D\log\rho}{Dt}\right)$$
$$+\left[p+(\lambda+2\mu)\frac{D\log\rho}{Dt}\right]\mathbf{grad}\,\frac{1}{\rho}-\frac{\mu}{\rho}\,\mathbf{curl}\,\mathbf{w}$$
$$+\frac{1}{\rho}\,\mathbf{grad}\,\mu\cdot[\mathbf{grad}\,\mathbf{v}+(\mathbf{grad}\,\mathbf{v})_c]$$
$$-2\,\mathbf{grad}\,\mu\frac{D(1/\rho)}{Dt}, \quad (10)$$

where p is the pressure, ρ the density, λ and μ the Poisson-Duhem coefficients of viscosity, and $\mathbf{f}$ the extraneous force per unit mass, which we shall suppose conservative. Hence the rate of diffusion of vorticity through an arbitrary surface $\mathfrak{S}$ is

$$-\oint_{\mathfrak{S}}\mathbf{a}\times\mathbf{dS}=-\oint_{\mathfrak{S}}\left[p+(\lambda+2\mu)\frac{D\log\rho}{Dt}\right]$$
$$\times\mathbf{grad}\,\frac{1}{\rho}\times\mathbf{dS}+\oint_{\mathfrak{S}}\frac{\mu}{\rho}\,\mathbf{curl}\,\mathbf{w}\times\mathbf{dS}$$
$$-\oint_{\mathfrak{S}}\mathbf{grad}\,\mu\cdot[\mathbf{grad}\,\mathbf{v}+(\mathbf{grad}\,\mathbf{v})_c]\times\mathbf{dS}$$
$$+2\oint_{\mathfrak{S}}\frac{D(1/\rho)}{Dt}\,\mathbf{grad}\,\mu\times\mathbf{dS}. \quad (11)$$

Thus the diffusion of vorticity is effected by three different mechanisms: The compressibility of the fluid at the boundary, the rotation of the vorticity field about axes tangential to the boundary, and the inhomogeneity of the fluid upon the boundary. In the special case when the surface $\mathfrak{S}$ is a surface of constant density and of constant viscosity μ, if the vorticity field rotates about the normals to $\mathfrak{S}$ or vanishes upon and in the vicinity of $\mathfrak{S}$, then vorticity is transported across $\mathfrak{S}$ by convection only.

For viscous incompressible fluids whose viscosity is constant, (11) becomes

$$-\oint_{\mathfrak{S}}\mathbf{a}\times\mathbf{dS}=\nu\oint_{\mathfrak{S}}\mathbf{curl}\,\mathbf{w}\times\mathbf{dS}, \quad (12)$$

and an easy transformation yields Jaffé's formula,

$$-\oint_{\mathfrak{S}}\mathbf{a}\times\mathbf{dS}=\nu\oint_{\mathfrak{S}}\mathbf{grad}\,\mathbf{w}\cdot\mathbf{dS}. \quad (13)$$

For an inviscid but compressible fluid the diffusion rate (11) becomes

$$-\oint_{\mathfrak{S}}\mathbf{a}\times\mathbf{dS}=-\oint_{\mathfrak{S}}p\,\mathbf{grad}\left(\frac{1}{\rho}\right)\times\mathbf{dS} \quad (14)$$
$$=\oint_{\mathfrak{S}}\frac{1}{\rho}\,\mathbf{grad}\,p\times\mathbf{dS}. \quad (15)$$

Hence, if the surface $\mathfrak{S}$ is either a surface of constant density or a surface of constant pressure, vorticity is transported across it by convection only. If the fluid is homogeneous we may employ the thermodynamic relation

$$\mathbf{grad}\,e=T\,\mathbf{grad}\,s-p\,\mathbf{grad}\left(\frac{1}{\rho}\right), \quad (16)$$

where e is the internal energy, T the absolute temperature, and s the specific entropy. The diffusion rate (14) now becomes

$$-\oint_{\mathfrak{S}}\mathbf{a}\times\mathbf{dS}=\oint_{\mathfrak{S}}T\,\mathbf{grad}\,s\times\mathbf{dS}, \quad (17)$$
$$=-\oint_{\mathfrak{S}}s\,\mathbf{grad}\,T\times\mathbf{dS}.$$

Thus if the surface $\mathfrak{S}$ is a surface of constant entropy or a surface of constant temperature, vorticity is transported across it by convection only. These theorems are closely connected to the Bjerknes circulation theorem.[5]

If the fluid cannot conduct heat, the entropy remains constant for each particle, so that a surface of constant entropy is a material surface. The last theorem above can then be extended so as to apply not only to an instant but to all time: The total vorticity within a material surface of constant entropy is changed by convection only. Since in plane motion there is no convection of vorticity through a material curve, it follows that the total vorticity within a closed curve of constant entropy is constant for all time.

[5] H. Lamb, see reference 3, p. 247. A. Vazsonyi, "On rotational gas flows", Quart. of App. Math. 3, p. 33, (1945).

On the Transfer of Energy in Continuous Media

C. TRUESDELL
*Naval Ordnance Laboratory, Washington, D. C.**
(Received October 27, 1947)

A formula for the rate of change of the kinetic energy of an arbitrary finite material volume of a Newtonian continuum is deduced. The general formula is then applied to the special case of a compressible viscous fluid, generalizing the theorem of Bobyleff and Forsyth. It is shown that the vorticity and the expansion play completely separate and exactly analogous parts in the dissipation of energy associated with viscosity.

THE *kinetic energy* T of a finite volume V of a continuum is given by the definition

$$T \equiv \tfrac{1}{2}\int_V \rho q^2 d\tau, \tag{1}$$

where ρ is the density and q is the magnitude of the velocity vector q^i. Let V be a material volume of the continuum, that is, a volume consisting always of the same particles. Then it is a consequence of the principal of conservation of mass, $\delta(\rho d\tau)/\delta t = 0$, that the material derivative of T is given by

$$\frac{\delta T}{\delta t} = \int_V \rho q^\alpha a_\alpha d\tau, \tag{2}$$

where a_i is the acceleration vector.

Let T^{ij} be the stress tensor and let a second stress tensor W^{ij} be given by the definition

$$W_j^i = \pi\delta_j^i + T_j^i, \tag{3}$$

where π is a scalar function called the *pressure*. For the validity of the subsequent analysis π may be an arbitrary scalar function. From other considerations,[1] however, if the medium is compressible,

$$\pi \equiv \left(\frac{\partial e}{\partial(1/\rho)}\right)_{s,a,b,c}, \tag{4}$$

where e is the energy per unit mass, s the entropy per unit mass, and a, b, and c are Lagrangian coordinates, while if the medium is incompressible,

$$\pi \equiv -\tfrac{1}{3}T_\alpha^\alpha. \tag{5}$$

In terms of the tensor W^{ij} the principle of conservation of momentum assumes the form

$$\rho a_i = F_i - \pi_{,i} + W_i^\beta{}_{,\beta}, \tag{6}$$

$$W^{ij} = W^{ji}, \tag{7}$$

where F_i is the extraneous force vector. Hence the formula (2) becomes

$$\frac{\delta T}{\delta t} = \int_V q^\alpha [F_\alpha - \pi_{,\alpha} + W_\alpha{}^\beta{}_{,\beta}] d\tau. \tag{8}$$

Then by the Gauss-Green theorem,

$$\frac{\delta T}{\delta t} = \int_V q^\alpha F_\alpha d\tau + \int_V \pi q^\alpha{}_{,\alpha} d\tau - \int_V q^\alpha{}_{,\beta} W_\alpha{}^\beta d\tau + \oint_S \pi q^\alpha dS_\alpha + \oint_S q^\alpha W_\alpha{}^\beta dS_\beta, \tag{9}$$

where the surface integrals are taken over the closed surface S bounding V. Rayleigh's *dissipation function* Φ is given by the definition

$$\Phi \equiv W^{\alpha\beta} d_{\alpha\beta}, \tag{10}$$

where d_{ij} is the *deformation tensor*:

$$d_{ij} = \tfrac{1}{2}(q_{i,j} + q_{j,i}). \tag{11}$$

Then by Eqs. (7),

$$\Phi = q^\alpha{}_{,\beta} W_\alpha{}^\beta. \tag{12}$$

If we insert this relation and the Eulerian form of the principle of conservation of mass,

$$\frac{\delta \log\rho}{\delta t} + q^\alpha{}_{,\alpha} = 0, \tag{13}$$

* This investigation was carried out under Contract No. 53-47 *Mechanics of Continuous Media* from the Office of Naval Research to the Naval Ordnance Laboratory.

[1] C. Truesdell and R. Schwartz, "The Newtonian mechanics of continua," Naval Ordnance Laboratory Memorandum No. 9223, July 18, 1947.

into the formula (9) we obtain the final form

$$\frac{\delta T}{\delta t} = \int_V q^\alpha F_\alpha d\tau - \int_V \pi \frac{\delta \log \rho}{\delta t} d\tau - \int_V \Phi d\tau + \oint_S \pi q^\alpha dS_\alpha + \oint_S q^\alpha W_\alpha{}^\beta dS_\beta. \quad (14)$$

We may interpret this general energy theorem by stating the significance of the five integrals as follows: The rate at which the kinetic energy of a finite volume is dissipated equals

(1) the rate at which work is done against the extraneous force, plus
(2) the rate at which work is done in the interior of the volume by the pressure in compressing the medium, plus
(3) the rate at which work is done by the stress tensor W_{ij} in the interior of the volume in deforming the medium, plus
(4) the rate at which work is done by the pressure in diminishing the boundary surface, plus
(5) the rate at which work is done by the stress tensor W^{ij} in diminishing the bounding surface.

If the finite material volume V is enclosed by stationary walls, to which it adheres without slipping, then the velocity q^i vanishes upon S, and hence the two surface integrals in formula (14) vanish also. If the extraneous force is conservative, $F_i/\rho = -\phi_{,i}$ then we may define a potential energy U

$$U \equiv \int_V \rho \phi d\tau, \quad (15)$$

from which, by the principle of conservation of mass, we may conclude that

$$\frac{\delta U}{\delta t} = -\int_V F_\alpha q^\alpha d\tau + \int_V \rho \frac{\partial \phi}{\partial t} d\tau, \quad (16)$$

and when the extraneous force is also steady,

$$\frac{\delta U}{\delta t} = -\int_V F_\alpha q^\alpha d\tau. \quad (17)$$

Thus for the motion of a finite volume of a continuum subject only to steady conservative extraneous forces and confined by stationary walls, to which it adheres without slipping,

$$\frac{d}{dt}(T+U) = -\int_V \pi \frac{\delta \log \rho}{\delta t} d\tau - \int_V \Phi d\tau. \quad (18)$$

We shall now apply the general energy transfer theorem to the motion of compressible viscous fluids, for which

$$W_j{}^i = \lambda \delta_j{}^i d_\alpha{}^\alpha + 2\mu d_j{}^i, \quad (19)$$

$$\Phi = \lambda (d_\alpha{}^\alpha)^2 + 2\mu d_\beta{}^\alpha d_\alpha{}^\beta, \quad (20)$$

where λ and μ are the Poisson-Duhem[2] coefficients of viscosity, not necessarily constant, but subject to the inequalities

$$\mu \geqq 0, \quad 3\lambda + 2\mu \geqq 0. \quad (21)$$

For the fifth integral in the formula (14), the formulas (19) and (20) yield

$$\oint_S q^\alpha W_\alpha{}^\beta dS_\beta = -\oint_S \lambda \frac{\delta \log \rho}{\delta t} q^\alpha dS_\alpha + \oint_S 2\mu q^\alpha d_\alpha{}^\beta dS_\beta. \quad (22)$$

The fourth, second, and first integrals in formula (14) do not simplify in any way. To transform the third integral we require the tensor identity

$$d_\beta{}^\alpha d_\alpha{}^\beta + \omega^\alpha{}_\beta \omega^\beta{}_\alpha = -q^\beta{}_{,\alpha\beta} q^\alpha + [(d_\alpha{}^\beta + \omega^\beta{}_\alpha) q^\alpha]_{,\beta}, \quad (23)$$

where the *vorticity tensor* ω_{ij} is given by

$$\omega_{ij} = \tfrac{1}{2}(q_{i,j} - q_{j,i}). \quad (24)$$

Since the space is Euclidean, the order of covariant differentiation in the first expression on the right in formula (23) is immaterial. Hence, by the Eulerian equation of continuity (13),

$$-q^\beta{}_{,\alpha\beta} q^\alpha = \left(\frac{\delta \log \rho}{\delta t}\right)_{,\alpha} q^\alpha = \left(\frac{\delta \log \rho}{\delta t} q^\alpha\right)_{,\alpha} + \left(\frac{\delta \log \rho}{\delta t}\right)^2. \quad (25)$$

Thus the expression (20) for the dissipation

[2] P. Duhem, "Récherches sur l'hydrodynamique," Annales de la faculté des sciences de l'université de Toulouse 3 (2nd series), 315–431 (1901).

function becomes finally

$$\Phi=(\lambda+2\mu)\left(\frac{\delta\log\rho}{\delta t}\right)^2+2\mu\omega^{\alpha\beta}\omega_{\alpha\beta}+\left\{2\mu\left[(d^\alpha{}_\beta+\omega^\alpha{}_\beta)q^\beta+\frac{\delta\log\rho}{\delta t}q^\alpha\right]\right\}_{,\alpha}-2\mu_{,\alpha}\left[q^\alpha{}_{,\beta}q^\beta+\frac{\delta\log\rho}{\delta t}q^\alpha\right]. \quad (26)$$

Then the third integral in formula (14) may be put into the form

$$\int_V\Phi d\tau=\int_V(\lambda+2\mu)\left(\frac{\delta\log\rho}{\delta t}\right)^2d\tau+\int_V 2\mu\omega^{\alpha\beta}\omega_{\alpha\beta}d\tau+\oint_S 2\mu\frac{\delta\log\rho}{\delta t}q^\beta dS_\beta+\oint_S 2\mu(d^\alpha{}_\beta+\omega^\alpha{}_\beta)q^\alpha dS_\beta-\int_V 2\mu_{,\alpha}\left[q^\alpha{}_{,\beta}q^\beta+\frac{\delta\log\rho}{\delta t}q^\alpha\right]d\tau. \quad (27)$$

Substitution of the evaluations (22) and (27) into the general energy transfer theorem (14) yields the energy transfer theorem for viscous compressible fluids:

$$\frac{\delta T}{\delta t}=\int_V q^\alpha F_\alpha d\tau-\int_V\pi\frac{\delta\log\rho}{\delta t}d\tau-\oint_S\pi q^\alpha dS_\alpha-\oint_S(\lambda+2\mu)\frac{\delta\log\rho}{\delta t}q^\alpha dS_\alpha-\oint_S 2\mu\omega^\beta{}_\alpha q^\alpha dS_\beta-\int_V(\lambda+2\mu)\left(\frac{\delta\log\rho}{\delta t}\right)^2d\tau-\int_V 2\mu\omega^{\alpha\beta}\omega_{\alpha\beta}d\tau+\int_V 2\mu_{,\alpha}\left[q^\alpha{}_{,\beta}q^\beta+\frac{\delta\log\rho}{\delta t}q^\alpha\right]d\tau. \quad (28)$$

The fourth, fifth, sixth, and seventh integrals show that both on the surface and in the interior of the region, energy is dissipated by the independent effects of dilatation and vorticity. The last integral represents the effect of variation of the viscosity μ. When the fluid is confined by stationary walls, to which it adheres without slipping, and when the variation of viscosity may be neglected, we have

$$\frac{dT}{dt}=\int_V q^\alpha F_\alpha d\tau-\int_V\pi\frac{\delta\log\rho}{\delta t}d\tau-(\lambda+2\mu)\int_V\left(\frac{\delta\log\rho}{\delta t}\right)^2d\tau-2\mu\int_V\omega^{\alpha\beta}\omega_{\alpha\beta}d\tau. \quad (29)$$

It is a consequence of the inequalities (21) that $\lambda+2\mu\geqq 0$, so that the last two terms above are always negative. When the fluid is incompressible, the formula (29) reduces to the theorem of Bobyleff and Forsyth.[3]

The energy theorem assumes its most elegant form for barotropic phenomena, for which $\pi=\pi(\rho)$. Then we may define an *intrinsic energy* E:

$$E\equiv\int_V\rho\left[-\int_{\rho_0}^{\rho}\pi(\xi)d\left(\frac{1}{\xi}\right)\right]d\tau, \quad (30)$$

such that

$$\frac{\delta E}{\delta t}=\int_V\pi\frac{\delta\log\rho}{\delta t}d\tau. \quad (31)$$

For barotropic phenomena of a viscous, compressible fluid of constant viscosity, subject to steady conservative extraneous force and confined by stationary walls to which it adheres without slipping,

$$\frac{d}{dt}(T+U+E)=-(\lambda+2\mu)\int_V\left(\frac{\delta\log\rho}{\delta t}\right)^2d\tau-2\mu\int_V\omega^{\alpha\beta}\omega_{\alpha\beta}d\tau. \quad (32)$$

[3] H. Lamb, *Hydrodynamics* (Cambridge University Press, Teddington, England, 1932), 6th edition, pp. 580–581.

Letters to the Editor

PUBLICATION of brief reports of important discoveries in physics may be secured by addressing them to this department. The closing date for this department is five weeks prior to the date of issue. No proof will be sent to the authors. The Board of Editors does not hold itself responsible for the opinions expressed by the correspondents. Communications should not exceed 600 words in length.

On the Positive Excess of the Penetrating Component at 17,000 Feet

I. F. QUERCIA, B. RISPOLI, AND S. SCIUTI
Istituto fisico dell'Università, Centro di fisica nucleare del C.N.R., Rome, Italy
January 19, 1948

RECENT experiments by Jánossy,[1] Rossi,[2] and others[3] indicate that mesons are produced considerably even at low height. These experiments moreover yield a rough value of the absorption coefficient of the meson producing primary radiation (about 150 g/cm²). These results, together with the usual assumption that the primary radiation is protonic, point out that the proton component might be noticeable even at not very great heights. Consequently, the positive excess would be expected to increase with the height.

However, an opposite result (i.e., a decrease of the positive excess with height) would be expected if the assumption[4] is made that a great fraction of low mesons is produced even at low heights (about 17,000 feet) by a neutral radiation.

Because of the interest of these problems, we have carried out some experiments on the positive excess of the penetrating component in substratosphere.

Our experimental arrangement (Fig. 1) similar to that described by the Rome group[5] consists of three G.-M. counters 52×4 cm², the charged particles being deflected by two magnetic lenses. The apparatus was placed in a Baltimore Martin and the following counting rates were simultaneously recorded photographically: (1) twofold coincidences (AB) for $E \geqslant 2.3 \cdot 10^8$ ev, (2) twofold coincidences (BC) for $E \geqslant 4.6 \cdot 10^8$ ev, (3) threefold coincidences (ABC) for $E \geqslant 4.6 \cdot 10^8$ ev. Here, for each type of event recorded, the minimum meson energy required to penetrate the iron plates, is indicated.

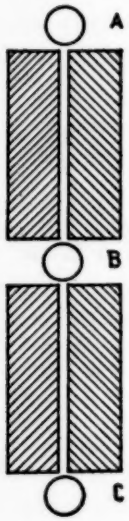

FIG. 1. Counter arrangement.

TABLE I. Positive excess of the penetrating component at 17,000 feet with control data taken before and after each flight.

Height (feet)	N^{+*} (AB)	N^{-*} (AB)	N^{+} (BC)	N^{-} (BC)	N^{+} (ABC)	N^{-} (ABC)
17,000	54.60±0.84	48.20±0.76	43.20±0.60	38.92±0.60	15.84±0.52	13.04±0.48
300	15.84±0.16	15.40±0.12	14.64±0.12	14.28±0.12	5.68±0.08	5.28±0.08

* N^{+}, N^{-} indicate coincidences per minute of positive and negative particles when the casual rate is subtracted.

TABLE II. Values of $\delta = 2(N^{+} - N^{-})/(N^{+} + N^{-})$ and the corrected value η of the positive excess.

Height (feet)	δ (AB)	η* (AB)	δ (BC)	η (BC)	δ (ABC)	η (ABC)
17,000	0.124±0.024	0.30	0.104±0.025	0.45	0.193±0.048	0.32
300	0.028±0.013	0.14	0.025±0.011	0.12	0.073±0.013	0.15

* We estimate that the accuracy of our values of η is of the order of 40 percent.

The signs of the various fields were so arranged as to focus either positive or negative particles. During each flight the sign of the particles recorded was alternately changed. The results of the first eight flights (four hours at 17,000 feet) are summarized in Table I, together with the control data recorded before and after each flight.

It should be noticed that there is no complete exclusion for particles of the "unwanted" sign. Consequently, the measured effect $\delta = 2(N^{+} - N^{-})/(N^{+} + N^{-})$ must be corrected, according to the calculations of Bernardini and others.[5] In Table II the values of δ and of *the corrected value η of the positive excess* are given for the three types of coincidences recorded.

The experiments are being continued at different heights in order to get more detailed information. Although the present results are still preliminary, the evidence of an increase in the positive excess with height is certain.

We wish to thank Professor Bernardini for his continuous help and for stimulating discussion.

The authors express their appreciation to the officers and men of the "132° Gruppo-Stormo Baltimore" who were so efficient and cooperative in flying a Baltimore airplane for this work.

[1] L. Jánossy, Phys. Rev. **64**, 345 (1943); Proc. Roy. Soc. **A183**, 190 (1944).
[2] H. Bridge, B. Rossi, and R. Williams, Phys. Rev. **72**, 257 (1947); H. Bridge and B. Rossi, Phys. Rev. **71**, 379 (1947).
[3] L. Leprince, Ringuet, Heritier, and Foy, Comptes Rendus **221**, 406 (1945); G. D. Rochester and L. Bound, Nature **146**, 745 (1940).
[4] M. Schein, William P. Jesse, and E. O. Wollan, Phys. Rev. **56**, 613 (1939); **57**, 847 (1940). Gerhart Groetzinger, E. O. Wollan, and Marcel Schein, Phys. Rev. **59**, 113 (1941).
[5] G. Bernardini, M. Conversi, E. Pancini, E. Scrocco, and G. C. Wick, Phys. Rev. **68**, 109 (1945).

Strain Sensitivity of Magnetic Susceptibility

T. S. HUTCHISON
University of St. Andrews, Scotland
AND
JAMES REEKIE
University of Toronto, Canada
January 12, 1948

STUDIES on the magnetic properties of cold worked metals have shown that magnetic susceptibility can be considerably affected by work hardening. This effect has been regarded by some investigators as a secondary one, brought about by the presence of small amounts of ferrous impurity in the metals.[1] During extensive experiments with copper and aluminum of the highest purity we have obtained results which appear to us to provide fairly conclusive evidence that marked changes in magnetic susceptibility are observable which cannot reasonably be attributed to the presence of ferromagnetic impurities. Some of this work has already been briefly reported,[2,3] and a considerably more complete account will be given later, but we would like at this stage to present certain of these results, which appear to be of considerable importance in that they allow a correlation between the observed magnetic changes and certain metallurgical changes occurring in cold worked metals.

In Fig. 1 we show the percentage change of susceptibility of both copper and aluminum, at room temperature, as a function of the degree of cold working. In the diagram χ_0 is the mass susceptibility of the annealed metal and $\Delta\chi$ the difference between the "cold worked" and the "annealed" values, the cold worked value being measured in every case one hour after completion of cold work. Cold working is expressed as the percentage reduction in area of a circular, rod-shaped specimen, cold working being carried out by wire drawing. Susceptibility is measured by the Gouy method, using apparatus which has already been described.[4]

In the case of copper the diamagnetic susceptibility rapidly decreases (numerically), becoming constant at about 15 percent below its annealed value after 10 percent cold working, and then, after 40 percent cold working, begins to revert towards its "annealed" value. In cold worked aluminum the paramagnetic susceptibility decreases, rather more slowly, reaching a stable value about 15 percent below the "annealed" value at 50 percent reduction of area.

Now, when a pure metal is subjected to cold working, both lattice distortion and grain fragmentation occur, together with a certain amount of grain orientation. Aluminum is spontaneously self-recovering from lattice distortion during cold working at room temperature; copper has been shown to undergo a similar self-recovery at room temperature, extending over a period of some hours, or even days.[5] We have already noted that copper shows a marked "magnetic self-recovery" at room temperature, measurable over some hours;[2] we have found by similar experiments that there is no detectable magnetic self-recovery in aluminum. Recovery from fragmentation, or "recrystallization," does not proceed to any appreciable

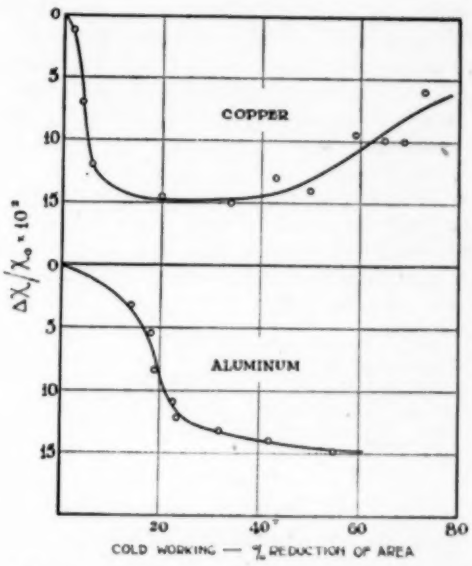

FIG. 1. Percentage change of susceptibility as a result of cold working, at room temperature. χ_0 for copper $= -0.085 \times 10^{-6}$. χ_0 for aluminum $= +0.62 \times 10^{-6}$.

extent until the metals are heated to about 200°C (the recrystallization temperature of copper and aluminum).

Therefore, we have come to the conclusion that the change in magnetic susceptibility on cold working is due to the combined effects of lattice distortion and fragmentation. The magnetic self-recovery observed in copper is a result of the recovery from lattice distortion; the fact that no such recovery is observed in aluminum is because aluminum, as noted above, recovers from lattice distortion *during* cold working. The remaining, stable change in susceptibility is regarded as the result of fragmentation.

It is known that, if cold working is sufficiently severe, recrystallization may occur in any metal, even at room temperature. This appears to be the case in copper for cold working in excess of 50 percent; spontaneous recrystallization would then result in a reversion of susceptibility towards its "annealed" value, as is seen in Fig. 1. Complete annealing of both cold worked copper and aluminum results in a return of the susceptibility to its original value.

If the above picture is correct, we should expect the major part of the stable change of susceptibility to be caused by the surface layers of the metal, where, with this

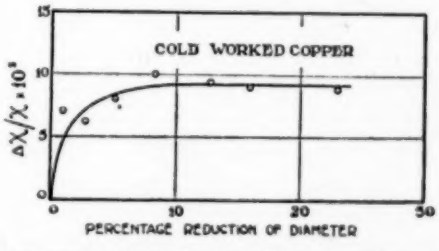

FIG. 2. Percentage change of susceptibility at room temperature on removal of surface layers of cold worked rod by etching. Value of χ before etching $= -0.076 \times 10^{-6}$.

method of cold working, fragmentation is most severe. A simple experiment in which the surface layers of a cold worked copper rod were gradually removed by etching in weak nitric acid shows this actually to be the case. Figure 2 gives the percentage change in susceptibility as a function of the percentage reduction in *diameter* caused by etching. Here χ is the initial value of susceptibility in the cold worked condition and $\Delta\chi$ is the difference between the "etched" and "initial cold worked" values. Clearly most of the change in χ is caused by the heavily fragmented surface layers, and on removal of these layers the susceptibility reverts very nearly to its original value for the annealed metal.

[1] A. Kussmann and H. J. Seemann, Zeits. f. Physik **77**, 567 (1932).
[2] J. Reekie and T. S. Hutchison, Nature **157**, 807 (1946).
[3] T. S. Hutchison and J. Reekie, Nature **159**, 537 (1947).
[4] T. S. Hutchison and J. Reekie, J. Sci. Inst. **23**, 209 (1946).
[5] H. Megaw, H. Lipson, and A. R. Stokes, Nature **154**, 145 (1944).

Polarization Correlation of Successive Gamma-Ray Quanta

DAVID L. FALKOFF*
University of Michigan, Ann Arbor, Michigan
January 14, 1948

RECENT successful experiments[1] on the angular correlation of γ-quanta emitted in successive nuclear transitions are in sufficient accord with theory[2,3] to make it worth while to inquire into what additional information can be gotten from this type of measurement. L. Madansky of this laboratory has suggested the possibility of detecting a polarization correlation between successive quanta by use of the photoelectric or Compton effect as analyzers, and is setting up apparatus to measure it.

The purpose of this note is to state what the theory predicts for such correlations and to point out that, aside from its intrinsic interest, the measurement of polarization correlation can be a useful tool in nuclear spectroscopy because, unlike the directional correlation, it provides a means of distinguishing between the electric and magnetic multipole character of the γ-transition and hence of determining the parity of the nuclear states.

The formalism for the calculation of polarization correlation differs in only one respect from that for the angular correlation,[2,3] namely, one has to specify the polarizations of the two quanta rather than average over them. One finds for the case of anti-parallel quanta, the first being a 2^{l_1}-pole transition between nuclear states of angular momentum quantum numbers J' and J, the second a 2^{l_2}-pole transition between nuclear states J and J'', that the probability of the polarizations of the two quanta, being at an angle φ with respect to each other, may always be expressed in the form:

$$W(\varphi)=1+A\cos 2\varphi. \tag{1}$$

Here $A=2N/D$ with

$$N=\sum_n \left(\begin{matrix}J'\\n+1\end{matrix}\middle|\, Y_{l_1}^{-1}\,\middle|\begin{matrix}J\\n+2\end{matrix}\right)\left(\begin{matrix}J'\\n+1\end{matrix}\middle|\, Y_{l_1}^{1}\,\middle|\begin{matrix}J\\n\end{matrix}\right) \times\left(\begin{matrix}J\\n+2\end{matrix}\middle|\, Y_{l_2}^{1}\,\middle|\begin{matrix}J''\\n+1\end{matrix}\right)\left(\begin{matrix}J\\n\end{matrix}\middle|\, Y_{l_2}^{-1}\,\middle|\begin{matrix}J''\\n+1\end{matrix}\right), \tag{2}$$

and

$$D=\sum_n\left[\left|\left(\begin{matrix}J'\\n-1\end{matrix}\middle|\, Y_{l_1}^{-1}\,\middle|\begin{matrix}J\\n\end{matrix}\right)\right|^2+\left|\left(\begin{matrix}J'\\n+1\end{matrix}\middle|\, Y_{l}^{1}\,\middle|\begin{matrix}J\\n\end{matrix}\right)\right|^2\right] \cdot\left[\left|\left(\begin{matrix}J\\n\end{matrix}\middle|\, Y_{l_2}^{-1}\,\middle|\begin{matrix}J''\\n+1\end{matrix}\right)\right|^2+\left|\left(\begin{matrix}J\\n\end{matrix}\middle|\, Y_{l_2}^{1}\,\middle|\begin{matrix}J''\\n-1\end{matrix}\right)\right|^2\right],$$

the summation being over the $(2J+1)$ magnetic quantum numbers of the intermediate state J. The $Y_l^{\pm 1}$ are spherical harmonics; their matrix elements are given by Condon and Shortley[4] for $l=1, 2$ and may be obtained by group theory methods for arbitrary l.

The coefficient A in (1) is always real and its sign is given by:

$$\text{sign of } A=(-1)^{l_1+l_2+J'-J''}+1+\delta, \tag{3}$$

where $\delta=1$ if both multipoles are electric or magnetic, 0 if one is electric, the other magnetic.

As an example, consider the $\gamma-\gamma$ transitions in Co^{60} and Sc^{46}. Deutsch and co-workers[1] identify these as quadrupole-quadrupole ($l_1=l_2=2$) transitions between nuclear states $J'=4$, $J=2$, $J''=0$. Hence here the sign of A is positive if both multipoles are electric or magnetic, and negative otherwise. Accordingly, in the first case one should observe a maximum coincidence rate when the polarizations are parallel ($\varphi=0$); in the second case the maximum occurs for perpendicular polarizations ($\varphi=\pi/2$). The magnitude of A is 2/7 so that the ratio of W max. to W min. is 1.8, which can be used as an additional experimental check on the assignment of multipole orders and quantum numbers. It should be remarked, however, that A has the magnitude 2/7 for any quadrupole-quadrupole $J+2$, J, $J-2$ transition irrespective of J.

In Table I, the absolute values of A as a function of J are listed for dipole-dipole transitions between states $J'=J-\Delta j$, J, $J+\Delta J=J''$. Similar tables for higher multipoles to complement those of Hamilton[2] are in preparation. The sign of A is given by (3) with $l_1=l_2=1$.

TABLE I. $|A(J)|$ for dipole-dipole transitions.

	$\Delta J=-1$	$\Delta J=0$	$\Delta J=1$
$\Delta j=-1$	$\frac{1}{7}$	$\frac{(2J-1)}{(6J+7)}$	$\frac{J(2J-1)}{(14J^2+33J+20)}$
$\Delta j=0$	$\frac{(2J+3)}{(6J-1)}$	$\frac{(2J-1)(2J+3)}{(8J^2+8J-1)}$	$\frac{(2J-1)}{(6J+7)}$
$\Delta j=1$	$\frac{(J+1)(2J+3)}{(14J^2-5J+1)}$	$\frac{(2J+3)}{(6J-1)}$	$\frac{1}{7}$

Comparison of this table with Table I of Hamilton,[2] shows that the magnitude of A is roughly twice that of the corresponding parameter R/Q for the angular correlation. Hence, whenever the angular correlation is easily measurable, one may also expect an appreciable polarization correlation. On the other hand, since the form of the polarization distribution (1) is the same for all multipoles, the main value of the polarization data will be to supplement the angular correlation data which do distinguish the various multipoles orders.

* National Research Council Predoctoral Fellow.
[1] E. L. Brady and M. Deutsch, Phys. Rev. **72**, 870 (1947).
[2] D. R. Hamilton, Phys. Rev. **58**, 122 (1940).
[3] G. Goertzel, Phys. Rev. **70**, 897 (1946).
[4] E. U. Condon and G. H. Shortley, *Theory of Atomic Spectra* (The Macmillan Company, Inc., New York, 1935), pp. 63 and 95.

Higher Order Field Equations

ALEX E. S. GREEN
Department of Physics, University of Cincinnati, Cincinnati, Ohio
January 16, 1948

CONSIDER the quadratic Lagrangian

$$L=(1/2a^2)(c_0\varphi_\alpha{}^2+c_1a^2\varphi_\alpha,_{\beta_1}{}^2+c_2a^4\varphi_\alpha,_{\beta_1\beta_2}{}^2 +c_3a^6\varphi_\alpha,_{\beta_1\beta_2\beta_3}{}^2+c_4a^8\varphi_\alpha,_{\beta_1\beta_2\beta_3\beta_4}{}^2), \quad (1)$$

where a is an arbitrary length and the c's are dimensionless natural constants. Higher derivatives, if admissible, may be treated by induction. Applying Hamilton's principle[1] we obtain the set of linear eighth-order field equations

$$(c_0-c_1a^2\Box+c_2a^4\Box^2-c_3a^6\Box^3+c_4a^8\Box^4)\varphi_\alpha(\mathbf{r},t)=0 \quad (2)$$

which may be written as

$$[\prod_{\sigma=1}^{4}(a^2\Box-s_\sigma{}^2)]\varphi_\alpha(\mathbf{r},t)=0, \quad (3)$$

where $s_\sigma{}^2$ represents the four roots of the auxiliary algebraic equation obtained by replacing $a^2\Box$ by s^2 in (2).

A solution of (3) expressed in Fourier integrals is

$$\varphi_\alpha(\mathbf{r},t)=(1/2\pi)^4\sum_\sigma\int[\varphi_{\sigma\alpha}(\mathbf{k})\exp(ix_\beta k_{\sigma\beta}) +\varphi_{\sigma\alpha}{}^*(\mathbf{k})\exp(-ix_\beta k_{\sigma\beta})]d\mathbf{k}, \quad (4)$$

where

$$k_{\sigma\beta}=(\mathbf{k},ik_\sigma) \quad \text{and} \quad k_\sigma{}^2=\mathbf{k}\cdot\mathbf{k}+s_\sigma{}^2/a^2. \quad (5)$$

Corresponding to our Lagrangian we can find an energy momentum density tensor $t_{\mu\nu}$, for which energy and momentum is conserved, i.e., $t_{\mu\nu},_\nu=0$. Expressing $t_{\mu\nu}$ in terms of Fourier amplitudes (we may discard all time-dependent terms) we get the Hamiltonian

$$H=-\int ict_{44}dV=\sum_{\sigma\alpha}2\gamma_\sigma\int k_\sigma 2\varphi_{\sigma\alpha}{}^*\varphi_{\sigma\alpha}d\mathbf{k} =\sum_{\sigma\alpha}\int hck_\sigma\eta_{\sigma\alpha}{}^*\eta_{\sigma\alpha}d\mathbf{k}, \quad (6)$$

where

$$\gamma_\sigma=(-c_1+2c_2s_\sigma{}^2-3c_3s_\sigma{}^4+4c_4s_\sigma{}^6), \quad (7)$$

and

$$\eta_{\sigma\alpha}(\mathbf{k})=(2\gamma_\sigma k_\sigma/ch)^{\frac{1}{2}}\varphi_{\sigma\alpha}(\mathbf{k}). \quad (8)$$

Going over to quantum-field theory the commutation rules are

$$[\varphi_{\sigma\alpha}{}^*(\mathbf{k}),\varphi_{\tau\beta}(\mathbf{k}')]=-\delta_{\sigma\tau}\delta_{\alpha\beta}\delta(\mathbf{k}-\mathbf{k}')ch/2k_\sigma\gamma_\sigma. \quad (9)$$

Suitable supplementary conditions which permit only transverse states of positive energy to exist in the "empty" field are

$$[(1-is_\sigma/ak)\mathbf{k}\cdot\mathbf{A}_\sigma(\mathbf{k})-k_\sigma\phi_\sigma(\mathbf{k})]\Omega=0. \quad (10)$$

The use of Dirac's expansors[2] is indicated here.

When nucleons are present in the field we find the interaction energy by a fourfold application of the formalism of Fock,[3] modified for bosons with finite masses ($m_\sigma=s_\sigma\hbar/ac$). From symmetry and superposition considerations we obtain the interaction energy[4]

$$U=\sum_\sigma(1/\gamma_\sigma)(\Sigma_{uv}{}'g_ug_v/8\pi)[(1-\tfrac{1}{2}\boldsymbol{\alpha}_u\cdot\boldsymbol{\alpha}_v) \times(1/R)\exp(-s_\sigma R/a)-\tfrac{1}{2}(\boldsymbol{\alpha}_u\cdot\mathbf{R}/R)(\boldsymbol{\alpha}_v\cdot\mathbf{R}/R) \times(s_\sigma/a+1/R)\exp(-s_\sigma R/a)]. \quad (11)$$

The $1/R$ singularity at short ranges, which is present in second-order field theory (i.e., when $c_2=c_3=c_4=0$), vanishes in fourth-[4] ($c_3=c_4=0$), sixth- ($c_4=0$), and eighth-order theories because $\Sigma(1/\gamma_\sigma)=0$, independent of the magnitudes of the natural constants. The self-energy is thus finite in the higher order theories. It is given by

$$U_s=-(\Sigma s_\sigma/\gamma_\sigma)(1-\tfrac{1}{2}\boldsymbol{\alpha}\cdot\boldsymbol{\alpha})g^2/8\pi a. \quad (12)$$

If we admit only field particles with real, positive, or zero masses then the c's must all have the same sign and the factor $(\Sigma s_\sigma/\gamma_\sigma)$ is positive or negative according to whether the c's are positive or negative.

Exploratory attempts to apply the results of fourth-order theory to the deuteron indicate that agreement with experiment in energy level and scattering questions can be achieved, with a reasonable choice of constants, if we introduce the isotopic spin formalism. Following Kemmer[5] for the charge-independent hypotheses one treats each component of $\varphi_\alpha(\mathbf{r},t)$ as a three vector in isotopic spin space. The modified formalism leads finally to the appearance of the isotopic spin operator T_{ab} as a factor in the interaction function. This approach is a radical one, however, if the more complicated interaction function of sixth- or eighth-order theories is used, because of the large number of field particles implied. In these cases the close similarity between Kemmer's Eq. (21) and Eq. (6) above invites consideration of the possibility of associating the sigma-quanta with the isotopic spin quanta themselves.

[1] Compare B. Podolsky and C. Kikuchi, Phys. Rev. **65**, 228 (1944).
[2] P. A. M. Dirac, Proc. Roy. Soc. **A183**, 284 (1945).
[3] V. Fock, Physik. Zeits. Sowjetunion **6**, 425 (1934).
[4] A. E. S. Green, Phys. Rev. **73**, 26 (1948).
[5] N. Kemmer, Proc. Camb. Phil. Soc. **34**, 354 (1938).

Spectroscopic Evidence of Methane in the Earth's Atmosphere*

MARCEL V. MIGEOTTE**
Mendenhall Laboratory of Physics, The Ohio State University, Columbus, Ohio
January 23, 1948

WHEN mapping the solar spectrum, under high resolving power, in the 3.3-μ region, fourteen regularly spaced and intense lines have been found between 3.33μ and 3.47μ. The wave numbers of these lines agree, within a maximum difference of ± 0.7 cm^{-1}, with the measurements of A. H. Nielsen and H. H. Nielsen[1] on the 3.3-μ fundamental band of CH_4. The intense central line (Q branch) of the CH_4 band falls in a spectral region absorbed by water vapor. For shorter wave-lengths than 3.3μ, many intense lines of water vapor prevent also the possibility of finding most of the CH_4 lines of the R branch.

The new lines have been found on spectrograms taken on January 10, 1948, with a new prism-grating recording spectrometer design by Dr. Robert Noble, under the direction of Professor H. H. Nielsen. This instrument is of the Pfund type, has an aperture of $f:5$, and parabolic mirrors with a focal length of 100 cm. An echelette grating with 7200 lines per inch was used for the observations.

The other fundamental band of CH_4 is situated at 7.7μ and is more intense than the 3.3-μ band. Consequently, a band of CH_4 is to be expected in the solar spectrum at 7.7μ. In fact, A. Adel[2] has found at low dispersion a band in the solar spectrum at 7.6μ and has proposed N_2O and perhaps N_2O_5, as possible identifications.[3] The 7.7-μ region of the solar spectrum was also mapped by A. Adel[4] at high dispersion by using a grating with 2400 lines per inch, and this author[5] has attributed part of the observed fine structure to N_2O. Adel's measurements have been compared with the data obtained by A. H. Nielsen and H. H. Nielsen[1] for the 7.7-μ band of CH_4. It is possible to find many corresponding lines, within the errors of observations. However, the solar spectrum in this region is complicated by the presence of many water vapor lines and probably also by the fine structure of N_2O.

With the aim of finding the CH_4 lines in the 7.7-μ region of the solar spectrum, an echelette grating with 3600 lines per inch has been placed in the spectrometer. A comparison between the expected spectrograms and the observations from Adel may also show if the detected methane is not due to a local impurity of the atmosphere.

Details concerning the identification of the 3.3-μ band of methane in the solar spectrum will be published, in the near future, in the Astrophysical Journal.

* Supported by Air Materiel Command, Wright Field, Dayton, Ohio.
** From the Institut d'Astrophysique de Cointe, University of Liége, Belgium.
[1] A. H. Nielsen and H. H. Nielsen, Phys. Rev. 48, 864 (1935).
[2] A. Adel, Ap. J. 87, 198 (1938).
[3] A. Adel, Ap. J. 90, 627 (1939).
[4] A. Adel, Ap. J. 94, 451 (1941).
[5] A. Adel, Ap. J. 93, 509 (1941).

Fluctuations in the Refractivity of Water

JOHN B. HAWKES AND ROBERT W. ASTHEIMER
Stevens Institute of Technology, Hoboken, New Jersey
December 26, 1947

AT the Chicago meeting of the American Physical Society Antonoff, Yakimac, and Randall report finding that the density of water fluctuates with time in a random manner. The density fluctuations are said to be in the fourth decimal place. Since the refractivity of water $(n-1)$ is roughly proportional to the density, a similar fluctuation in the index should exist.

We are able to measure changes of index with temperature, by means of a Jamin interferometer, to a precision of 1×10^{-6} index units per degree Centigrade. Light is supplied from a sodium arc. Fluctuations in density of 10^{-4} g/cc as reported by Antonoff would result in fluctuations of 3×10^{-5} index unit. This, in turn, would produce a fringe shift of about 10 fringes in our instrument.

We find that when the temperature of the water is held constant to 0.005°C, we observe fringe fluctuations no greater than $\frac{1}{2}$ fringe. This fluctuation is believed to be due to small temperature variations arising from the operation of the thermostat. This $\frac{1}{2}$-fringe fluctuation corresponds to an index change of 1.5×10^{-6} and a density fluctuation of no greater than 5×10^{-6} g/cc. Continuous observation of the fringe pattern has been made over periods of several hours. The fringe fluctuations in our apparatus have a period of about 30 seconds, which is of the same order as the operating period of the thermostat.

The Neutron-Proton Scattering Formula

S. FLÜGGE AND E. HÜCKEL
University of Marburg, Marburg, Germany
January 12, 1948

THE neutron-proton scattering cross section can be described easily by the often used Bethe formula[1]

$$\sigma=\frac{3}{4}\sigma_T+\frac{1}{4}\sigma_S=\frac{3}{4}\frac{4\pi}{k^2+\kappa^2}+\frac{1}{4}\frac{4\pi}{k^2+\kappa'^2},$$

which is derived for a square well of radius a and a *real* singlet state of the deuteron. In this equation, k^2 is the kinetic energy of the incident neutron, measured in the center of gravity frame, in units of $\hbar^2/M$. The first term belongs to the triplet interaction with κ^2 being the binding energy of the deuteron in the same units. In the second term, κ'^2 is the binding energy of the real singlet state. If κa or $\kappa' a$ is not much less than unity, a correction has to be made by a factor $1+2\kappa a$ or $1+2\kappa' a$, respectively, not $1+\kappa a$ as suggested by Bethe.

We should like to point out in this letter that the second term of this expression does not hold for a *virtual* singlet state of the deuteron as commonly supposed. An easy calculation used instead gives

$$\sigma_S=\frac{4\pi}{k^2+(a^2/4)(\kappa'^2-k^2)^2},$$

where $\kappa'^2>0$ is now the energy of the virtual level in the same units. This expression is of the same form as Breit and Wigner's well-known resonance dispersion formula with a line breadth which is proportional to k and of the same order of magnitude as the resonance energy. In consequence of this large line breadth we do not get a maximum for $k^2=\kappa'^2$ but a cross section monotonously falling with growing energy in the same manner as Bethe's formula suggests and experiments[2] show.

The limit for $k=0$ comes out to be $\sigma_S=16\pi/(a^2\kappa'^4)$ instead of Bethe's $\sigma_S=4\pi/\kappa'^2$, i.e., larger by a factor $4/(\kappa' a)^2$. With the usual values for the virtual level energy of about 100 kev, this factor is much larger than unity. In order to get the right observed slow neutron scattering cross section of about 20.10^{-24} cm^2, it is necessary to take a much larger virtual level energy, about 1.5 Mev.

The change in order has many consequences, e.g., for the capture cross section of slow neutrons by protons, and for the field theory of nuclear forces. Details of the deduction of the new formula and of these consequences will be published elsewhere.

[1] H. A. Bethe and R. F. Bacher, Rev. Mod. Phys. 8, 114 (1936); J. Schwinger and E. Teller, Phys. Rev. 52, 286 (1937); C. Kittel and G. Breit, *ibid.* 56, 744 (1939).
[2] Compare Bailey, Bennett, Bergstrahl, Nuckolls, Richards, and Williams, Phys. Rev. 70, 583 (1946); D. H. Frisch, *ibid.* 70, 589 (1946).

On Heavy Mesons and the Cosmic Rays Far Underground

KENNETH I. GREISEN
Cornell University, Ithaca, New York
January 12, 1948

IT is well known that the intensity of mesons as a function of depth down to 300 meters water-equivalent exhibits a form which is entirely explainable in terms of the known processes of decay and ionization loss, provided the mesons have an energy spectrum given by $f(E)$ const.$E^{-1.8}$, in which $f(E)$ is the number of mesons (at the place of production high in the atmosphere) with energy above E. Beyond 400 meters depth, however, the range distribution of the mesons changes from $f(R)$=const.$R^{-1.9}$ to $f(R)$=const.$R^{-2.9}$, which indicates that for mesons of energy 10^{11} ev and above either the energy spectrum becomes more steep or energy losses become important that increase with energy.

The first explanation which comes to mind for this change is that the primary cosmic rays may have a steeper energy distribution above 10^{11} ev than below. This explanation, however, is refuted by the evidence on large bursts observed under thick shields at sea level, and particularly the data on the density-frequency distribution of extensive air showers, both of which indicate that the energy distribution continues without change in form up to higher energies than 10^{11}.

A second explanation which has been offered[1] is the energy loss by radiation, which becomes appreciable for mesons of energy large compared with 10^{10} ev, and which increases in proportion to the energy. Lyons[2] has shown that the effect of radiation loss is to give the absorption curve the form

$$F(T)=\text{const.}\,T^{-\gamma}e^{-T/\lambda},$$

where λ is the "radiation length," defined so that

$$\overline{(dE/dx)}_{\text{rad}}=-(E/\lambda).$$

Such a relation might fit the underground data approximately if λ were about 10^5 g/cm² for rock and soil. However, the radiation length cannot be assigned so arbitrarily. The data on bursts under thick shields at sea level[1,3,4] agree with the collision probabilities deduced by Christy and Kusaka for mesons of spin zero. From the same probabilities, one may calculate* $\lambda \gtrsim 10^6$ g/cm² for a material of average atomic number around 11. Thus, the *experimental* radiation probabilities are too small by a factor 10 to account for the change in slope of the absorption curve.

The recent discovery of the heavy meson by Lattes, Muirhead, Occhialini, and Powell[5] and of its spontaneous decay into the ordinary meson offers a new explanation. Suppose that the heavy mesons are produced high in the atmosphere. They may then either lose most of their energy by interacting with nuclei of air, or disintegrate into ordinary mesons and some neutral particle. Presumably the mean free path is short (around 100 g/cm²), independent of energy, and approximately equal to the mean free path of the primary rays. The probability of decay, however, is inversely proportional to the density of the air and the momentum of the particle. For the number of heavy mesons of a particular energy as a function of depth, one therefore obtains the equation**

$$dn/dt=Ae^{-t}-r(1+(B/t)),$$

where Ae^{-t} is proportional to the number of primary rays of sufficiently high energy. $B=8\times10^5\mu/c\tau_0E$, μ=rest energy, τ_0=proper lifetime, and E=energy of the heavy meson. t is measured in units of the mean free path. From this one may calculate the number of ordinary mesons of a particular energy:

$$m=\int_0^{\infty}\frac{B}{t}r\,dt\approx\frac{B}{B+1}A.$$

Thus, one obtains from the intermediate step in creation of mesons a new factor $B/B+1$ in the spectrum. For $B\gg1$ there is no change, while for $B\ll1$, the factor is just B, which is inversely proportional to the energy. This is precisely the sort of factor needed to explain the change in slope of the absorption curve. The transition occurs at an energy around 8×10^{10} ev, where B must equal 1. From this, taking $\mu=1.7\times10^8$, we find for the proper lifetime, $\tau_0=6\times10^{-8}$ second, which is within the range of values deduced by Marshak and Bethe[6] from independent considerations.

Further support is given to this hypothesis by Forro's report[7] of a positive temperature coefficient for the rays observed at 1000 meters depth. This is expected because of the dependence of the decay probability on the density of the air. Unfortunately, no correlation was possible with the upper air temperatures, which should have been much more significant than the ground temperatures.

* This calculation depends logarithmically on the energy of the meson, according to the formula of Christy and Kusaka. However, the logarithmic increase should be cut off by the screening which has been neglected. $\lambda=10^6$ was calculated for an energy 10^{11} ev and, therefore, is probably too small.

** The method of computation was suggested by H. A. Bethe.

[1] W. Heisenberg, *Cosmic Radiation*, translated by T. H. Johnson (Dover Publications, New York, 1946), pp. 76–83.
[2] D. Lyons, Physik. Zeits. **42**, 166 (1941).
[3] R. E. Lapp, Phys. Rev. **69**, 321 (1946).
[4] R. F. Christy and S. Kusaka, Phys. Rev. **59**, 414 (1941).
[5] C. M. Lattes, H. Muirhead, G. P. S. Occhialini, and C. F. Powell, Nature **159**, 694 (1947).
[6] R. E. Marshak and H. A. Bethe, Phys. Rev. **72**, 506 (1947).
[7] M. Forro, Phys. Rev. **72**, 868 (1947).

On Neutral Mesons in Cosmic Rays

KENNETH I. GREISEN
Cornell University, Ithaca, New York
January 12, 1948

NUMEROUS phenomena which have defied even qualitative explanation up to the present are made understandable in the light of the neutral meson hypothesis, coupled with the recent discovery of the heavy meson. One such phenomenon is Anderson's photograph of a decay electron of 24-Mev energy,[1] which Marshak[2] has explained in terms of the neutral meson. Another is the shape of the meson absorption curve far underground, and the positive temperature effect far underground, which are explained in the previous letter.

A third is the variation of burst frequency under thick shields as a function of altitude. Since the number of high energy mesons ($E>10^{10}$ ev) does not change appreciably

with altitude, the radiative collisions of ordinary mesons cannot account for the rapid increase of large bursts ($E>10^{11}$ ev) with altitude.[3-6] It has been noted[3,4] by Schein, Gill, and Lapp that the largest bursts increase with altitude much more rapidly than the smaller bursts, in fact, even more rapidly than the giant air showers. Bridge *et al.*[5] found an increase in bursts by a factor 400 in going to 30,000 ft. altitude, a much larger increase than is found for large air showers. These results are explainable if, in addition to the radiative collisions of mesons, one invokes the following process of burst production. Either a primary proton or a heavy meson may interact with a nucleus to produce a group of mesons containing both neutral mesons and charged heavy mesons of both signs. The neutral mesons decay immediately into two photons each, which initiate the cascade shower. The frequency of the process should increase very rapidly with altitude because of the short mean free path of the primaries and heavy mesons. Moreover, the effect should be most noticeable for bursts of energy greater than 10^{11} ev, because heavy mesons of smaller energy are removed from the atmosphere also by decaying into ordinary mesons.

A fourth phenomenon is the giant air showers. Cocconi, Loverdo, and Tongiorgi[7] have shown* that in the giant showers, a few percent of the particles are penetrating particles, presumably mesons. This implies too many mesons for them to be produced in a single nuclear interaction, and too many electrons in comparison with the mesons for the electrons to have originated either from the mesons or from the single explosive process (followed by cascade development) in which the mesons may have been formed. But if one supposes that groups of mesons can be produced by nuclear interactions of heavy mesons as well as primary protons, and that principally only the heavy mesons of $E<10^{11}$ ev decay into ordinary mesons instead, one has a cascade production which can easily account for the large number of mesons in a single shower. Moreover, if in each interaction $\frac{1}{3}$ of the particles produced are neutral mesons that decay into photons, one can easily account for finding most of the energy of the shower ultimately in the soft component.

Cocconi *et al.* have shown, indeed, that *every* large shower of penetrating particles in air is accompanied by an extensive shower of photons and electrons. This is exactly as required by the neutral meson postulate.

Associated with the above phenomena are the cloud-chamber observations of Fretter,[8] in which the simultaneous production of heavy particles and electrons has been seen. Fretter has already suggested that the electrons in these photographs may have arisen through decay of short-lived neutral mesons.

A fifth phenomenon is the relation between the electron spectrum and the meson spectrum throughout the lower atmosphere. According to the neutral-and-heavy-meson postulates, the chief sources of electrons in the lower atmosphere should be two: (1) the cascades resulting from photons produced by decay of neutral mesons, and (2) the decay of ordinary light mesons. From the second source one expects a rather soft spectrum of electrons approximately in equilibrium with the ordinary mesons (varying as the ratio of meson intensity to the density of the air). From the first source, however, one expects a primary spectrum of photons having exactly the same form as the energy spectrum of heavy mesons; this is the same as the spectrum of ordinary mesons at sea level except for an extra factor $8\times10^{10}/E+8\times10^{10}$ in the spectrum of light mesons (see previous letter). Moreover, the first source (which is the only appreciable source for the giant air showers) should vary strongly with altitude, as though the cascades were all begun near the top of the atmosphere. Not only the neutral mesons but also the heavy mesons should decay mostly in the top quarter of the atmosphere, hence the mesons also should behave as if they originated near the top. Such an hypothesis accounts perfectly for the variation of relative electron and meson intensity with altitude, a problem which has long puzzled investigators.[9,10] It also provides a reason for the similarity of the high energy electron and meson spectra.

Thus, the consequences of the neutral meson postulate, coupled with the strongly interacting heavy charged mesons, are so fruitful that one is strongly tempted to accept the postulate, perhaps too hastily. A few experiments are suggested which may either disprove the postulate or add considerable weight to it.

(1) The transition curve for large bursts should be carried out to greater thicknesses of lead, to measure the absorption of the burst producing radiation. Thus one could tell whether the bursts were made by ordinary mesons or by strongly interacting particles. This should be done at an elevation of 3000 meters or more.

(2) A comparison of burst production under thick shields of different but low atomic numbers (e.g., iron and aluminum or concrete). This may distinguish between radiation processes and nuclear explosions as the origin of the bursts.

(3) A search for anomalous absorption of burst-producing and penetrating-shower-producing radiation in air, by comparing absorption in air with that in dense materials. A comparison of bursts under 15-cm lead at sea level with those under 50-cm lead at Mt. Evans, for instance, would show whether or not the burst-producing radiation undergoes decay in the atmosphere with a lifetime $\sim10^{-7}\mu/E$ second.

(4) A search for penetrating particles in the large bursts. The above postulates would predict that Geiger counters placed in thick lead under the ionization chamber (which in turn is under thick lead) would frequently be discharged when bursts occurred in the ionization chamber. This could not occur if the bursts were due to atmospheric electron showers, or to radiative collisions of ordinary mesons.

* Recent experiments of J. E. Treat and K. Greisen (unpublished) give about 30 electrons per meson at 3200 meters elevation.

[1] C. D. Anderson, R. V. Adams, Paul E. Lloyd, and R. R. Rau, Phys. Rev. 72, 724 (1947).
[2] R. E. Marshak, Am. Phys. Soc. Bulletin 22, No. 6, 14.
[3] M. Schein and P. S. Gill, Rev. Mod. Phys. 11, 267 (1939).
[4] R. E. Lapp, Phys. Rev. 69, 321 (1946).
[5] H. Bridge, B. Rossi, and R. W. Williams, Phys. Rev. 72, 257 (1947).
[6] E. F. Fahy and M. Schein, Am. Phys. Soc. Bulletin 22, No. 6, 15.
[7] G. Cocconi, A. Loverdo, and V. Tongiorgi, Phys. Rev. 70, 852 (1946).
[8] W. B. Fretter, Phys. Rev. 72, 743 (1947); *ibid.* 73, 41 (1948).
[9] B. Rossi and K. Greisen, Phys. Rev. 61, 121 (1942).
[10] H. Bridge and B. Rossi, Phys. Rev. 71, 379 (1947).

The Magnetic Moments of Cu^{63} and Cu^{65}

R. V. POUND
Lyman Laboratory of Physics, Harvard University, Cambridge, Massachusetts
January 12, 1948

THE magnetic moments of the two stable copper isotopes, Cu^{63} and Cu^{65}, have been determined by measurements of nuclear magnetic resonance absorption. Previously, Ritschl[1] had shown the spins of the two isotopes to be $\frac{3}{2}$ and had calculated their magnetic moments as 2.5 nuclear magnetons from measurements of the hyperfine structure of spectral lines. Schüler and Schmidt[2] confirmed these spin values and calculated 2.5 and 2.6 nuclear magnetons for the magnetic moments of Cu^{63} and Cu^{65}, respectively.

The lines were found with the recording radiofrequency spectrometer previously reported,[3] in the region of 3 Mc/sec., using a constant magnetic field of about 3000 gauss. The sample was cuprous chloride powder, compressed into a cylindrical pellet in a mold. In this way, a factor of two or three in signal strength can be gained over that obtained for the uncompressed powder. The copper lines were unusually intense for a crystalline sample and the ratio of the amplitudes of the two lines was about 2:1, as can be seen from the reproduction of a record from the spectrometer shown in Fig. 1. The lines recorded are derivatives of the absorption curves, which are similar to, but should not be confused with, dispersion curves. In agreement with Schüler and Schmidt, the larger magnetic moment is possessed by the less abundant isotope, Cu^{65}. The amplitude ratio is in good agreement with the known abundance ratio of 7:3.

The frequencies of the two lines were measured by making marks on the paper of the recording milliammeter at about 1-kc/sec. intervals as the spectrometer slowly passed through zero beat with a heterodyne-frequency meter. To minimize errors from drift of the magnetic field, measurements were made first at one line, then at the other, and finally at the first again. The frequency ratio was determined by an interpolation based on the assumption of a uniform rate of drift of the field. The total time taken for one set of three readings was about 30 minutes, and the total drift was never greater than about 1 part in 1000. Errors caused by short-period fluctuations in the field are unlikely because the magnet current is supplied from a bank of large storage cells. The procedure was repeated and the result of both measurements is

$$\nu_{Cu^{65}}/\nu_{Cu^{63}} = 1.0711 \pm 0.0002.$$

A compressed sample of sodium bromide was used to compare the frequency of the Na^{23} line with that of Cu^{63} by the same procedure. The result of these measurements is

$$\nu_{Cu^{63}}/\nu_{Na^{23}} = 1.0022 \pm 0.0002.$$

Taking the magnetic moment of Na^{23} to be 2.217 ± 0.002 nuclear magnetons and its spin as $\frac{3}{2}$,[4] and making a small correction for the diamagnetism of the electrons in the two ions,[5] the magnetic moments of the copper isotopes, in nuclear magnetons, are found to be

$$\mu_{Cu^{63}} = 2.2265 \pm 0.0025,$$

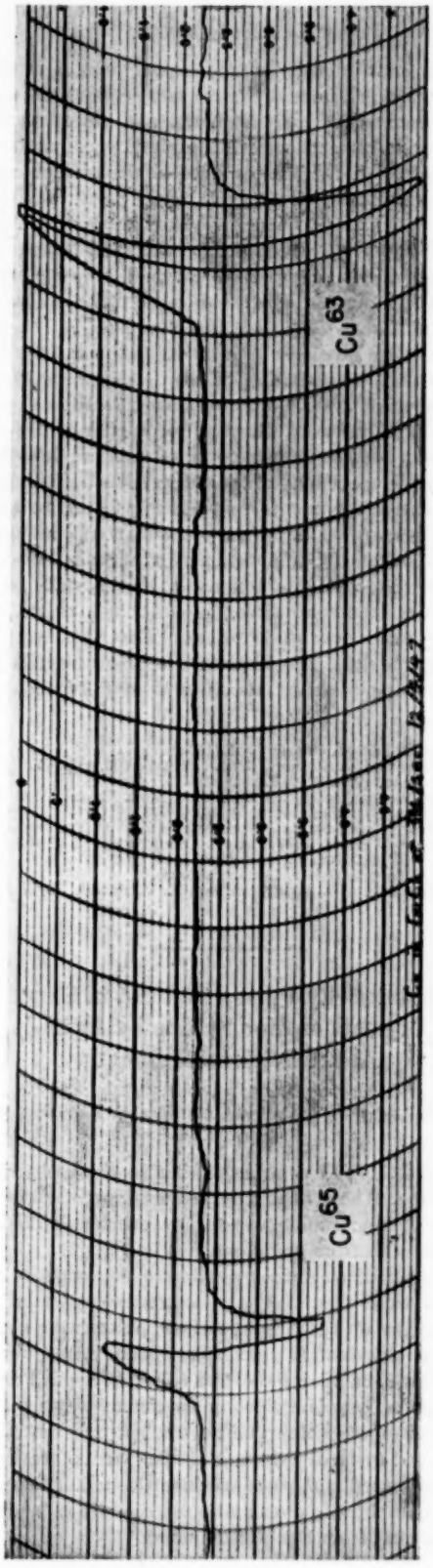

FIG. 1. Record from the r-f spectrometer. Frequency decreased toward the right at a rate of about 10 kc/sec. per division, and the paper speed was four divisions per hour.

and

$$\mu_{Cu^{65}} = 2.3847 \pm 0.0030.$$

The unusual intensity of the copper lines is probably caused by a cupric impurity in the sample. Since the cupric ion is electronically paramagnetic, and since electronic paramagnetic relaxation occurs rapidly,[6] compared with the frequency of the nuclear lines in the present experiment, a fluctuating local field would result having an intensity much larger than in crystals not having a paramagnetic impurity. Therefore, the relaxation time T_1 of the nuclei of the cuprous ions would be considerably shortened. A similar effect has been observed for the protons in $CuSO_4 \cdot 5H_2O$ by Bloembergen.[7] A shortened relaxation time gives rise to relatively intense lines under the conditions of operation of the spectrometer because partial saturation is common for most crystalline samples.

The widths of the two lines as recorded, about 5 gauss or 5 kc/sec. between maxima and minima, are determined partly by inhomogeneity of the magnetic field. The magnet used for these experiments has poles only $3\frac{3}{4}$ in. in diameter and a $1\frac{1}{8}$-in. gap, while the sample was about $\frac{3}{4}$ in. long by $\frac{1}{2}$ in. in diameter. Computation of the r.m.s. line width from the spin-spin interactions in the crystal, using a formula developed elsewhere,[8] gives about 2 kc/sec., if an average is taken over all directions of the crystal axes, with respect to the field. The observed line breadth sets a lower limit on the spin-lattice relaxation time T_1 of about 10^{-4} second.

[1] R. Ritschl, Zeits. f. Physik **79**, 1 (1932).
[2] H. Schüler and T. Schmidt, Zeits. f. Physik **100**, 113 (1936).
[3] R. V. Pound, Phys. Rev. **72**, 527 (1947).
[4] J. B. M. Kellogg and S. Millman, Rev. Mod. Phys. **18**, 323 (1946).
[5] W. E. Lamb, Jr., Phys. Rev. **60**, 817 (1941).
[6] C. J. Gorter, *Paramagnetic Relaxation* (Elsevier Publishing Company, Inc., New York, 1947); R. T. Cummerow, D. Halliday, and G. E. Moore, Phys. Rev. **72**, 1233 (1947).
[7] N. Bloembergen, *Thesis*, Leiden, in press.
[8] N. Bloembergen, E. M. Purcell, and R. V. Pound, Phys. Rev., in press.

Conductivity Pulses Induced in Single Crystals of Zinc Sulfide by Alpha-Particle Bombardment

A. J. Ahearn
Bell Telephone Laboratories, Murray Hill, New Jersey
January 12, 1948

CONDUCTIVITY pulses similar to those observed in diamond[1] have been observed with specimens of single crystals of zinc sulfide when they are bombarded with alpha-particles from polonium.

The types of electrodes used were the same as in the diamond experiments. With electrodes separated by a 0.003-cm gap on the crystal surface, pulses were observed when a potential of 30 volts was applied. Pulses were also observed when a potential of 100 volts was applied between electrodes on opposite sides of specimens about 0.050-in. thick. Pulses were observed both when polished surfaces and cleaved surfaces were used. Pulses were observed with all of the limited number of specimens tested. The response both in numbers of pulses and pulse height is substantially less than that from the best diamond.

The specimens* used were natural crystals of sphalerite which is the cubic form of zinc sulfide. A qualitative spectrochemical analysis of one of the specimens showed an impurity content of the order of 0.1 percent, chiefly germanium. Similarly, the other specimens exhibited impurity contents in the neighborhood of 0.01 percent of one or more of the elements gallium, mercury, cadmium, and manganese. The appearance of pulses in zinc sulfide with this relatively high impurity content contrasts strikingly with the absence of pulses in some diamonds where the impurity content is known to be much smaller.

[1] D. E. Wooldridge, A. J. Ahearn, and J. A. Burton, Phys. Rev. **71**, 913 (1947).
* Some of the specimens were obtained through the courtesy of Dr. Keith Boyer, Massachusetts Institute of Technology, and others from Dr. M. F. Distad, Naval Research Laboratory.

A Note on Relativistic Quantum Mechanics

Hartland S. Snyder
Brookhaven National Laboratory, Upton, New York
January 14, 1948

THE usual method for obtaining a Hamiltonian for systems of interacting particles and fields is by the use of a Lorentz invariant Lagrangian or an equivalent method. An alternative method is the direct examination of the transformation properties of an assumed form for a Hamiltonian. This note reports the results of such an examination for the following example. Suppose the Hamiltonian, H, of a system may be written in the form

$$H = \int \epsilon_{\mathbf{k}} da_{\mathbf{k}}^{+} da_{\mathbf{k}} + \int \epsilon_{\mathbf{K}} da_{\mathbf{K}}^{+} da_{\mathbf{K}} + \int V(\mathbf{k}, \mathbf{k}', \mathbf{K}) da_{\mathbf{k}}^{+} da_{\mathbf{k}'}^{+} da_{\mathbf{K}} + \int V^{*}(\mathbf{k}, \mathbf{k}', \mathbf{K}) da_{\mathbf{k}'}^{+} da_{\mathbf{k}} da_{\mathbf{K}}^{+}$$

and the total momentum, $\mathbf{P}$, may be written

$$\mathbf{P} = \int \mathbf{k} dn_{\mathbf{k}} + \int \mathbf{K} dN_{\mathbf{K}}.$$

In the above equations $da_{\mathbf{k}}^{+}$ are creation operators and $da_{\mathbf{k}}$ are annihilation operators for Fermi particles and satisfy the commutation relations $da_{\mathbf{k}}^{+} da_{\mathbf{k}'}^{+} + da_{\mathbf{k}'}^{+} da_{\mathbf{k}}^{+} = 0$ if $\mathbf{k} \neq \mathbf{k}'$ and $= d_{\mathbf{k}}$ if $\mathbf{k} = \mathbf{k}'$, and $dn_{\mathbf{k}} = da_{\mathbf{k}}^{+} da_{\mathbf{k}} / d_{\mathbf{k}}$. Also, $da_{\mathbf{K}}^{+}$ is a creation operator and $da_{\mathbf{K}}^{+}$ is an annihilation operator for Bose particles and satisfy $da_{\mathbf{K}} da_{\mathbf{K}'}^{+} - da_{\mathbf{K}'}^{+} da_{\mathbf{K}} = 0$ if $\mathbf{K} \neq \mathbf{K}'$ and $= d_{\mathbf{K}}$ if $\mathbf{K} = \mathbf{K}'$, and $dN_{\mathbf{K}} = da_{\mathbf{K}}^{+} da_{\mathbf{K}} / d_{\mathbf{K}}$.

The requirement that H, $\mathbf{P}$ constitute a four vector with respect to homogeneous Lorentz transformations gives the following results. First, $\epsilon_{\mathbf{k}} = \pm(M^2 + \mathbf{k}^2)^{\frac{1}{2}}$ in which the constant M may be identified with the mechanical mass of the Fermi particle. Second, $\epsilon_{\mathbf{K}} = \pm(u^2 + \mathbf{K}^2)^{\frac{1}{2}}$ in which the constant u is the mechanical mass of the Bose particle. Third,

$$V(\mathbf{k}, \mathbf{k}', \mathbf{K}) = U_0 \delta(\mathbf{k} - \mathbf{k}' - \mathbf{K}) \exp\{2g(\mathbf{k}) - 2g(\mathbf{k}') - 2f(\mathbf{K})\}$$

in which U_0 is a constant, f and g are real functions of their arguments, and $\delta(\mathbf{k} - \mathbf{k}' - \mathbf{K})$ is the Dirac δ-function. This particular Hamiltonian does not give convergent results. Other forms for Hamiltonians are being examined at the present time.

Secondary Electrons Produced by Mesons

J. G. WILSON
The Physical Laboratories, University of Manchester, Manchester, England
January 12, 1948

IN a recent paper[1] Nassar and Hazen have measured the number of secondary electrons in equilibrium with the meson beam at sea level. In particular, they find the number of electrons with energy greater than 10^7 ev to be about 2 percent of the total number of mesons, and state this result to be in disagreement with an early measurement of my own[2] which is quoted to be 4.8 percent of electron secondaries of energy greater than 10^7 ev. This discrepancy arises from a misreading of my paper, in which the incident mesons were divided into two categories, with momenta respectively greater and less than 3×10^9 ev/c, which were considered separately.

The mesons of the high momentum group, comprising about 44 percent of the whole meson beam, were accompanied by about 4.4 percent (of their own number) of electrons; those of the lower momentum group, comprising the remaining 56 percent, were accompanied by only 0.4 percent of electrons. The measurement by Nassar and Hazen is to be compared with the mean value over both groups, taken together, that is, with $(0.44\times4.4+0.56\times0.4)$ percent or 2.2 percent, and not with $(4.4+0.4)$ percent. There is thus no significant discrepancy between the two sets of observations.

[1] S. Nassar and W. Hazen, Phys. Rev. **69**, 298 (1946).
[2] J. G. Wilson, Nature **142**, 73 (1938).

The Hyperfine Structure and Nuclear Moments of Chlorine*

L. DAVIS, JR., B. T. FELD, C. W. ZABEL, AND J. R. ZACHARIAS
Research Laboratory of Electronics, Massachusetts Institute of Technology, Cambridge, Massachusetts
January 12, 1948

TWO of us[1] have recently reported an atomic-beam magnetic resonance experiment, in which the hyperfine structure splittings of the ground states of the natural isotopes of potassium were separately observed, with a mass spectrograph supplementing the usual hot wire detector. In the experiments herein reported, a discharge tube, previously used to supply atomic hydrogen, was used to provide a beam of chlorine atoms. To detect the beam, a fraction of the Cl atoms and the Cl_2 molecules are converted to negative ions on evaporation from the usual hot tungsten filament despite its high work function. These ions are then analyzed by the mass spectrograph. We have, therefore, been able to measure the hyperfine structure splittings of the $^2P_{3/2}$ ground states of Cl^{35} and Cl^{37}.

Townes, Holden, Bardeen, and Merritt[2] as well as Gordy, Simmons, and Smith[3] have shown that for Cl^{35} and Cl^{37} the nuclear spin $I=\frac{3}{2}$ and that various molecules exhibit large electric quadrupole interactions. Townes[4] has estimated the nuclear electric quadrupole moments Q from such data.

The energy level system for an atom of nuclear spin $I=\frac{3}{2}$ and electronic state $J=\frac{3}{2}$ is sketched in Fig. 1. The

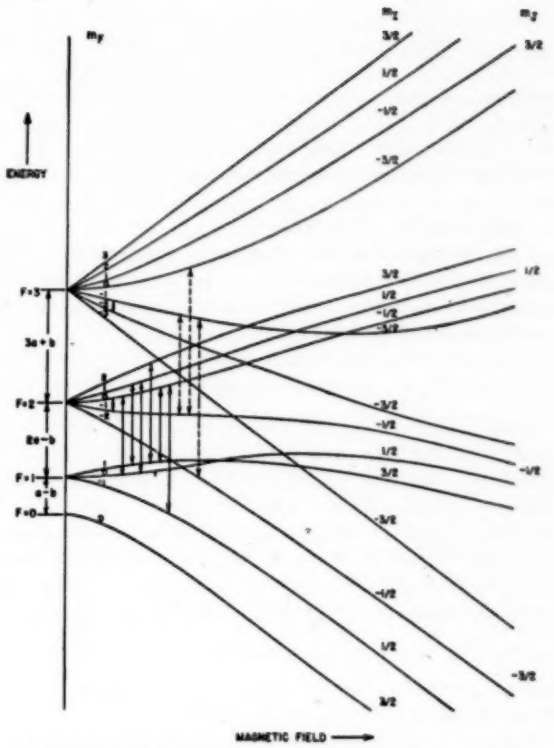

FIG. 1. A rough plot of the h.f.s. level energies as a function of applied magnetic field for a nucleus of $I=3/2$ in an atom with $J=3/2$, derived from the Hamiltonian

$$H=aI\cdot J+b\left\{\frac{3/2(I\cdot J)^2+3/4I\cdot J-\frac{1}{2}I(I+1)J(J+1)}{I(2I-1)J(2J-1)}\right\}+\mu_0 g_J J\cdot H-\mu_0(m/M_p)g_I I\cdot H,$$

for small b/a and $a>0$. The abscissa runs from $x=0$ to ~6, where $x=\mu_0 g_J H/a$.

vertical lines between levels show transitions which can be observed in this apparatus,[5] which requires, for proper refocusing, that m_J change sign. Of the eleven such transitions which obey selection rules $\Delta F=\pm1,0$ $\Delta m_F=\pm1.0$, we have observed 8; 2 for $\Delta F=0$ and 6 for $\Delta F=1$, between $F=2$ and $F=1$. For Cl^{35} these observations were made in the h.f.s. Zeeman region and in the region of intermediate coupling; for Cl^{37}, only in the Zeeman region. A set of lines typical of Cl^{35} at fixed intermediate field is:

$$\begin{aligned}\nu(3,-1\leftrightarrow3,-2)&=35.414\pm0.02\text{ mc/sec.},\\ \nu(2,0\leftrightarrow2,-1)&=36.890,\\ \nu(2,0\leftrightarrow1,1)&=336.266,\\ \nu(2,0\leftrightarrow1,0)&=340.075,\\ \nu(2,1\leftrightarrow1,1)&=368.066,\\ \nu(2,1\leftrightarrow1,0)&=371.872,\\ \nu(2,2\leftrightarrow1,1)&=395.702.\end{aligned}$$

Assuming the hyperfine structure to be given by a magnetic dipole interaction constant a and an electric quadrupole interaction constant b, we can draw the following conclusions:

(1) Both isotopes have nuclear spins $I=\frac{3}{2}$;

(2) the separations $\Delta\nu_{2,1}=2a-b$ are: $(\Delta\nu^{35}{}_{2,1})=355.231\pm0.02$ mgc/sec. and $(\Delta\nu^{37}{}_{2,1})=298.116\pm0.02$ mgc/sec.;

TABLE I.

Isotope	a(mgc/sec.)	b(mgc/sec.)	$Q(10^{-26}\,\text{cm}^2)$ (DFZZ)	$Q(10^{-26}\,\text{cm}^2)$ (Townes)
Cl^{35}	205.2 ± 4.6	55.2 ± 1.2	-7.95 ± 0.2	-6.7
Cl^{37}	170.6 ± 3.9	43.1 ± 1.0	-6.20 ± 0.2	-5.1

(3) $(b/a)^{35}=0.269\pm0.006$;

(4) by observing the trajectory of the atoms giving rise to the line $(2,0)\rightarrow(1,-1)$ we conclude that the magnetic moment of Cl^{35} is positive, confirming the observation of Kusch and Millman;[6]

(5) assuming their[6] value of $g^{35}/g^{37}=1.203\pm0.005$ to give a^{35}/a^{37}, we obtain the a and b values of Table I.

From atomic h.f.s. measurements of this sort, it is possible to obtain accurate values of the nuclear quadrupole moment Q, without resorting to fine structure data and estimates of an effective nuclear charge Z_i, since both the magnetic dipole and electric quadrupole interactions have the same r dependence on the electronic wave functions. From the formulae for a and b given by Casimir[7] neglecting relativity corrections, we obtain, in an obvious notation:

$$Q=-(b/a)g_I(\mu_z^2/e^2)(m/M_p)(L+1)(2L+3)/J(J+1),$$

and we get the Q values of Table I. The Q values given by Townes[4] are included for comparison.

In view of the fact that Q values can be determined quite accurately, we believe that the significance of these values lies not in the fact that they disagree with the estimates of Townes, but rather that, when combined with microwave spectroscopy measurements of $eQ\partial^2V/\partial z^2$, they provide a method of actually measuring $\partial^2V/\partial z^2$ at the position of the halogen nucleus in a wide variety of molecules.

Values for a and b of considerably greater accuracy can be obtained when the transitions $\Delta\nu_{1,2}=3a+b$ are found. We plan to apply this method to other halogens, including radioactive ones, and to measure the interaction constants to higher precision than the present apparatus can achieve. We believe that ultimately this method is suitable for observing these atomic interactions to a few cycle/sec., for atoms in concentration of less than 10^{-5}.

* This work has been supported in part by the Signal Corps, the Air Materiel Command, and the Office of Naval Research.

[1] L. Davis, Jr. and J. R. Zacharias, Bull. Am. Phys. Soc. 22, No. 6, B2 (1947).
[2] C. H. Townes, A. N. Holden, J. Bardeen, and F. R. Merritt, Phys. Rev. 71, 644 (1947).
[3] W. Gordy, J. W. Simmons, and A. G. Smith, Phys. Rev. 72, 344 (1947).
[4] C. H. Townes, Phys. Rev. 71, 909 (1947).
[5] J. R. Zacharias, Phys. Rev. 61, 270 (1942).
[6] P. Kusch and S. Millman, Phys. Rev. 56, 527 (1939).
[7] H. B. G. Casimir, *On the Interaction Between Atomic Nuclei and Electrons* (Teyler's Tweede Genootshap, Amsterdam, 1936).

Instantaneous Rates of Grain Growth

PAUL A. BECK, M. L. HOLZWORTH, AND HSUN HU
Department of Metallurgy, University of Notre Dame, Notre Dame, Indiana

January 9, 1948

PREVIOUS work[1,2] showed that the isothermal increase of the average grain size (D) with the annealing time (t) in high purity aluminum follows the relation

TABLE I. Heat treatment and grain size of specimens.

Specimen No.	Heat treatment	D mm
1	125 min. at 400°C	0.235
2	125 min. at 400°C and 120 min. at 450°C	0.340
3	5 min. at 450°C	0.230
4	125 min. at 450°C	0.344

$$D=K\cdot t^n, \tag{1}$$

where K and n are parameters depending on the temperature. The exponent n increases from 0.056 at 350°C to 0.32 at 600°C. From (1) the instantaneous rate of growth is

$$dD/dt=nK\cdot t^{n-1}. \tag{2}$$

Since $n<1$, dD/dt decreases with continued annealing. The absolute value of the negative exponent $n-1$ and, therefore, the rate of decay of dD/dt is increasing with decreasing temperature.

More recent experiments demonstrated that the rate of grain growth in high purity aluminum after 33 percent reduction of area by rolling depends only on the instantaneous grain size and on the temperature, but that it is independent of the particular prior heat treatment used to produce the instantaneous grain size considered. A typical experiment was the following. Four specimens 0.020 in. thick, from ingot No. 18 (see reference 2), were annealed at the temperatures and for the periods given in Table I. The table also gives the average grain sizes obtained.

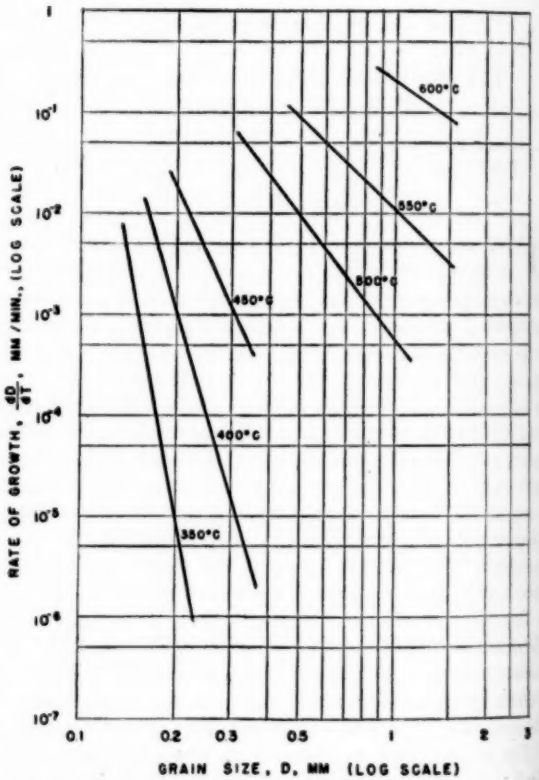

FIG. 1. Rate of grain growth as a function of grain size for aluminum.

It is seen that, in accordance with the earlier data,[2] annealing for 125 min. at 400°C produces a grain size equal to that produced by a 5 min. anneal at 450°C (specimens 1 and 3). The data also show (specimens 2 and 4) that the final grain size obtained by an anneal of 125 min. at 400°C and a subsequent anneal of 120 min. at 450°C was equal to that produced by a single anneal of 125 min. at 450°C. The period of annealing at 450°C necessary for increasing the grain size from 0.23 mm to 0.34 mm was, therefore, the same (120 min.) regardless of whether the initial grain size of 0.23 mm had been obtained by a prior 125-min. anneal at 400°C or by annealing for 5 min. at 450°C.

Since the rate of growth is determined by the instantaneous grain size and the temperature, it is desirable to express dD/dt as a function of these variables. From (1)

$$t=(D/K)^{1/n}.$$

By substituting this into (2) one obtains:

$$dD/dt=n\cdot K^{1/n}\cdot D^{1-1/n}, \qquad (3)$$

or in logarithmic form:

$$\log(dD/dt)=\log n+1/n\,\log K+(1-1/n)\log D. \qquad (4)$$

If $\log(dD/dt)$ is plotted *vs.* $\log D$, a straight line is obtained for each temperature with a slope of $1-1/n$. Figure 1 gives this plot for high purity aluminum at 350° to 600°C, from data previously published.[3] The slight initial deviations from the $D=K\cdot t^n$ relationship at the lowest temperatures are here neglected. It is seen that the rate of decay of dD/dt increases considerably with decreasing temperature.

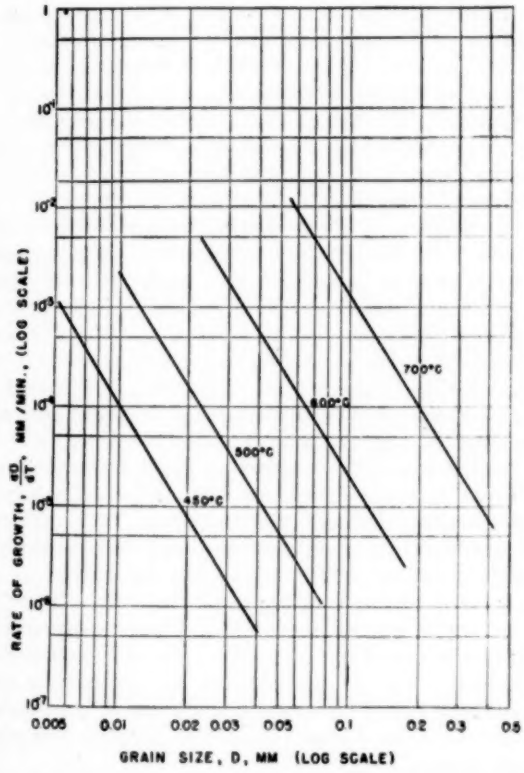

FIG. 2. Rate of grain growth as a function of grain size for 70-30 brass.

As shown in Fig. 1 by the variation of slope with temperature, the ratio of the instantaneous rates of growth at two different temperatures depends on the grain size. Since the temperature dependence of dD/dt varies with the grain size, the "heat of activation" which might be calculated from instantaneous rates will also be grain size dependent. For instance, the "heat of activation" calculated for dD/dt at $D=0.15$ mm is about 38 K cal./g atom, but at $D=0.5$ mm it is roughly 60 K cal./g atom. It has been shown previously[1] that for high purity aluminum, strictly speaking, no heat of activation value can be derived from the temperature dependence of the total time of growth to a certain grain size (average rate of growth), because the value obtained depends on the grain size. The above results show that the same difficulty is also encountered if, in accordance with a recent suggestion by Hollomon,[3] instantaneous rates of growth are used instead of average rates.

For 70-30 brass, where the exponent n is independent of temperature,[4] it is possible to derive a heat of activation value from *either* the total time for a certain grain size, *or* from the instantaneous rate dD/dt, as given in Fig. 2. It can be easily shown that both methods give the *same* numerical value of $Q=61.8$ K cal./g atom, which is independent of the grain size.

This work was supported by the Office of Naval Research, U. S. Navy.

[1] P. A. Beck, J. C. Kremer, and L. J. Demer, Phys. Rev. 71, 555 (1947).
[2] P. A. Beck, J. C. Kremer, L. J. Demer, and M. L. Holzworth, "Grain growth in high purity aluminum and in an aluminum-magnesium alloy," AIME Tech. Pub. No. 2280 Metals Technology, September 1947.
[3] Discussion of reference 2 by J. J. Hollomon.
[4] P. A. Beck, J. Towers, Jr., and W. D. Manly, "Grain growth in 70-30 brass," AIME Annual Meeting, February 1948.

Laue Photography of Neutron Diffraction

E. O. WOLLAN, C. G. SHULL, AND M. C. MARNEY
Clinton National Laboratory, Oak Ridge, Tennessee
January 19, 1948

THE photographic technique has played so important a role in the field of x-ray diffraction that it is of interest to develop this technique for use in neutron diffraction problems. With this idea in mind, we have obtained the Laue photograph, shown in Fig. 1, of the diffraction of neutrons by a NaCl crystal.

The experimental arrangement used in obtaining this and other Laue photographs with neutrons is shown schematically in Fig. 2. A collimated beam of thermal neutrons possessing a continuous wave-length distribution in the region from 0.5 to 3.0 angstroms was taken from the Clinton pile. The collimating system consisted of a hole through a 2½-foot shield block. The exit aperture of this hole was ¼ inch in diameter, and in order to increase the intensity it was successively stepped to larger diameters (up to ¾ inch) toward the inside of the shield block. The final two inches of the collimating shield consisted of boron carbide impregnated plastic for strong neutron absorption.

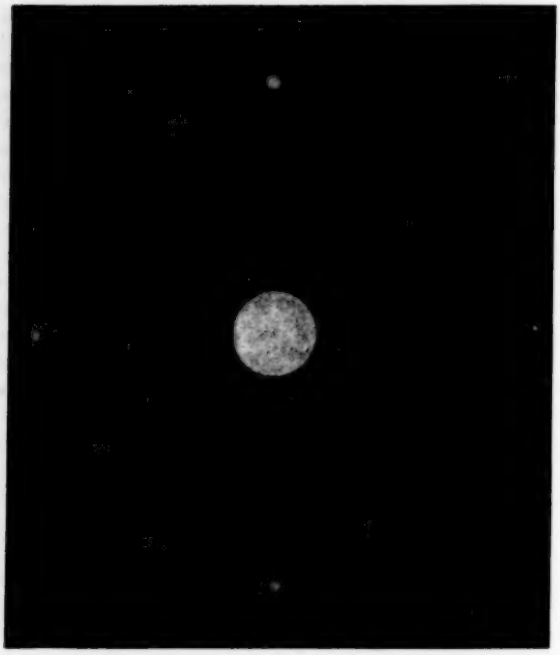

FIG. 1. Laue photograph showing neutron diffraction by NaCl.

Since photographic film (in our case x-ray double emulsion film) is quite insensitive to neutrons, it is necessary to use some type of sensitive screen in conjunction with the film. For this purpose, a sheet of indium 0.5 mm thick has been placed in contact with the film, and the beta-particles resulting from neutron capture in the indium produce the photographic effect. A 1½-inch hole was cut in the center of the indium sheet to reduce the darkening in the vicinity of the primary beam, and the outline of this hole can be seen in Fig. 1. The film was backed by a ¼-inch boron carbide plastic shield through which a ¾-inch hole was cut for the primary beam. The white area in the center of the photograph arises from neutrons and gamma-rays backscattered from the film cassette into the region not covered by the boron carbide shield.

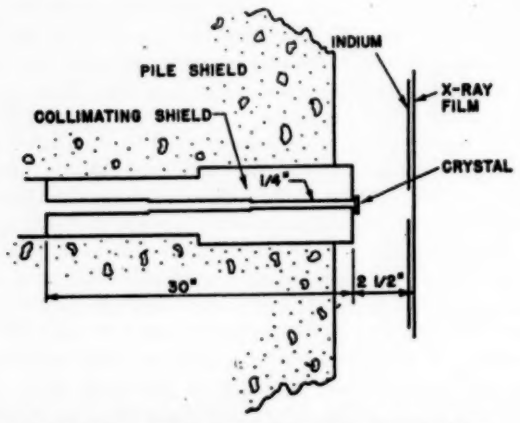

FIG. 2. Schematic diagram of Laue camera for obtaining neutron diffraction patterns.

The photograph in Fig. 1 was obtained with a NaCl crystal 0.35 cm thick, with the incident beam parallel to one of the cube axes and with a crystal to film distance of 6.40 cm. An exposure time of 10 hours was used. By the usual gnomonic projection the Laue spots have been identified as (402), (422), and their permutations for the outer series, and (311) and permutations for the inner series. Other spots such as the (442) and (513) are visible on the original negative but are too weak to show on the reproduction. The relative intensities of the spots on the pattern are in agreement with those expected from the distribution of intensity in the neutron spectrum of the incident beam.

Patterns have also been obtained for a variety of other crystals, including quartz, calcite, LiF, and $NaNO_3$, and several activating materials other than indium have been tried. Details on these and related studies will be published later.

Note on Angular Distributions in Nuclear Reactions

L. WOLFENSTEIN
University of Chicago, Chicago, Illinois
AND
R. G. SACHS
University of Wisconsin, Madison, Wisconsin
January 20, 1948

IN a recent paper[1] of the same title a proof is given of the general theorem that in a nuclear reaction produced with an unpolarized beam of given orbital angular momentum incident on an unpolarized target, the angular distribution of the outgoing intensity cannot be more complicated than that of the incoming intensity. In the last two paragraphs of that paper, an error is made in the application of the treatment to reactions which lead to an arbitrary number of particles of arbitrary spin.

The theorem may be applied to the angular distribution of one of the outgoing particles provided no other independent outgoing particle direction and no state of polarization of any of the particles is specified. This distribution is obtained by summing the absolute square of the wave function describing outgoing particles over all of the unspecified variables. It is shown in the original paper that the absolute square of the wave function may be analyzed into products of the form $\psi_j{}^{\mu'}\psi_l{}^{M}\psi_{l'}{}^{-M'}\psi_s{}^{M''}\psi_s{}^{-M'''}\cdots$, where the first factor describes the angular distribution of the particle under observation and the remaining factors describe the orbital and spin distributions over which the integration is to be performed. Because of the orthogonality relations for the $\psi_l{}^{M}\psi_s{}^{M''}$, the integration eliminates all terms except those for which $\mu'=m-m'$ with $-L\leq m\leq L$, $-L\leq m'\leq L$, where L is the orbital angular momentum of the incident particle. At this point the basic argument of reference 1 may be applied, with the consequence that only terms with $j'\leq 2L$ remain in the intensity expression after integration (rather than before integration as originally stated).

[1] E. Eisner and R. G. Sachs, Phys. Rev. 72, 680 (1947).

Errata: On the Tripartition of Heavy Elements

[Phys. Rev. 72, 1257 (1947)]

TSIEN SAN-TSIANG
Laboratoire de chimie Nucléaire, Collège de France, Paris, France

AND

The Uncertainty Principle and the Yield of Nuclei Formed in Fission

[Phys. Rev. 72, 1265 (1947)]

P. F. GAST
The General Electric Company, Hanford Engineer Works, Richland, Washington

THE Editor regrets that Fig. 1 of the first of the above letters has been interchanged with Fig. 1 of the second paper. The captions, however, are correct as they stand.

In addition, in the correct figure in the letter by Tsien San-Tsiang, the diagram on the left should be labeled *A*, and that on the right, *B*.

The Relative Energies of the Gamma-Radiations from Co^{60} and Zn^{65}

ERLING N. JENSEN, L. JACKSON LASLETT, AND WILLIAM W. PRATT
Institute for Atomic Research and Department of Physics, Iowa State College, Ames, Iowa

December 1, 1947

THE energies of the gamma-rays from Co^{60} and from Zn^{65} have been previously reported[1–4] by a number of investigators who made use of magnetic spectrometers. The energy given[2,4] for the Zn^{65} gamma-ray (1.14 Mev is slightly greater than that originally cited by Deutsch *et al.*[1] for the lower energy Co^{60} line (1.10 Mev) but below that subsequently reported by Miller and Curtiss[2] (1.16 Mev) for this latter radiation. Although the probable errors given in the above investigations were such that no real inconsistency is implied, we would like to present here evidence to the effect that the radiation from Zn^{65} has the lower energy.

We have examined the gamma-ray spectra of Co^{60} and Zn^{65} with a thin-lens magnetic spectrometer,[5] using the photoelectrons ejected from a thin lead foil. The energies obtained for the Co^{60} lines were 1.16 and 1.32 Mev, and that for Zn^{65} was 1.11 Mev. The calibration of the spectrometer was based on the use of annihilation radiation from Zn^{65}. To effect a direct comparison of the gamma-ray energies in question, a source with *both* activities was placed in the spectrometer and the composite spectrum obtained. The results of this test are shown in Fig. 1 and, when compared with our previous curves for these materials, permitted the individual peaks to be definitely identified. It therefore appears that the gamma-ray from Zn^{65} is of lower energy than either of the Co^{60} lines.

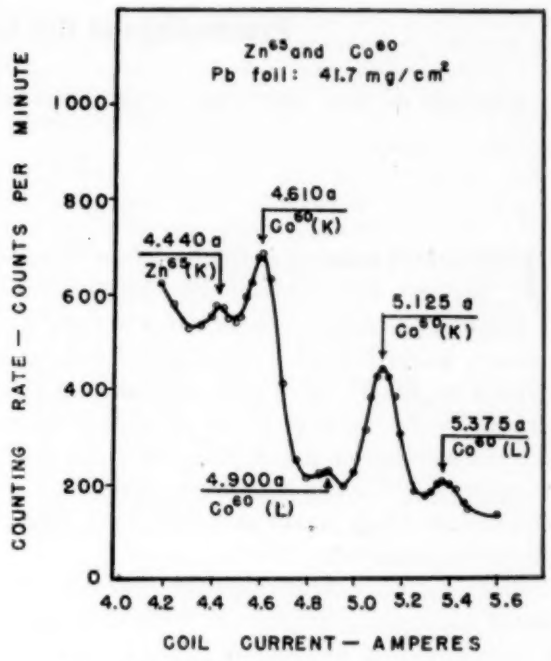

FIG. 1. Composite curve for the comparison of Co^{60} and Zn^{65} gamma-ray energies.

We are indebted to Dr. A. Roberts for calling to our attention the apparent inconsistency between our data and some of the earlier work and for discussing with us the practicality of a direct comparison of the gamma-rays in question.

* Work performed under contract W-7405-eng-82 between the Atomic Energy Commission and the Iowa State College Institute for Atomic Research. Paper No. 26 from the Institute for Atomic Research.

[1] M. Deutsch and L. G. Elliott, Phys. Rev. 62, 558(A) (1942); M. Deutsch, L. G. Elliott, and A. Roberts, Phys. Rev. 68, 193 (1945).

[2] L. C. Miller and L. F. Curtiss, J. Research Nat. Bur. Stand. 38, 359 (1947).

[3] C. E. Mandeville and H. W. Fulbright, Phys. Rev. 64, 265 (1943).

[4] M. Deutsch, A. Roberts, and L. G. Elliott, Phys. Rev. 61, 389(A) (1942).

[5] This work is described in a paper shortly to be submitted for publication. The effect of the radiator thickness is considered and a suitable correction made.

Proceedings of the American Physical Society

Minutes of the Meeting at the University of California, Los Angeles, California

January 2–3, 1948

THE 283rd meeting of the American Physical Society was held at the University of California, Los Angeles on Friday and Saturday, January 2 and 3, 1948. The growth of interest in physics on the Pacific Coast was again demonstrated by the doubling of the number of papers and the attendance as compared with the winter meeting of 1947. The maximum attendance was about 410. Once again a number of Eastern physicists attended.

President L. A. DuBridge, who presided over one of the sessions, announced the probable dates for the Pasadena Meeting as June 24, 25, and 26, 1948. This meeting will be part of a series of scientific gatherings honoring Dr. Robert A. Millikan's 80th birthday. In addition to this meeting, it has now been agreed that the 1949 winter meeting will be held at Berkeley and the 1949 summer meeting at the University of Washington, Seattle. Excellent invited papers attracted large audiences and added much to the meeting. Other presiding officers were J. W. Ellis, R. B. Brode, R. T. Birge, and J. Kaplan.

J. KAPLAN
Local Secretary for the Pacific Coast
University of California
Los Angeles, California

Invited Papers

Physics of the Upper Atmosphere. C. T. ELVEY, *U. S. Naval Ordnance Test Station. Inyokern.*

Linear Electron Accelerators. W. W. HANSEN, *Stanford University.*

Magnetization and Rotation. S. J. BARNETT, *California Institute of Technology and University of California, Los Angeles.*

Nuclear Transmutations with High Energy Particles. G. T. SEABORG, *University of California, Berkeley.*

The Metabolism of the Fission Products and the Heaviest Elements. J. G. HAMILTON, *University of California, Berkeley.*

Contributed Papers

A3. Collisions of the Second Kind. JOSEPH KAPLAN, *University of California, Los Angeles.*—Ta-You Wu[1] has listed thirty-two possible excitation processes in the upper atmosphere and among these were eighteen collisions of the second kind in which the energy of electronic excitation of one particle is transferred into the energy of electronic and vibrational excitation of a molecule. A typical example is $N_2(A^3\Sigma)+O(^1S)\rightarrow O(^1D)+N_2(B^3\Pi)$, the latter in the fifth vibrational level. The resonance in this case is very close and the spin rule is obeyed, hence Wu states that the cross section for this process may be of the same order as the gas kinetic values. The Franck-Condon principle is obeyed.[2] The writer has studied this and similar collisions involving metastable nitrogen molecules and metastable atoms of oxygen and nitrogen. The results suggest that such collisions have much smaller cross sections than have hitherto been assumed. These results are consistent with new ideas concerning the nature of excitation processes in the auroral afterglow,[3] and point the way to new experiments designed to make careful determinations of collision cross sections.

[1] Ta-You Wu, Proc. Ind. Acad. Sci. **18A**, 47 (1943).
[2] R. E. Meyerott, Phys. Rev. **71**, 553 (1947).
[3] J. Kaplan, Phys. Rev. (to be published).

A4. Anomalous Dispersion and Absorption of Ultra-Short Electromagnetic Waves in some Fatty Acids. G. POTAPENKO AND D. WHEELER, *California Institute of Technology.*—The dielectric constant and the coefficient of absorption of electric waves 25 cm long has been measured in dilute solutions of formic, acetic, propionic, and butyric acids in dioxane. Second Drude's method has been used, with Slatis' correction for the eddy currents in the condenser leads. A new method has been developed for computing the effective volume of the rotating portion of the molecule from the data obtained. The computed volumes are found to be proportional to the molecular volume. This shows that the anomalous dispersion and absorption of ultra-high frequency waves in acids investigated is due to the orientation of the entire molecule as a unit. In this respect fatty acids differ from simple alcohols in which, as it has been shown earlier,[1] the anomalous dispersion and absorption is due to the orientation of the dipole-bearing group (hydroxil), which rotates in the high frequency field independently of the rest of the molecule. This difference between the acids and the alcohols is attributed to the difference in the interatomic forces which in acids hinder greatly the rotation of carboxyl group.

[1] E. Keutner and G. Potapenko, Phys. Zeits. **38**, 635 (1937); **40**, 100 (1939).

A5. Propagation Characteristics in a Coaxial Structure with Two Dielectrics. ALFREDO BAÑOS, JR., H. GRUEN, AND DAVID S. SAXON, *University of California.*—The propagation characteristics for circularly symmetric TM-modes in a coaxial structure with two dielectrics offer many points of interest. For a given mode, the pertinent parameters are the ratio of the dielectric constants of the two media involved, the ratio of the two radii, and the operating frequency, expressed, say, in terms of the cut-off frequency for the *empty* guide. Among the results of special interest are the facts that, as already pointed out by Frankel,[1] the phase velocity for a given propagating mode may lie between the phase velocities corresponding to each of the two unbounded dielectrics and that, by proper choice of parameters, it is always possible to obtain a phase velocity of a pre-assigned value higher, of course, than the lower of the two velocities for the unbounded media. This suggests the possibility of using such structures in linear accelerators. Some results of an extensive computational program are presented in the form of families of curves showing the dependence of the propagation constant and of the phase velocity on the parameters of interest. Some discussion of field distributions is also given.

[1] Sidney Frankel, J. App. Phys. 18, 650 (1947).

A6. On the Hyperfine Structure of Gallium. G. E. BECKER* AND P. KUSCH, *Columbia University.*—The hyperfine structures of the ground $^2P_{1/2}$ and the metastable $^2P_{3/2}$ states of Ga^{69} and Ga^{71} have been determined by the atomic beam magnetic resonance method. The h.f.s. levels for an atom whose nucleus has a magnetic dipole, electric quadrupole, and magnetic octupole moment are given by the formula $W=aC/2+bC(C+1)+c(C^3+4C^2+4C/5)$, where $C=F(F+1)-I(I+1)-J(J+1)$. For the metastable state of gallium, with $I=J=\frac{3}{2}$, there are four levels at zero external magnetic field, corresponding to $F=3$, 2, 1, and 0. The determination of the separations of these levels permits the calculation of the constants a, b, and c in the equation above. It was found that only the first two terms are needed to explain the hyperfine splitting of each Ga isotope, within the precision of these measurements. An upper limit for the value of c is $3\cdot10^{-9}$ cm^{-1}. Other results are: $a_{71}=8.0868$ and $a_{69}=6.3644\cdot10^{-3}$ cm^{-1}; $b_{71}=5.4759$ and $b_{69}=8.6894\cdot10^{-5}$ cm^{-1}; $Q_{71}=.117$ and $Q_{69}=.186\cdot10^{-24}$ cm^2. The $\Delta\nu$ of the normal state of each isotope has been determined by the use of transitions in which $\Delta m_J=\pm1$, $\Delta m_J=0$ in the Paschen-Back region. $\Delta\nu_{71}=.113488$ and $\Delta\nu_{69}=.089319$ cm^{-1}. The ratio $(\Delta\nu_{71}/\Delta\nu_{69})=1.27059$ is in good agreement with $(a_{71}/a_{69})=1.27063$.

* Now at Stanford University.

A7. On the Absorption Spectrum of Active Nitrogen. R. EDWIN WORLEY,* *University of California.*—The problem of absorption through active nitrogen has been reattacked, using a 13-meter path,[1] at pressures of a few millimeters. An observation of the O_3 "atmospheric" bands (magnetic dipole, intercombination) showed that *allowed* transitions should be detected for a concentration of 10^{10} molecules/cm^3 in the initial vibrational level. Absence of the 0−0 band of N_2^+ indicates that the (unexcited) ion is not a primary carrier of the energy, as was proposed by Mitra.[2] Failure to observe first positive bands (N_2, $B^3\Pi\leftarrow A^3\Sigma$)—either from $v''=0$ or from v'' levels favored by the afterglow—is evidently due in part to the small fraction of molecules that reach $A^3\Sigma$ via the afterglow.[3] In addition, traces of mercury vapor probably reduced the life of this metastable state. Results obtained by Rayleigh[3] suggest that certain states of the neutral molecule, lying above the first ionization limit and apparently 'metastable,'[4] may play a role in activation. A test of this possibility is planned.

* Now at the University of Southern California.
[1] H. D. Smith and J. K. Marshall, J. Opt. Soc. Am. 30, 338 (1940).
[2] S. K. Mitra, "Active Nitrogen—A New Theory," Indian Press Ltd., Calcutta (1945).
[3] Lord Rayleigh, Proc. Roy. Soc. 151, 567 (1935); 176, 1, 16 (1940); 180, 123, 140 (1942).
[4] R. E. Worley, Phys. Rev. 64, p. 215 (1943).

A8. Parallel-Plate Counters and the Measurement of Very Small Time Intervals. J. W. KEUFFEL, *California Institute of Technology.*—The counter characteristics of a discharge tube using plane parallel electrodes are being investigated, especially with regard to the short time-lags ($\sim10^{-9}$ sec.) which have been reported in the breakdown of overvolted spark gaps.[1] A parallel-plate counter using copper plates 35 cm^2 in area and spaced 2.4 mm was found to have the following characteristics, when filled with $\frac{1}{2}$-atmos. of argon and 6-mm xylene: threshhold 1500 volts; plateau 1500 volts, with a slope of 4 percent/100 volts; pulse rise time, $\sim5\times10^{-9}$ sec. A multivibrator quenching circuit, with a quench time of .05 sec., was employed. The rise-time was measured by means of a timing circuit similar to that described by Neddermeyer *et al.*[2] Construction of a multi-detector model of the timing circuit, which should permit the measurement of very small time intervals between ionizing events, as well as an estimate of the uncertainty in reaction time of the counters, is now under way.

[1] L. B. Loeb, *Fundamental Processes of Electrical Discharge in Gases* (John Wiley and Sons, Inc., New York, 1939), p. 447ff.
[2] Neddermeyer, Althaus, Allison, and Schatz, Rev. Sci. Inst. 18, 488 (1947).

B2. The Gravitational, Electromagnetic, and Vector Meson Fields and the Similarity Geometry. BANESH HOFFMANN,* *Institute for Advanced Study, Princeton* (by title).—In the general conformal geometry of space-time, the null geodesics are invariant. There is a special case, which may be called the similarity geometry, in which all geodesics are invariant. Let $S_{\sigma\tau}$ be a symmetric tensor, of index $2N$, belonging to this similarity geometry, and let S and Z be respectively the determinant and the curvature scalar formed from it. Then,[1] since $Z(S)^{\frac{1}{2}}/(S_{00})^2$ is gauge invariant, consider the four-dimensional variational principle

$$\delta\int\{Z(S)^{\frac{1}{2}}/(S_{00})^2\}dx^1dx^2dx^3dx^4=0. \qquad (1)$$

If $S_{\sigma\tau}$ is subject to the invariant restrictions $S_{04}=0$, S_{44}/S_{00} independent of the coordinates, (1) yields the general relativity field equations for the gravitational, electromagnetic, and vector meson fields. Removing the restrictions on

S_{rr} introduces two additional scalar fields which are under investigation.

* On leave from Queens College.
[1] Compare Hoffmann, Phys. Rev. 72, 458 (1947).

B3. Dust Electrostatics. JAMES W. HANSEN, *University of California.* (Introduced by Leonard B. Loeb.)—The work reported on at the June 1947 Stanford meetings has been continued. Varying the length of the dusting tower has shown that the charge-size relationship and the particle-size distribution change markedly after the dust leaves the duster. Considerable evidence is available to show that this change is due primarily to aggregate formation. Details of such changes in distribution which it is impossible to summarize in this abstract will be presented.

B4. Water Drop Corona at Reduced Pressures. W. N. ENGLISH, *University of California.* (Introduced by Leonard B. Loeb.)—An extension of the experiments[1] with a water drop point, in a point to plane corona gap, to the pressure range 205- to 760-mm Hg has clarified the results obtained at atmospheric pressure, and furnished a striking proof of the dependence of negative point corona on secondary electron emission from the cathode. It appears that normal negative corona cannot occur on a water point, owing to the extremely low secondary electron emission coefficient. The luminosity observed with a negative drop point may then be attributed to streamer discharge from the positive end of the receding spray droplets in the high field region, as observed by Macky[2] with larger drops in a uniform field. The effect will also take place with a positive point, the streamers occurring from the lower positive ends of the droplets. The complex oscilloscope pulses obtained on positive and negative polarity, and the other features of the corona, can be convincingly explained with the aid of this mechanism.

[1] W. N. English, Phys. Rev. 72, 741(A) (1947).
[2] W. A. Macky, Proc. Roy. Soc. 133, 565 (1931).

B5. Positive and Negative Point to Plane Corona. L. B. LOEB AND W. N. ENGLISH, *University of California, Berkeley.*—A comparison of positive and negative metal point to plane corona in air has been made in the pressure range 205- to 760-mm Hg. Current-voltage characteristics reveal that the onsets, Vg, are almost identical and that the curve for negative point lies always above that for positive point, doubtless because of the more efficient generation of space charge in the latter. Reasonable negative point characteristics were most difficult to obtain, and the dependence of this corona on surface properties of the point is evident. A study of the intermittent regime onset, Vg, as a function of pressure shows very nearly the expected linear relationship for a positive point, but a decided curvature for the negative. This means a small difference in positive and negative onset near 500-mm Hg pressure, which can however be readily accounted for within the mechanism suggested by Loeb,[1] when the effect of absorbed gas films on the secondary electron emission of the point is considered. A preliminary experiment with non-metallic points of FeS and CuO has yielded an unexpected difference in the onsets Vg^+ and Vg^- at atmospheric pressure.

[1] L. B. Loeb, Phys. Rev. 71, 712 (1947).

B6. Low Energy Mesotrons at High Altitudes.* DONALD C. MOORE AND ROBERT B. BRODE, *University of California, Berkeley.*—A series of cloud-chamber photographs have been taken in the flights of a B-29 at 30,050 feet and at 18,300 feet. To observe the frequency of occurrence of the various components of the cosmic radiation the cloud chamber was operated at random. The presence of six horizontal metal plates in the cloud chamber enabled one to distinguish between slow mesotrons, slow protons, electrons, and fast penetrating particles. Both the diffuse tracks due to pre-expansion particles and the sharp tracks due to fast expansion particles have been analyzed. The necessary corrections for chamber sensitive time, gas pressure in the chamber, and solid data angle of observation have been applied to these data. These measurements give the number of mesotrons with a range between 0.7 cm and 3.3 cm of lead and those with ranges greater than 3.3 cm of lead per square cm, per minute, per unit solid angle at the zenith. Combining the data obtained in these flights with data of other observers for higher energy mesotrons, energy spectra are obtained from 28 Mev to 520 Mev. The 30,050 feet energy spectrum has a maximum of 32 mesotrons per square cm, per minute, per unit solid angle at the zenith per Bev energy interval at 0.2 Bev. At 0.4 Bev the intensity is about 3. For the 18,300 feet spectrum the maximum is also at 0.2 Bev and has a value of 14. At 0.4 Bev the intensity is about 1. The 18,300 feet spectrum cannot be accounted for by higher energy mesotrons coming from upper layers of the atmosphere, but rather, represents more nearly the creation spectrum of mesotrons. The absorption coefficient of a primary radiation that would produce the observed altitude variation of the slow mesotrons is calculated to be about 170 grams per square cm.

* The research described in this abstract was supported in part by the Office of Naval Research.

B7. The Mass of Cosmic-Ray Mesotrons.* J. G. RETALLACK AND R. B. BRODE, *University of California, Berkeley.*—Forty-one new measurements of the mass of individual cosmic ray mesotrons have been obtained with the equipment previously described. The cloud chamber in the magnetic field was filled with air at 1.13 atmosphere. A curvature correction of 0.03 ± 0.04 meter^{-1} has been derived from the measurement of 60 no-field tracks. The mesotrons whose masses were determined had energies from 50 to 600 Mev as measured in a field of 4750 gauss. The probable errors due to turbulence are 3 to 8.5 percent and are much larger than the scattering probable errors which are 1.5 to 2.5 percent for this energy range. 37 of the 41 measurements are consistent with the assumption of a unique mass of $192m_e$. The probable error based on external consistency is $\pm 5m_e$. The remaining four mass values (474, 538, 588, $717m_e$) do not seem to be consistent with the other observations. The 37 values from this experiment and the 26 measurements of

W. B. Fretter[1] are consistent with the assumption of a unique mass of $196 \pm 5 m_e$.

* The research described in this abstract was supported in part by the Office of Naval Research.

[1] W. B. Fretter, Phys. Rev. 70, 625 (1946).

B8. An Apparatus for Mesotron Mass Measurements at High Altitudes.* R. B. BRODE, *University of California, Berkeley.*—To measure the momentum of cosmic-ray particles, cloud chambers have been mounted above and below the gap in a permanent magnet. Thin beryllium foil windows separate the cloud chambers from a helium filled box in the gap of the permanent magnet. The change in direction of the particles above and below the magnet can be accurately measured. The induction in the magnet gap is about 5000 gauss. 20 cm of track are visible in each chamber, and about 20 cm are obscured by the magnet between the chambers. Below this set of chambers is placed a large cloud chamber containing 15¼-inch thick lead plates. The range of a particle that passes through the momentum analyzer is observed in the lower chamber. The entire apparatus with its controls occupies a space of about 75 cubic feet, and is mounted on a rigid framework for installation in a B-29. The weight of the apparatus is about 2000 pounds. Sea level operation of this unit furnishes about one measurable mass value per day out of 125 coincidence-tripped observations. The spectrum of low energy mesotrons now indicates that one should, at 30,000 feet, measure about 15 mass values per hour out of 30 counter-controlled expansions. The measurements of masses with this apparatus appears to be about as reliable as the data obtained in this laboratory with a large electromagnet and cloud chamber for range determination.

* The research described in this abstract was supported in part by the Office of Naval Research.

B9. Some Discharge Characteristics of Geiger-Müller Counters. H. V. NEHER, *California Institute of Technology.*—For the usual self-quenching or fast cylindrical Geiger counter for a given potential above threshold, there is a definite relationship between the duration, τ, of the pulse, the maximum change in potential of the wire, ΔV, and the resistance in the circuit. It is found that $\Delta V\tau/R$ is approximately a constant, independent of the capacitance in the circuit. This is to be expected if the quantity of charge that flows is independent of the circuit constants. For a counter 6" long, 1" in diameter and a wire 0.0015" in diameter working at 150 volts above threshold, $\Delta V\tau/R$ was found to have an average value of 2.6×10^{-9} coulombs.

B10. New Measurements on the Variation with Latitude of the Cosmic-Ray Intensity at the Vertical at High Altitudes. A. T. BIEHL, R. A. MONTGOMERY, H. V. NEHER, W. H. PICKERING, WM. C. ROESCH, *California Institute of Technology.*—To achieve a higher degree of accuracy combined with a better angular resolution than could be achieved with the equipment used by Millikan, Neher and Pickering[1] in 1939–42 in their balloon flights, apparatus of an entirely new design was constructed. Three trays of counters were used consisting of 8 counters in each. Each tray had a sensitive area of approximately 25×25 cm². The distance between the outside trays was 1 meter. This arrangement gave an angular resolution of approximately $\pm 15°$ from the vertical. To achieve constancy of counter voltage, light weight dry cells were used. The whole equipment including wrapping and lines ready for launching weighed about 8 kg. At least two flights, measuring the radiation coming in near the vertical, were made at San Antonio, Fort Worth, St. George (Utah), Omaha, Rapid City, Bismarck and Saskatoon. Preliminary results from these flights will be presented.

[1] H. V. Neher and W. H. Pickering, Rev. Sci. Inst. 13, 143 (1941). See also W. H. Pickering, Proc. I.R.E. 31, 479 (1943).

B11. Stars in Photographic Emulsions. Part I. Experimental. EUGENE GARDNER AND VINCENT PETERSON, *University of California, Berkeley.*—Photographic plates have been bombarded in the 184" Berkeley cyclotron for the purpose of studying stars initiated by deuterons and alpha particles. We have tabulated the number of prongs (i.e., the number of charged particle tracks making up the star) for 1200 stars initiated by deuterons and 200 stars initiated by alpha particles. Protons of energy more than about 10 Mev do not make recognizable tracks in the emulsions which we are using, so our results will not include prongs due to high energy protons. For stars initiated by deuterons the average number of prongs per star is 3.0. This is true for all incident deuteron energies from 35 Mev to 190 Mev. Preliminary results indicate that for stars initiated by alpha-particles the average number of prongs is slightly higher. For deuteron-initiated stars there are about three times as many prongs in the direction of the beam as in the backward direction. The cross section for formation of stars by alpha particles is being measured by counting sections of tracks made by alpha-particles and the stars originating on these tracks. This paper is based on work performed with the support of the Atomic Energy Commission under Contract W-7405-Eng-48 with the Radiation Laboratory, University of California, Berkeley, California.

B12. Stars in Photographic Emulsions. Part II. Theoretical. WENDELL HORNING, *University of California.*—The number of stars observed as a function of the number of prongs has been computed on the basis of a nuclear model described by R. Serber.[1] The method of the calculation is to compute first the distribution of excitation energies of a nucleus, for a given energy of the bombarding particle. The statistical model is then used to predict what particles will be evaporated from the nucleus at each excitation. The average number of prongs per star thus obtained varies somewhat with energy, from 3.0 for 35-Mev deuterons to 3.9 for 190-Mev deuterons. This agrees roughly with the observed average prong number of 3.0 for all incident energies used. Since the ratio of neutron to charged particle evaporation is greater for heavier elements, the lighter elements in the photographic emulsion contribute strongly to the visible stars. The recoil of these lighter nuclei accounts roughly for the observed angular distribution of star prongs, if we assume that evaporation is spherically

symmetric with respect to the parent nucleus. This paper is based on work performed with the support of the Atomic Energy Commission, under Contract W-7405-Eng-48 with the Radiation Laboratory, University of California, Berkeley, California.

[1] R. Serber, Phys. Rev. 72, 1114 (1947).

C3. Heavily-Ionizing Cosmic-Ray Particles at 30,000 Ft. Altitude.* R. RONALD RAU,** CARL D. ANDERSON, RAYMOND V. ADAMS, AND PAUL E. LLOYD, *California Institute of Technology.* Out of 3914 cloud-chamber photographs obtained in a B-29 aircraft at 30,000 ft. altitude, 378 photographs show the occurrence of single heavily-ionizing particles which cannot arise from radioactive contamination, and 72 photographs each show from 2 to 17 particles which arise from nuclear disintegrations in the walls or the gas of the cloud chamber. Of the singly occurring particles 79 are identified as protons and 9 as mesotrons. The particles which are observed to arise from disintegrations are protons in all cases where identification is possible. The heavily-ionizing particles of low energy (of energy up to 20 Mev) occur isotropically; those of higher energy favor the vertical direction, and in only 3 percent of the cases are they time-coincident with electron showers. Heavily-ionizing particles are observed 7.2 times as frequently per exposure at 30,000 ft. as at 14,000 ft.

* This work was carried out under contract with the Office of Naval Research.
** Now at the Princeton University.

C4. Photo-Effects in Middle-Weight Nuclei. L. I. SCHIFF, *Stanford University.*—Recent data[1] on photo-effects in light and middle-weight nuclei obtained with Li γ-rays give considerably larger values for the ratio $\sigma(\gamma, p)/\sigma(\gamma, n)$ than predicted by the usual statistical theory.[2] This theory assumes that all states of the two residual nuclei can arise from the states of the compound nucleus initially excited. Excitation by a γ-ray whose wave-length is greater than the nuclear radius is expected to yield compound states that correspond to a more regular kind of oscillation than those excited by nucleon bombardment. We suppose that most of the states of the residual nuclei from the photo-effects have similar regularities. The effective level densities then increase only as a small power of the excitation energy, rather than exponentially as in the case of nucleon bombardment. This shifts the spectrum of emitted protons and neutrons towards higher energies, and increases the cross section ratio since the protons can penetrate the Coulomb barrier more easily. Numerical estimates agree in order of magnitude with the experiments, and are insensitive to the power of the energy in the level density.

[1] O. Hirzel and H. Wäffler, Helv. Phys. Acta (to be published).
[2] V. F. Weisskopf and D. H. Ewing, Phys. Rev. 57, 472 (1940).

C5. The Berkeley Four Million Volt Electrostatic Generator. CLARENCE TURNER, BRUCE CORK, JOSEPH BALLAM, AND HAYDEN GORDON, *University of California.*—The Berkeley pressure Van de Graaff machine was designed to inject 4-Mev protons into the linear accelerator. The Wisconsin horizontal design was extrapolated to insure dependable operation at 4 million volts. The pressure tank is 8 feet inside diameter, with a maximum operating pressure of 200 p.s.i.g. The 20″ air gap between high potential electrode and tank is divided into two 10″ gaps by a second shell operating at half the total voltage. The length of insulating column is 15 feet. The high potential electrode is 54″ o.d. and 6 feet long to provide space for extensive equipment for operation of a high current pulsed ion source. Provision was made for two accelerating tubes—one for the proton beam and one for an electron beam to be used for voltage control. Reasonably dependable operation at 4 million volts has been attained with 100 p.s.i.g. nitrogen pressure and about 40 pounds of Freon. Proton beams of several microamperes have been obtained, but results are very preliminary. This work was sponsored by the Atomic Energy Commission.

C6. Ion Source Equipment for Berkeley Electrostatic Generator. FRANKLIN FILLMORE, ARTHUR HUDGINS, AND MORRIS JEPPSON, *University of California.*—The ion source in this generator was designed to produce high current proton pulses 15 times per second and of 300 microseconds duration. This permits a high injection current during the on time of the linear accelerator without overloading the electrostatic generator. The protons are generated in a Zinn-type arc equipped with a differential pumping system which removes 95 percent of the H_2 gas escaping from the arc chamber. The protons are accelerated to 50 kv and focused into the accelerating tube through a small aperture. The differential pumping system consists of an air-cooled diffusion pump backed by a mechanical pump operating inside a small steel tank. Hydrogen pumped from the ion source discharges into this tank and is recirculated to the ion source through an oil filter and palladium leak. Power to operate the equipment is provided by two 400-cycle generators driven by the charging belt. Cold air from a heat exchanger is blown through the Textolite support tubes to cool the diffusion pump and other shell equipment. Control is accomplished by small d.c. motors which are switched on and off by a selector switch system which in turn is operated by a nylon fishline. This work was sponsored by the Atomic Energy Commission.

C7. Physical Design of the Berkeley Linear Accelerator. HUGH BRADNER, RICHARD CRAWFORD, HAYDEN GORDON, AND JOHN R. WOODYARD, *University of California, Berkeley.*—Thirty-two megavolt protons have been obtained from a resonant cavity linear accelerator. The cavity is a 12-sided copper cylinder approximately 40 feet long and 38 inches in diameter, operating at 202.5 mc in the TM_{010} mode which has a Q of about 70,000 and shunt impedance of 330 megohms. Protons are injected on the axis and accelerated in the gaps between 46 "drift tubes." These tubes range in diameter from 4.75″ to 2.75″ and in length from 4.4″ to 10.9″, and in center-to-center distance from 5.43″ to 14.5″. Tube dimensions were chosen to maintain the resonant frequency of the cavity constant throughout its length. Tungsten wire grids are used for focusing. Drift tubes are supported by conducting stems which permit accurate

adjustment of drift tube position. Peak power of 2.15 megawatts is supplied by 26 triode oscillators through 24 transmission lines terminating in low inductance loops inside the cavity. The cavity is supported in a steel tank which is evacuated to a working pressure of 4×10^{-6} mm mercury. Both the vacuum tank and the resonant cavity split longitudinally for access. This work was sponsored by the Atomic Energy Commission.

C8. Control of the Field Distribution in the Linear Accelerator Cavity. WOLFGANG K. H. PANOFSKY, CHAIM RICHMAN, AND FRANK OPPENHEIMER,* *University of California.*—The cavity of the 40-foot linear accelerator consists of a long cylindrical pipe loaded with "drift tubes" of graduated lengths.** Such a system has a spectrum of resonant modes near the desired operating mode, which is the mode giving uniform peripheral magnetic flux density as a function of the axial coordinate. The spectrum becomes more closely spaced as the length increases. Analysis of the field equations in the cavity has shown that the critical problem is not the problem of preventing jumping of the frequency from the proper mode to the next mode, but is the problem of controlling the uniformity of field distribution in the proper mode. This problem has been analyzed by means of simple perturbation theory. This method results in a simple procedure of adjusting the distribution using a Fourier analysis of the magnetic field distribution at the edge of the cavity. The procedure has been used experimentally with satisfactory results. The mechanical tolerances of the accelerator cavity and the problems associated with multiple cavity coupling can be studied by this method. This work was sponsored by the Atomic Energy Commission.

* Now at the University of Minnesota, Minneapolis, Minnesota.
** Phys. Rev. 70, 447(A) (1946).

C9. Linear Accelerator Oscillator and Coupling System. W. R. BAKER, J. V. FRANCK, AND J. D. GOW, *University of California.* (Introduced by Dr. L. W. Alvarez.)—An oscillator capable of delivering 150 kw of 200-mc radio frequency power into the high "Q" resonant load of the linear accelerator has been developed. This oscillator, using four GL-434A triodes in parallel, is operated with a pulse length of 300 microseconds and a pulse repetition rate of 15 c.p.s. The operating frequency is controlled primarily by the linear accelerator cavity. A 50-ohm coaxial transmission line approximately one wave-length long and essentially unity coupled to the oscillator, operates with a voltage standing wave ratio of about 7 to supply power to the coupling loop in the linear accelerator. A resistor is placed across the transmission line at a voltage minimum for the fundamental frequency to suppress the unwanted 170-mc and 260-mc modes of the oscillator. This resistor absorbs less than three percent of the power in the fundamental frequency. The oscillator has been designed to have optimum grid drive at high power level and so requires preexcitation to obtain short build-up time. No problem is encountered in phasing 24 oscillators which automatically lock into the resonant frequency of the cavity. This work was sponsored by the Atomic Energy Commission.

C10. Beam Dynamics in the Linear Accelerator. ROBERT SERBER, *University of California.*—The orbits of particles in the linear accelerator are stable, both for displacements in phase and for radial displacements from the axis of the machine. Stability in the latter case is achieved by the use of grids or foils in the drift tubes. The lengths, L, of the drift tubes form a linear progression, $L=l_1n$. For small displacements, the frequency of phase oscillation is $\nu=(\cot\phi_s/2\pi n)^{\frac{1}{2}}$, where ϕ_s is the synchronous phase, and the amplitude of oscillation is $A\sim(n^{3-2\zeta}\cot\phi_s)^{-\frac{1}{4}}$. Here ζ is a number which depends on the shape of the field in the accelerating gaps ($\zeta<0.2$ in the present machine). For the radial oscillations, $\nu=(1/2\pi)(K/n)^{\frac{1}{2}}$ and $A\sim(n/K)^{\frac{1}{4}}$ where K is a number of order one which depends on field shape. Multiple scattering in the foils would cause the beam to spread to a diameter d; $d^2=[(32\pi NtZ^2e^4/KE^2)\times\ln(4\pi NtZ^{4/3}\hbar^2/m^2v^2)][(n/n_1)^{\frac{1}{2}}-1]$. Here t is the thickness of a foil, E is the mean accelerating electric field, and n_1 is the number of the first drift tube. If a is the internal diameter of a drift tube, the fraction of the beam transmitted is $I/I_0=1.6\exp\{-1.45d^2/a^2\}$. This work was sponsored by the Atomic Energy Commission.

D1. Near Infra-Red Dichroism Involving Aligned CH_2 Groups. LEONARD GLATT, *University of California.* (Introduced by Joseph W. Ellis.)—An investigation of dichroism in substances containing aligned single bond CH_2 groups is being conducted. Marked dichroism has been found in stretched polyethylene films, the E-vector being oriented respectively parallel and perpendicular to the molecular chain axes (stretch direction). Some assignments of observed bands to combination and overtone modes of CH_2 oscillators were attempted. Polarization evidence of coupling between CH_2 groups is presented. An interesting band, present only when there is an E-vector component parallel to the molecular chain axis was found at 4216 cm^{-1}. Semi-crystalline "Parowax" films from 40 to 500μ thick have been prepared by slowly cooling a melt on a hot water surface. Spectrograms of these films with unpolarized light, in conjunction with spectrograms of polyethylene with polarized light, gave convincing proof of an excellent alignment of the molecular chain axes normal to the surface.

D2. Geometrical Optics of Grazing Incidence Reflectors. PAUL KIRKPATRICK, A. V. BAEZ, AND ALLEN NEWELL, *Stanford University.*—Production of mirror images with x-rays is subject to the restriction that grazing angles of incidence must not exceed the small critical angle of total reflection. Such cases seem to have been neglected by optical theorists. A spherical mirror possesses the two focal lengths $Ri/2$ and $R/2i$, where R is the radius of curvature and i the grazing angle. Convergence of the former type readily produces a real line image of a point source. Two crossed mirrors yield a point image. Focal length, being dependent upon i, is conveniently variable. Two crossed mirrors produce anamorphotic images of extended objects, but this defect may be corrected by use of a third mirror. As with the concave grating, the focal surface is steeply inclined to the principal ray, but this may be reduced by

successive reflections from two mirrors in the parallel position, an arrangement which also reduces spherical aberration. This aberration causes pronounced doubling of images beyond the point of best focus. Presently recognized limitations would hold speeds to the order of f:100.

D3. Effect of Water of Crystallization on Absorption Bands of Neodymium Bromate Crystals. ARNOLD BENTON AND E. L. KINSEY, *University of California.*—Experimental evidence of the coupling of the 3μ vibrations of the water molecule with electronic transitions of the Nd^{+++} ion in $Nd(BrO_3)_3 \cdot 9H_2O$ crystals was obtained. The evidence is provided by the shifting of certain lines when H_2O is replaced by D_2O in the crystals, by the fact that the spacings of these lines agree with those known to be caused by pure electronic transitions, and by the fact that the displacements of these lines from the electronic lines are in good agreement with the known values of the vibration frequencies of water. The lines have been observed in the visible region of the spectrum at liquid nitrogen temperature using polarized light. As in the case of the pure electronic lines, the intensities are functions of the direction of the polarization of the light relative to the hexagonal axis of the crystal.

D4. Stellar Electromagnetic Fields. LEVERETT DAVIS, JR., *California Institute of Technology.*—The electromagnetic field in the neighborhood of a rotating magnetized body such as the earth or sun is best treated in an inertial system, one that does not rotate with the body. The stellar model considered is one in which the magnetic field is that of a dipole parallel to the axis of rotation, the field strength at the surface of the star at the pole being B_p. Rationalized m.k.s. units will be used. If the field due to the ions in the neighborhood of the star is negligible, the electrostatic potential outside the star is $V = V_p(a/r)^3 P_2(\cos\theta)$ where $V_p = B_p \omega a^2/3$, a is the radius of the star, ω its angular velocity, and (r, θ, ϕ) are spherical polar coordinates. Consideration of the motion of the ions in such a field shows that a space charge will accumulate that cannot be neglected. When a steady state has been attained, if one neglects the effect of unionized interstellar material, it appears that the external space charge rotates with the same angular velocity as does the star, that the change in the magnetic field is very small, but that the electrostatic potential is now, to a first approximation, $V = -\frac{3}{5} V_p(a/r) \sin^2\theta$.

D5. Rates of the Carbon Reactions in the Sun. REVEREND J. O'REILLY AND R. F. CHRISTY, *California Institute of Technology.*—Recent measurements in this laboratory (to be published soon) on the reactions C^{12} plus protons and C^{13} plus protons in the region of .4 to 1.3 Mev have led to values for the proton width Γ_p of 35 and 40 kev at their respective resonances at .45 and .55 Mev. The use of these values, together with the γ-ray widths which were confirmed to be .63 and 15 ev, respectively, permits an estimate of the rates of these reactions in the sun. The cross sections were extrapolated to the very low energies associated with stellar reactions by means of the one level dispersion formula. This procedure is admittedly crude but is perhaps the best that can be done in the absence of actual measurements at lower energies. The new value for the rate of the C^{12} reaction is 40 times that obtained by Bethe, by using a rough general estimate of Γ_p. The ratio of the rates of the C^{13} and C^{12} reactions is 9 whereas the inverse abundance ratio on the earth is 90. The rate of the C^{13} reaction compared to the $N^{15}(p\alpha)$ reaction is now however 3×10^{-4} which corresponds more nearly to their abundance ratio. This work was carried out under contract with the Office of Naval Research.

D6. Investigation of a Lens Type β-Ray Spectrograph. T. LAURITSEN AND R. F. CHRISTY, *California Institute of Technology.*—A lens type β-ray spectrograph able to focus electrons of energy up to ~3 Mev has been constructed to investigate low energy γ-radiation and to study various design parameters such as spherical aberration, background, etc. Calculations of the spherical aberration of a magnetic field with a minimum at the center of the spectrograph have been made.[1] Variation of the shape of the magnetic field has been accomplished by axial separation of the two coils which constitute the magnetic lens resulting in a considerable increase in the ratio of intensity to aberration over that obtained with a single thin lens. These considerations are being applied to the design of a high energy spectrograph intended to focus electrons up to 17.5 Mev. This work was carried out under contract with the Office of Naval Research.

[1] Kai Siegbahn, Phil. Mag. 37, 162 (1946).

D7. Proton Scattering by Beryllium. GEORGE S. KENNY AND SYLVAN RUBIN, *California Institute of Technology.*—The angular distribution of protons scattered from thin beryllium foils has been measured in the range 720 to 1310 kev, at angles of 25° to 155°, using a photographic type scattering camera. The camera used for previous work on Be^9 scattering has been modified by the addition of a drum shaped plate holder which permits 5 exposures before reloading. Observations have been made at significant points of the proton excitation curve, discussed in an accompanying abstract by R. G. Thomas, W. A. Fowler, and C. C. Lauritsen. The effect of the narrow γ-ray resonances at 988 and 1077 kev has been investigated in detail. Bombarding energies were accurately determined by measurement of the γ-ray excitation curve just prior to exposure of the plates. This work was carried out under contract with the Office of Naval Research.

D8. Beryllium-Proton Reactions and Scattering. R. G. THOMAS, W. A. FOWLER, AND C. C. LAURITSEN, *California Institute of Technology.*—The cross sections of the reactions $Be^9(p, d)Be^8$ and $Be^9(p, \alpha)Li^6$ and of the scattering $Be^9(p, p)Be^9$ have been measured for bombarding proton energies from 500 to 1200 kev at 90° and 135° to the incident beam. The protons, deuterons, and alpha-particles were separated by magnetic analysis. In this region the $Be^9(p, \gamma)B^{10}$ reaction shows marked resonances at 988 and 1077 kev.[1] The scattering cross section shows anomalies corresponding to these resonances. The anomaly corre-

sponding to the wide resonance at 988 kev is very large, the ratio to Rutherford scattering at 135° varying from a minimum of 2 at 910 kev to 6 at 1020 kev. The corresponding scattering cross sections are 1 and 3 barns. The deuteron and alpha-particle cross sections are of the order of 0.1 barn with the deuteron yield curve showing marked variations while the alpha-particle curve does not. This work was carried out under contract with the Office of Naval Research.

[1] C. C. Lauritsen, T. Lauritsen, W. A. Fowler, Phys. Rev. 72, 739 (1947).

D9. Catalytic Isomerization of Propane Containing C^{13}. O. Beeck, J. W. Otvos, D. P. Stevenson, and C. D. Wagner, *Shell Development Company.*—Using propane containing 17 percent C^{13} in the end position, the moist aluminum bromide catalyzed isomerization to propane containing C^{13} in the middle position has been shown to occur in this three-carbon molecule at a rate comparable to ordinary normal-isobutane isomerization under the same conditions. Tracing the carbon atom shift was accomplished in a single step by the mass spectrometer (see following abstract), the change in the ratio of the intensities of the ionic fragments of mass 30 and 29 being a measure of progress toward equilibrium. Direct proof has been obtained that the isomerization reaction is intramolecular in character; no detectable increase in the number of propane molecules containing two C^{13} atoms (ion weight 46) was obtained after 600 hours at room temperature, although after only 65 hours the isomerization reaction had proceeded half way to equilibrium. No side reactions were observed. This technique is now being applied to the butane isomerization reaction.

D10. Analyses of Isotopic Propanes. D. P. Stevenson, *Shell Development Company.* (Introduced by O. Beeck.)—In order to determine mass spectrometrically the isotopic species of a substance, one of the following two conditions must obtain: (a) Isotopic substitution must leave unchanged the dissociation probabilities of the various bonds of the molecular ion produced by low energy (50–100 volts) electron impact, or (b) samples of all isotopic species of interest must be available for calibration purposes. It has long been known that condition (a) does not hold for deuterium substituted compounds and thus that (b) must be satisfied for such compounds. Heretofore it has been necessary to assume that condition (a) holds for substances in which C^{12} has been replaced by C^{13}, although small deviations would be expected on theoretical grounds. Comparison of the mass spectrum of a propane with an abnormal terminal C^{13} content (see preceding abstract) with the mass spectrum of ordinary propane indicates that the dissociation probabilities of C–H bonds are unchanged within the experimental error. However, it is found that the dissociation probability of the C^{12}–C^{13} bond in the isotopic propane is slightly greater, 4–5 percent, than that of a C^{12}–C^{13} bond in ordinary propane. Although the complementary decrease of the dissociation probability of the C^{12}–C^{13} bond is indicated, the concentration of C^{13} available for this investigation is too low to permit quantitative evaluation. The analytical implications of these observations will be discussed.

D11. Ionization by C^{14} Radiation in the Ionization Chamber. John W. Otvos, *Shell Development Company.* (Introduced by O. Beeck.)—In order to measure C^{14} concentrations in gases by the ionization chamber technique, the relative ionization probabilities of ten hydrocarbons and of CO_2, CO, N_2, O_2, N_2O, He, Ne, and A have been determined for the beta particles emitted by C^{14}. $C^{14}O$ and $C^{14}O_2$ were used as the source for beta particles. The results show several expected regularities: (1) For the series of hydrocarbons the ionization probabilities increase linearly with the number of valence electrons. (2) For gases composed of the neighboring elements carbon, nitrogen, and oxygen the ionization probabilities obey simple additivity relationships based again on valence electrons. (3) Although methane and neon are isoelectronic the value for methane is considerably higher due to the lack of centralization of nuclear charge. Ionization probabilities measured at the relatively high energies of C^{14} beta particles bear no relation to ionization potentials or chemical properties but seem rather to be governed by quasi-geometrical factors, such as molecular volume. Interpolation of ionization probabilities for high electron energies should be possible on the basis of valence electrons, distribution of nuclear charge, and position in the Periodic Table, with values for helium, neon, and argon serving to relate the first, second, and third rows.

D12. The Bulk Viscosity of Liquids.* L. N. Liebermann, *University of California.*—The existence of bulk viscosity in liquids has been suggested as a possible explanation for the disagreement between the absorption of sound calculated from shear viscosity and the observed absorption. Eckart[1] recently has shown that forces responsible for streaming of fluids caused by sound waves are viscous forces of the bulk as well as the shear type and suggested that streaming might be used for their measurement. The velocity of streaming in a fluid is proportional to the power in the sound beam and to b where $b=(\frac{4}{3}\nu+\nu')/\nu$ and ν and ν' are the coefficients of shear and bulk viscosity. Whenever viscosity alone is responsible for sound absorption b is also the ratio of the observed absorption to that calculated using shear viscosity. The quantity b may be obtained from the ratio of the streaming pressure to the radiation pressure, together with an observation of the streaming velocity. The latter is obtained by suspending finely divided particles in the liquid and photographing their motion. The ratio of the pressures is obtained by suspending a disk in the axis of the sound beam. The disk is supported by strain gauge wire so that forces on the disk result in changes in resistance of the wire. In order that the relatively large radiation pressure effect produce a force on the disk of the same order as the streaming pressure, the reflectivity of the disk was made small by using aluminum foil of known thickness. Preliminary results show that b for CCl_4 is of the order of 13; this is in agree-

ment with b calculated from sound absorption data. Values for other liquids are being determined.

* This work represents one of the results of research carried out under contract with the Bureau of Ships, Navy Department.

D13. The Stability of Gas Bubbles in Water.* E. GERJUOY, *University of Southern California.*—Values of the tensile strength of water range from 0 to 200 atmospheres, depending on the observer and the method of measurement.[1] To account for these discrepancies, the presence of minute bubbles in the water, which expand rapidly at some critical negative pressure, has been hypothesized. To investigate this question, calculations have been made on the following idealized problem. A bubble of an ideal insoluble gas is in equilibrium under an external pressure of one atmosphere, the surface tension T being 75 dynes/cm. The external pressure is then slowly decreased, the bubble expanding isothermally in accordance with the ideal gas law. For positive external pressures the bubble always has an equilibrium radius, but for sufficiently large negative pressure there is no equilibrium radius, and in fact the bubble becomes unstable and grows rapidly when $pr+4T/3\sim 0$. The smaller the bubble at atmospheric pressure, the greater the negative pressure required to produce instability. However an initial bubble radius of 5×10^{-5} cm produces breakdown at a negative pressure of one atmosphere, while to postpone breakdown to negative pressures greater than 100 atmospheres, the initial "bubble" radii must be less than 5×10^{-7} cm. Although the model is crude, these results support the view that rupture will be observed at relatively small negative pressures unless the liquid is thoroughly degassed.

* This work supported by the Office of Naval Research.

[1] H. N. V. Temperley and Ll. G. Chambers, Proc. Phys. Soc., London **58**, 420 (1946).

D14. Measurement of Tensile Strengths of Liquids by Centrifuge Method.* J. J. DONOGHUE, E. GERJUOY, AND R. E. VOLLRATH, *University of Southern California.*—Measurements of the tensile or rupture strength of water and benzene have been made, using a centrifuge. A tube of liquid is rotated about a vertical axis, the speed of rotation being slowly increased until rupture is observed. The rupture manifests itself by the appearance of a bubble at the center of rotation, easily visible with the naked eye. The centrifuge speed is measured with a stroboscope, and the tensile strength at rupture is then readily calculable from the known length of the liquid column and the r.p.m. at rupture. Test specimens are prepared in a closed outgassed system. The liquids are distilled in a fractionating column to remove gases and other impurities. A tube of liquid is then sealed off while in equilibrium with a known small air pressure. Initial results with partially degassed water confirm predictions that the observed rupture strength is greatly lowered by the presence of dissolved gases and/or gas nuclei.

* Work supported by the Office of Naval Research.

E1. The Dynamics of Large Horizontal Eddies (Axis Vertical) in the Ocean off Southern California. GEORGE F. MCEWEN, *University of California.*—The circulation at depths zero and fifty meters is characterized by large horizontal counter-clockwise eddies between a northward inshore current and a southward offshore current. The eddy velocity decreases and the eddy size increases over a period of several months. Equivalent circular eddies computed from the usually oval shaped ones serve as convenient models for mathematical investigation. Each series of eddies conformed to the principle of the conservation of the moment of momentum, and their kinetic energy decreased progressively in accordance with a law of energy dissipation expected from a coefficient of lateral turbulence, 10^8 c.g.s. Next, a transformation of the two hydrodynamical equations of horizontal motion in the sea, involving both the deflecting force due to the earth's rotation, and lateral turbulence, resulted in the following single differential equation of vorticity diffusion:

$$\frac{\partial \zeta}{\partial t}=\mu\left(\frac{\partial^2\zeta}{\partial r^2}+\frac{1}{r}\frac{\partial \zeta}{\partial r}\right)+2\frac{\partial \mu}{\partial r}\frac{\partial \zeta}{\partial r}+\zeta\left(\frac{\partial^2\mu}{\partial r^2}+\frac{1}{r}\frac{\partial \mu}{\partial r}\right).$$

The theoretical relation of velocity to distance from the center corresponding to a solution assuming $\mu=10^8$ c.g.s. with boundary conditions, $t=0$, $\zeta=\zeta_1$, $r=r_1$, $\zeta=0$, $r>r_1$, agreed well with observations.

E2. Use of Plasma Sheaths as Variable Capacitances. W. E. PARKINS AND J. M. LEFFLER, *University of Southern California.*—The problem of cyclotron frequency modulation brought forth an unpublished suggestion by R. L. Thornton and B. Peters that the speed and magnitude of the frequency variation required might be achieved using controlled changes in the thickness of a plasma sheath serving as a capacitance. Some study of the feasibility of capacitance variation by such an approach has been made. Any current receiving electrode placed in a gas discharge will have a capacitance which depends on the discharge operating conditions. This capacitance also depends on the applied frequency as can be illustrated in the case of a flat probe maintained negative with respect to the plasma. At very high frequencies the capacitance will be determined by the space charge oscillations of the electrons.[1] At somewhat lower frequencies the electrons will continuously assume new equilibrium positions, but the ion current to the probe will be nearly steady. In this range the capacitance may be estimated by treating the sheath as the gap of a vacuum condenser. This has been verified in frequency modulation experiments. At still lower frequencies the sheath boundary will be able to adjust continuously. Here variations in ion current to the probe during the adjustment become important and calculations show the capacitance can be large compared to that indicated by the sheath dimensions. Circuits and operating data will be given.

[1] Tonks, Phys. Rev. **37**, 1458 (1931).

E3. Workfunctions of a Gas-Coated Surface. G. L. WEISSLER AND R. W. KOTTER, *University of Southern California.*—By using C. W. Oatley's[1] method for measuring contact potentials between a surface and a hot W-filament ($\phi_W=4.67$ ev), we determined the average work-

functions, ϕ, of a Ta-surface (slightly contaminated with W) after the following treatments: (1) baked out at 400°C for 24 hrs., heated to 1100°C by electron bombardment for 40 min.: $\phi=4.77$ ev; (2) surface bombarded with N_2 glow discharge: $\phi=4.43$ ev; (3) surface heated by electron bombardment: $\phi=4.77$ ev; (4) surface bombarded with argon glow-discharge: $\phi=4.71$ ev; (5) surface heated by electron bombardment: $\phi=4.66$ ev; (6) surface bombarded with O_2 glow-discharge: $\phi=5.87$ ev; (7) surface bombarded with argon glow-discharge: $\phi=4.62$ ev; (8) surface heated by electron bombardment: $\phi=4.71$ ev, and later $\phi=5.03$ ev (this latter increase in ϕ is due to residual O_2 diffusing to the surface); (9) surface bombarded with H_2 glow-discharge: $\phi=4.20$ ev, and later $\phi=4.50$ ev; (10) surface heated by electron bombardment: $\phi=5.38$ ev, and later $\phi=5.29$ ev.—N_2 and H_2 lower ϕ significantly, O_2 raises it. The lowering due to H_2 would have been greater if it were not for the previous O_2 treatment. Further similar work on evaporated metal surface is in progress.

[1] C. W. Oatley, Proc. Phys. Soc., London **51**, 318 (1939).

E4. Isotope Shifts in Some Previously Unexplored Lines of Nitrogen.* JOHN R. HOLMES, *University of Southern California*.—By using the Hilger E478 spectrograph in series with a Fabry-Perot interferometer it has been found possible to measure the isotope shifts in lines of N I which were previously unmeasured because of their low intensity and also the large dispersion required.[1] The lines could be obtained with high intensity and very few background N_2 bands by exciting a mixture of 0.01 mm N_2 and 4–6 mm He with an electrodeless discharge of about 30 megacycles. In order to get lines sharp enough to resolve the isotope structure it is necessary to immerse the discharge in liquid nitrogen; furthermore a marked improvement in sharpness was found upon making the cross section of the tube a thin rectangle rather than a circle. Preliminary results are approximately:

Transition	Wave-length	Isotope shift	
$3p\ ^4D_{3/2}\rightarrow 3s\ ^4P_{3/2}$	8719*A*	-0.06 ± 0.01	(Shift toward longer wave-lengths from N^{14} to N^{15})
$3p\ ^4D_{3/2}\rightarrow 3s\ ^4P_{3/2}$	8711.9*A*	-0.06 ± 0.01	
$3p\ ^4D_{1/2}\rightarrow 3s\ ^4P_{1/2}$	8703.4	-0.06 ± 0.01	
$3p\ ^4P_{3/2}\rightarrow 3s\ ^4P_{3/2}$	8210.9	-0.05 ± 0.01	
$3p\ ^4P_{3/2}\rightarrow 3s\ ^4P_{1/2}$	8188.2	-0.05 ± 0.01	
$3p\ ^4P_{1/2}\rightarrow 3s\ ^4P_{3/2}$	8185.0	-0.05 ± 0.01	
$3p\ ^4S_{3/2}\rightarrow 3s\ ^4P_{1/2}$	7423.9	-0.04 ± 0.01	

It is intended to try the same method for a measurement of the isotope shift of $3s\ ^1P_1\rightarrow 2p\ ^1S_0$ line of C I ($C^{12}-C^{13}$).

* This work has been partly supported by Contract ONR 238 Task III.
[1] J. R. Holmes, Phys. Rev. **63**, 41 (1943).

E5. Graphical Evaluation of Jacobi Polynomials. S. LEROY BROWN AND MARY GOWEN FOULKS, *University of Texas*.*—The Jacobi polynomials can be expressed in terms of the hypergeometric series** as

$$P_n(x)^{(\alpha,\beta)}=\binom{n+\alpha}{n}F\left(-n,\ n+\alpha+\beta+1;\ \alpha+1;\ \frac{1-x}{2}\right) \quad (1)$$

and will form an orthogonal set in the interval $+1$ to -1 with respect to the weight function $(1-x)^\alpha(1+x)^\beta$. Evaluation of such a polynomial may be accomplished with a mechanical harmonic synthesizer by the substitution $x=\cos\theta$, where the powers of $\cos\theta$ are expressed in terms of cosines of multiple angles. The ordinates of the continuous curve traced by the mechanical synthesizer give the values of the polynomial with respect to θ as the angle varies from 0 to π.

* Assisted by Office of Naval Research.
** Whittaker and Watson, *Modern Analysis*, Chap. XIV.

E6. A New Type of Dive Angle Indicator and Servo Accelerometer. DONALD H. JACOBS.* (Introduced by W. E. Frye.)—Work on a war time military research project revealed a need for a non-gyroscopic device for measuring the dive angle of aircraft and servoing this information at a high power level to other mechanisms. The device was required to remain unaffected by the forward acceleration of the aircraft in a dive. A need for a servo accelerometer also arose. Compactness and light weight were mandatory for both these devices. An instrument to meet these requirements was developed. The complete device, including a small servo motor with gear reduction, may be fitted into a standard aircraft instrument case. Several experimental models were built and were tested extensively in the laboratory and in aircraft. The theory of the instrument, data on sensitivity, design details, and the results of laboratory and field tests will be presented, together with some suggestions as to applications.

* Now at Aerophysics Laboratory, North American Aviation, Inc., Los Angeles, California.

E7. Metallic Carbide Lattice Energies and the Electron Affinity of C_2^{--}. I. HODES, *University of Southern California*. (Introduced by E. Gerjuoy.)—The fact that CaC_2 and other carbides form ionic crystals suggests that the structure C_2^{--} may be stable. The electrostatic energies of a number of carbides, specifically the crystals CaC_2, SrC_2, and BaC_2, have recently been calculated.[1] These calculations have been repeated by us, and the resultant values used to calculate the electron affinity E of C_2^{--}, defined by the equation $C_2^{--}+E=C_2+2e^-$. By analyzing a Born-Haber cycle for a metallic carbide, the expression $E+Q$, where Q is the heat of formation of molecular C_2 vapor from diamond, can be evaluated in terms of the crystal lattice energy U and known heats of formation. U equals the computed electrostatic energy plus corrections, the most important of which arises from the repulsive interaction. If the repulsive potential varies as $1/r^n$, a simple argument shows the correction should be $-1/n$ of the electrostatic energy. A value of $n=10$, indicated from other considerations, gives a result for $E+Q$ which for all three crystals is close to -245 kcal. mole. Q is not accurately known; the best available value yields $E=-2.9$ electron volts.

[1] L. I. Kazarnovskaya, J. Phys. Chem. U.S.S.R. **XX**, 1403 (1946).

E8. A Method for Incorporating into the Fourier Equations for X-Ray Studies Previously Established Structural Information. DAN MCLACHLAN, JR., *University of Utah*—When the structure of a compound is to be determined from

x-ray data by use of the Fourier equations a great deal of computation is necessary in order to establish the $3-n$ parameters indicative of the coordinates of the atoms in the unit cell. When n is large the Patterson projections are often too complicated for interpretation. Although previously established structural knowledge (either from the organic chemist, electron diffraction, or x-ray diffraction) is commonly used qualitatively to assist in the trials or to recognize similarities in the projection, there have not to date been any procedures developed by which the known structural facts may be incorporated into the initial Fourier equations so that the number of parameters are reduced or the computations simplified. In this paper a procedure is described by which the known interatomic distances and angles are introduced at the start and only the unknown distances are involved in the computation. A many-atom problem of a large organic compound may be so reduced in unknown parameters by virtue of previously established knowledge that the Patterson synthesis is easily interpreted. The method is based on the postulate that if

$$\rho(u) = \Sigma_h F^2(h_{\sigma\sigma}) \cos 2\pi hu,$$

then

$$\rho(u/g) = \Sigma_h F^2(h_{\sigma\sigma}) \cos 2\pi h^* u,$$

where $h^* = gh$.

E9. Cyclotron Frequency Modulation. K. R. MACKENZIE, *University of California.*—A method of modulation with a frequency range of 2.4 to 1 has been developed in the Radiation Laboratory, making it possible for the 184-inch cyclotron to accelerate either protons or deuterons in the near future. The system utilizes a capacitor consisting of a rotor with 6 rows of blades, 50 blades to a row, which mesh with two stator rows. One stator row is held at one end of a large rectangular cross-section transmission line, ¼ wave-length long, which is grounded at the other end. The other row is held at the end of a similar line which is connected to the dee. When fully meshed the whole system resembles a ¼-wave line. At the high frequency limit the system oscillates in approximately three ¼-wave sections with twice the dee voltage across the capacitor. Power is supplied by grounded grid tubes coupled to the resonant system by two lines whose lengths are adjusted to limit amplitude modulation to around 20 percent. This paper is based on work performed under Contract W-7405-eng-48B, with the Atomic Energy Commission.

E10. Scattering of High Energy Neutrons. A. BRATENAHL, R. H. HILDEBRAND, AND B. J. MOYER, *University of California.*—Measurements have been made of the angular distribution of high energy neutrons scattered into angles between 3° and 25° from spheres of Pb and Cu placed in the neutron beam of the 184-inch cyclotron. The scattered neutrons above 20 Mev were detected by pieces of carbon in which the n, $2n$ reaction produces C^{11} which has a 20-minute half life. The experimental curves relating intensity with angle show widths and central amplitudes characteristic of diffraction patterns for the nuclear sizes involved. Nuclear radii for calculating the diffraction were those corresponding to one-half the total cross sections measured for Pb and Cu in this neutron beam by the same detectors.* An average value of wave-length for the neutrons of the beam was employed in the calculations. Theoretical curves have been adjusted to the experimental data for Cu and Pb separately, plotted on the basis of intensity per scattering atom. The ratio of the peak intensities at 0° from these curves, after correction for attenuation in the scatterer, is 4.05 ± 0.4. The predicted value for this ratio on the basis of diffraction by the nuclei is 4.16. Experimental pattern half widths at one-fourth of peak height are 6.5° and 11° for Pb and Cu, respectively; whereas for the adjusted theoretical curves the corresponding values are 7° and 10°. This paper is based on work done at the Radiation Laboratory of the University of California under Contract W-7405-Eng-48 with the United States Atomic Energy Commission.

* E. M. McMillan, D. C. Sewell, J. M. Peterson, L. J. Cook, "Total cross sections for 90-Mev neutrons," Phys. Rev. (to be published).

E11. Positive Temperature Coefficient of the Soft Component of Cosmic Rays. L. E. SMITH, JR.,* *University of Washington.*—Studies of the data from a cosmic-ray telescope correlated with surface air temperatures yielded a temperature coefficient for the soft component (½- to 10½-cm lead) of $+.14 \pm .08$ percent/°C with an average correlation of $+.27 \pm .12$. Since the soft component is about 58 percent electrons from mesotron decay, 25 percent electrons produced by collision, and 17 percent slow mesotrons, there should be partial agreement of the coefficients of the soft component with the theory for coefficients of shower electrons produced by mesotron decay. This theory[1] predicts a difference between the electron and the mesotron component of -1.4 percent/cm Hg and $+.35$ percent/°C for the barometric and temperature coefficients. If for the mesotron coefficients we use the coefficients of the cosmic rays which penetrate 10½-cm lead and for the electron component the coefficients of the soft component, we get $(-3.5 \pm 0.4) - (-1.8 \pm 0.2) = -1.7 \pm 0.6$ percent/cm Hg and $(+.14 \pm .08) - (-.13 \pm .05) = +.27 \pm .13$ percent/°C. These are in agreement with the values predicted by the above theory.

* Now at San Diego State College.
[1] J. Barnothy and M. Forro, Phys. Rev. 55, 868 (1939).

E12. Recoil Protons in the Neutron Beam of the 184-Inch Cyclotron. WILSON M. POWELL, *University of California.*—A well collimated beam of neutrons from a half-inch beryllium target in the 195-Mev deuteron beam of the 184-inch cyclotron is allowed to pass through a Wilson cloud chamber. The beam enters the chamber through a 5-mil aluminum window. The chamber contains a half atmosphere of hydrogen as well as alcohol and water vapors and is in a magnetic field of 13,000 gauss. Measurements have been made of the angle and energy of recoil of the protons arising in the gas of the chamber. Curves will be given showing the distribution of the protons with angle and comparisons of these results with similar data obtained from carbon and paraffin with proportional counters will be made. This paper is based on work done at the Radiation Laboratory of the University of California under

Contract W-7405-Eng 48 with the United States Atomic Energy Commission.

E13. Excitation of Na^{24} and Na^{22} by Deuteron and Alpha Bombardment of Al. A. C. HELMHOLZ AND J. M. PETERSON, *University of California.*—Using essentially the technique of Thornton and Senseman,[1] the yield of Na^{24} and Na^{22} as a function of the bombarding energy of deuterons and alpha-particles has been studied. The bombarded element was Al. After the decay of periods of a few minutes, half-life measurements identified the 14.8 hr. period of Na^{24} and a long period which chemistry showed to be Na (almost certainly Na^{22}). The energy of the incident deuterons was 190 Mev with a spread of about ±5 Mev; of the alphas, 380 Mev with a spread of ±10 Mev. With deuterons, the Na^{24} activity as a function of distance from the end of the range rises rapidly to a maximum, falls to about half the maximum, and then remains essentially constant to the highest deuteron energy. The background effects of high energy neutrons are troublesome, and no accurate method of separating them out has been found. For deuteron induced Na^{22}, the activity rises to a maximum, then stays rather constant to highest energy. With alpha-particle excitation the Na^{24} activity shows a steady drop from the maximum, while the Na^{22} curve stays rather constant to highest energy as in the deuteron case. In the case of $Al(d, \alpha p)Na^{24}$ the values can be connected with those of Clark[2] at low energies, but the spread in deuteron energy in this case makes any conclusions questionable. This paper is based on work performed under the auspices of the Atomic Energy Commission in connection with Contract W-7405-Eng 48 with the Radiation Laboratory of the University of California, Berkeley, California.

[1] R. L. Thornton and R. W. Senseman, Phys. Rev. **72**, 872 (1947).
[2] E. T. Clark, Phys. Rev. **71**, 187 (1947).

E14. 90 Mev Neutron-Proton Scattering Angular Distribution. J. HADLEY, C. LEITH, H. YORK, E. KELLY, AND C. WIEGAND, *University of California.*—The angular distribution of protons in neutron-proton scattering has been measured for angles between 5° and 55° from the direction of the incident neutron beam. The average neutron energy for these measurements was 90 Mev produced by the stripping of 190-Mev deuterons in a ½-inch Be target in the 184-inch frequency modulated cyclotron. Thin paraffin scatterers of known carbon and hydrogen content were used; the number of protons originating in neutron-carbon reactions was determined by using pure carbon scatterers. The scattered protons were detected in a telescope of four proportional counters used in coincidence and set at a constant distance from the scatterer but at a variable angle with the neutron beam. Between the scatterers and counters were placed carbon absorbers whose thickness varied with the angle from the beam, so that only protons scattered by neutrons with energies greater than 66 Mev were counted. It was found that in the center of mass system the ratio of proton intensity per unit solid angle for perpendicular compared to forward scattering is 0.5. This forward proton peak is expected on the basis of exchange scattering. This paper is based on work done at the Radiation Laboratory of the University of California under Contract W-7405-Eng-48 with the United States Atomic Energy Commission.

SUPPLEMENTARY PROGRAMME

SP1. Near Infra-Red Dichroism Involving Hydrogen Bonds. LEONARD GLATT, *University of California.* (Introduced by Joseph W. Ellis.)—A striking example of dichroism has been found in (010) cleavage sections of β-succinic acid. Very intense absorption, appearing only in *E*-vector components parallel to the crystallographic *c* axis, caused complete opacity in the broad region from roughly 1.87μ to beyond 2.7μ, the limit of our spectrograph. This uni-directional absorption is ascribable to the intramolecular (O—H···O) hydrogen bonds which x-ray evidence has placed parallel to the *c* axis. The reasonable inference made by x-ray investigators that the H-atoms lie on the line connecting the O-atoms of neighboring molecules is thus confirmed. An anomalous ratio of overtone (and combination) to fundamental mode intensities for the hydrogen bond absorption is indicated by a contrast of our findings with those recently reported for the fundamental vibration region by D. A. Crooks. Adipic acid showed results similar to, but not so marked as, those of succinic acid.

Author Index to Abstracts of Papers Presented at the Los Angeles Meeting

Baker, W. R., J. V. Franck, and J. D. Gow—No. C9
Baños, A., Jr., H. Gruen, and D. S. Saxon—No. A5
Barnett, S. J.—No. B1
Becker, G. E. and P. Kusch—No. A6
Beeck, O., J. W. Otvos, D. P. Stevenson, and C. D. Wagner—No. D9
Benton, Arnold and E. L. Kinsey—No. D3
Biehl, A. T., R. A. Montgomery, H. V. Neher, W. H. Pickering, and Wm. C. Roesch—No. B10
Bradner, H., R. Crawford, H. Gordon, and J. R. Woodyard—No. C7
Bratenahl, A., R. H. Hildebrand, and B. J. Moyer—No. E10
Brode, R. B.—No. B8

Brown, S. Leroy and M. G. Foulks—No. E5
Davis, Leverett, Jr.—No. D4
Donoghue, J. J., E. Gerjuoy, and R. E. Vollrath—No. D14
Elvey, C. I.—No. A1
English, W. N.—No. B4
Fillmore, F., A. Hudgins, and M. Jeppson—No. C6
Gardner, E. and Vincent Peterson—No. B11
Gerjuoy, E.—No. D13
Glatt, Leonard—Nos. D1 and SP1
Hadley, J., C. Leith, H. York, E. Kelly, and C. Wiegand—No. E14
Hamilton, J. G.—No. C2
Hansen, J. W.—No. B3
Hansen, W. W.—No. A2
Helmholz, A. C. and J. M. Peterson—No. E13
Hodes, I.—No. E7
Hoffmann, Banesh—No. B2
Holmes, J. R.—No. E4
Horning, Wendell—No. B12
Jacobs, D. H.—No. E6
Kaplan, Joseph—No. A3
Kenny, G. S. and S. Rubin—No. D7
Keuffel, J. W.—No. A8
Kirkpatrick, Paul, A. V. Baez, and A. Newell—No. D2
Lauritsen, T. and R. F. Christy—No. D6
Liebermann, L. N.—No. D12
Loeb, L. B. and W. N. English—No. B5
MacKenzie, K. R.—No. E9
McEwen, G. F.—No. E1
McLachlan, D., Jr.—No. E8
Moore, D. C. and R. B. Brode—No. B6
Neher, H. V.—No. B9
O'Reilly, J. and R. F. Christy—No. D5
Otvos, J. W.—No. D11
Panofsky, W. K. H., C. Richman, and F. Oppenheimer—No. C8
Parkins, W. E. and J. M. Leffler—No. E2
Potapenko, G. and D. Wheeler—No. A4
Powell, Wilson M.—No. E12
Rau, R. Ronald, C. D. Anderson, R. V. Adams, and P. E. Lloyd—No. C3
Retallack, J. G. and R. B. Brode—No. B7
Schiff, L. I.—No. C4
Seaborg, G. T.—No. C1
Serber, Robert—No. C10
Smith, L. E., Jr.—No. E11
Stevenson, D. P.—No. D10
Thomas, R. G., W. A. Fowler, and C. C. Lauritsen—No. D8
Turner, C., B. Cork, J. Ballam, and H. Gordon—No. C5
Weissler, G. L. and R. W. Kotter—No. E3
Worley, R. Edwin—No. A7

Minutes of the Meeting of the New England Section at Wesleyan University, Middletown, Connecticut

November 1, 1947

THE 29nth meeting of the New England Section of the American Physical Society was held at Scott Laboratory, Wesleyan University in Middletown, Connecticut, on Saturday, November 1, 1947. One hundred and two members of the Section registered. The programme included five invited papers, four of which formed a symposium on physics of the solid state. There follow the titles of the invited papers and the abstracts of the ten minute contributed papers.

At the business meeting, the following officers were elected for 1948:

Chairman, K. T. Bainbridge, Harvard University.
Vice Chairman, Mildred Allen, Mount Holyoke College.
Secretary-Treasurer, G. F. Hull, Jr., Dartmouth College.
Programme Committee, W. P. Allis, Massachusetts Institute of Technology.
Programme Committee, C. T. Lane, Yale University.

Gordon F. Hull, Jr.
Secretary-Treasurer

Invited Papers

The Demonstration Lecture—Art or Craft? V. E. Eaton, *Wesleyan University.*

Symposium on Physics of the Solid State

Recent Experiments at High Pressures. P. W. Bridgman, *Harvard University.*

The Dependence of Dry Friction on the Bulk Properties of Metals. J. T. Burwell, Jr., *Massachusetts Institute of Technology.*

The Use of the Print-Out Effect in Studying the Motion of Electrons in Silver Chloride Crystals. J. R. Haynes, *Bell Telephone Laboratories, Inc.*

Properties of Quartz Crystals. K. S. Van Dyke, *Wesleyan University.*

Contributed Papers

1. Design of Double-Focusing Mass Spectrographs. H. E. DUCKWORTH, *Wesleyan University.* During recent years a number of double-focusing mass spectrographs have been constructed. In the course of making plans for a new double-focusing instrument, it has been desirable to compare critically these existing arrangements with certain other possible ones. The relative merits of the several arrangements with respect to resolving power, dispersion, magnification, and length of ion path will be discussed.

2. Arc Motion Reversal in Transverse Magnetic Field by Heating Cathode.* CHARLES G. SMITH, *Raytheon Manufacturing Company.* An arc between concentric tantalum electrodes in argon and mercury vapor was driven around by an axial magnetic field. The inner electrode was a cathode and so constructed that the arc spot played upon its outer surface and could in a few seconds bring it to a white heat. When the cathode was only at a red heat or less, the arc raced rapidly in the retrograde direction, but would turn suddenly and travel very slowly in the proper direction (the way the electromagnetic forces were acting) when the cathode at the arc spot was white hot and presumably thermionic. Argon pressure was from 5- to 30-mm Hg. Estimated Hg vapor pressure was above 0.1 mm. Arc current was approximately 13 amperes for a cathode 2.5 cm in diameter. Arc drop was 16 volts when the cathode was relatively cool, and 14 when white hot. No conditions of pressure, field intensity, or arc current could be found that would make the thermionic arc go in the retrograde direction.

* Part of the work was done at Harvard University.

3. High Frequency Corona Applications. M. D. O'DAY AND E. H. CULLINGTON, *Air Materiel Command, Cambridge Field Station.* A high frequency corona to be used in V-2 rocket experiments will be demonstrated. Using such a corona, spectrographs may be made at various altitudes for the purpose of studying the composition of the atmosphere. A compact, variable frequency kilowatt transmitter, designed for the rocket experiments, will be used in this demonstration.

The use of such a corona for producing monochromatic light by means of electrodes of several metal salts will be demonstrated also. The importance of such a convenient method of obtaining characteristic spectra of various salts will be emphasized.

4. Some Characteristics of a Delay-Line Coupled Wide-Band Pulse Amplifier.* H. GUNTHER RUDENBERG,** *Harvard University.* Measurements of gain and time delay have been made on pulse amplifier stages which use a traveling-wave delay-line circuit[1] to obtain short resolving times in spite of capacitive loading. Almost any number of tubes may be used in "parallel," their control grids connected to the nodes of one artificial delay line and their respective anodes connected to the corresponding nodes of a second identical delay line. A stage gain of 2.7 times permits optimum utilization of tubes, and *m*-derived delay-line terminations reduce reflection losses. A band width of more than 40 megacycles has been obtained with one stage using six 6J6 tubes, each having 30 micromicrofarads added capacitance shunting the electrodes. This stage has a resolving time of about 0.02 microsecond and introduces a pulse delay of 0.05 microsecond. An amplifier with a band width of 200 megacycles is now under construction.

* The experimental work was partly supported by Signal Corps and Navy Contract N5ori-76, Task Order I.
** Now National Research Council, RCA Predoctoral Fellow.
[1] W. S. Percival, British Patent, 460,562 (1937).

5. Propagation of Sound in Liquids under High Pressure. GERALD HOLTON, *Harvard University.* A multiple-echo method has been adapted to investigations of the velocity and absorption of sound in water and other liquids under high pressures, and measurements have been carried out with short pulses of 15-M c.p.s. sound to about 6000 kg/cm². A modified Loran DAS was used as timing mechanism. Data in water at various temperatures have been compared with velocities predicted by known thermodynamic coefficients. Incidentally, a zero temperature coefficient region has been found and investigated. Measurements of absorption proved, as so often, more difficult and less accurate than those of velocity. Anomalies are found in absorption coefficients and are found to obey a simple law. The behavior of other liquids (e.g., Toluene and ethyl ether) has also been investigated and will be reported on.

6. Silver Chloride Used as an Ionization Detector for Cosmic Rays.* W. L. WHITTEMORE AND J. C. STREET, *Harvard University.* Certain pieces of AgCl cut from single or rolled crystals give constant and satisfactory performance as an ionization detector over several days if cooled by liquid N_2 immediately after annealing, and if not exposed to strong radiation. Approximate saturation is obtained with 2000 volts/cm in agreement with results for photo-conductivity. Our tests have shown that annealed crystals kept several days at room temperature require considerably higher voltage for saturation. Preliminary measurements show that a crystal not easily saturated can be improved by controlled gamma-irradiation at low temperatures without field. This can be explained as a filling of trapping centers. Tests of stability of crystals treated in this way have been made for short periods only (½-hour). Radiation from 2 milligrams of radium, shielded with one centimeter of lead and placed 5 centimeters from a crystal, first gave the improvement cited above, but after eight hours of exposure resulted in a peculiar behavior characterized by pulses at least 100 times larger than usual, occurring with and without applied potential, and whose frequency was markedly affected by the radium source. The results of a preliminary study of pulse heights for identical events will be reported.

* This work is supported by Navy Contract N5ori-76.